Universidade da Coruña

Doctoral Thesis

# Structural optimization of steel jackets for offshore wind turbines considering dynamic response and fatigue constraints

Iván Couceiro Aguiar

*Supervisors:*

Dr. José París López
Dr. Fermín Navarrina Martínez

Programa de doctorado en Ingeniería Civil
Febrero 2018

# Abstract

It takes time for society to digest changes, but we are changing. We can not deny climate change anymore and, as a species, we have come to realize there is an urgent need to change our energy generation habits. They have changed indeed and, in the last decades, renewable energies have clearly colored the picture of energy sources. Particularly, wind energy is called to be one of the most valuable cards in the hand of renewable energies in the near future. However, the current trend, and target of this thesis, are not the typical wind turbines installed inland. In the last years, the preferred location for the placement of wind farms has traveled, or we better say sailed from land to the seas, seeking for higher efficiency and exploitation of wind's potential. Even though there are reasons to carry wind turbines offshore, the trip is neither easy nor low-cost and implies the analysis and design of new substructures to bear the weight of the turbines. Those substructures are called jackets.

This thesis defines a procedure of analysis of the dynamic behavior of offshore wind turbines supported by jackets. Upon that analysis, a structural optimization problem is defined and solved using mathematical and numerical optimization techniques. The goal is to reduce the amount of material needed to manufacture the jackets and therefore reduce the investment of offshore wind turbine structures and consequently the indirect cost of energy production.

The structural model is based on a non-linear dynamic analysis of three dimensional framed structures for fully coupled offshore wind turbines considering the rotation of the blades. Special care is taken in the description of the environmental loading conditions. Wind and wave actions and forces on the elements of the structure are thoroughly modeled. One of the most decisive aspects in the design of offshore structures is fatigue in steel elements arising from cyclic loads. In this thesis fatigue damage is assessed in terms of S-N curves by means of the Palmgren-Miner rule and using the Rainflow algorithm for counting stress cycles. Long-term fatigue damage in the joints of the jackets is accurately estimated from the damage computed for short-term computational simulations.

Since the analysis of the jackets is addressed in the time domain, the problem is faced as a dynamic response optimization. Although there are a few methodologies to handle time-dependent constraints, none is able to accomplish the task efficiently and still retaining all the valuable information about the structural status. A novel methodology

is introduced to efficiently deal with the time-dependent structural constraints imposed to the dynamic response of the structure.

The optimization model is presented as a weight minimization of the steel jacket under Ultimate Limit Stress, Fatigue Limit State and frequency constraints. Cross-sections of the tubular elements and bottom and top widths of the jacket are chosen as design variables to perform a simultaneous shape and size optimization while preserving the straight alignment of the legs. The optimization is addressed using Sequential Linear Programming which requires a first order sensitivity analysis. The sensitivities are obtained through Direct Differentiation and analytic derivatives except for the fatigue damage constraint since it lacks analytic derivative. The sensitivity core of the computational code constitutes an extremely expensive part in terms of CPU time and storage.

The optimization methodology developed is applied to real jacket structures bearing fully coupled rotating wind turbines. The optimization results show fair robustness of the algorithm when facing different problems and substantial reductions in the weight of the steel jackets are obtained while guarantying the fulfillment of the conditions imposed by the structural standards.

# Contents

# List of Figures

# List of Tables

# Prologue

*"Estáis esperando mis palabras. Me conocéis bien y sabéis que soy incapaz de permanecer en silencio. Callar, a veces, significa mentir, porque el sliencio puede interpretarse como aquiescencia."*
**Miguel de Unamuno**

Not many accept the challenge of reading a whole PhD thesis. Some will do it for pleasure, some will be forced to do so (sorry). Probably, most of them will read just the parts they are particularly interested in, the mathematical description, the numerical approach, the results (only the pictures)... But, some will tragically, yet inevitably, leave their bookmarks forever in the introduction chapter.

So, I am going to do my best and try to lure you towards reading the rest of the document on the first pages.

I hope I can do so.

*"Autotelic: It refers to a self contained activity, one that is not done with the expectation of future benefit, but simply because the doing itself is the reward."*
**Mihaly Csikzentmihalyi**

Chapter 1

# Introduction

*"A man's true honour cannot be outraged by what he suffers, but only and alone by what he does; for there is no saying what may befall any one of us"*
**Arthur Schopenhauer**, The art of being right.

Once upon a time, a man encountered a river in his path. Since he was granted the gift of rational thinking, he asked himself three questions before even start doing anything. The first question, that was already answered by its inborn determination, was: *What am I doing?*, to which he replied relentlessly: *I'm crossing this river*. The second question, which is the most meaningful, was: *Why am I doing it?*, and the third: *How do I do it?*...

I would like to think those three questions, *What?*, *Why?* and *How?*, not particularly in that order, are absolutely necessary for any activity claiming to be called rational. While the frontier between them is sometimes blurred and we could argue for days about the extent of each question and yet never reach an understanding; by responding to them we are undoubtedly revealing our purpose, motive and the means we plan to use to reach our end.

This chapter is about answering those questions. More precisely this chapter deals with the first two questions, and the remaining 219 pages of this document are a hopeful attempt of response to the third.

There is actually a fourth question that is not up to me to answer which is: *Did I do it?*. In this matter, I would be the lawyer on the trial against my own work and you would be the judge (let's hope not the prosecutor) to decide whether I did it or not. Although in this case, I would rather be guilty.

## 1.1. Background

It takes time for society to digest changes, but we are changing. We can not deny climate change anymore and, as a species, we have come to realize there is an urgent need to change our energy generation habits.

They have changed indeed and, in the last decade, renewable energies have clearly colored the picture of energy sources where fossil fuels, nuclear energy and natural gas were the primary elements. Particularly, energy extracted from the wind will be one of the most valuable cards in the hand of renewable energies in the near future.

The use of the wind resource is not new whatsoever. Windmills are undoubtedly the ancestors of modern wind turbines. They are said to be nearly 3000 years old although, the first reliable record is from 644 A.D. Regardless of their age and origin, they were an economic stilt during the Early and Late modern period[1].

**Figure 1.1. Traditional windmill (Goliath 1897) and modern wind turbines in Eemshaven, Netherlands.**

The fact is, wind power is now the main bet in terms of changing our energy resources. The worldwide power generation capacity from wind has grown in the last

[1] A detailed and enjoyable historical background on windmills and windwheels that can be read in [Hau, 2006] is highly encouraged.

decade from less than 100 GW to almost 500 GW in 2016 [2]. Particularly in the European Union (EU) the installed wind power capacity reached in 2016 the second largest form of power generation capacity, overtaking coal[3]. Figure 1.3 shows some of the main indicators of the wind energy evolution in the EU since 2005.

However, the current trend, and target of this thesis, are not the typical wind turbines installed inland. In the last years, the preferred location for the placement of wind farms has traveled, or we better say sailed from land to the seas. In the field's jargon, one is called onshore wind and the other offshore wind (1.2).

**(a) Onshore wind farm (source: inhabitat).** **(b) Offshore wind farm (source: Siemens).**

**Figure 1.2. Onshore vs Offshore wind farms.**

Offshore wind is not the only card alone in the deck, it is half of a bigger strategy to squeeze the raw energy of the oceans: Offshore Renewable Energy (OWE). The other half is known as ocean energy which is the extraction of energy from waves, currents, tides, etc. There are even combined proposals to merge both strategies in singular structures or devices [Karimirad, 2014; Pérez-Collazo et al., 2015].

Even though there are reasons to carry wind turbines offshore, the trip is neither easy nor low-cost. The main justification to plant the seeds of wind energy harvesting out in the seas is simple: wind is steadier and stronger offshore. The latter means higher efficiency and exploitation of wind's potential. Nevertheless, the drawbacks are easy to see. We are severely separating generation from consumption, so there is a need to wire new subsea transmission lines and built both, offshore and onshore substations. Also, the erection of wind turbines out in the middle of the sea means the development of new methods to sustain or hold their weight. While the tower, nacelle and blades remain similar to their onshore cousins, we need some method to support the whole structural system below the tower.

There are numerous types and concepts of substructures as supports of Offshore Wind Turbines (OWT). Each of them is particularly suitable or viable at certain ranges of depths. Even though the depth frontiers for each technology are not firmly estab-

[2]Source: Global Wind Energy Council
[3]Source: WindEurope

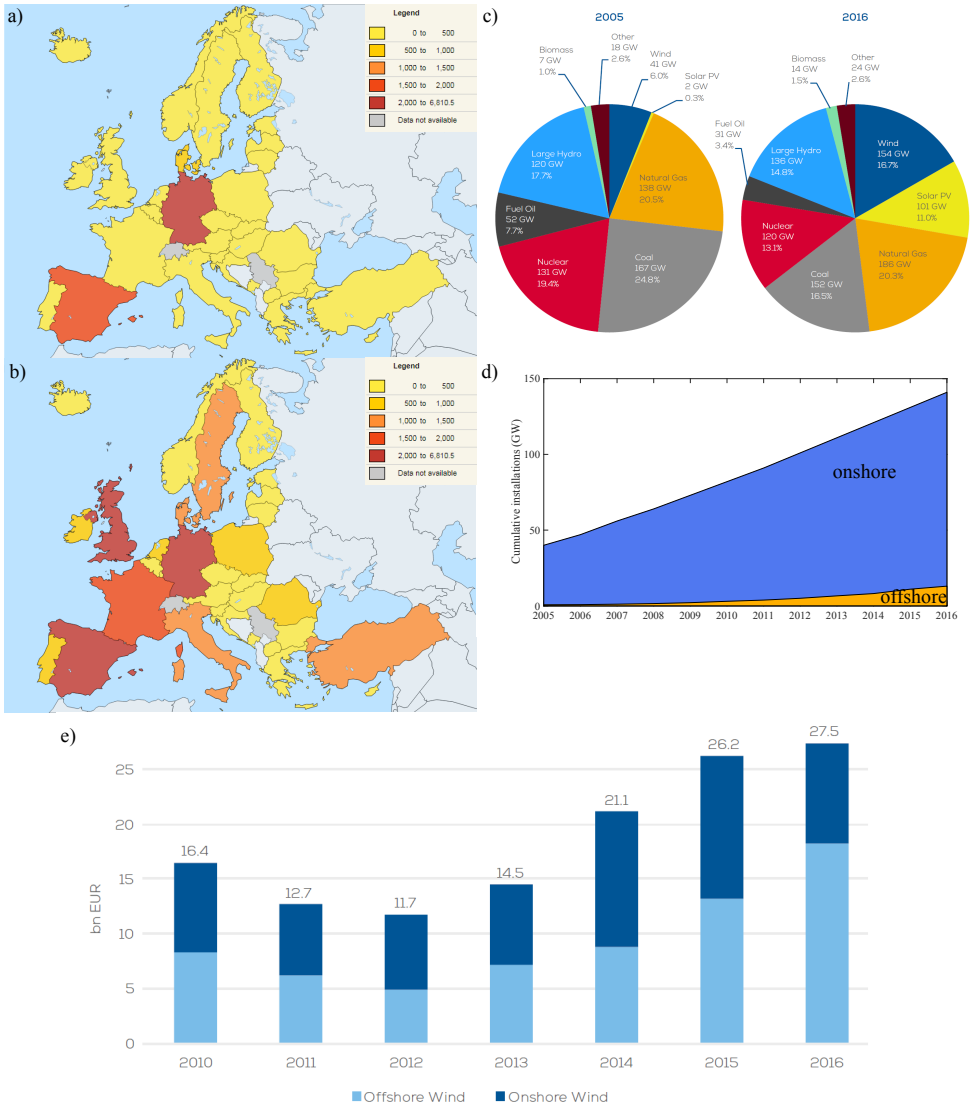


**Figure 1.3. Wind power trend in the EU. a)Primary production of energy from wind 2005, 1000 tonnes of oil equivalent. b)Primary production of energy from wind 2015, 100 tonnes of oil equivalent. c)Shares ins installed capacity 2005/2016 from energy sources. d)Onshore and offshore cumulative installed capacity 2005-2016 in GW. e)New asset in wind energy 2010-2016 in onshore and offshore. Sources: Eurostat, WindEurope, International Renewable Energy Agency (IRENA).**

lished, there is a wide gap between two conceptually different substructure approaches: bottom supported and floating.

While floating substructure concepts are mostly drafts and prototypes, bottom supported structures are solidly endorsed by engineering experience, in fact, they come from the old offshore oil and gas platforms substructures[4]. Additionally, bottom supported structures can be divided in bottom fixed and compliant. The former behave as a rigid body and must resist the full dynamic forces and the latter are designed to deflect with the action of environmental loads and reduce the dynamic force suffered. Either way, bottom supported OWT build a structure that connects the base of the tower with the sea bottom and floating OWT do not. Figure 1.4 draws the most common types of substructures arranged by recommended depth suitability.

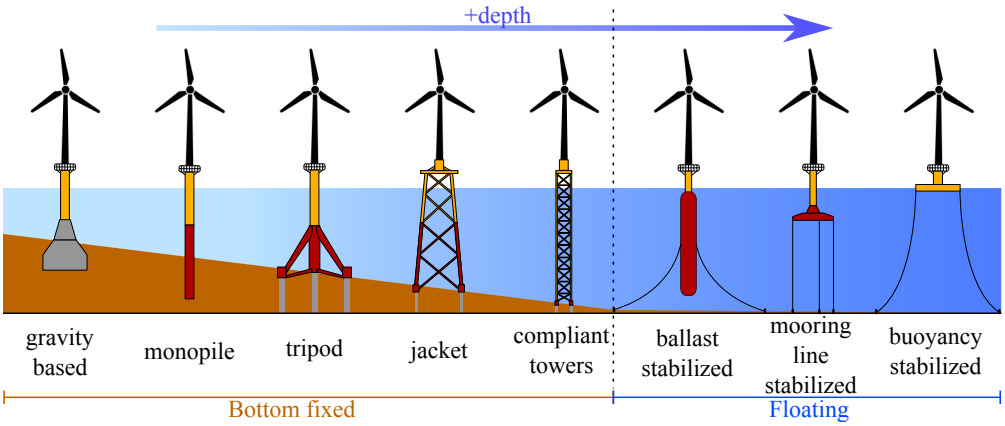


**Figure 1.4. Main offshore wind turbines substructure concepts.**

Among the common substructures pictured in figure 1.4, there is one that overcomes the rest in terms of number of units actually installed: monopiles. Monopiles are simple steel pipes ranging 2.5-6.0 m of diameter, hammered into the seabed and allowing straightforward calculation, fabrication and transport. However, monopiles are highly limited. The limit for them is said to be at 25-30 m deep and bearing 5-6 MW turbines, and that using 6.0 m diameter tubes which generate quite heavy structures.

In the deployment of offshore technology, the current challenge are the intermediate water depths 30-60 m, for which the developers have traditionally preferred the jacket type foundations. Jackets are 3D framed rigid structures formed by steel tubes of 0.5-2.0 m of diameter and around 500-600 t of weight. Most of the offshore wind farms up to the date are supported by monopiles, representing in 2016 more than 80% of OWT substructures while jackets only a 6.6% in Europe. One of the key factors is that, the share increase for Gravity based and tripod foundations already stopped in 2016 and jackets are just now starting to rise in new projects and future plans. Most of the actual

[4]If curious, one can consult the first chapters of [Chakrabarti, 2005], [El-Reedy, 2015] and [Wilson, 2003] for a deep historical review in offshore developments

projects under construction or already authorized to begin that tackle intermediate depths and big wind turbines of 7-8 MW use jacket foundations: Aberdeen, Beatrice, East Anglia 1, Hornsea Project, Neart na Gaoithe, Thanet Extension (UK projects with more than 600 wind turbines of 7 and 8 MW and depths ranging 30-56 m); Borkum Riffgrund 2, Wikinger (Germany projects with almost 100 turbines in depths up to 40 m); Nissum Bredning Vind (Denmark); Éolien en mer de la Baie de Saint-Brieuc (France, 62 8MW turbines in 28-36m depths); Longyuan Jiangsu Dafeng (China, 80 turbines); Tamra, Southwest (South Korea, 30 3 MW turbines up to 20 meters deep); Block Island Project[5], Fisherman's Atlantic City Windfarm Phase I, Coastal Virginia (USA windfarms in depths of 20-40 meters).


**Figure 1.5. Share of substructures types in EU offshore wind farms in 2016 (source: WindEurope) and examples of most used bottom-fixed structures.**

So the trend is clear, jackets are developers' weapon that will help them face the challenge of conquer deeper waters and more powerful turbines.

Yet, there are many engineering and technological features of jackets' analysis and design subject to uncertainties or unresolved. The mere structural analysis of the jackets and the definition and fulfillment of the particular strength requirements is a cumbersome process. Some of the physical phenomena critical to the design life of the structure, such as fatigue in steel, are hard to assess accurately. The impact of the in-place environmental conditions implies the definition of an unmanageable number of load cases which also generate an even greater amount of structural output data.

Above those issues arises the question if the designs of the steel jackets could be improved and optimized in terms of reducing the investment cost of the structure while meeting the same structural and strength requisites.

[5]The Block Island Project was the first USA offshore wind farm, located near Rhode Island with just 5 turbines powering more than 20000 homes annually

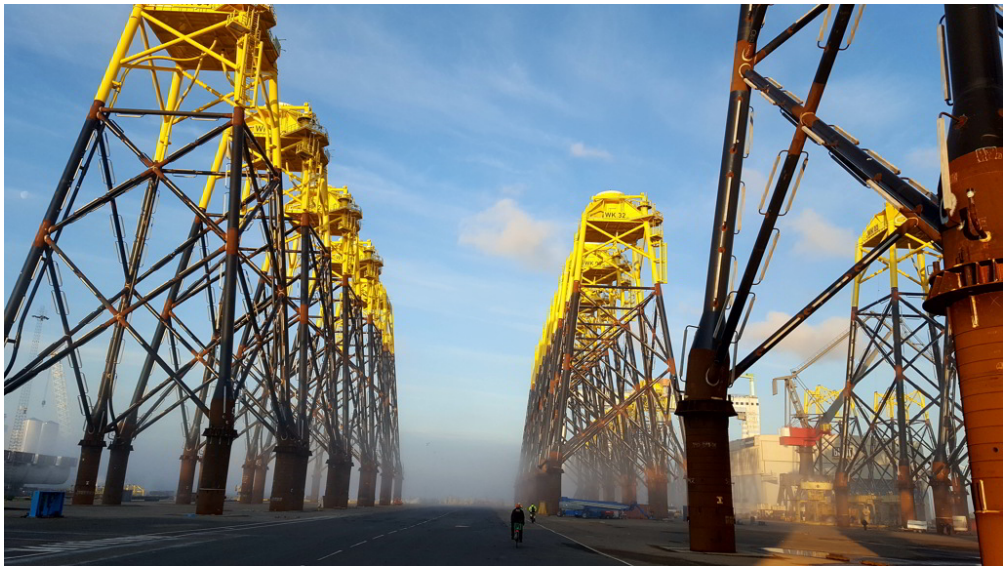

**Figure 1.6. Wikinger jackets ready to be shipped in Denmark (Source: Bladt Industries).**

## 1.2. Review

Although jacket structures for offshore wind turbines are relatively new, marine bottom-fixed steel structures exist from early 1900s. The Kerr-McGee drilling platform in figure 1.7a, known as Kermac Rig No. 16, was the first offshore rig in the Gulf of Mexico that was out of sight of land. From that very first milestone in 1947 to the 50.000 tonnes Bullwinkle colossal placed also in the Gulf of Mexico only 41 years passed. This fact may be seen as a reflection of how quickly the development for offshore petroleum structures grew based on strong economic interest. History is being repeated now but luckily for us the sought resource is wind instead of oil.

Even though mathematical optimization techniques, and particularly structural optimization, is older than these developments, the actual industry has always been reluctant to include them in the design process. Moreover, the advances in the optimization of offshore structures are still far from matured as we are yet in the phase when several works begin to appear without a common approach. Even the mere modelization of offshore wind turbines is still unclear and subjected to many uncertainties, the first world offshore wind farm dates 1991 and the first one to use jacket substructures was the Beatrice Demonstration in 2007.

Regarding the structural analysis, although frequency domain analysis is common for offshore structures, time domain analysis is becoming the preferred method as it is proven more accurate and reliable, not to mention it is the method prescribed for certification by the standards [DNV-OS-C101, 2014]. Despite the obvious drawback of high computing-time and resources demand it is the trend in the analysis of offshore structures.

**(a) Kermac Rig 16 from New Orleans Times-Picayune.**

**(b) Shell's Bullwinkle Jacket.**

**Figure 1.7. First offshore jacket structures.**

One of the first works noteworthy is [Yoshida, 2006], even though it is focused on an onshore turbine, they performed an optimization of the turbine tower in the time domain considering extreme and fatigue constraints. In [Karadeniz et al., 2010], a reliability-based optimization is proposed to account for uncertainties in the design of the jackets. The probabilistic constraints are based in extreme conditions but authors mention that the formulation can be extended to take into account fatigue probabilistic design. [Yan et al., 2010] performed an optimization of a platform jacket based on the ANSYS analysis and optimization toolbox under extreme loading. Their work considered the dimensions of the deck and the cross-sections of the main jacket's piles as design variables. [King et al., 2013] compared the influence in the design optimization of considering either superposition approaches or partially integrated and fully integrated models using Damage Equivalent Loads (DEL). In [Nasseri et al., 2014], authors optimize another jacket for a platform using a genetic algorithm with the weight of the jacket as objective function and diameter and thickness of the tubular members as variables under extreme loading. They use directional environmental data for the load cases.

Particularly, the Norwegian University of Science and Technology has been extremely active in this field in the past years. Their progress is reflected in many scientific publications in journals and conferences as well as the ABYSS project funded by The Danish Council for Strategic Research [Zwick et al., 2012; Chew et al., 2013; Muskulus & Schafhirt, 2014; Schafhirt et al., 2014, 2016; Chew et al., 2016]. A common feature of those works is the optimization only of the cross-sections of the members of the jacket structures and the utilization of the FEDEM software either for the dynamic analysis or for load calculations. The use of the rainflow counting algorithm is also extended in all works.

In [Zwick et al., 2012] authors study the use of a full-height lattice tower substituting the typical tubular tower. The improvement of the designs is made by locally

modifying the dimensions of the elements based on which one is the farthest from its behavioral limit. In [Chew et al., 2013] a comparison between 3-legged and 4-legged jackets is carried out with an optimization of the 3-legged version. DELs are used and the stability of the members is incorporated as a check out of the optimization loop. Later their work expanded to a gradient based optimization with analytical sensitivities of the constraints and the use of Sequential Quadratic Programming (SQP) method of MATLAB [Chew et al., 2016]. The time-dependent constraints are treated with the worst-case approach which considers only the maximum of the constraint in time without regard of whether that maximum can appear at another time point in the next optimization iteration. In [Schafhirt et al., 2014] authors based their analysis in 30 seconds simulations using Genetic Algorithm for the optimization and also for analysis shortcuts. In later works a local optimization approach is proposed in which it is assumed that changes in the properties of the members do not affect the response of the structure [Schafhirt et al., 2016]. This is assumed valid for simultaneous changes in all members of the structure which are optimized individually.

It is also worth mention the work developed in [Oest et al., 2017]. Analytical gradients are used for the optimization. However, the loads are considered independent of the design variables and a quasi-static structural analysis is performed to evaluate the behavior of the structure. The optimization is carried out using the Sequential Linear Programming (SLP) method implemented in the CPLEX optimizer of ILOG-IBM. This is one of the most complete works in optimization of offshore jacket structures up to date, together with [Chew et al., 2016].

## 1.3. Motivation

Question *Why?* is actually a chain of questions that have already been answered in the background section. For example, questions *Why wind?, why offshore?* or *why jackets?* have already been addressed in this dissertation. I would also like to think we have reached a point where there is no need to answer *why renewable sources?*

But, the final question of *Why optimize jackets?* is still unanswered.

The fact is, jackets are becoming the preferred support structure to reach deeper waters and bear more powerful turbines. So presumably, there is going to be countless jackets across the seas in the near future. Thus, those jackets, they better be perfectly designed so we do not end up unnecessarily wasting useful resources. Moreover, jackets represent a significant part of the budget in the deployment of an offshore wind farm and, the deeper the waters the higher the cost of the structure (figure 1.8). It is also noteworthy the few works bold enough to face the optimization of offshore jackets, not only because the novelty of the problem but because how hard it is to approach and solve accurately and efficiently.

Therefore, the motivation is the need to find, objectively, the most efficient support structure for OWT, not only in order to reduce costs but to improve the designs themselves so they can vanquish deeper waters.

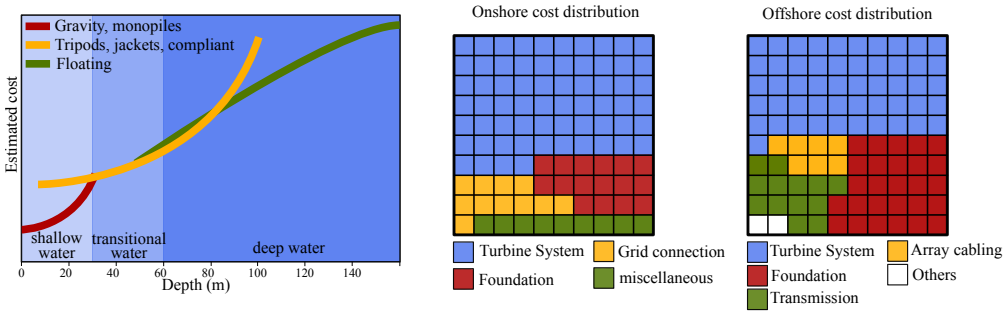


**Figure 1.8. Conceptual estimated cost vs depths for OWT substructures (Adapted from: [Musial et al., 2006] and typical cost distribution comparison in Onshore and Offshore windfarms (Data Source: WindEurope)**

## 1.4. Objective

What this thesis approaches is the description of a procedure of analysis of the dynamic behavior of offshore wind turbines supported by jackets. Upon that analysis, a structural optimization problem is defined and solved using mathematical and numerical optimization techniques. The goal is to reduce the amount of material needed to manufacture the jackets and therefore reduce the investment of OWT substructures and consequently the indirect cost of energy production.

In summary, the main objective of this thesis is the development of a structural optimization methodology to find the optimum designs of fixed steel jackets for offshore wind turbines.

Additionally, the main goal can be divided in intermediate or second level objectives that, although is soon to discussed them here, can be summarized as:

- Set the characteristics of the dynamic structural analysis of a fully-coupled offshore wind turbine and solve the time dependent response of the structure.
- Define a procedure to asses or estimate the fatigue damage during the whole life of the structure without the need of too long numerical simulations.
- Define an optimization problem in accordance to the structural requisites.
- Make the optimization problem manageable.
- Solve the optimization problem proposed and test its robustness in numerical examples.

## 1.5. Organization

Now comes the hard part. The part that requires 3 years of devoted work and 219 pages to get explained. So here we are just going to write the thesis overview.

- Chapter 1: The present chapter serves as introduction to the matter, gives a little background on the subject, sets the objective, the motivation and the outline of the document.
- Chapter 2: It is by far the longest chapter of the thesis. It contains the description of how the structural model is built, the modelization of the environmental loads, the numerical techniques used to solve the structural dynamic problem and the definition of the method for fatigue life assessment.
- Chapter 3: It defines step by step all the elements that conform the optimization problem proposed for jackets of offshore wind turbines and how can it be handled efficiently.
- Chapter 4: It describes the first order sensitivity analysis carried out which is necessary to solve the optimization problem proposed.
- Chapter 5: It defines the optimization methodology and describes the algorithm utilized to achieve the optimum designs of the jackets.
- Chapter 6: This chapter presents the application of the optimization method to several jacket examples with emphasis in the explanation of the optimum designs reached.
- Chapter 7: Finally, a few conclusions are drawn and some key topics are marked as interesting for future research developments.

There are two additional appendices as support information considered useful but not worthy of the space they would take within the main chapters.


**Figure 1.9. Wikinger jackets installed.**

Chapter 2

# Mathematical and numerical modeling

*"Eventually I concluded that language was bigger than the universe, that it was possible to talk about things in the same sentence which could not both be found in the real world. The real world might conceivably contain some object which had never so far been moved, and it might contain a force that had never successfully been resisted, but the question of whether the object was really immovable could only be known if all possible forces had been tried on it and left it unmoved. So the matter could be resolved by trying out the hitherto irresistible force on the hitherto immovable object to see what happened. Either the object would move or it wouldn't, which would tell us only that either the hitherto immovable object was not in fact immovable, or that the hitherto irresistible force was in fact resistible"*

**Mike Alder**

## 2.1. Introduction

This might be the longest, densest and most heterogeneous chapter of this thesis. Even though it is not about optimization, and it may not be appropriate to talk about it here, this thesis certainly is about optimization and so, everything in this document is somehow related to it.

Despite the fact that optimization techniques are seen more as an academic than technological field, the mathematical and numerical representation of the phenomenon and physics, on which the optimization methods are to be applied, need to accurately reproduce the reality of the events. Offshore engineering involves knowledge from numerous disciplines, each one of them being an extensive and profound area of research itself. So, modeling "*what is happening*" in an offshore wind turbine and jacket substructure means gathering all that scattered wisdom and join it together. Obviously,

one can only begin to scratch the surface of those deep expertise areas in an effort to extract the necessary pieces, and this chapter is all about that.

This chapter deals with: how the whole structure; including the jacket, the tower, the rotor-nacelle assembly and the blades, is modeled; how the different nature loads affect the structure, and how they are computationally represented and applied; how is this all merged to replicate the behavior of the structure dynamically as realistic and accurate as possible; and how do we fight with a phenomenon not yet fully understood as fatigue.

And there it is the reason why this chapter is the longest, densest and by far the most heterogeneous.

## 2.2. Previous considerations and hypotheses

Particular hypotheses are made and described in each of the forthcoming sections, however some bigger picture assumptions are given here since it would be confusing to justify them later.

One of the first and unsettled dilemmas was: Could the tubular members of the jacket be considered beams or given their diameter to length ratio and their thickness do they need to be considered as shells? From a local approach, each tubular element conforming the jacket is indeed a shell.

However, calculating the natural frequencies of individual elements it can be seen that the first vibration modes are beam type modes. Moreover, when combining all members in the whole jacket structure, the global natural vibration of the structure is dominated by beam modes. Thus, the dynamic behavior of the jacket structure can be modeled with beam elements accurately enough. Additionally, the optimization problem proposed in this thesis using shell elements instead of beam elements would grow in a size unmanageable for the current computational resources and lacking justification given the reasonable accuracy of the beam elements model.

There are three types of connections: hinged, rigid and semi-rigid. While the joints of the jacket structures are design and built as rigid as possible it might be more precise to take them for semi-rigid, although it would imply to introduce a stiffness coefficient for the rotation of each joint around each axis reflecting the actual rotational restraint of the node. Nevertheless, the gain in accuracy can be easily lost if those coefficients are not accurately obtained. Also, even though the joints are not perfectly built, the rigid connection model gives a proper representation of the actual behavior of the union.

And the same goes for the bottom fixed legs of the jacket. The soil in which they are fixed is at the best an elastic media. There are models actually considering the soil-structure interaction for offshore structures, however in this work the hypothesis of clamped legs at the bottom is made.

## 2.3. Structural model

Previous to the structural analysis, all the details and characteristics that define the numerical model which represents the actual structure, and its particularities, needs to be settled. The following describes step by step how the numerical model of the structure is built.

### 2.3.1. Global and local coordinate systems

Three dimensional space frames and their structural analysis call for a definition of two different coordinate systems. The overall geometry of the space frame, loads, displacements and restraints are described with reference to a global right-handed coordinate system $XYZ$ (defined by the unit vectors $\boldsymbol{e}_X$, $\boldsymbol{e}_Y$ and $\boldsymbol{e}_Z$). With three coordinates for each joint there are 6 degrees of freedom per joint, three displacements and three rotations. The solution of the dynamic equations of motion is as well performed in the global reference system.

However, for each member, a local reference frame ($xyz$ defined by the unit vectors $\boldsymbol{e}_x$, $\boldsymbol{e}_y$ and $\boldsymbol{e}_z$) is established to be able to derive the stiffness and mass relations for each element. We also need the transformation matrix that relates the coordinates of both systems for each element [Kassimali, 2012].

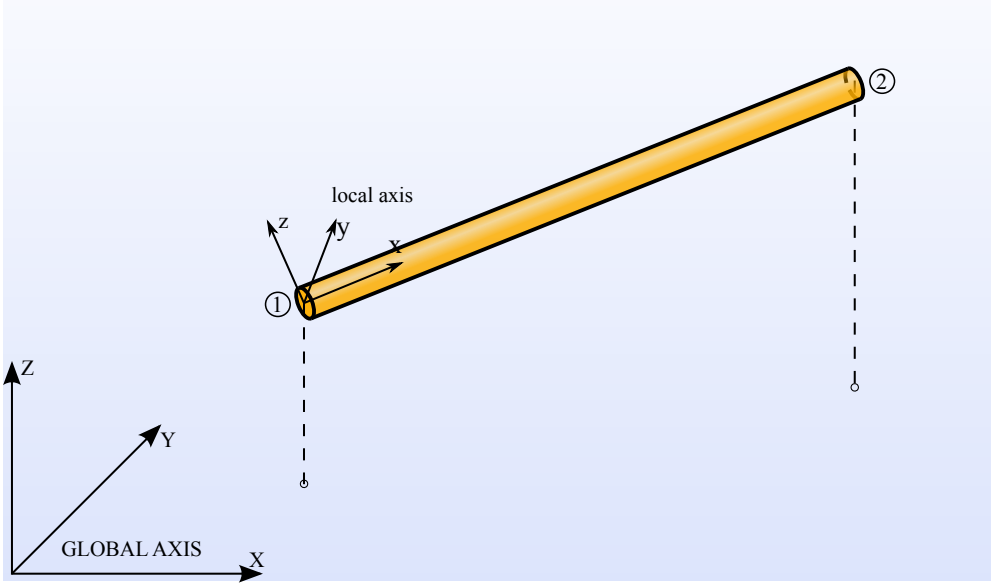


**Figure 2.1. Global and local axes of a structural member.**

The common practice to define the local axes is to align the local $x$ axis along the orientation of the straight member and define the $y$ axis as the cross product between

the global $Z$ axis and the local $x$ axis. This leads to a vertical $xz$ plane and a parallel to the horizontal $y$ axis.

Let the direction of the unit vector $\boldsymbol{e}_x$ of the local $x$ axis be defined by its direction cosines denoted by $r$:

$$r_{xX} = \cos(\theta_{xX}) = \frac{X_2 - X_1}{L} \qquad r_{xY} = \cos(\theta_{xY}) = \frac{Y_2 - Y_1}{L}$$
$$r_{xZ} = \cos(\theta_{xZ}) = \frac{Z_2 - Z_1}{L} \tag{2.1}$$

where $X_1$, $Y_1$, $Z_1$, $X_2$, $Y_2$ and $Z_2$ are the global coordinates of nodes 1 and 2.

Then the direction of the $y$ axis is defined as:

$$\boldsymbol{e}_y = \boldsymbol{e}_Z \times \boldsymbol{e}_x = \det \begin{vmatrix} \boldsymbol{e}_X & \boldsymbol{e}_Y & \boldsymbol{e}_Z \\ 0 & 0 & 1 \\ r_{xX} & r_{xY} & r_{xZ} \end{vmatrix} = -r_{xY}\,\boldsymbol{e}_X + r_{xX}\,\boldsymbol{e}_Y \tag{2.2}$$

Finally, the $z$ axis is defined as the cross product between the $x$ axis and the normalized $y$ axis:

$$\begin{aligned} \boldsymbol{e}_z = \boldsymbol{e}_Z \times \boldsymbol{e}_y &= \det \begin{vmatrix} \boldsymbol{e}_X & \boldsymbol{e}_Y & \boldsymbol{e}_Z \\ r_{xX} & r_{xY} & r_{xZ} \\ \dfrac{-r_{xY}}{\sqrt{r_{xX}^2 + r_{xY}^2}} & \dfrac{r_{xX}}{\sqrt{r_{xX}^2 + r_{xY}^2}} & 0 \end{vmatrix} \\ &= -\frac{r_{xX} r_{xZ}}{\sqrt{r_{xX}^2 + r_{xY}^2}}\boldsymbol{e}_X - \frac{r_{xY} r_{xZ}}{\sqrt{r_{xX}^2 + r_{xY}^2}}\boldsymbol{e}_Y + \sqrt{r_{xX}^2 + r_{xY}^2}\boldsymbol{e}_Z \end{aligned} \tag{2.3}$$

Thereby, the transformation matrix from global to local axes is:

$$\boldsymbol{R} = \begin{pmatrix} r_{xX} & r_{xY} & r_{xZ} \\ \frac{-r_{xY}}{\sqrt{r_{xX}^2 + r_{xY}^2}} & \frac{r_{xX}}{\sqrt{r_{xX}^2 + r_{xY}^2}} & 0 \\ -\frac{r_{xX} r_{xZ}}{\sqrt{r_{xX}^2 + r_{xY}^2}} & -\frac{r_{xY} r_{xZ}}{\sqrt{r_{xX}^2 + r_{xY}^2}} & \sqrt{r_{xX}^2 + r_{xY}^2} \end{pmatrix} \tag{2.4}$$

In addition, there is another step. The local axes defined until now can be rotated by an roll angle $\varphi$ to achieve a second pair of axes $y'$ and $z'$ oriented according to the principal axes of the member. This is not relevant when dealing with the tubular members of the jacket but has to be considered for the non axisymmetric cross-sections of the blades. This second transformation is achieved rotating the transformation matrix of (2.4) as:

$$\boldsymbol{R'} = \boldsymbol{\Phi}\,\boldsymbol{R} \tag{2.5}$$

where the rotation matrix $\boldsymbol{\Phi}$ is:

$$\boldsymbol{\Phi} = \begin{pmatrix} 1 & 0 & 0 \\ 0 & \cos\varphi & \sin\varphi \\ 0 & -\sin\varphi & \cos\varphi \end{pmatrix} \tag{2.6}$$

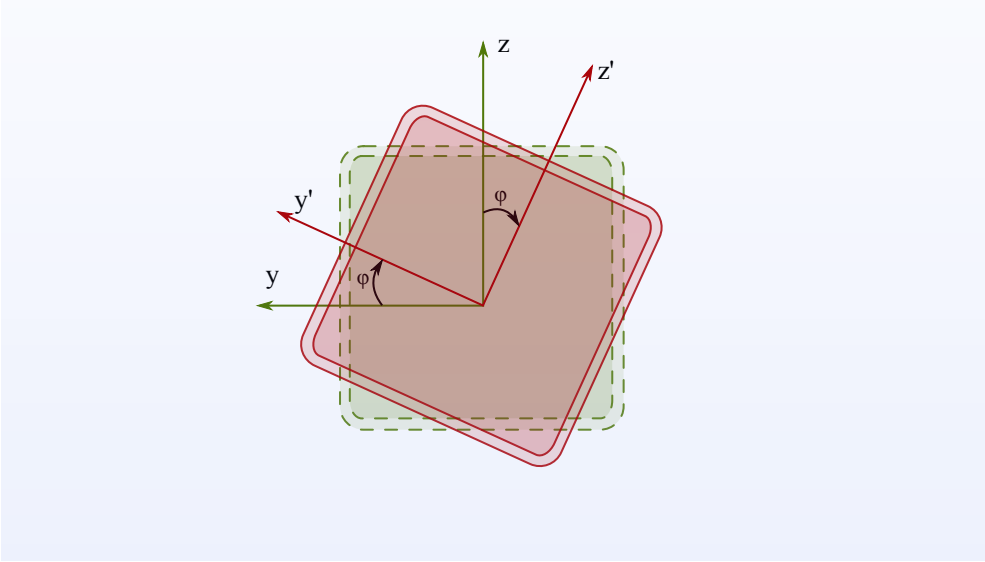


**Figure 2.2. Roll angle of the member.**

Thereby, the full transformation matrix including the roll angle of the cross-section is:

$$\boldsymbol{R'} = \begin{pmatrix} r_{xX} & r_{xY} & r_{xZ} \\ \frac{-r_{xY}\cos(\varphi) - r_{xX} r_{xZ}\sin(\varphi)}{\sqrt{r_{xX}^2 + r_{xY}^2}} & \frac{r_{xX}\cos(\varphi) - r_{xY} r_{xZ}\sin(\varphi)}{\sqrt{r_{xX}^2 + r_{xY}^2}} & \sqrt{r_{xX}^2 + r_{xY}^2}\sin(\varphi) \\ \frac{r_{xY}\sin(\varphi) - r_{xX} r_{xZ}\cos(\varphi)}{\sqrt{r_{xX}^2 + r_{xY}^2}} & \frac{-r_{xX}\sin(\varphi) - r_{xY} r_{xZ}\cos(\varphi)}{\sqrt{r_{xX}^2 + r_{xY}^2}} & \sqrt{r_{xX}^2 + r_{xY}^2}\cos(\varphi) \end{pmatrix} \tag{2.7}$$

This transformation matrix changes any given orientation or direction from the global axes to the local base. In order to do the inverse transform, the inverse of the transformation matrix would be needed although, matrix (2.7) is orthogonal and thus its inverse is equal to its transpose.

$$\boldsymbol{v'} = \boldsymbol{R'}\,\boldsymbol{v} \qquad \longrightarrow \qquad \boldsymbol{v} = \boldsymbol{R'}^{t}\,\boldsymbol{v'} \tag{2.8}$$

There is an exception to this definition of local axes, and it happens when the member is oriented vertically, meaning that its local $x$ axis is in fact the global $Z$ axis.

When this happens, equation (2.2) can not be used, as the cross product would be **0**. Thus, for vertically oriented members, we can simply choose the local axes to be: $(x, y, z) \Leftrightarrow (Z, Y, -X)$.

Still, there is another exception: Equations (2.2) through (2.7) are valid for fixed elements, whereas for moving objects and, more specifically in our case, rotating objects, if we use the local axes definition explained so far we may find out that the orientation of $y$ and $z$ changes with every rotation. This would not be an issue when dealing with tubular sections but, when dealing with non axisymmetric sections, it means that the roll angle $\varphi$ that relates the orientation of the local axes with the principal axes of the cross-section, changes with every rotation $\theta$. So we would have to define a particular $\varphi(\theta)$ function for every element.

However, we can change the derivation of the local axes for rotating elements so their roll angle remains constant with the rotating motion. Considering that the spinning of the turbine occurs around the $X$ axis, the new local axes are:

$$\begin{aligned} \boldsymbol{e}_z &= \boldsymbol{e}_X \times \boldsymbol{e}_x \\ \boldsymbol{e}_y &= \boldsymbol{e}_z \times \boldsymbol{e}_x \end{aligned} \tag{2.9}$$

This definition guarantees that the new local $z$ axis remains always in the $YZ$ plane and the roll angle of the cross-sections is constant along the rotation. Using equation (2.9) to derive the new transformation matrix leads to:

$$\boldsymbol{R'} = \begin{pmatrix} r_{xX} & r_{xY} & r_{xZ} \\ -\sqrt{r_{xZ}^2 + r_{xY}^2}\cos(\varphi) & \frac{r_{xX} r_{xY}\cos(\varphi) - r_{xZ}\sin(\varphi)}{\sqrt{r_{xZ}^2 + r_{xY}^2}} & \frac{r_{xX} r_{xZ}\cos(\varphi) + r_{xY}\sin(\varphi)}{\sqrt{r_{xZ}^2 + r_{xY}^2}} \\ \sqrt{r_{xZ}^2 + r_{xY}^2}\sin(\varphi) & \frac{-r_{xX} r_{xY}\sin(\varphi) - r_{xZ}\cos(\varphi)}{\sqrt{r_{xZ}^2 + r_{xY}^2}} & \frac{-r_{xX} r_{xZ}\sin(\varphi) + r_{xY}\cos(\varphi)}{\sqrt{r_{xZ}^2 + r_{xY}^2}} \end{pmatrix} \tag{2.10}$$

The exception for this particular case would arise when the local axis $x$ falls parallel to the global $X$ axis. In this case, the local axes are just oriented as the global axes and only the transformation (2.6) given by the roll angle needs to be applied.

Figure 2.3 shows the mistake made in the dynamic behavior of the structure by not considering the rotating local axes since the angles of roll of the rotating blades are referred to different local axes at each time step. In fact whenever one of the blades is oriented vertically, the non-rotating local axes interchange positions of $z$ and $y$ axis and thus the first two natural bending modes are miscalculated. The above mentioned definition of local axes corrects this effect.

### 2.3.2. Stiffness matrix

The derivation of the full stiffness matrix for beam elements is well explained in [Oñate, 1992; Wilson, 2001; Pilkey, 2005; Carrera et al., 2011] however, the process will

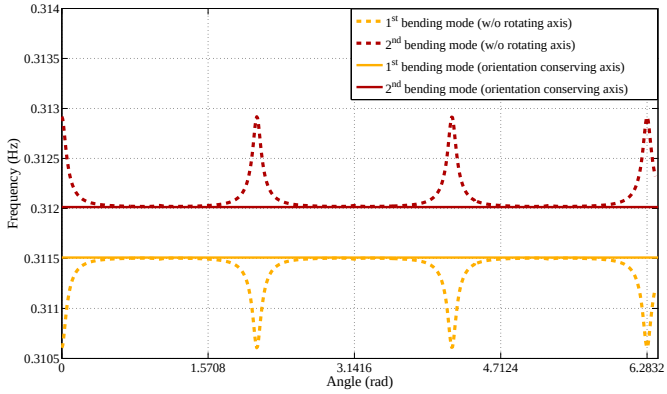


**Figure 2.3. First and second natural vibration modes with and without the additional local axes formulation.**

be outlined here as some of the terms would be later needed in forthcoming sections and chapters.

Given an element of the three dimensional structure, it is already known that we have six degrees of freedom per node so, we end up with twelve degrees of freedom per element. Representing the vector of displacements in both global and local axes:

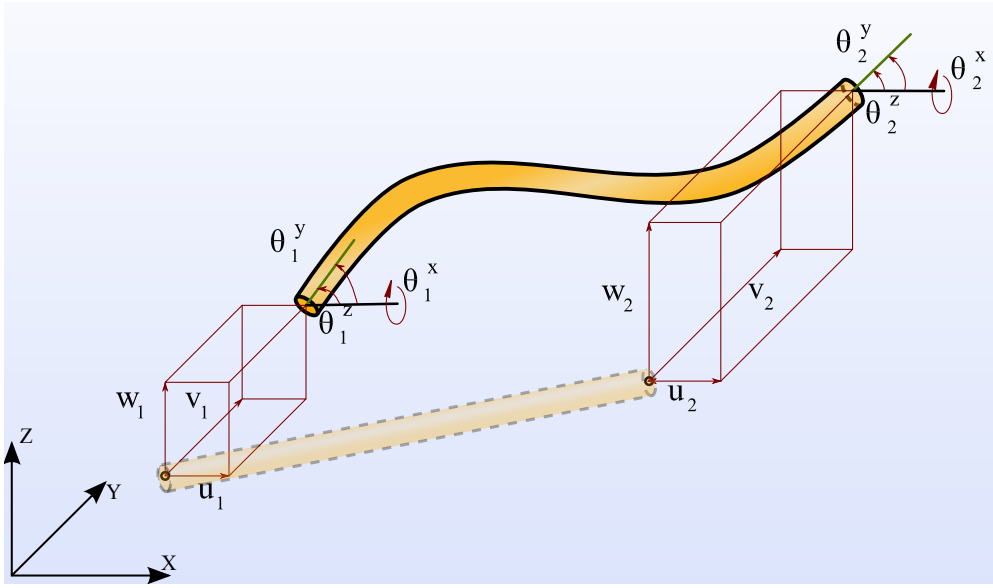


**Figure 2.4. Global axes displacements.**

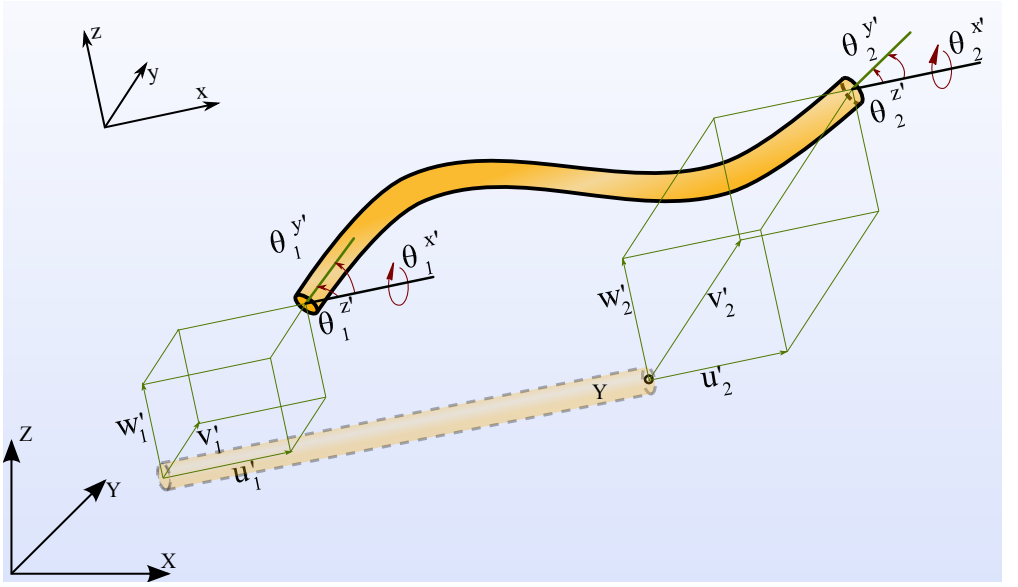


**Figure 2.5. Local axes displacements.**

$$\boldsymbol{u} = \left\{ \begin{array}{c} \boldsymbol{u}_1 \\ \boldsymbol{u}_2 \end{array} \right\} \quad ; \quad \boldsymbol{u}_1 = \left\{ \begin{array}{c} u_1 \\ v_1 \\ w_1 \\ \theta_1^x \\ \theta_1^y \\ \theta_1^z \end{array} \right\} \quad ; \quad \boldsymbol{u}_2 = \left\{ \begin{array}{c} u_2 \\ v_2 \\ w_2 \\ \theta_2^x \\ \theta_2^y \\ \theta_2^z \end{array} \right\} \tag{2.11}$$

$$\boldsymbol{u'} = \left\{ \begin{array}{c} \boldsymbol{u'}_1 \\ \boldsymbol{u'}_2 \end{array} \right\} \quad ; \quad \boldsymbol{u'}_1 = \left\{ \begin{array}{c} u'_1 \\ v'_1 \\ w'_1 \\ \theta_1^{x'} \\ \theta_1^{y'} \\ \theta_1^{z'} \end{array} \right\} \quad ; \quad \boldsymbol{u'}_2 = \left\{ \begin{array}{c} u'_2 \\ v'_2 \\ w'_2 \\ \theta_2^{x'} \\ \theta_2^{y'} \\ \theta_2^{z'} \end{array} \right\} \tag{2.12}$$

Given those movements in the local reference frame, the strains produced by those displacements shown in figure 2.6 can be expressed as:

$$\boldsymbol{\varepsilon} = \left\{ \begin{array}{c} \Delta L \\ \Delta\theta_1^y \\ \Delta\theta_2^y \\ \Delta\theta^x \\ \Delta\theta_1^z \\ \Delta\theta_2^z \end{array} \right\} = \left\{ \begin{array}{c} u'_2 - u'_1 \\ \theta_1^{y'} + \frac{w'_2 - w'_1}{L} \\ \theta_2^{y'} + \frac{w'_2 - w'_1}{L} \\ \theta_2^{x'} - \theta_1^{x'} \\ \theta_1^{z'} + \frac{v'_2 - v'_1}{L} \\ \theta_2^{z'} + \frac{v'_2 - v'_1}{L} \end{array} \right\} \tag{2.13}$$

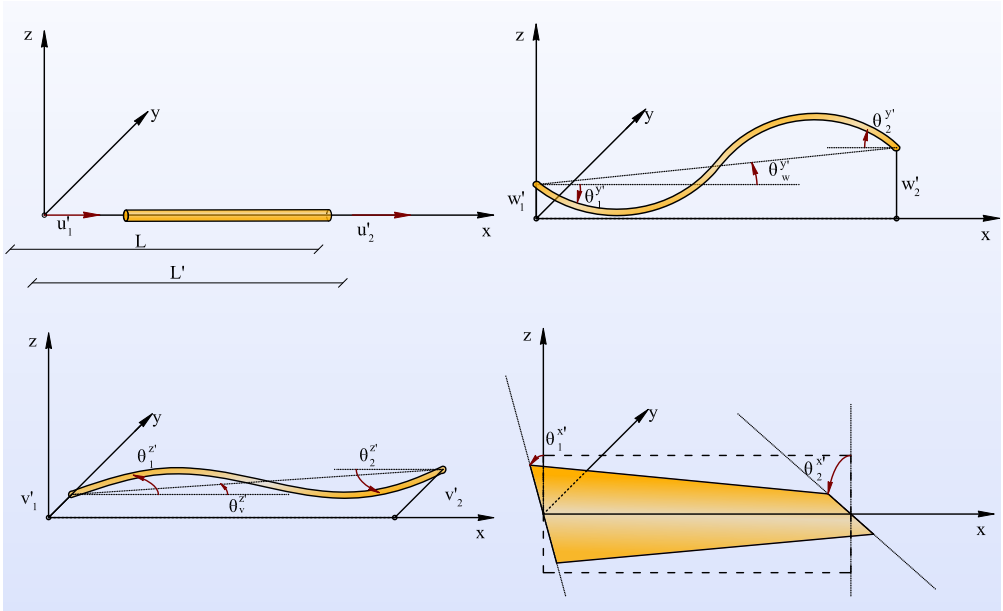


**Figure 2.6. Local movements and strains of an element.**

Thus, the relation between local displacements and strains can be expressed as:

$$\boldsymbol{\varepsilon} = \boldsymbol{E}\,\boldsymbol{u'} \tag{2.14}$$

where the matrix $\boldsymbol{E}$ is:

$$\boldsymbol{E} = \begin{pmatrix} -1 & 0 & 0 & 0 & 0 & 0 & 1 & 0 & 0 & 0 & 0 & 0 \\ 0 & 0 & -1/L & 0 & 1 & 0 & 0 & 0 & 1/L & 0 & 0 & 0 \\ 0 & 0 & -1/L & 0 & 0 & 0 & 0 & 0 & 1/L & 0 & 1 & 0 \\ 0 & 0 & 0 & -1 & 0 & 0 & 0 & 0 & 0 & 1 & 0 & 0 \\ 0 & 1/L & 0 & 0 & 0 & 1 & 0 & -1/L & 0 & 0 & 0 & 0 \\ 0 & 1/L & 0 & 0 & 0 & 0 & 0 & -1/L & 0 & 0 & 0 & 1 \end{pmatrix} \tag{2.15}$$

Given the matrix that transforms from local to global coordinates:

$$\boldsymbol{T} = \begin{pmatrix} \boldsymbol{R'} & & & \\ & \boldsymbol{R'} & & \\ & & \boldsymbol{R'} & \\ & & & \boldsymbol{R'} \end{pmatrix} \tag{2.16}$$

We can finally relate the strains with the global displacements with the compatibility equation as:

$$\left.\begin{array}{l} \boldsymbol{u'} = \boldsymbol{T}\,\boldsymbol{u} \\ \boldsymbol{\varepsilon} = \boldsymbol{E}\,\boldsymbol{u'} \end{array}\right\} \Rightarrow \boldsymbol{\varepsilon} = \boldsymbol{E}\,(\boldsymbol{T}\,\boldsymbol{u}) = \underbrace{(\boldsymbol{E}\,\boldsymbol{T})}_{\boldsymbol{B}}\boldsymbol{u} \Leftrightarrow \boldsymbol{\varepsilon} = \boldsymbol{B}\,\boldsymbol{u} \tag{2.17}$$

The strains can also be related with the stresses of the element through the constitutive equation:

$$\boldsymbol{\sigma} = \begin{Bmatrix} N \\ M_1^y \\ M_2^y \\ M^x \\ M_1^z \\ M_2^z \end{Bmatrix} = \boldsymbol{D}\,\boldsymbol{\varepsilon}, \quad ; \quad \boldsymbol{D} = \begin{pmatrix} \frac{EA}{L} & 0 & 0 & 0 & 0 & 0 \\ 0 & \frac{4EI_y}{L} & \frac{2EI_y}{L} & 0 & 0 & 0 \\ 0 & \frac{2EI_y}{L} & \frac{4EI_y}{L} & 0 & 0 & 0 \\ 0 & 0 & 0 & \frac{GJ}{L} & 0 & 0 \\ 0 & 0 & 0 & 0 & \frac{4EI_z}{L} & \frac{2EI_z}{L} \\ 0 & 0 & 0 & 0 & \frac{2EI_z}{L} & \frac{4EI_z}{L} \end{pmatrix} \tag{2.18}$$

where $E$ is the elastic modulus of the element, $A$ is the cross-sectional area, $I_y$ and $I_z$ are the section moment of inertia in $y$ and $z$ respectively, $G$ is the shear modulus and $J$ is the torsional moment of inertia.

Then, the generalized stresses $\boldsymbol{\sigma}$ can be transformed to nodal forces on the element $\boldsymbol{f}$ in a similar way movements are transformed to strains with the equilibrium equation:

$$\boldsymbol{f'} = \boldsymbol{E}^t\,\boldsymbol{\sigma} \Rightarrow \boldsymbol{f} = \boldsymbol{T}^t\left(\boldsymbol{E}^t\,\boldsymbol{\sigma}\right) = \left(\boldsymbol{T}^t\boldsymbol{E}^t\right)\boldsymbol{\sigma} = \underbrace{\left(\boldsymbol{T}\boldsymbol{E}\right)^t}_{\boldsymbol{B}^t}\boldsymbol{\sigma} \Leftrightarrow \boldsymbol{f} = \boldsymbol{B}^t\,\boldsymbol{\sigma} \tag{2.19}$$

where the local and global vectors of nodal forces are:

$$\boldsymbol{f'} = \begin{Bmatrix} \boldsymbol{f'}_1 \\ \boldsymbol{f'}_2 \end{Bmatrix} \quad ; \quad \boldsymbol{f'}_1 = \begin{Bmatrix} f_1^{x'} \\ f_1^{y'} \\ f_1^{z'} \\ m_1^{x'} \\ m_1^{y'} \\ m_1^{z'} \end{Bmatrix} \quad ; \quad \boldsymbol{f'}_2 = \begin{Bmatrix} f_2^{x'} \\ f_2^{y'} \\ f_2^{z'} \\ m_2^{x'} \\ m_2^{y'} \\ m_2^{z'} \end{Bmatrix} \tag{2.20}$$

$$\boldsymbol{f} = \begin{Bmatrix} \boldsymbol{f}_1 \\ \boldsymbol{f}_2 \end{Bmatrix} \quad ; \quad \boldsymbol{f}_1 = \begin{Bmatrix} f_1^{x} \\ f_1^{y} \\ f_1^{z} \\ m_1^{x} \\ m_1^{y} \\ m_1^{z} \end{Bmatrix} \quad ; \quad \boldsymbol{f}_2 = \begin{Bmatrix} f_2^{x} \\ f_2^{y} \\ f_2^{z} \\ m_2^{x} \\ m_2^{y} \\ m_2^{z} \end{Bmatrix} \tag{2.21}$$

Finally, the stiffness matrix that relates forces and movements can be obtained using the three equations, compatibility, constitutive and equilibrium:

$$\left.\begin{array}{l} \boldsymbol{\varepsilon} = \boldsymbol{B}\,\boldsymbol{u} \\ \boldsymbol{\sigma} = \boldsymbol{D}\,\boldsymbol{\varepsilon} \\ \boldsymbol{f} = \boldsymbol{B}^t\,\boldsymbol{\sigma} \end{array}\right\} \rightarrow \left\{\begin{array}{l} \boldsymbol{\sigma} = \boldsymbol{D}\left(\boldsymbol{B}\boldsymbol{u}\right) = \overbrace{\left(\boldsymbol{D}\boldsymbol{B}\right)}^{\boldsymbol{S}}\boldsymbol{u} \\ \boldsymbol{f} = \boldsymbol{B}^t\left(\boldsymbol{S}\boldsymbol{u}\right) = \underbrace{\left(\boldsymbol{B}^t\boldsymbol{S}\right)}_{\boldsymbol{K}}\boldsymbol{u} \end{array}\right\} \Rightarrow \boldsymbol{K} = \boldsymbol{T}^t\,\underbrace{\boldsymbol{E}^t\,\boldsymbol{D}\,\boldsymbol{E}}_{\boldsymbol{K'}}\,\boldsymbol{T} \rightarrow \boldsymbol{K}\boldsymbol{u} = \boldsymbol{f} \tag{2.22}$$

where $\boldsymbol{K'}$ is often called the elemental stiffness matrix:

$$\boldsymbol{K'} = \left(\begin{array}{cccccc|cccccc}
\frac{EA}{L} & 0 & 0 & 0 & 0 & 0 & \frac{-EA}{L} & 0 & 0 & 0 & 0 & 0 \\
0 & \frac{12EI_z}{L^3} & 0 & 0 & 0 & \frac{6EI_z}{L^2} & 0 & \frac{-12EI_z}{L^3} & 0 & 0 & 0 & \frac{6EI_z}{L^2} \\
0 & 0 & \frac{12EI_y}{L^3} & 0 & \frac{-6EI_y}{L^2} & 0 & 0 & 0 & \frac{-12EI_y}{L^3} & 0 & \frac{-6EI_y}{L^2} & 0 \\
0 & 0 & 0 & \frac{GJ}{L} & 0 & 0 & 0 & 0 & 0 & \frac{-GJ}{L} & 0 & 0 \\
0 & 0 & \frac{-6EI_y}{L^2} & 0 & \frac{4EI_y}{L} & 0 & 0 & 0 & \frac{6EI_y}{L^2} & 0 & \frac{2EI_y}{L} & 0 \\
0 & \frac{6EI_z}{L^2} & 0 & 0 & 0 & \frac{4EI_z}{L} & 0 & \frac{-6EI_z}{L^2} & 0 & 0 & 0 & \frac{2EI_z}{L} \\
\hline
\frac{-EA}{L} & 0 & 0 & 0 & 0 & 0 & \frac{EA}{L} & 0 & 0 & 0 & 0 & 0 \\
0 & \frac{-12EI_z}{L^3} & 0 & 0 & 0 & \frac{-6EI_z}{L^2} & 0 & \frac{12EI_z}{L^3} & 0 & 0 & 0 & \frac{-6EI_z}{L^2} \\
0 & 0 & \frac{-12EI_y}{L^3} & 0 & \frac{6EI_y}{L^2} & 0 & 0 & 0 & \frac{12EI_y}{L^3} & 0 & \frac{6EI_y}{L^2} & 0 \\
0 & 0 & 0 & \frac{-GJ}{L} & 0 & 0 & 0 & 0 & 0 & \frac{GJ}{L} & 0 & 0 \\
0 & 0 & \frac{-6EI_y}{L^2} & 0 & \frac{2EI_y}{L} & 0 & 0 & 0 & \frac{6EI_y}{L^2} & 0 & \frac{4EI_y}{L} & 0 \\
0 & \frac{6EI_z}{L^2} & 0 & 0 & 0 & \frac{2EI_z}{L} & 0 & \frac{-6EI_z}{L^2} & 0 & 0 & 0 & \frac{4EI_z}{L}
\end{array}\right) \tag{2.23}$$

This elemental stiffness matrix in local coordinates is computed for each element, transformed to global coordinates and then assembled in the global stiffness matrix according to the structure's connectivity of the elements.

### 2.3.3. Mass matrix

The structural mass matrix tries to represent the inertial properties of the members in a dynamic system. The procedures for modeling the mass of three dimensional beams are various [Paz, 2003; Clough & Penzien, 1995; Cheng, 2001]. When using the displacement matrix method for structural analysis two typical approaches for the mass matrix are used: Lumped mass and consistent mass. The lumped mass method is the simplest way of considering the inertial properties, consisting in concentrate the mass of the elements at the nodal coordinates resulting in a diagonal matrix. This method considers the translation mass effects but neglects the inertia of the flexural rotations. The diagonal lumped mass matrix for a three dimensional beam element would be:

$$diag\left(\boldsymbol{M'}_L\right) = \frac{\rho\, A\, L}{2}\left\{1\ ,1\ ,1\ ,I_0/A\ ,0\ ,0\ ,1\ ,1\ ,1\ ,I_0/A\ ,0\ ,0\ \right\} \tag{2.24}$$

being $\rho$ the density of the material and $I_0$ the polar moment of inertia. The density and area considered for the element have to take into account the possibility of flooded members (considering the mass of the entrapped water) and elements covered with marine growth.

However it is possible to generate a mass matrix using the finite element method and the same shape functions used to derive the stiffness matrix [Paz, 2003] and applying the principle of virtual work. The consistent mass matrix obtained this way considers all the translation and rotation effects and has a similar structure to (2.23):

$$\boldsymbol{M'}_C = \frac{\rho AL}{420}\left(\begin{array}{cccccc|cccccc} 140 & 0 & 0 & 0 & 0 & 0 & 70 & 0 & 0 & 0 & 0 & 0 \\ 0 & 156 & 0 & 0 & 0 & 22L & 0 & 54 & 0 & 0 & 0 & -13L \\ 0 & 0 & 156 & 0 & -22L & 0 & 0 & 0 & 54 & 0 & 13L & 0 \\ 0 & 0 & 0 & \frac{140I_0}{A} & 0 & 0 & 0 & 0 & 0 & \frac{70I_0}{A} & 0 & 0 \\ 0 & 0 & -22L & 0 & 4L^2 & 0 & 0 & 0 & -13L & 0 & -3L^2 & 0 \\ 0 & 22L & 0 & 0 & 0 & 4L^2 & 0 & 13L & 0 & 0 & 0 & -3L^2 \\ \hline 70 & 0 & 0 & 0 & 0 & 0 & 140 & 0 & 0 & 0 & 0 & 0 \\ 0 & 54 & 0 & 0 & 0 & 13L & 0 & 156 & 0 & 0 & 0 & -22L \\ 0 & 0 & 54 & 0 & -13L & 0 & 0 & 0 & 156 & 0 & 22L & 0 \\ 0 & 0 & 0 & \frac{70I_0}{A} & 0 & 0 & 0 & 0 & 0 & \frac{140I_0}{A} & 0 & 0 \\ 0 & 0 & 13L & 0 & -3L^2 & 0 & 0 & 0 & 22L & 0 & 4L^2 & 0 \\ 0 & -13L & 0 & 0 & 0 & -3L^2 & 0 & -22L & 0 & 0 & 0 & 4L^2 \end{array}\right) \tag{2.25}$$

The full derivation of (2.25) using the finite element method can be found in [Cheng, 2001]. Using both models (2.24) and (2.25) has major impact when computing the natural frequencies of individual elements, specially when rotations are important since the lumped mass matrix is unable to emulate the rotational inertia. Moreover, using the consistent mass matrix tends to overestimate the natural frequencies of the structure while using the lumped mass underestimates them. The discrepancies between both models tend to converge when discretizing the beams in multiple elements, in fact, the influence is significantly lower over the dynamic behavior of a structure formed by numerous bars. Even though the consistent matrix involves a greater storage size it is computationally convenient as the shape of the matrix its equal to that of the stiffness matrix. Consistent mass matrix has been used in this work to account for the mass of the structure.

### Hydrodynamic added mass

A submerged body in motion has to move the fluid around it thus, more force is required to accelerate the body inside a fluid than in vacuum. Using Newton's Second Law we can assimilate that additional force as an imaginary additional or added mass. According to [El-Reedy, 2015] and also [ISO19902:2007, 2013] the added mass may be estimated as the mass of the displaced water for transverse motions, and neglected for longitudinal motions. Thus, the term added to the translation degrees of freedom of (2.24) or (2.25) for submerged cylinders is:

$$m_a = \rho \frac{\pi}{4} D^2 \, L \tag{2.26}$$

being $D$ the diameter of the cylindrical submerged element, $L$ its length and $\rho$ water's density.

### 2.3.4. Damping matrix

The term damping in structural dynamics refers to the mechanisms whereby the structural system dissipates its vibrating energy. The characterization of damping in dynamically excited systems is still an open research area since neither the actual physical mechanisms involved in damping or the best approach to model them have been found yet [Adhikari, 2000]. Sources of damping are multiple: friction between elements, fluid resistance, structural joints, material damping...

Modal analysis is a common practice in the dynamic analysis of structures. In order to apply modal analysis of undamped systems to damped systems it is common to assume proportional damping so the modes of vibration of the damped system preserves the simplicity of the normal modes of the undamped case [Caughey & O'Kelly, 1965]. Thus, the classical damping or Rayleigh damping [Rayleigh, 1877] that expresses the damping matrix as a linear combination of the mass and stiffness matrices has been extensively used not only in modal analysis but in time history integration methods.

$$\boldsymbol{C} = \alpha_1 \boldsymbol{M} + \alpha_2 \boldsymbol{K} \tag{2.27}$$

where the coefficients $\alpha_1$ and $\alpha_2$ are obtained selecting two modes of vibration $\omega_1$ and $\omega_2$ and assigning damping ratios for each mode $\xi_1$ and $\xi_2$ [Chopra, 1995]:

$$\alpha_1 = 2\xi_1 \frac{\omega_1 \omega_2}{\omega_1 + \omega_2} \quad ; \quad \alpha_2 = \frac{2\xi}{\omega_1 + \omega_2} \tag{2.28}$$

The damping ratios are usually given in standards for steel structures according to experimental data [Elshafey et al., 2009]. In this work, the classical damping approach is used selecting damping ratios according to the standards or modelization recommendations for each particular case. For example, [DNV-OS-C101, 2014] recommends a 1% damping ratio for the jacket support for all vibration modes, while [ISO19902:2007, 2013] establishes an upper limit of 5% damping ratio but recommends values of 1% or 2%. [Lindenburg, 2002] shows values for the aerodynamic damping of the blades for different wind speeds. Normally, a 10% damping ratio is used for the blades to account for the aerodynamic effects.

## 2.4. Loading conditions and loads modelization

Offshore structures are subjected to a wide range of different nature, sources and types of loads. It is also important to describe the loads acting at different stages of the process of mounting an offshore structure. For example, jackets are always assembled at workshops and then shipped to the offshore situation to be then "launched" as figure 2.7 draws. Motions in transport, lifting, launching and other operations generate loads that differ so much than those of an in-place situation [ISO19902:2007, 2013]. There are as well accidental loads as collision from vessels, fire, explosions or impacts from objects.

Nevertheless, in the scope of this work, the loads applied are restricted to in-place and service situations such as gravity, buoyancy, wind and waves. Also, in this section only how the loads are modeled and considered is explained, not referring to the particular load cases that can be applied to a certain model.

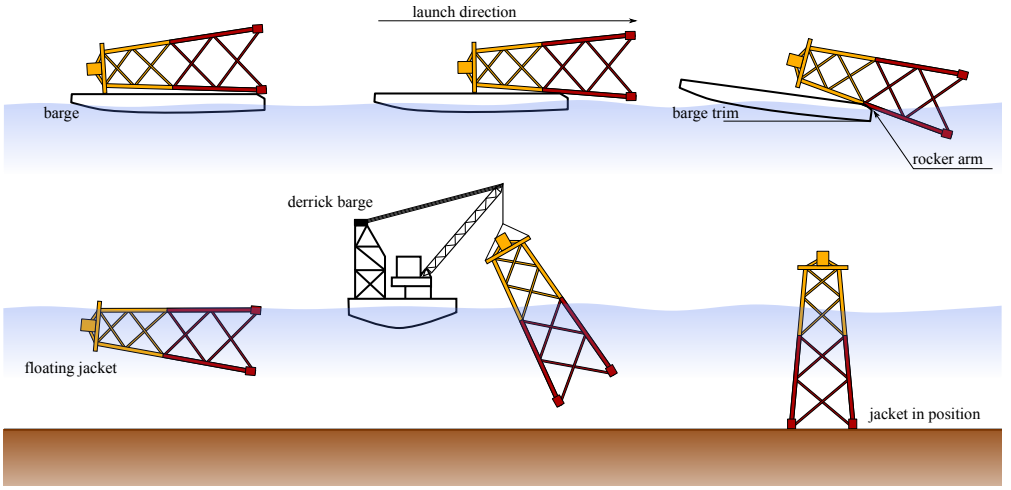


**Figure 2.7. Jacket launching operation.(Adapted from ESDEP)**

### 2.4.1. Gravity

Gravity loads considered in this work are referred mainly to self weight of all the elements of the structure, jacket, transition piece, tower, rotor-nacelle assembly and blades. Most of the elements are discretized as beam elements so their self weight is calculated with their cross-sectional area and the density of the material they are made of. In some cases, as the rotor-nacelle assembly or the transition piece, since they are not actual beams, the density introduced is an equivalent density to achieve the desired mass and weight in the structure with the modeled beams.

The model has also been developed taking into account the possibility of point masses at certain nodes of the structure. This is of use at the stiffeners of the tower and to model the mass of the hub. Point masses are also considered in the structural mass matrix as lumped masses at the nodal points having influence only over the translation degrees of freedom.

Regarding the jacket structure, the weight of each member is computed considering the weight of the steel tubular section, the weight added by marine growth when necessary and the weight of the entrapped water for flooded members. Thus, the weight for each jacket element is taken as:

$$W_e = g\, L\, (\rho_s\, A_s + \rho_{mg}\, A_{mg} + \rho_w\, A_w) \tag{2.29}$$

where $W_e$ is the total weight of the element, $g$ is the acceleration of gravity and $\rho_s$, $\rho_{mg}$, $\rho_w$, $A_s$, $A_{mg}$ and $A_w$, are the density and area of the steel section, marine growth around the element and entrapped water respectively.

**Figure 2.8. Marine growth over tubular elements.(Source: Offshore energy today)**

### 2.4.2. Buoyancy

Submerged elements experience an upward force equal to the weight of the displaced volume of water. This load is called buoyancy. Typically, for offshore structures there are two approaches to calculate the buoyancy of the members:

- Rational method: buoyancy is the resultant of fluid pressure acting on the surface of the submerged body. The rational method takes this pressure distribution along the members perpendicular to their axis.
- Marine method: it assumes that the element will have a rigid body motion so the weight of the member is calculated considering its submerged position. In other words the weight of the member is calculated with its submerged density. Thus, buoyancy somehow lightens the total weight of the element.

In this work the marine method has been used as more convenient. Thus, the weight load described in (2.29) is modified as:

$$W_e = g\, L\, (\rho_s\, A_s + \rho_{mg}\, A_{mg} + \rho_w\, A_w - \rho_w\, A_t) \tag{2.30}$$

where $A_t$ refers to the total area of the element. Note that, terms in (2.30) are included when needed for each case.

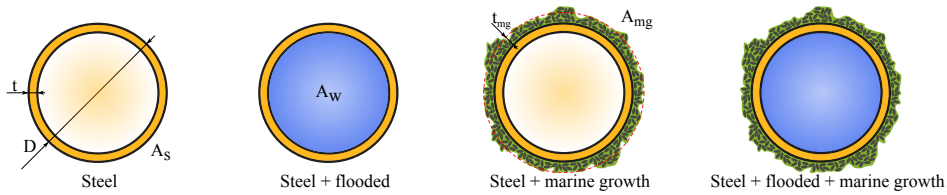


**Figure 2.9. Conditions for the cross sections of the jacket.**

The buoyancy load is only considered in non flooded elements of the jacket. Buoyancy may seem negligible but structural tubular members of offshore structures are often carefully selected such that their buoyancy/weight ratio is greater than 1.0. This means that the member will float in water. Thus the total buoyancy load acting on the structure has the order of magnitude of the total weight of the jacket steel components and can not be neglected.

### 2.4.3. Wind

Wind is the main load acting on the non-submerged part of the structure: the wind turbine tower and the blades. In the scope of this work, wind acting on the non-submerged elements of the jacket structure is neglected. This section explains how the wind forces are extracted and applied to the model, this section will not deal with how the wind itself is modeled. The main objective of this section is to provide a method to extract the wind loads acting on the blades and tower which will be finally supported by the jacket structure.

To study the aerodynamics of wind turbines some if not heavy knowledge on fluid dynamics is imperative. Any possible simplified description made in this thesis about Computational Fluid Dynamics will not have done justice to an extensive scientific research field such as CFD.

#### Wind forces on the blades

In order to extract the aerodynamic forces acting on the blades the Blade Element Momentum (BEM) theory is used (not to be mistaken with Boundary Element Method [Brebbia & Domínguez, 1992; Aliabadi, 2002; Guizán, 2018]). The basics of BEM method for horizontal axis wind turbines can be consulted in [Burton et al., 2001], [Hansen, 2015] and [Hau, 2006].

Wind turbines extract kinetic energy from the wind, thus, the mass of air which passes through the rotor disc must reduce its speed and the affected air mass must expand its area downstream forming what is called stream-tube as represented in figure 2.10. Assuming the hypothesis that there is no air flowing in and out of the stream-tube, the mass flow rate of air along the steam-tube must remain constant. Right before the actuator disc, the loss in kinetic energy is absorbed by an increment in the pressure and as the air passes through the rotor disc, the pressure drops below the

atmospheric level. This region is called the wake. This principle is known as the Betz's Momentum Theory [Betz, 1919].

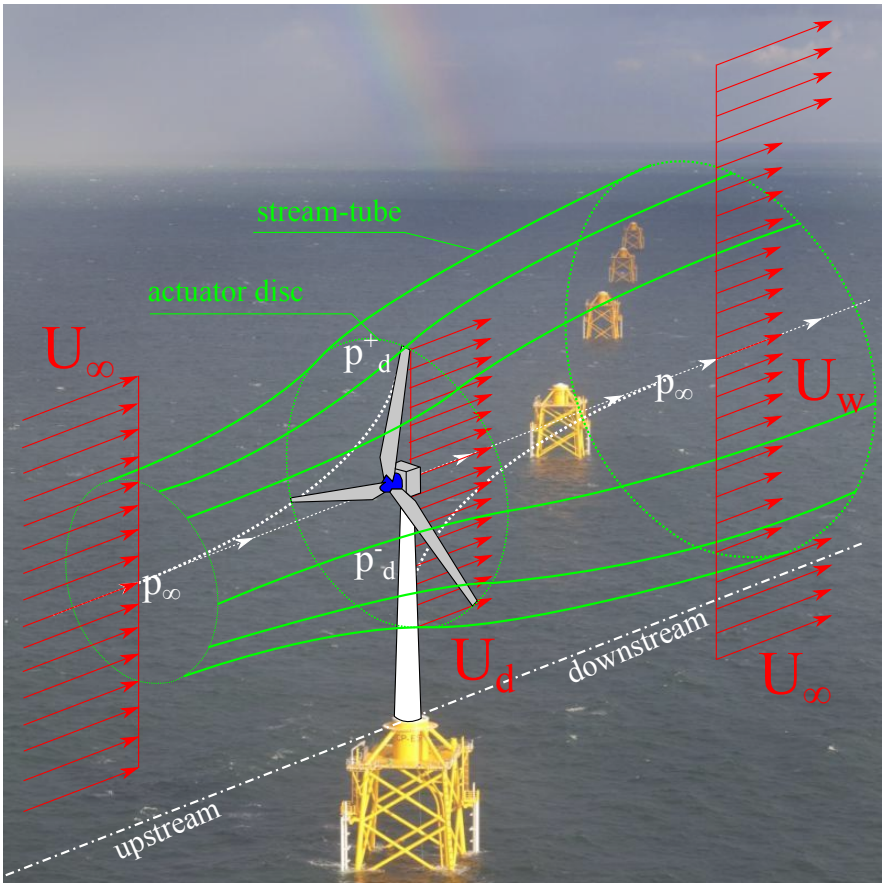


**Figure 2.10. Stream-tube and wind velocity profiles across the actuator disc.**

In figure 2.10, $U_\infty$, $U_d$ and $U_w$ are the air velocities far upstream, at the disc and in the far wake. $p_d^+$ and $p_d^-$ represent the increased and decreased pressure before and after the rotor disc.

Thereafter, the air undergoes a change in velocity and a rate change of momentum caused only by the pressure difference:

$$\left(p_d^+ - p_d^-\right)\, A_d = (U_\infty - U_w)\, \rho\, A_d\, U_d \tag{2.31}$$

Applying Bernoulli's principle upstream and downstream separately, the pressure difference can be obtained since the total energy upstream and downstream must remain constant separately. Note that the flow is considered incompressible and horizontal.

$$\left.\begin{array}{lll} \text{downstream} & \Longrightarrow & \frac{1}{2}\rho\, U_\infty^2 + p_\infty = \frac{1}{2}\rho\, U_d^2 + p_d^+ \\ \text{upstream} & \Longrightarrow & \frac{1}{2}\rho\, U_w^2 + p_\infty = \frac{1}{2}\rho\, U_d^2 + p_d^- \end{array}\right\} \Rightarrow \left(p_d^+ - p_d^-\right) = \frac{1}{2}\rho\left(U_\infty^2 - U_w^2\right) \tag{2.32}$$

Introducing also the axial induction factor $a$ that represents the velocity variation as $U_d = U_\infty(1-a)$ and using (2.31) and (2.32) gives:

$$U_w = (1-2a)U_\infty \tag{2.33}$$

Thus, half of the speed loss occurs upstream and half downstream.

We have not described yet how can all this be applied to extract the actual forces acting on the blades of the turbine, which is done by means of the BEM method [Glauert, 1935]. The pressure on the blades makes them rotate by virtue of their aerodynamic design translating the loss of axial momentum in a torque exerted on the rotor disc. Thus, there is also an equal and opposite torque imposed upon the air generating a rotating motion opposite to that of the blades downstream. This change in tangential velocity of the air can be expressed by terms of a tangential induction factor $a'$. Immediately downstream, the tangential velocity is $2(\Omega r a')$ [Burton et al., 2001] where $r$ is the radial distance and $\Omega$ the angular velocity of the rotor.

The change of axial and angular momentum of the air are the lift and drag forces on the span-wise elements of the blades. It is assumed that the lift and drag can be obtained with the aerodynamic characteristics of the cross-section of the blade, the velocity components and the flow induction factors. Given the tangential velocity of a blade element $\Omega r$ and the tangential velocity of the air at the wake $\Omega r a'$, the total tangential speed experienced by the blade element would be $\Omega' = \Omega r(1+a')$.

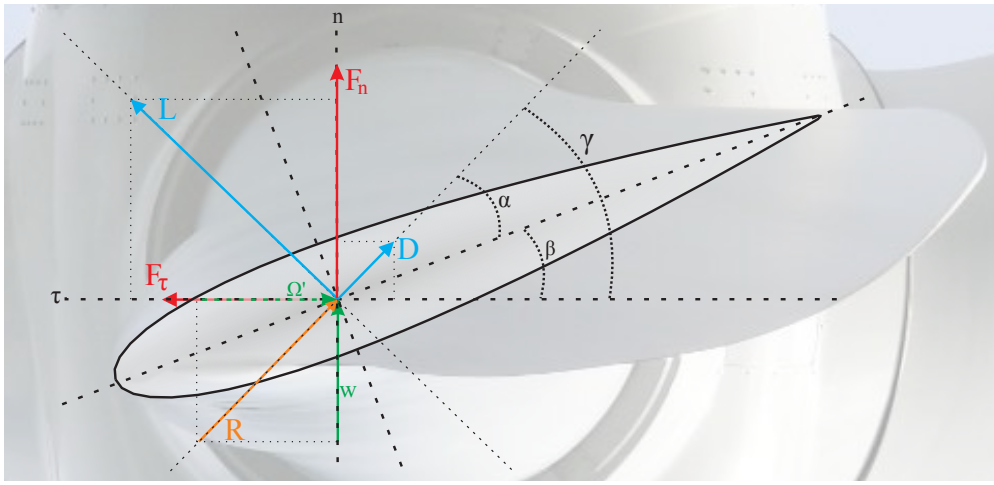


**Figure 2.11. Velocities and forces on the blade element.**

The aerodynamics of the blade element are depicted in figure 2.11 where $w$ denotes the velocity of the wind at the airfoil ($w = U_d$), $R$ is the resultant of the flow direction on the airfoil. $D$ and $L$ are the drag and lift forces respectively and $F_\tau$ and $F_n$ are the projected forces on the normal an tangential axis considering the axis of the turbine. The parameter $\alpha$ is the angle of attack of the inflow direction with respect to the chordwise axis and $\beta$ is called the pitch angle.

The angle of attack is obtained as:

$$\left.\begin{array}{l} w = U_\infty(1-a) \\ \Omega' = \Omega r(1+a') \end{array}\right\} \rightarrow R = \sqrt{w^2 + \Omega'^2} \longrightarrow \sin(\gamma) = \frac{U_\infty(1-a)}{R} \longrightarrow \alpha = \gamma - \beta \tag{2.34}$$

For a given airfoil shape, drag and lift coefficients are described for a range of angles of attack [Spera, 2008; Ramírez, 2015], thus the drag and lift forces, and thereby the normal and tangential forces acting on a blade element of length $\delta r$, can be calculated as:

$$\left.\begin{array}{l} D = \frac{1}{2}\,\rho\, R^2\, C_d\, c\, \delta r \\ L = \frac{1}{2}\,\rho\, R^2\, C_l\, c\, \delta r \end{array}\right\} \Rightarrow \left\{\begin{array}{l} F_n = D\sin(\gamma) + L\cos(\gamma) \\ F_\tau = -D\cos(\gamma) + L\sin(\gamma) \end{array}\right. \tag{2.35}$$

Actually, the induction factors, axial and tangential, are not known so equations (2.34) and (2.35) can not be directly applied. Hence they require the following iterative process:

1. Initialize $a = 0$ and $a'$=0.
2. Calculate the inflow angle $\gamma$ and the angle of attack as $\alpha = \gamma - \beta$
3. Obtain the drag and lift coefficients $C_d$ and $C_l$ given the angle of attack and the selected airfoil section.
4. Project the coefficients in normal and tangential direction as:

$$\begin{array}{l} C_n = C_d\sin(\gamma) + C_l\cos(\gamma) \\ C_\tau = -C_d\cos(\gamma) + C_l\sin(\gamma) \end{array} \tag{2.36}$$

5. Update induction factors [Hansen, 2015]:

$$a = \frac{1}{\dfrac{4\sin^2(\gamma)\,F}{\sigma\, C_n} + 1} \quad ; \quad a' = \frac{1}{\dfrac{4\sin(\gamma)\,\cos(\gamma)\,F}{\sigma\, C_\tau} - 1} \tag{2.37}$$

6. Return to 2 and repeat until convergence.

Expressions written in (2.37) account for effects like the Prandtl's blade tip loss and a discrete number of blades through the parameters $F$ (tip loss factor) and $\sigma$ (chord solidity) respectively [Burton et al., 2001], which are obtained as:

$$F = \frac{2}{\pi} \arccos\left( e^{-\frac{B(R-r)}{2\,r\,\sin(\gamma)}} \right) \tag{2.38}$$

$$\sigma = \frac{B\,c}{2\,\pi\,r} \tag{2.39}$$

where $B$ is the number of blades, $r$ is the radial position of the blade element in consideration and $c$ the chord length of the airfoil.

Methodology described in (2.36) through (2.39) is valid for values of the axial induction factor under the critical axial induction factor $a_c = 0.2$. For greater values the momentum theory breaks down and the coefficients need to be corrected accordingly [Spera, 1994]:

$$a = \frac{1}{2}\left[2 + K(1-2a_c) - \sqrt{(K(1-2a_c)+2)^2 + 4(Ka_c^2 - 1)}\right] \tag{2.40}$$

$$K = \frac{4\,F\,\sin^2(\gamma)}{\sigma\,C_n} \tag{2.41}$$

Figure 2.12 shows the comparison between the resultant torque and thrust on the rotor using the above described method to calculate the forces for different wind speeds at the hub with those of the reference work [Jonkman et al., 2009]. It can be seen that whereas the tangential force, resulting in global torque is quite well obtained, the normal forces are a 5% underestimated.

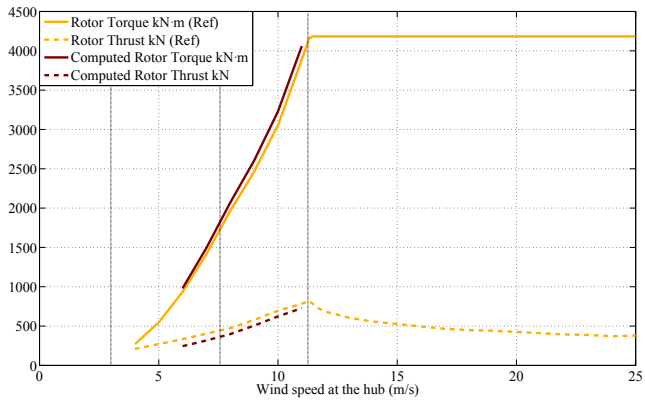


**Figure 2.12. Torque and thrust comparison with the reference model [Jonkman et al., 2009].**

### Wind forces on the tower

The forces on the tower are computed just as a drag force acting on the tubular section as:

$$F = \frac{1}{2}\,\rho\,U_h^2\,C_d\,D\,\delta l \tag{2.42}$$

where $U_h$ is the wind speed at elevation $h$, $D$ is the diameter of the tubular section, $\delta l$ is the length of the considered element and $C_d$ is the drag factor of the cylindrical section (typically 0.6-0.7).

So far so simple. However, under normal operating conditions the rotating blades move in close proximity to the tower, leaving a relatively small clearance between the two elements. The flow around the tower influences the wind speed at the blades and two effects are perceptible:

- Tower dam: When the rotor is mounted up-wind, wind encounters the blade before the tower. The effect is merely a delay of the flow and a decrease on the wind speed (figure 2.13a).
- Tower shadow: In down-wind rotors the torque pulsations are more significant as wind is directly blocked by the tower.

This work considers only the tower dam effect for up-wind mounted turbines. The effect is thoroughly studied in [Dolan & Lehn, 2006] and included in this work by means of a modified wind speed for the blade passing in front of the tower.

$$U_h^* = U_h + W_{dam} \qquad \text{with} \quad W_{dam} = -U_h\,\frac{D^t}{2\pi}\,\frac{d_x}{d_x^2 + d_y^2} \tag{2.43}$$

where $d_x$ and $d_y$ are the distances in global $x$ and $y$ axis between the passing blade and the tower.

The effect on the exerted torque is depicted in figure 2.13b. As stated in [Dolan & Lehn, 2006] torque is reduced to a minimum 94% when the blade is exactly in front of the tower.

## 2.4.4. Waves

Waves are the main load acting on the submerged part of the structure, in this case the jacket. Wave loading has an inherent dynamic nature. As opposed to wind, which is a dynamic load, but in some cases can be considered steady, waves must always be treated as dynamic forces. As for the wind in the previous section, the forward is intended to deal with how the loads from waves are computed and applied to the model, no reference is made about different load cases or combinations.

The first step is to define how the waves themselves are modeled and then how the forces on the submerged elements are extracted.

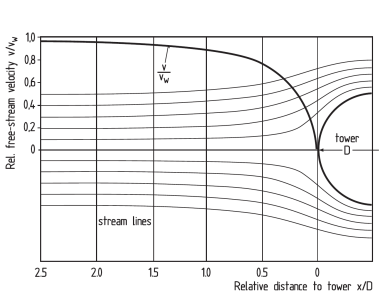


**(a) Flow in an up-wind turbine from [Hau, 2006].**

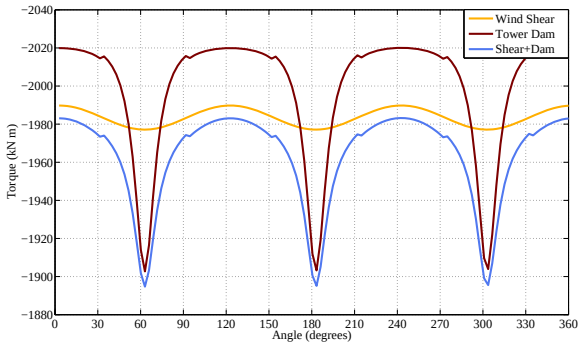


**(b) Torque comparison.**

**Figure 2.13. Tower dam effect.**

### Wave theory

The wave theory comprises the equations that represent the movement and characteristics of the waves. The full analysis of the effects of real waves slamming into structures is again a competence of CFD researchers. Waves have a nonlinear, irregular and often apparently random nature. However, wave description may be given in a regular wave form and described by a deterministic theory [Chakrabarti, 2005]. In regular waves the properties of the wave are invariant from cycle to cycle. Those characteristics are dominated by three parameters: Period ($T$), height ($H$) and water depth ($d$). A number of regular wave theories have been developed but two classical theories, the linear Airy wave theory and the second order Stokes wave theory, are usually applied and show good predictions in practice.

The linear Airy theory is the simplest theory. Waves take the form of a sine (cosine) curve and thus the equation that describes the motion of the free surface can be written as:

$$\eta(x,t) = \frac{H}{2}\,\cos\left(k\,x - \omega\,t\right) \tag{2.44}$$

where $k$ is called the wave number, $x$ is the coordinate in direction of wave's propagation, $\omega$ is the frequency of the wave and $t$, time.

We can also consider the relations:

$$\omega = \frac{2\pi}{T} \qquad k = \frac{2\pi}{L} \qquad c = \frac{\omega}{k} \tag{2.45}$$

with $L$ the length of the wave and $c$ the celerity or speed of propagation of the wave.

The water particles velocities and accelerations may then be given by:

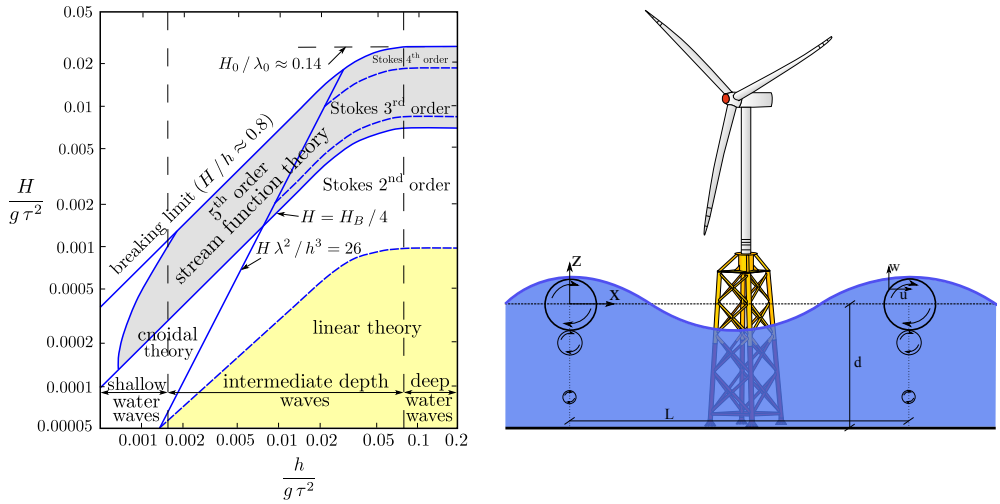


**Figure 2.14. Wave theories applicability from [Méhauté, 1976] and wave kinematics.**

$$u(x,z,t) = \frac{\alpha}{\omega}\frac{\cosh(k(z+d))}{\cosh(kd)}\cos(kx-\omega t) \qquad \dot{u}(x,z,t) = \alpha\frac{\cosh(k(z+d))}{\cosh(kd)}\sin(kx-\omega t)$$

$$w(x,z,t) = \frac{\alpha}{\omega}\frac{\sinh(k(z+d))}{\cosh(kd)}\sin(kx-\omega t) \qquad \dot{w}(x,z,t) = -\alpha\frac{\sinh(k(z+d))}{\cosh(kd)}\cos(kx-\omega t) \tag{2.46}$$

being $\alpha = gkH/2$ and $u$ and $w$ the particles velocities in $x$ and $z$ axes respectively and $\dot{u}$ and $\dot{w}$ the particles acceleration

However, the linear theory does not account for the water level at the free surface. In order to account for this effect, stretching formulas have to be used to modify the above equations. In this work, the stretching formulas used are found in [Chakrabarti, 2005]. Thus, equation (2.46) can be rewritten as:

$$u(x,z,t) = \frac{\alpha}{\omega}\frac{\cosh(kz)}{\cosh(k(d+\eta))}\cos(kx-\omega t) \qquad \dot{u}(x,z,t) = \alpha\frac{\cosh(kz)}{\cosh(k(d+\eta))}\sin(kx-\omega t)$$

$$w(x,z,t) = \frac{\alpha}{\omega}\frac{\sinh kz}{\cosh(k(d+\eta))}\sin(kx-\omega t) \qquad \dot{w}(x,z,t) = -\alpha\frac{\sinh(kz)}{\cosh(k(d+\eta))}\cos(kx-\omega t) \tag{2.47}$$

The linear Airy wave is considered useful in intermediate to deep depths and for low wave heights. Thereby it is considered the adequate theory for computing fatigue life design calculations under average situations but not for ultimate limit stress under extreme conditions [ISO19902:2007, 2013; DNV-OS-C101, 2014].

When increasing the height of the waves, the linear theory begins to fall and non-linear theories are more suitable. There is a wide range of nonlinear theories developed but the most commonly used is the second order Stokes' theory.

The second order Stokes wave has two frequency components for the wave kinematics. The first frequency is equal to that of the Airy wave and the second is at twice the wave frequency. Expressions for the surface elevation and wave kinematics can be then written as sum of a linear component (Airy expressions) and a second order term:

$$\begin{aligned}
\eta(x,t) &= \eta_{Airy}(x,t) + \frac{\pi H^2}{8L}\frac{\cosh(kd)}{\sinh^3(kd)}\left(2+\cosh(2kd)\right)\cos\left(2(kx-\omega t)\right) \\
u(x,z,t) &= u_{Airy}(x,z,t) + \frac{3}{4c}\left(\frac{\pi H}{T}\right)\frac{\cosh\left(2k(z+d)\right)}{\sinh^4(kd)}\cos\left(2(kx-\omega t)\right) \\
\dot{u}(x,z,t) &= \dot{u}_{Airy}(x,z,t) + \frac{3\pi}{2L}\left(\frac{\pi H}{T}\right)\frac{\cosh\left(2k(z+d)\right)}{\sinh^4(kd)}\sin\left(2(kx-\omega t)\right) \\
w(x,z,t) &= w_{Airy}(x,z,t) + \frac{3}{4c}\left(\frac{\pi H}{T}\right)\frac{\sinh\left(2k(z+d)\right)}{\sinh^4(kd)}\sin\left(2(kx-\omega t)\right) \\
\dot{w}(x,z,t) &= \dot{w}_{Airy}(x,z,t) - \frac{3\pi}{4L}\left(\frac{\pi H}{T}\right)\frac{\sinh\left(2k(z+d)\right)}{\sinh^4(kd)}\cos\left(2(kx-\omega t)\right)
\end{aligned} \tag{2.48}$$

The second order component is smaller in magnitude than the first order one and when it is added, the profile of the wave becomes peaked at the crest yielding a shallower trough. This form is quite prevalent in the ocean where the height of the waves is finitely large.

In this work, linear Airy waves are used in terms of modeling regular weather conditions for fatigue life design and second order Stokes waves are used for storm and extreme conditions for ultimate limit stress [DNV-OS-J101, 2010].

#### Forces due to waves

Forces arising from waves on submerged elements can be computed considering either that the structure is large or small with respect to the waves magnitude. For jacket structures, the force acting on the individual members forming the structures can be calculated considering the theory of wave induced loads on slender members.

In general the hydrodynamic force exerted on a submerged cylinder has three separated components: a normal force that is perpendicular to the member's axis, a tangential force that is parallel to the member's axis and a lift force that is normal to the direction of the fluid flow. In this work, tangential forces and lift forces that are due to friction, wake effects, vortex shedding and other phenomena are disregarded before the normal force.

For slender members it is accepted that wave loads may be assessed by Morison's formula [Morison et al., 1950]. The normal force per unit of length exerted by fluid

flow in a given direction perpendicular to a slender cylinder can be decomposed into two sources: an inertial force $f_I$ and a drag force $f_D$. Then,

$$f_N(x,z,t) = \underbrace{\frac{\pi}{4}\,\rho\,C_M\,D^2\,\dot{s}(x,z,t)}_{f_I} + \underbrace{\frac{1}{2}\,\rho\,C_D\,D\,s(x,z,t)\,|s(x,z,t)|}_{f_D} \tag{2.49}$$

being $C_M$ and $C_D$ the inertia and drag coefficients respectively (that depend on the Reynolds and Keulegan-Carpenter numbers [Haritos, 2007]) and $s$ and $\dot{s}$, the particles velocities and acceleration in the direction of the fluid. When dealing with compliant structures the effect of the movements in the structure can be accounted for in (2.49) in terms of relative velocities and accelerations.

Although, equation (2.49) is prescribed to cylinders perpendicular to the flow direction or in other words vertical submerged pipes. Consequently, to compute the forces on inclined submerged members the procedure would be:

1. Discretize the element in $n$ parts to compute the force at the $n+1$ points with global and local coordinates $(X,Y,Z)$ and $(x,y,z)$.
2. Compute the velocity and acceleration of the particles in wave's direction at the discretized points $s(X,Y,Z,t)$ and $\dot{s}(X,Y,Z,t)$.
3. Project velocity and acceleration to the local axes of the element to obtain the velocities and accelerations $u'(x,t)$, $\dot{u'}(x,t)$, $v'(x,t)$, $\dot{v'}(x,t)$, $w'(x,t)$ and $\dot{w'}(x,t)$ of the fluid in the local axes of the element.
4. Use Morison's formula to compute the normal force on the element in the local $y$ and $z$ axes $\rightarrow f'_y(x,t)$ and $f'_z(x,t)$.
5. Integrate the forces along the length of the element to obtain the resultant forces on the element[1]:

$$F'_y = \int_{x_1}^{x_{n+1}} f'_y(x,t)dx \approx \sum_{i=1}^{n+1} f'_y(x_i,t)\delta l_i \tag{2.50}$$

$$F'_z = \int_{x_1}^{x_{n+1}} f'_z(x,t)dx \approx \sum_{i=1}^{n+1} f'_z(x_i,t)\delta l_i \tag{2.51}$$

6. Calculate the point of application of the resultant force that will be later needed to compute the equivalent forces and moments concentrated at the nodes of the element.

$$x_{F'_y} = \frac{\displaystyle\int_{x_1}^{x_{n+1}} x f'_y(x,t)dx}{\displaystyle\int_{x_1}^{x_{n+1}} f'_y(x,t)dx} \approx \frac{\displaystyle\sum_{i=1}^{n+1} x_i f'_y(x_i,t)\delta l_i}{\displaystyle\sum_{i=1}^{n+1} f'_y(x_i,t)\delta l_i} \tag{2.52}$$

[1] Actually, the force on the first and last discretized point is considered only acting on $\delta l_i/2$.

$$x_{F'_z} = \frac{\int_{x_1}^{x_{n+1}} x f'_z(x,t)dx}{\int_{x_1}^{x_{n+1}} f'_z(x,t)dx} \approx \frac{\sum_{i=1}^{n+1} x_i f'_z(x_i,t)\delta l_i}{\sum_{i=1}^{n+1} f'_z(x_i,t)\delta l_i} \tag{2.53}$$

7. Project the resultant local forces to the global axes to obtain the global forces due to waves acting on the element: $F_X(X,Y,Z,t)$, $F_Y(X,Y,Z,t)$ and $F_Z(X,Y,Z,t)$.

It is worth saying that the upper limit for the integrals of the forces and their numerical approximation is either the end of the element or the free surface of the water (2.44) if the element is partially submerged.

The force due to current (which is depth dependent) can be accounted for by vectorially combining the wave kinematics with the current velocities [ISO19901-1, 2005]. There are combined models with wave kinematics and current profile that gave the best estimate of the hydrodynamic actions over a framed structure [Dalrymple & Heideman, 1989].

With the exception of more complex models merging CFD with structural analysis or Fluid Structure Interaction (FSI), the above described procedure is the most suitable and adequate approach to extract the wave forces upon the submerged elements of the structure.

### 2.4.5. Distributed loads treatment

It is already known that beams and thus, framed structures modeled by beams, are designed to naturally deal with loads concentrated on the structural joints or nodes. However, every load described so far is actually a distributed load acting along the length of each element (self weight, buoyancy, wind, waves, current). Almost every natural source of load will exert a distributed load between the nodes of the bars.

Luckily there is a way to overcome this issue. Applying linear superposition the analysis of a given element subject to distributed loads along its length can be decomposed in sum of two states. State I having equivalent loads acting on the nodes of the structures. And State II subjected to the distributed load and the member's fixed-end forces produced by the load ($\boldsymbol{f'_{eq}}$). This is well known in structural engineering but is briefly described here as it would be needed later. By superposition, the movements of the structure would be the sum of movements of the two states but, movements of state II are zero and thereby the movements of the structure can be computed using only state I. However, final element end forces, and consequently stresses are due to the two states, since both produce stresses on the structure. Thus, to obtain the stresses of the structure the contributions from both states have to be added [Weaver & Gere, 1990].

As a result, when computing the member end forces of a given element $\boldsymbol{f'}$, the typical matrix formulation states that:

$$\boldsymbol{\sigma} = \boldsymbol{S}\,\boldsymbol{u} \Rightarrow \boldsymbol{f'} = \boldsymbol{E}^t\,\boldsymbol{\sigma} \tag{2.54}$$

where the matrices $\boldsymbol{S}_e$ and $\boldsymbol{E}_e$ were derived in previous sections and movements $\boldsymbol{u}_e$ are those obtained as a result of state I.

The total member end forces (State I + State II) are:

$$\boldsymbol{f'} = \boldsymbol{E}^t\,\boldsymbol{\sigma} + \boldsymbol{f'_{eq}} \tag{2.55}$$

## 2.5. Dynamic analysis

Up to this point, the basic structural and numerical model as well as the type of loading and the modelization of those loads have been depicted. The following sections illustrate the procedure applied for the dynamic analysis of the structure.

### 2.5.1. Natural frequencies and modes of vibration

The natural frequencies of any structure are the frequencies at which the structure vibrates freely without any exerted force. The natural modes are the shapes of those vibrations. Although structures do have an infinite number of natural modes it is impossible to capture them all. Structural models possess a number of natural frequencies equal to the number of degrees of freedom. In practice, it is not necessary to achieve all the natural modes reachable as the high frequencies will also be associated with small amplitudes so, just a few of the first natural vibration modes of the structure need to be obtained.

Natural frequencies are of great importance since any time dependent force acting on the structure with the same frequency would produce resonance. Offshore wind turbines are indeed subject to dynamic forces but there is another major issue: wind turbines are designed to move (or rotate more precisely). Thus, the natural frequencies of the structure must not coincide with the frequencies of the rotation movement. The main excitation frequencies produced by the rotation are called 1P and 3P. 1P corresponds to the frequency of the constant rotational speed while 3P is called the blade-passing frequency [van der Tempel & Molenaar, 2002]. The frequencies are also needed for the definition of the damping matrix (2.27), (2.28).

Natural frequencies can be obtained as the generalized eigenvalue problem:

$$(\boldsymbol{K} - \lambda_i\,\boldsymbol{M})\,\boldsymbol{\phi}_i = 0 \tag{2.56}$$

where $\boldsymbol{K}$ and $\boldsymbol{M}$ are the global stiffness an mass matrices and $\lambda_i$ and $\boldsymbol{\phi}_i$ are the $i$-th eigenvalue and eigenvector. The natural frequency is calculated as $\omega_i^2 = \lambda_i$.

The problem can be transformed to a standard eigenvalue problem and then solved by means of the Power Method [von Mises & Pollaczek-Geiringer, 1929]. However, the power method gives the highest vibration frequency or the largest eigenvalue. As mentioned, the interest is focused on the first modes of vibration which have the lowest

vibration frequency. Thus, in order to obtain first the lower modes, problem (2.56) has to be approached as the inverse problem:

$$\left(\boldsymbol{M} - \frac{1}{\lambda_i}\,\boldsymbol{K}\right)\boldsymbol{\phi}_i = 0 \tag{2.57}$$

The above generalized problem can be transformed to the standard eigenvalue problem, given the decomposition of $\boldsymbol{K}$ as:

$$\boldsymbol{K} = \boldsymbol{L}\,\boldsymbol{D}\,\boldsymbol{L}^T = \boldsymbol{L}\,\boldsymbol{D}^{1/2}\,\boldsymbol{D}^{1/2}\,\boldsymbol{L}^T \tag{2.58}$$

Hence, if we denote $\rho_i = \frac{1}{\lambda_i}$, the generalized inverse eigenvalue problem:

$$\begin{aligned}
\boldsymbol{M}\,\boldsymbol{\phi}_i = \rho_i\,\boldsymbol{K}\,\boldsymbol{\phi}_i \quad &\Leftrightarrow \quad \boldsymbol{M}\,\boldsymbol{\phi}_i = \rho_i\,\boldsymbol{L}\,\boldsymbol{D}^{1/2}\,\boldsymbol{D}^{1/2}\,\boldsymbol{L}^T\,\boldsymbol{\phi}_i \\
&\Leftrightarrow \quad \boldsymbol{L}^{-1}\boldsymbol{M}\,\boldsymbol{\phi}_i = \rho_i\,\boldsymbol{D}^{1/2}\,\boldsymbol{D}^{1/2}\,\boldsymbol{L}^T\,\boldsymbol{\phi}_i \\
&\Leftrightarrow \quad \boldsymbol{D}^{-1/2}\,\boldsymbol{L}^{-1}\boldsymbol{M}\,\boldsymbol{\phi}_i = \rho_i \underbrace{\boldsymbol{D}^{1/2}\,\boldsymbol{L}^T\,\boldsymbol{\phi}}_{=\hat{\boldsymbol{\phi}}_i \Rightarrow \boldsymbol{\phi}_i = \boldsymbol{L}^{-T}\boldsymbol{D}^{-1/2}\,\hat{\boldsymbol{\phi}}_i} \\
&\Leftrightarrow \quad \underbrace{\boldsymbol{D}^{-1/2}\,\boldsymbol{L}^{-1}\boldsymbol{M}\,\boldsymbol{L}^{-T}\boldsymbol{D}^{-1/2}}_{\hat{\boldsymbol{M}}}\,\hat{\boldsymbol{\phi}}_i = \rho_i\,\hat{\boldsymbol{\phi}}_i \\
&\Leftrightarrow \quad \hat{\boldsymbol{M}}\,\hat{\boldsymbol{\phi}}_i = \rho_i\,\hat{\boldsymbol{\phi}}_i
\end{aligned} \tag{2.59}$$

The eigenvalues of the standard problem are computed with the power method [von Mises & Pollaczek-Geiringer, 1929] and the natural frequencies are obtained as $\omega_i = (1/2\pi)\sqrt{1/\rho_i}$

Additionally, we need more than the first natural frequency and mode. Therefore the deflation procedure is applied to achieve the subsequent frequencies. Given the eigenvalue $\rho_k$, the $k+1$ eigenvalue and eigenvector are computed shifting the value of $\rho_k$ to 0 without altering the rest. However, modifying problem (2.56) implies the recursive factorization of matrix $\boldsymbol{K}$ in order to transform the inverse generalized eigenvalue problem to the inverse standard problem. In order to bypass the recursive factorization the deflation approach is directly applied to the inverse problem in (2.59).

$$\begin{aligned}
\boldsymbol{M'}_{k+1} &= \boldsymbol{M} - \sum_{j=1}^{k} \rho_j \left[\left(\boldsymbol{K}\boldsymbol{\phi}_j\right)\left(\boldsymbol{K}\boldsymbol{\phi}_j\right)^t\right] \\
\boldsymbol{K'}_{k+1} &= \boldsymbol{K}
\end{aligned} \tag{2.60}$$

The Offshore Code Comparison jacket (OC4) natural frequencies and those obtained in this work are depicted in figure 2.15 as well as the eigenmodes or natural modes of vibration in figure 2.16. In figure 2.15 the black dashed line reflects the first five natural frequencies computed in this thesis. The first modes are in good agreement with the

rest of the existing codes except for the first torsional mode, where there is a 10% of deviation from the average frequency of the OC4 codes. The other modes, match perfectly both frequency and mode of vibration with the reference, pointing out that the mass and stiffness of the structure is indeed well modeled with the so far described methodology.

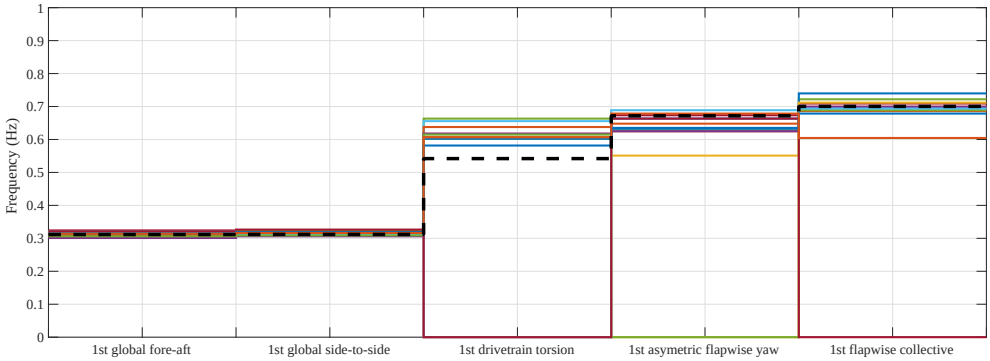


**Figure 2.15. Comparison of natural frequencies from existing codes [Popko et al., 2014] and this thesis.**

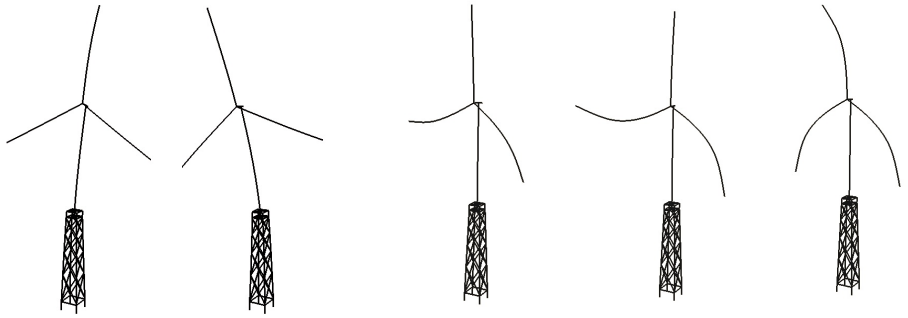

**(a) 0.31151 Hz** **(b) 0.31201 Hz** **(c) 0.54196 Hz** **(d) 0.67184 Hz** **(e) 0.70036 Hz**

**Figure 2.16. First natural frequencies and modes of the OC4 jacket computed in this thesis.**

### 2.5.2. Equation of motion and time integration

The well known discrete equation of motion for structures with multiple degrees of freedom is:

$$\boldsymbol{M}\,\ddot{\boldsymbol{u}} + \boldsymbol{C}\,\dot{\boldsymbol{u}} + \boldsymbol{K}\,\boldsymbol{u} = \boldsymbol{f} \tag{2.61}$$

which is an initial value problem where the matrices $\boldsymbol{M}$, $\boldsymbol{C}$ and $\boldsymbol{K}$ are the global mass, damping and stiffness matrices resulting from the elemental matrices assembly (2.23),(2.25),(2.27). Vectors $\boldsymbol{u}$, $\dot{\boldsymbol{u}}$ and $\ddot{\boldsymbol{u}}$ are the global displacements, velocities and accelerations of the degrees of freedom of the structural nodes.

The final purpose of this work is to optimize the design of the jacket structures. In order to do that we need to find the lightest structural design that still satisfies the required conditions or constraints, which often depend on the stresses of the structure. Those stresses are obtained from the structural displacements through the compatibility, constitutive and equilibrium equations as seen in (2.22), and displacements are reached solving the equations of motion (2.61).

It is mandatory to evaluate the dynamic response of the structure during a period of time sufficiently large, at least 10 min or 600 s [DNV-OS-J101, 2010] which is also the averaging time for short-term wind conditions [DNV-RP-C205, 2010].

Running such simulations call for a large enough time step in order to compute a reasonable number of integration steps while keeping the required accuracy. Furthermore, a great number of load cases has to be considered to catch a reliable representation of the environmental conditions affecting the structure. This also generates an enormous amount of outputs and data to be processed.

Consequently, the problem needs an extremely efficient and low resource-demanding numerical integration scheme. One of the most extended direct integration methods might be the Newmark family methods [Hughes, 1987].

The equations for the Newmark family read:

$$\begin{aligned} \boldsymbol{M}\,\ddot{\boldsymbol{u}}_{k+1} + \boldsymbol{C}\,\dot{\boldsymbol{u}}_{k+1} + \boldsymbol{K}\,\boldsymbol{u}_{k+1} &= \boldsymbol{f}_{k+1} \\ \boldsymbol{u}_{k+1} &= \boldsymbol{u}_k + \Delta t\,\dot{\boldsymbol{u}}_k + \tfrac{\Delta t^2}{2}\left[(1-2\,\beta)\,\ddot{\boldsymbol{u}}_k + 2\,\beta\,\ddot{\boldsymbol{u}}_{k+1}\right] \\ \dot{\boldsymbol{u}}_{k+1} &= \dot{\boldsymbol{u}}_k + \Delta t\left[(1-\gamma)\,\ddot{\boldsymbol{u}}_k + \gamma\,\ddot{\boldsymbol{u}}_{k+1}\right] \end{aligned} \tag{2.62}$$

where the formulas for $\boldsymbol{u}_{k+1}$ and $\dot{\boldsymbol{u}}_{k+1}$ arise from simple finite difference formulas [Newmark, 1959], and $\beta$ and $\gamma$ are two parameters that define the particular Newmark method and determine the stability and accuracy of the technique. For example, $\beta = 1/6$ and $\gamma = 1/2$ give the linear acceleration method where the acceleration of the degrees of freedom is considered to vary linearly between time steps. For $\beta = 1/4$ and $\gamma = 1/2$ we have the average acceleration method or commonly known as the trapezoidal rule, which is the method used in this thesis. There are a number of methods derived from the Newmark scheme: Wilson-$\theta$, Houbolt and others. The advantage of the trapezoidal rule is that it is unconditionally stable and yields accurate results. A long record of comparison between direct integration schemes can be further read in the works of Bathe [Bathe & Wilson, 1973; Bathe & Noh, 2012].

Using the mentioned trapezoidal rule with $\beta = 1/4$ and $\gamma = 1/2$, the procedure of solving the dynamic equation is:

1. Calculate the initial accelerations:

$$\boldsymbol{M}\ddot{\boldsymbol{u}}_0 = \boldsymbol{f}_0 - \boldsymbol{C}\,\dot{\boldsymbol{u}}_0 - \boldsymbol{K}\,\boldsymbol{u}_0 \tag{2.63}$$

2. Compute the predictors for the displacements and velocities:

$$\begin{aligned} \tilde{\boldsymbol{u}}_{k+1} &= \boldsymbol{u}_k + \Delta t\dot{\boldsymbol{u}}_k + \beta\Delta t^2(1-2\beta)\ddot{\boldsymbol{u}}_k \\ \tilde{\dot{\boldsymbol{u}}}_{k+1} &= \dot{\boldsymbol{u}}_k + (1-\gamma)\Delta t\ddot{\boldsymbol{u}}_k \end{aligned} \tag{2.64}$$

3. Solve for the accelerations at step $k+1$:

$$\left(\boldsymbol{M} + \gamma\Delta t\boldsymbol{C} + \beta\Delta t^2\boldsymbol{K}\right)\,\ddot{\boldsymbol{u}}_{k+1} = \boldsymbol{f}_{k+1} - \boldsymbol{C}\,\tilde{\dot{\boldsymbol{u}}}_{k+1} - \boldsymbol{K}\,\tilde{\boldsymbol{u}}_{k+1} \tag{2.65}$$

4. Update predictors with the computed acceleration:

$$\begin{aligned} \boldsymbol{u}_{k+1} &= \tilde{\boldsymbol{u}}_{k+1} + \beta\Delta t^2\,\ddot{\boldsymbol{u}}_{k+1} \\ \dot{\boldsymbol{u}}_{k+1} &= \tilde{\dot{\boldsymbol{u}}}_{k+1} + (1-\gamma)\Delta t\,\ddot{\boldsymbol{u}}_{k+1} \end{aligned} \tag{2.66}$$

The process above described can also be laid out in terms of solving displacements and using predictors for the velocities and accelerations. In step 1, the initial condition can be also obtained as the displacements of the static analysis.

The average acceleration method or trapezoidal rule is unconditionally stable for $\Delta t$ which allows to reduce the number of integration steps in benefit of computational cost.

Figure 2.17 shows results comparison for the shear reaction at the mudline considering a wave loading with $H = 6\,m$ and $T = 10\,s$ for the OC4 jacket.

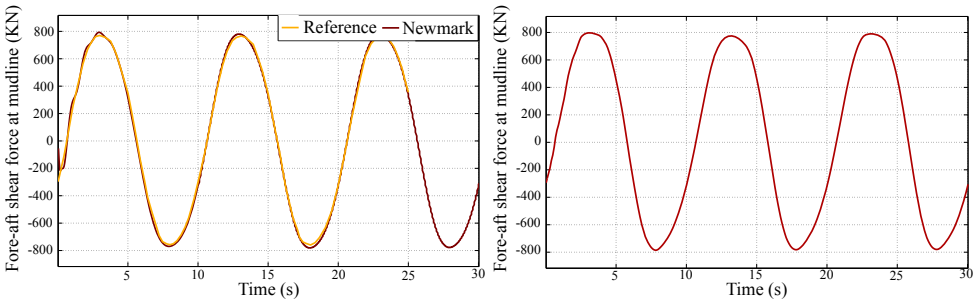


**(a) Fore-aft shear at mudline comparison with results of [Popko et al., 2014].** **(b) Fore-aft shear at mudline with initial condition.**

**Figure 2.17. Fore-aft shear at mudline.**

Introducing the initial condition obtained with the linear static analysis also eliminates the small perturbations at the beginning of the simulation.

### 2.5.3. Blades rotation and time integration with variable geometry

So far, we have depicted the coupled structural model for the wind turbine, tower and jacket substructure, the loading conditions and the solution of the equations of motion. However, wind turbines are designed to move (rotate more specifically), and this is something to account for.

The usual approach in offshore wind turbines is to build separate models for the aerodynamic part (rotor-nacelle and blades) and the structural part (tower and jacket) [Passon & Branner, 2014; Yeter et al., 2015]. It is usually decomposed again to analyze each structure separately. Most models use a multibody dynamics approach for the aerodynamic part to compute the loads which are later applied to the support structure as a time history loading record. Multibody dynamics comprise the mathematical and computational methodologies to deal with constrained deformable bodies subjected to large deformations and movements. The movements of the structure are restricted by what are called kinematic joints that restrict the relative motion between objects. A thoroughly review of typical multibody dynamics can be found at [Shabana, 1997].

However, the highly non-linear multibody dynamic equations have to be merged-in with the finite element method in order to be able to analyze the complete structural behavior of flexible bodies. While this approach can be used if the analysis is going to be carried out once and only to get the loading conditions, it is not desirable to repeat it again and again with every design modification, and even less to include it in a design sensitivity analysis loop in terms of efficiency [Zhu, 2014].

This work differs from those approaches. It is obvious that the loads of the wind acting on the blades are the ones responsible for their rotation. Nevertheless, in this work the rotation of the blades is an imposed movement between time steps with loads also calculated at each time step. Then the structure is subjected to large deformations but not in a typical sense, the large deformations are not a result of the loads. Therefore the model is not strictly a non-linear structural model but something we can call variable geometry. Even though it is not a regular non-linear problem, the properties of the structure do change between time steps due to the deformation, imposed or not, and therefore the mass, stiffness and damping properties change. Those changes in the mass, stiffness and damping matrices are something we can calculate with each change but the solution of the equations of motion has to be performed by means of a non-linear methodology. In this work, the non-linear Newmark integration method is employed. It adds Newton iterations to each time step of the Newmark algorithm described in (2.63) through (2.66).

Let us define the acceleration at step $k+1$ as:

$$\ddot{\boldsymbol{u}}_{k+1} = \ddot{\boldsymbol{u}}_k + \boldsymbol{\delta}\ddot{\boldsymbol{u}} \tag{2.67}$$

Then equation (2.62) leads to:

$$\left\{ \begin{array}{l} \boldsymbol{u}_{k+1} = \boldsymbol{u}_k + \Delta t\, \dot{\boldsymbol{u}}_k + \dfrac{\Delta t^2}{2} \ddot{\boldsymbol{u}}_k - \Delta t^2\, \beta\, \ddot{\boldsymbol{u}}_k + \Delta t^2\, \beta\, \ddot{\boldsymbol{u}}_k + \Delta t^2\, \beta\, \boldsymbol{\delta \ddot{u}} \\ \dot{\boldsymbol{u}}_{k+1} = \dot{\boldsymbol{u}}_k + \Delta t\, \ddot{\boldsymbol{u}}_k - \Delta t\, \gamma\, \ddot{\boldsymbol{u}}_n + \Delta t\, \gamma\, \ddot{\boldsymbol{u}}_n + \Delta t\, \gamma\, \boldsymbol{\delta \ddot{u}} \end{array} \right\} \Leftrightarrow \tag{2.68}$$

$$\left\{ \begin{array}{l} \boldsymbol{u}_{k+1} = \underbrace{\boldsymbol{u}_k + \Delta t\, \dot{\boldsymbol{u}}_k + \dfrac{\Delta t^2}{2} \ddot{\boldsymbol{u}}_k}_{\tilde{\boldsymbol{u}}_{k+1}} + \underbrace{\Delta t^2\, \beta\, \boldsymbol{\delta \ddot{u}}}_{\boldsymbol{\delta u}} \\ \dot{\boldsymbol{u}}_{k+1} = \underbrace{\dot{\boldsymbol{u}}_k + \Delta t\, \ddot{\boldsymbol{u}}_k}_{\tilde{\dot{\boldsymbol{u}}}_{k+1}} + \underbrace{\Delta t\, \gamma\, \boldsymbol{\delta \ddot{u}}}_{\boldsymbol{\delta \dot{u}}} \end{array} \right\} \Leftrightarrow \left\{ \begin{array}{l} \boldsymbol{u}_{k+1} = \tilde{\boldsymbol{u}}_{k+1} + \boldsymbol{\delta u} \\ \dot{\boldsymbol{u}}_{k+1} = \tilde{\dot{\boldsymbol{u}}}_{k+1} + \boldsymbol{\delta \dot{u}} \end{array} \right\} \tag{2.69}$$

and the residual:

$$\boldsymbol{r} = \boldsymbol{f}_{k+1} - \boldsymbol{M} \ddot{\boldsymbol{u}}_{k+1} - \boldsymbol{C} \dot{\boldsymbol{u}}_{k+1} - \boldsymbol{K} \boldsymbol{u}_{k+1} \tag{2.70}$$

The Newton iterations are performed on the residual considering a linearized increment $\boldsymbol{\delta r}$ such that $\boldsymbol{r} + \boldsymbol{\delta r} = 0$, where the nonlinear contribution can be obtained as:

$$\begin{aligned} \boldsymbol{\delta r} &= \frac{\partial \boldsymbol{r}}{\partial \boldsymbol{u}}\, \boldsymbol{\delta u} + \frac{\partial \boldsymbol{r}}{\partial \dot{\boldsymbol{u}}}\, \boldsymbol{\delta \dot{u}} + \frac{\partial \boldsymbol{r}}{\partial \ddot{\boldsymbol{u}}}\, \boldsymbol{\delta \ddot{u}} = \\ &= \frac{\partial \boldsymbol{r}}{\partial \boldsymbol{u}}\, \Delta t^2\, \beta\, \boldsymbol{\delta \ddot{u}} + \frac{\partial \boldsymbol{r}}{\partial \dot{\boldsymbol{u}}}\, \Delta t\, \gamma \boldsymbol{\delta \ddot{u}} + \frac{\partial \boldsymbol{r}}{\partial \ddot{\boldsymbol{u}}}\, \boldsymbol{\delta \ddot{u}} = \\ &= \left( \Delta t^2\, \beta\, \frac{\partial \boldsymbol{r}}{\partial \boldsymbol{u}} + \Delta t\, \gamma\, \frac{\partial \boldsymbol{r}}{\partial \dot{\boldsymbol{u}}} + \frac{\partial \boldsymbol{r}}{\partial \ddot{\boldsymbol{u}}} \right) \boldsymbol{\delta \ddot{u}} \end{aligned} \tag{2.71}$$

From equation (2.70) we know that:

$$\frac{\partial \boldsymbol{r}}{\partial \boldsymbol{u}} = -\boldsymbol{K} \quad ; \quad \frac{\partial \boldsymbol{r}}{\partial \dot{\boldsymbol{u}}} = -\boldsymbol{C} \quad ; \quad \frac{\partial \boldsymbol{r}}{\partial \ddot{\boldsymbol{u}}} = -\boldsymbol{M} \tag{2.72}$$

And thus:

$$\boldsymbol{\delta r} = -\underbrace{\left( \Delta t^2\, \beta\, \boldsymbol{K} + \Delta t\, \gamma\, \boldsymbol{C} + \boldsymbol{M} \right)}_{\boldsymbol{K^*}} \boldsymbol{\delta \ddot{u}} \tag{2.73}$$

Then, the following equation has to be solved iteratively:

$$\boldsymbol{r} = -\boldsymbol{\delta r} \Leftrightarrow \boldsymbol{r} = \boldsymbol{K^*}\, \boldsymbol{\delta \ddot{u}} \tag{2.74}$$

There are several convergence criteria for the iterative process. It seems reasonable to stop the process when the increments in the displacements are small enough. However, this rule may not be satisfactory since the norm of the displacements vector involves different units of measure. Displacements and rotations use to differ in its order of magnitude. Thus, a typical convergence criterion may fall as it may indicate

convergence because the displacements dominate the norm of the vector while rotations might still be far from the right result. Consequently, the proposed convergence criterion is [Chopra, 1995] :

$$\frac{(\boldsymbol{\delta r}_{k+1})^t \ \boldsymbol{\delta u}_{k+1}}{(\boldsymbol{r})^t \ \boldsymbol{\delta u}_k} < \epsilon \tag{2.75}$$

The solution of the variable geometry problem with the above non-linear algorithm and the update at each time step of the finite element matrices yields an increase in the computing effort needed. In practice the computational time needed for the simulation is triplicated. That proportionality is conserved with $\Delta t$. Figure 2.18 shows the computational time needed for the simulations of a model with 1428 degrees of freedom. It is noteworthy that even for a relatively small $\Delta t = 0.1$ the rotating model has a computing time to simulated time ratio slightly greater than 1/10. This computational time will be increased with implementations described in further chapters.

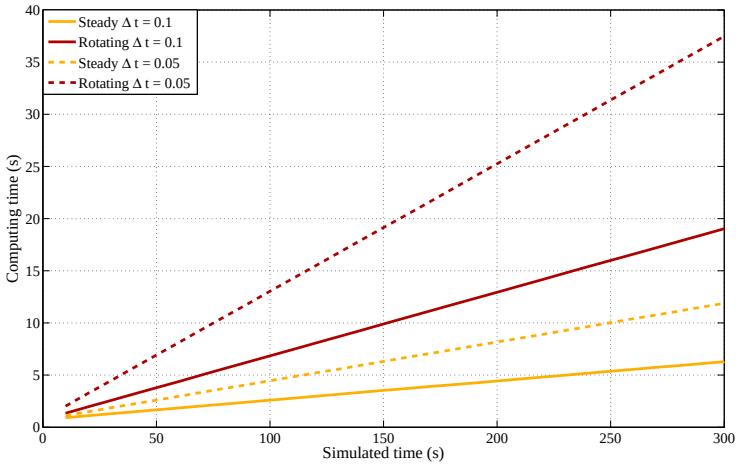


**Figure 2.18. Computing time for the steady and rotating case for different time steps.**

In fact, the average acceleration method looses its unconditional stability property in its non-linear version [Chang, 2004a]. The main problem is that it is a step by step integration method, and the changes in the structure are updated only at the beginning of each step. The linearization of the structural changes between time steps may lead to poor accuracy or even instability. Thus, we have to limit the time step $\Delta t$ in order to guarantee the stability of the integration method. According to [Chang, 2004a,b] the stability of the method depends on the rate of change of the stiffness and the natural frequencies of the system. Figure 2.19 shows the movement of the hub for a test case using different time steps. Instabilities and high inaccuracies are found for $\Delta t > 0.2$. It has been tested that for $\Delta t \leq 0.1$ differences on the solutions are not perceptible.

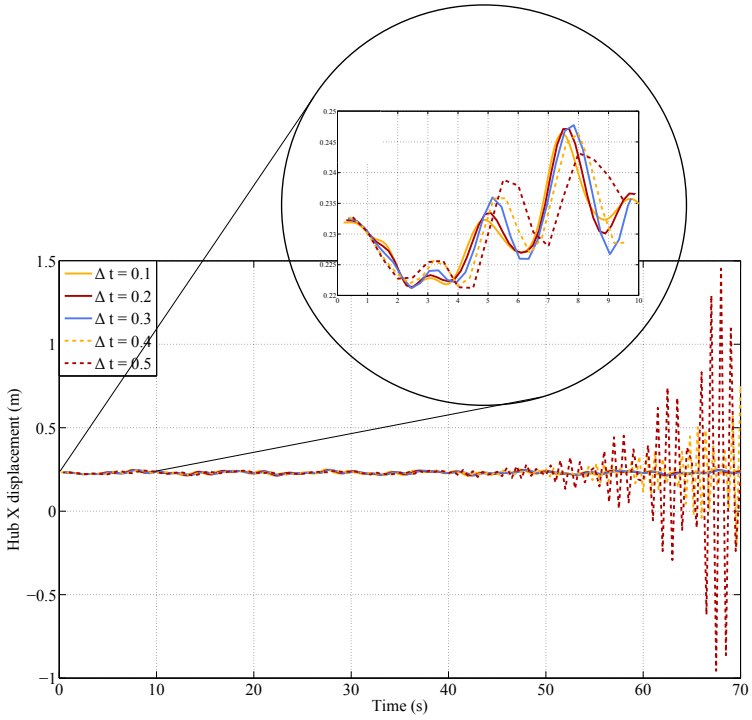


**Figure 2.19. Hub displacement in X direction. Comparison of the time history analysis with the nonlinear Newmark method for different time steps.**

Still, the rotation of the structure has an extent further than the simple resolution of the equations of motion. The following describes some of the additional considerations that have to be accounted for in the rotating structure.

### Previous step displacements rotation

The Newmark integration method uses the information of displacements, velocities and accelerations in step $k$ to obtain those of step $k+1$. The solution of the equations is performed in the global reference frame presenting no issues when the structure is still. However, for the moving blades, elements are rotated between time steps and therefore between two consecutive solutions of the equations of motion. Thus, the displacements obtained in the step $k$ do not represent the deformed shape of the blade, at step $k+1$, with respect to the same axes after rotating the blade; since that deformed shape which is now the initial condition for the $k+1$ step, has rotated as well (2.20). Therefore, the rotated displacement, velocity and acceleration vectors have to be referenced to the global axes.

$$\begin{aligned} \boldsymbol{u'}_y^k &= \boldsymbol{u}_y^k \cos(\theta) - \boldsymbol{u}_z^k \sin(\theta) \\ \boldsymbol{u'}_z^k &= \boldsymbol{u}_y^k \sin(\theta) + \boldsymbol{u}_z^k \cos(\theta) \end{aligned} \tag{2.76}$$

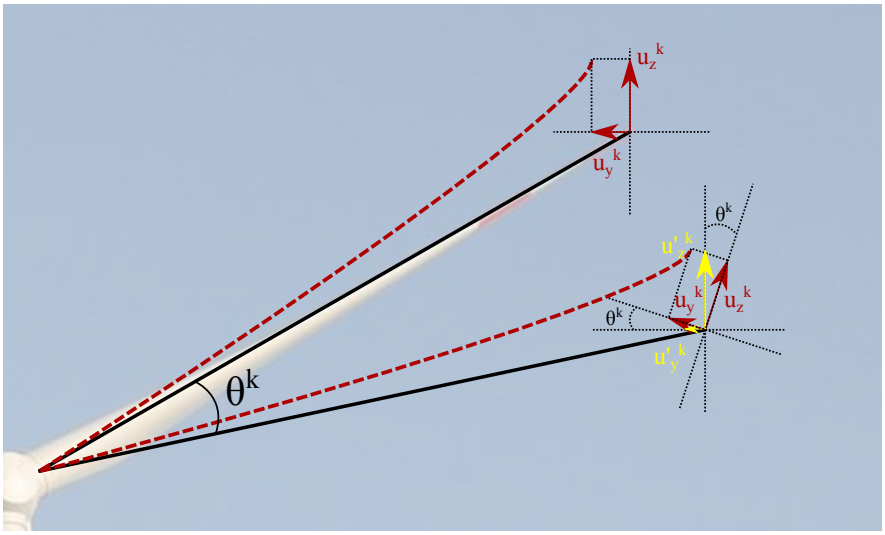


**Figure 2.20. Rotation of the displacement vectors for the nodes of the blades.**

### Rotation effects

The rotation of the blades carries several physical implications that have an impact in the way the structure and its response are accurately modeled. The most important effects would be the gyroscopic and centrifugal stiffening effect. There is an extensive record of studies on these topics [Geradin & Kill, 1984; Sauer & Wolf, 1989; Wallrapp & Schwertassek, 1991; Gans & Anderson, 1991; Hamdi et al., 2014] that refer to a number of approaches to model these effects within finite element formulations. [Sauer & Wolf, 1989] defined a consistent gyroscopic matrix to evaluate the gyroscopic forces on the elements which is then added to the damping matrix in (2.61). Centrifugal stiffening however, is a nonlinear effect that takes into account that the centrifugal forces acting on a rotating deformed element have a restoring effect and thus stiffen the structure. The additional stiffness can be modeled as a geometric stiffness matrix using the centrifugal force over the elements which depends on the mass, rotational speed and distance to the center of rotation [Przemieniecki, 1968]. Nevertheless, both effects depend directly on the speed of rotation of the elements. Thus their influence is more acute in high speed applications and rotating machinery. According to [Burton et al., 2001] one blade change its first natural frequency only a 0.5% due to centrifugal stiffening, consequently it has minor impact on the natural frequencies and dynamic response of the overall structure. Both effects are neglected in this work.

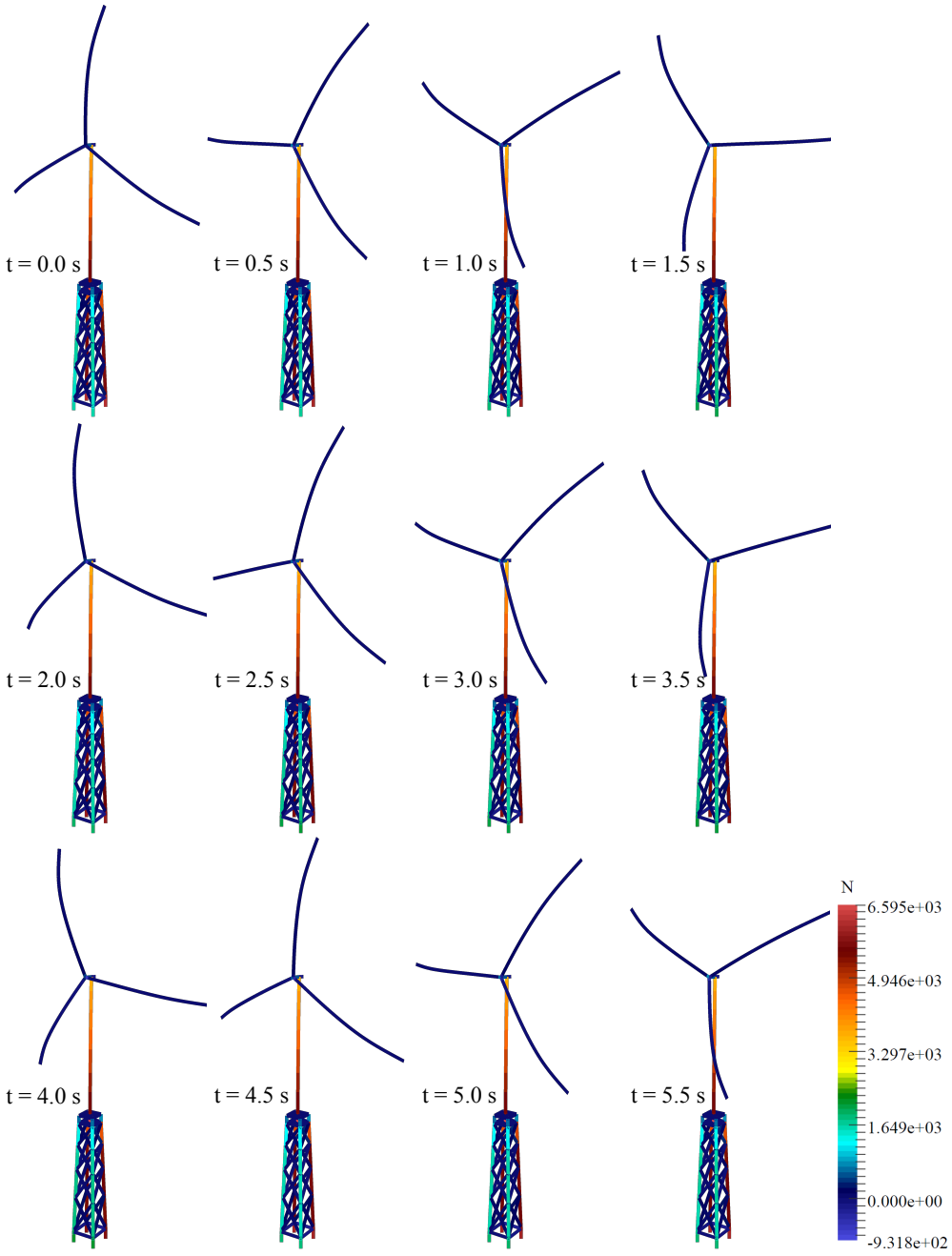


**Figure 2.21. Rotating structure and axial force on the elements.**

## 2.6. Fatigue analysis

### 2.6.1. Introduction and fatigue theories

The most significant load actions on an offshore structure are wind and waves. Wind and waves have a cyclic nature and so the structure is subject to cycles of stresses and strains. The structure undergoes a finite amount of damage with each cycle. The accumulated damage caused by the cyclic stresses and strains is called fatigue. This effect is particularly critical at locations where the stresses are extremely concentrated, in our case at the welds of the joints. Fatigue damage is closely related to crack formation and propagation thus, fatigue is associated with the appearance of the first crack, modifying the mechanical properties of the structure due to plastic deformations [Cui et al., 2014].

There are two big theories or approaches to calculate the fatigue damage. The first would be the study of fracture mechanics, which is a vastly research field itself whose extent goes far beyond the scope of this thesis. The other theory involves methods to account for the accumulated damage of the cyclic loading. The latter is the dominant method and the one recommended by the standards in offshore engineering [DNV-RP-C203, 2011; ABS, 2003].

Particularly, the Stress-Cycle (S-N) approach is the one used in this work. The S-N curves or Wöhler curves represent the number of cycles N of a given constant stress range S that can cause the failure of the structure by fatigue. S-N curves are fully documented in the cited standards and are based upon extensive collections of experimental data.

Some hypothesis and considerations are taken when using the S-N approach to estimate the fatigue damage. First, it is assumed that each stress range produces a linear damage based only on the number of appearances. Thus, for a given stress range $\Delta\sigma_i$ the damage $D_i$ produced in the structure at the spot where that stress occurs would be:

$$D_i = \frac{n_i}{N_i} \tag{2.77}$$

where $n_i$ is the number of stress cycles with amplitude $\Delta\sigma_i$ and $N_i$ is the number of cycles to failure for that stress range given by the S-N curve.

Second, it is assumed that damage associated with different stress ranges is completely independent, meaning that the moment and order of the stress ranges is irrelevant. These hypothesis and methodology to compute the damage is known as the Palmgren-Miner rule [Palmgren, 1924]. The total damage suffered by a certain point of the structure for a given time history would be:

$$D = \sum_{i=1}^{k} \frac{n_i}{N_i} = \frac{1}{a} \sum_{i=1}^{k} n_i \ (\Delta\sigma_i)^m \tag{2.78}$$

where $\overline{a}$ and $m$ are parameters of the S-N curve, and $k$ is the number of stress blocks considered representative of the time history record.

The [DNV-RP-C203, 2011] describes different S-N curves for different geometries and conditions. The curve for tubular joints in seawater with cathodic protection is the adequate for the analyzed problem in this thesis. Also, equation (2.78) is modified to account for the particular thickness of each section by:

$$D = \sum_{i=1}^{k} \frac{n_i}{N_i} = \frac{1}{\overline{a}} \sum_{i=1}^{k} n_i \left(\frac{t}{t_r}\right)^{k'm} (\Delta\sigma_i)^m \tag{2.79}$$

where $t_r$ is the reference thickness, 32 mm for tubular joints and $k'$ is a thickness exponent taken as 0.1 for tubular welds.

Equation (2.79) establishes the method used in this work to compute the fatigue damage. However there are crucial aspects yet to be defined:

- Where is the damage evaluated? We have to define the particular points of the structure susceptible to suffer high fatigue damage.
- How are the stress ranges calculated? Given a time history of loads the time history of stresses or strains for any point of the structure can be directly obtained. Nevertheless, it is far from trivial to extract the stress ranges and the number of times they appear from a time history record computationally. For that matter there is a number of known counting algorithms [Lalanne, 1999].
- How is the fatigue damage at design life assessed? Fatigue damage tries to describe the long-term behavior of the structure subjected to cyclic loads. In fact, the objective is to obtain and limit the fatigue damage on the structure during its whole design life. Since it is not reasonable nor affordable to simulate the whole life of the structure, the total fatigue damage has to be assessed with other techniques.

The following sections detail all these aspects.

### 2.6.2. Hot Spots

For fatigue assessment purposes it is considered that the welds of tubular joints are the points susceptible of undergoing crack growth due to cyclic loading. At those points, the nominal stresses can be obtained through the proposed method as the beam stresses. However, joints present a critical concentration of stresses due to their geometry. That is called the hot spot stress, which is calculated as the nominal stress affected by a Stress Concentration Factor (SCF). The SCFs depend exclusively on geometrical parameters of the joint and the elements it links. The values of the SCFs come from numerous experimental and numerical data. A short explanation of where do the SCFs come from and the specific expressions used in this work can be found

in Appendix A. The factors used are the ones found in the corresponding standard [DNV-RP-C203, 2011].

Each joint is also considered to have eight hot spots uniformly distributed at the circumference of the intersection. The hot spot stress for each point is then calculated as:

$$\sigma_1 = (SCF_{AC})\,\sigma_x + (SCF_{MIP})\,\sigma_{my} \tag{2.80}$$

$$\sigma_2 = \tfrac{1}{2}(SCF_{AC} + SCF_{AS})\,\sigma_x + \tfrac{1}{2}\sqrt{2}\,(SCF_{MIP})\,\sigma_{my} - \tfrac{1}{2}\sqrt{2}\,(SCF_{MOP})\,\sigma_{mz} \tag{2.81}$$

$$\sigma_3 = (SCF_{AS})\,\sigma_x - (SCF_{MOP})\,\sigma_{mz} \tag{2.82}$$

$$\sigma_4 = \tfrac{1}{2}(SCF_{AC} + SCF_{AS})\,\sigma_x - \tfrac{1}{2}\sqrt{2}\,(SCF_{MIP})\,\sigma_{my} - \tfrac{1}{2}\sqrt{2}\,(SCF_{MOP})\,\sigma_{mz} \tag{2.83}$$

$$\sigma_5 = (SCF_{AC})\,\sigma_x - (SCF_{MIP})\,\sigma_{my} \tag{2.84}$$

$$\sigma_6 = \tfrac{1}{2}(SCF_{AC} + SCF_{AS})\,\sigma_x - \tfrac{1}{2}\sqrt{2}\,(SCF_{MIP})\,\sigma_{my} + \tfrac{1}{2}\sqrt{2}\,(SCF_{MOP})\,\sigma_{mz} \tag{2.85}$$

$$\sigma_7 = (SCF_{AS})\,\sigma_x + (SCF_{MOP})\,\sigma_{mz} \tag{2.86}$$

$$\sigma_8 = \tfrac{1}{2}(SCF_{AC} + SCF_{AS})\,\sigma_x + \tfrac{1}{2}\sqrt{2}\,(SCF_{MIP})\,\sigma_{my} + \tfrac{1}{2}\sqrt{2}\,(SCF_{MOP})\,\sigma_{mz} \tag{2.87}$$

where $\sigma_x$, $\sigma_{my}$ and $\sigma_{mz}$ are the nominal stresses due to axial forces, and moments. $SCF_{AC}$, $SCF_{AS}$, $SCF_{MIP}$ and $SCF_{MOP}$ are the Stress Concentration Factors for axial loading for the crown and the saddle (figure A.3) and for the in-plane and out-of-plane bending moment respectively.

The above equations need to be particularized for each element assembled at each joint.

### 2.6.3. Counting algorithms

Once we have the locations to calculate the accumulated damage, we need to somehow acquire the number of cycles and amplitude of the stress-history for those points. In other words, count. The problem is that, we do not have an harmonic signal of constant amplitude and frequency which would simplify the counting process. We rather have a random shaped peaks distribution that complicates the determination of the number of cycles the structure suffers. For this matter we need to use counting algorithms, in fact, counting algorithms were developed in origin to study fatigue in aerodynamic problems [Lalanne, 1999].

There are numerous counting algorithms which can be classified in two main types. Methods whose outputs are not related to fatigue calculations and damage, and methods whose outputs are directly referred to the quantities needed for fatigue assessment. The former are always preferred for fatigue analysis in engineering.

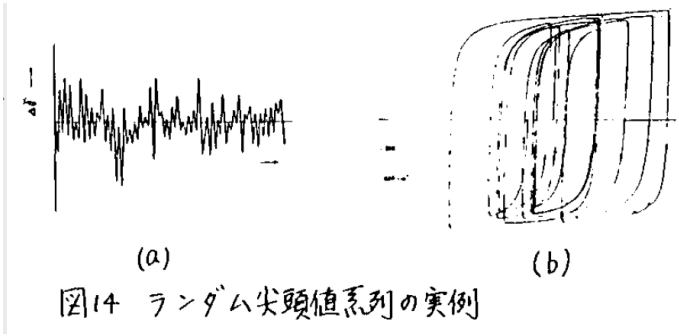


**Figure 2.22. Original image of the Rainflow counting algorithm [Endo et al., 1967a].**

Among the most used methods (range-count, range-mean count, range-pair, Haye's counting method ...) the Rainflow counting method or Pagoda roof method is consistently the used method in fatigue analysis. The rainflow method was first proposed by Tatsuo Endo in 1967 [Endo et al., 1967a,b]. It was not until 1974 when the method was first officially published in English [Endo et al., 1974]. The procedure was intentionally developed to count the cycles of strain in metals to account for fatigue. Several upgrades and modifications have come afterwards [Murakami, 1992; Zengah et al., 2013; Marsh et al., 2016] though the American Society for Testing and Materials (ASTM) adopted a version of the Rainflow algorithm which has been the main reference since 1985 [ASTM-E1049-85(2011)e1, 2011]. The standard comprises a set of rules to extract the cycles and half cycles from a given stresses signal time history but is out of the scope of this work to discuss them here although it is important to bear in mind that the Rainflow counting algorithm identifies a cycle as when the stress record forms a closed stress-strain hysteresis loop.

### 2.6.4. Fatigue life assessment

Even though there is a method to count the number of cycles the jackets are subjected to, it is completely unreasonable to count every single cycle during the whole design life of the structure and for all the possible load scenarios. Thereby it is mandatory to develop techniques to estimate the long-term damage from shorter calculations.

Early attempts where based either on simulating very short time series or even singular events as one wave cycle or such, or either simulating excessively long intervals and adjust probability functions of the stress cycles. Neither the short time series were capable of assessing the damage for the long term nor the long computations were manageable or the probabilities obtained were representative enough. One of the most famous alternatives is to estimate the fatigue damage based on spectral methods by using the power spectrum. In this regard, the Probability Density Function (PDF) of the stress ranges can be estimated using the Dirlik's method [Dirlik, 1985].

However, a well-known limitation of the method is that it is unable to capture any

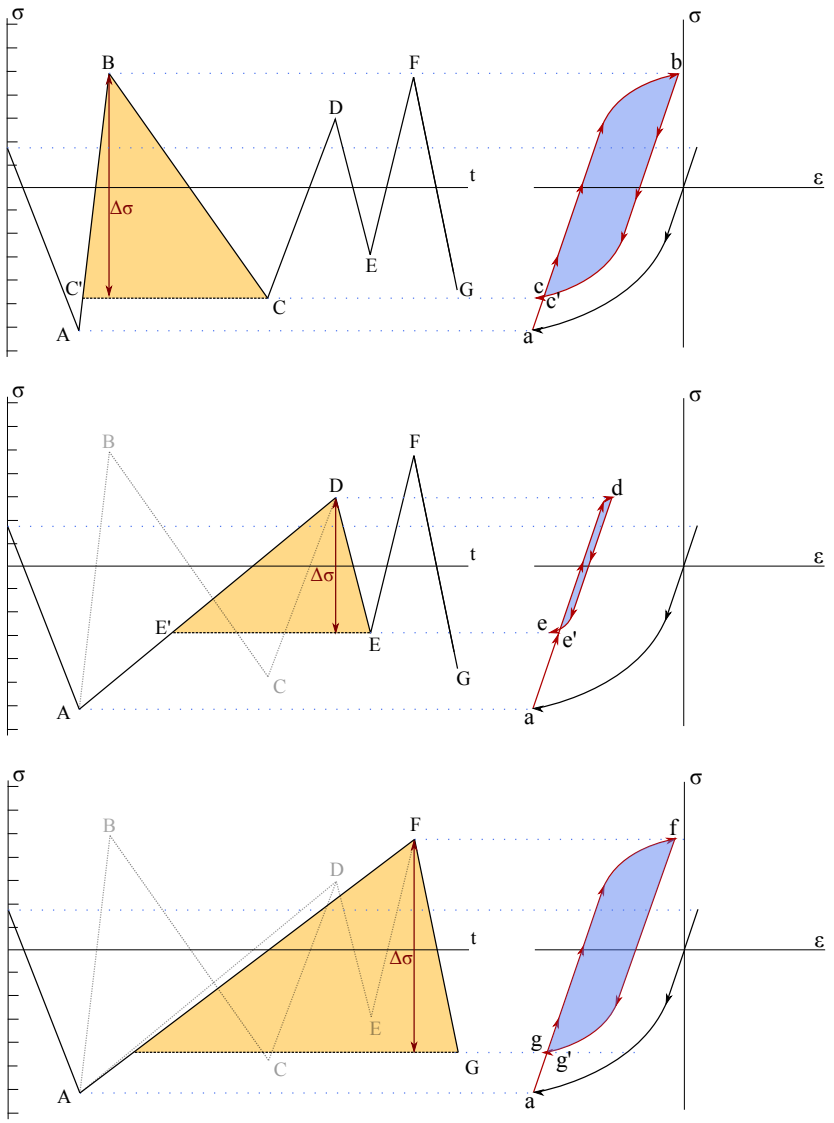


**Figure 2.23. Rainflow counting process.**

bimodal character of an stress signal and fails to model signals with large periodicity, which often appear in wind turbines [Ragan & Manuel, 2007]. Moreover, since the Dirlik's method is based on the power spectrum it only contains information about the amplitudes but not the phases, so it can not account for two or more signals that are in phase producing larger damage. Spectral analysis and frequency domain analysis allow an easier handle of the problem statistically but deliver a poor or low accuracy compared to time history methods [Mohammadi et al., 2016].

Thus, the common trend in offshore engineering and particularly in the assessment

of fatigue for wind turbines is the time history analysis [Jia, 2014; Yeter et al., 2015; Kvittem & Moan, 2015]. Nevertheless, the problem of how do we estimate the long term damage while keeping the computational cost manageable is still there. In this regard, there are current works devoted to find a solution [Stieng et al., 2015]. Authors have explored the estimation of fatigue from a linear regression based on Damage Equivalent Loads (DEL) for 10 minutes time series with promising results. Others performed a topology optimization of a jacket using 30 seconds long simulation and then considering that the cycles found in that interval where repeated a number of times design life/simulation time [Martens, 2014].

One thing is clear, we are going to need to extrapolate. Thus, we need to choose the short term computation or computations used for the extrapolation first and then the extrapolation model. Based on Martens' idea [Martens, 2014] and given the assumption made that the damage is accumulated linearly based on the Palmgren-Miner rule it is reasonable to think that the damage will continue to increase linearly. So, in this work, the extrapolation model is linear.

Regarding the short term simulations used as extrapolation base we need to use data significant enough and also long enough so the loads and the structural response are completely developed and make sure we are not cutting out high period cycles. Again, while keeping the computational cost manageable. Offshore standards seem to agree in the 10 minutes period for the simulation of loads, actually wind is commonly represented by 10 minutes mean wind speed. Researchers about this field have compared results of short-term simulations of 1 -minutes with simulations of 60 minutes for fatigue design analysis [Zwick, 2015].

In this work, a linear extrapolation based on the damage computed for 300 and 600 seconds is proposed. Also, the extrapolation is performed in the damage values not in the number of cycles and the 300 s damage is taken as the first value, not 0.

Then, for a design life $T_{life}$ in seconds, the expected damage is:

$$D_{life} = D_{300} + \frac{D_{600} - D_{300}}{300} (T_{life} - 300) \tag{2.88}$$

where $D_{life}$ is the damage at design life and $D_{300}$ and $D_{600}$ the damages computed for 300 and 600 seconds respectively.

Figures 2.24 and 2.25 show two examples of the damage calculated and linearly estimated for the OC4 jacket example considering a singular load case with self weight, buoyancy, wind and waves. In both figures the points represent the damage obtained with simulations of the whole interval for 300 s, 600 s, 3600 (1 hour), 86400 s (1 day) and 630720000 s (20 years) while the dashed lines draw the estimated damage calculated with (2.88). Simulations were carried out with a time step of 0.5 seconds in order to actually be able to run the simulation and store the output data. The values for the 20 years long simulation were also estimated from the values of 1 year simulation (31536000 s) as it was not reasonable to run the implemented rainflow algorithm through all the stress-history. The simulations were also performed for all the 3968 hot-spots of the jacket. The mean error for the estimation remained under

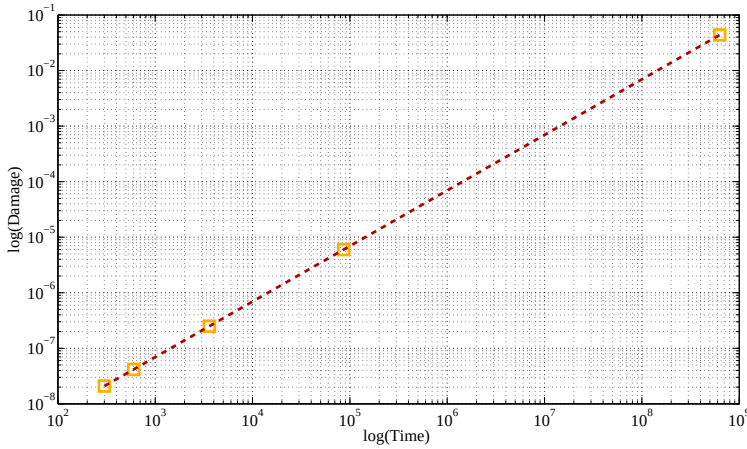


**Figure 2.24. Calculated and estimated damage for bar 121, node 2, hot spot 1, of the OC4 jacket.**

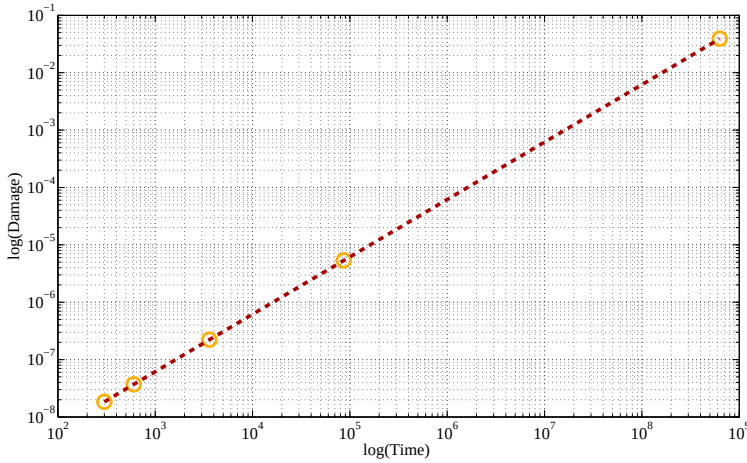


**Figure 2.25. Calculated and estimated damage for bar 33, node 1, hot spot 2, of the OC4 jacket.**

the 10%, which seems quite large but it is worth noting that the high error arises from a few hot-spots where the estimation deeply fails. Additionaly, those points where the hot-spots less susceptible of undergoing significant values of damage and represent less than a 5% of the hot-spots.

## 2.7. Summary and conclusions

From the basic structural and dynamic properties of the members forming the structure, stiffness, mass and damping, to the computation of the dynamic response of the structure and the assessment of the fatigue life damage, this chapter establishes the foundations on which the following ones are supported. The whole model of the offshore wind turbine is built up with beam elements which are proved sufficiently accurate to represent the dynamic properties of the structure. Static and dynamic loading is considered in the three dimensional framed structure with regard to distributed loads between the nodes of the beam elements. Wind loads are taken into account for the blades through the BEM method considering as well the tower dam effect. For the wave loading computation, Airy and second order Stokes wave theories are used while the forces on the elements are obtained with the Morison's formula.

The natural frequencies of the structure are computed and in good agreement with the values of the reference models and the dynamic equation of motion is integrated with the Newmark method, in particular the average acceleration method is used guaranteeing unconditional stability. However, this work includes the rotation movement of the blades introducing a change in the geometry between time steps requiring the use of a non-linear integration algorithm although centrifugal stiffening and gyroscopic effects due rotation are neglected. In this case the non-linear Newmark integration method is utilized. The use of the non-linear integration method needs a reduction of the time step and a subsequent increase in the computational effort which is still manageable in terms of analysis but will shortly become an important issue in the following chapters.

For fatigue analysis purposes the S-N approach of the current standards is applied using the Palgrem-Miner rule that considers the linearity of the accumulated damage. Also, fatigue is computed in the hot-spots of the tubular joints considering as well the SCFs. In terms of counting life-span stresses the rainflow counting algorithm is used for computations of 300 and 600 seconds to calculate the damage at those ages. The design life damage is linearly extrapolated from those two values for each hot-spot.

The whole formulation described on the chapter for the dynamic analysis of jacket structures as supports for offshore wind turbines is considerably demanding in terms of computational resources although it is also consistently accurate and robust. The methodology of analysis represents the main external actions and the dynamic and structural behavior of the whole structure assembly. It also serves as base to assess the fatigue damage expected in the joints of the structure during the design life.

Chapter 3

# Optimization problem

*"Elegance is effortless beauty"*
**Mike Schlaich**

## 3.1. Introduction

The former chapter describes the details for the mathematical and numerical modelization of what in the recent past was an engineering challenge. Challenges are still there but solid steps forward have been made and to prove it, there are many examples of actual completely functional offshore wind farms and many projects in development, each of them humbly pushing the limits of innovation. But, for something to be just "functional" is not enough. If there is something we can learn from nature, it is that only the best ones survive. This obviously depends on how do we define the word "best" for each case, which is a semantic problem although it is one that we can sort of express mathematically.

This is where optimization steps in.

Particularizing for structural engineering, every structure is designed for a purpose which is normally accomplished by satisfying some conditions that can indeed be defined through mathematical functions. For the optimization problem those conditions that the structure needs to fulfill are the constraints. Every structure is as well defined by its properties, that could be mechanical properties, shape, dimensions or others. If we fix some properties and modify others that we will call design variables, we could try to improve the structural design keeping the conditions or constraints satisfied. And here is the key point, we need to establish some system to measure the improvement, superiority or betterness of one design over another. That is mathematically expressed with an objective function. As we are trying to get the best design, we would have to find the design variables that, satisfying the constraints, define the structure that takes the objective function to the extreme, maximum or minimum.

Any optimization problem can be stated in those terms as:

$$min\ f(\boldsymbol{x}) \tag{3.1}$$

subject to:

$$\begin{aligned} g_j(\boldsymbol{x}) &\leq 0 \qquad j = 1, m \\ h_k(\boldsymbol{x}) &= 0 \qquad k = 1, l \\ x_i^m \leq x_i &\leq x_i^M \quad i = 1, n \end{aligned} \tag{3.2}$$

the above problem represents the standard optimization problem where $f$ is the objective function that depends on the set of $n$ design variables $\boldsymbol{x}$, $g_j$ are the $m$ inequality constraints, $h_k$ are the $l$ equality constraints and $x_i^m$ and $x_i^M$ are minimum and maximum values for the design variables usually called side constraints[1].

There are numerous mathematical techniques to solve the above problem depending on the nature of the objective function, constraints and design variables. Solving methodology aside, a crucial aspect in optimization is the particularization of 3.1 and 3.2 for the desired problem. It is important to bear in mind that optimization delivers the best solution under the criteria established in the definition of the mathematical problem.

This chapter is devoted to define the mathematical optimization problem for the design of steel jackets for offshore wind turbines.

## 3.2. Definition of the optimization problem

As stated in former sections the particularization of (3.1) and (3.2), say the definition of the optimization problem, is of major importance to accomplish the final purpose. We need to keep in mind that the optimized design that the methodology delivers will only be the best design of the set of designs that match the particular definition of the problem.

Again, the optimization problem is defined through:

- The objective function: Represents the criterion imposed to decide the betterness or improvement of the solutions.
- The constraints: Limit the designs to satisfy the required conditions.
- The design variables: They are the properties susceptible of being modified to improve the design.

[1] They could also be found as bound constraints or box constraints

### 3.2.1. Objective function

Even though there are greater ends worth pursuing by society, one of the most used objective functions in structural optimization as a measure of efficiency of the design is the cost of the structure. There are countless factors affecting the final budget of a structural project from its conception to its final construction. Since accounting for every one of them is impossible in practice, the common approach is to use the amount of material the structure is made of as an economic measure. In these terms, the total weight of the structure is stated as the objective function to minimize in the optimization process.

The weight of the structure is simply computed as:

$$W = \sum_{i=1}^{n} \rho_i \, A_i \, l_i \tag{3.3}$$

where $\rho_i$, $A_i$ and $l_i$ are the density, cross-sectional area and length of the $i$th element, being $n$ the total number of elements. In our case $\rho_i$ can be assumed constant and the area of the tubular elements can be expressed in terms of the diameter and thickness of each member ($D_i$,$t_i$)

$$W = \rho \sum_{i=1}^{n} \left( \frac{\pi}{4} \left( D_i^2 - (D_i - 2t_i)^2 \right) \right) \, l_i \tag{3.4}$$

The above equation constitutes the objective function of the optimization problem. Note that only the elements of the jacket are accounted for since only the design of the support structure is aimed in this work. Moreover, it will be described later but the objective function is expressed in terms of the optimization design variables[2] $(D_i, t_i, l_i)$.

### 3.2.2. Structural and design constraints

Every part of the definition of the optimization problem is important in its way, however the constraints imposed to the design are more relevant since they decide whether the new design is valid or not. Traditionally, design constraints in structural optimization are limits imposed to the stresses and deformations of the structure. Those limits are related to the forces acting on the elements, their dimensions and their material. A very noble approach is to compute the pure stresses the material is subject to at each point to guarantee that the elastic limit is not exceeded. However, it has been long since engineering structures are strongly regulated by structural standards. Those documents specify the particular limits and conditions needed to be imposed for the structure to be able to be constructed and functional. The following sections describe the constraints imposed to the jacket structure in this work[ISO19902:2007, 2013; DNV-OS-C101, 2014; Norsok, 2004].

[2]The length of the elements $l_i$ are not design variables per se but are directly related to them.

All constraints are particularized for tubular elements. Further description and conditions can be consulted in the cited standards.

**Ultimate Limit State constraints**

The restrictions for the structure under Ultimate Limit States (ULS) specify the ultimate resistance of the structure under the maximum carrying loads.

All the expressions share the same basic shape of a normalized ratio acting force to design strength. In order to resemble to (3.2) they are expressed as that ratio minus 1.

Requirements are also different for submerged and non-submerged elements.

1. Combined actions only for non-submerged elements.

   *a*) Axial tension and bending moment:

$$g_{TB} = \frac{\gamma_{R,t}\, N}{f_t\, A} + \frac{\gamma_{R,b}\, \sqrt{{M_y}^2 + {M_z}^2}}{f_b\, W_e} - 1 \leq 0 \tag{3.5}$$

   where $N$, $M_y$ and $M_z$ are the axial tension and bending moments respectively, $\gamma_{R,t}$ and $\gamma_{R,b}$ are the partial resistance factors, $A$ is the cross-sectional area of the bar and $W_e$ is the elastic section modulus $\left(\frac{\pi}{32}\frac{\left(D^4-(D-2t)^4\right)}{D}\right)$. The representative axial tensile strength $f_t$ is equal to the yield strength $f_y$ in this case. The representantive bending strength $f_b$ is defined as:

$$f_b = \begin{cases} \dfrac{W_p}{W_e} f_y & ; \quad \dfrac{f_y\, D}{E\, t} \leq 0.0517 \\ \left(1.13 - 2.58\left(\dfrac{f_y\, D}{E\, t}\right)\right)\dfrac{W_p}{W_e} f_y & ; \quad 0.0517 \leq \dfrac{f_y\, D}{E\, t} \leq 0.1034 \\ \left(0.94 - 0.76\left(\dfrac{f_y\, D}{E\, t}\right)\right)\dfrac{W_p}{W_e} f_y & ; \quad 0.1034 \leq \dfrac{f_y\, D}{E\, t} \leq 120\dfrac{f_y}{E} \end{cases} \tag{3.6}$$

   being $W_p$ the section plastic modulus $\left(\frac{1}{6}\frac{\left(D^3-(D-2t)^3\right)}{D}\right)$, $E$ the material's modulus of elasticity and $D$ and $t$, the tubular diameter and thickness respectively.

   *b*) Axial compression and bending moment: Elements subject to combined compression and bending need to satisfy two conditions:

$$g_{CB} = \frac{\gamma_{R,c}\, N}{f_c\, A} + \frac{\gamma_{R,b}}{f_b\, W_e}\sqrt{\frac{C_{m,y}\, {M_y}^2}{1-\frac{N}{N_{e,y}}} + \frac{C_{m,z}\, {M_z}^2}{1-\frac{N}{N_{e,z}}}} - 1 \leq 0 \tag{3.7}$$

   and

$$g_{CB2} = \frac{\gamma_{R,c}\, N}{f_{yc}\, A} + \frac{\gamma_{R,b}\, \sqrt{{M_y}^2 + {M_z}^2}}{f_b\, W_e} - 1 \leq 0 \tag{3.8}$$

The second equation limits the combined force acting on the element like the one in (3.5) for tensile forces and the first takes into account limitations due to buckling. Coefficients are obtained as follows:

$$f_{yc} = \begin{cases} f_y & ; \quad \dfrac{f_y}{f_{xe}} \leq 0.170 \\ \left(1.047 - 0.274 \dfrac{f_y}{f_{xe}}\right) f_y & ; \quad \dfrac{f_y}{f_xe} > 0.170 \end{cases} \tag{3.9}$$

$$f_{xe} = 2\, C_x\, E \frac{t}{D} \tag{3.10}$$

$$f_c = \begin{cases} \left(1 - 0.278\, \lambda^2\right) f_{yc} & ; \quad \lambda \leq 1.34 \\ \dfrac{0.9}{\lambda^2} f_{yc} & ; \quad \lambda > 1.34 \end{cases} \tag{3.11}$$

$$\lambda = \frac{K\, L}{\pi\, r} \sqrt{\frac{f_{yc}}{E}} \tag{3.12}$$

$$N_{e,y} = \frac{\pi\, E\, A}{\left(K_y\, L/r\right)^2} \quad ; \quad N_{e,z} = \frac{\pi\, E\, A}{\left(K_z\, L/r\right)^2} \tag{3.13}$$

$$C_{m,y} = 1 - 0.4 \frac{N}{N_{e,y}} \leq 0.85 \quad ; \quad C_{m,z} = 1 - 0.4 \frac{N}{N_{e,z}} \leq 0.85 \tag{3.14}$$

In the above equations $f_{yc}$ is called the representative local buckling strength, $f_c$ is the representative axial compressive strength and $f_{xe}$ is the representative elastic local buckling strength. $C_x$ is the reduced elastic critical buckling coefficient which takes the value 0.3. $\lambda$ is the column slenderness parameter which is a function of the effective length factor $K$ and $r = \sqrt{I/A}$ is the radius of gyration of the section. Coefficients $C_m$ and $N_e$ are the moment reduction factors and the Euler buckling limits for the section.

2. Combined actions only for submerged elements:

   *a)* Hoop Buckling:

$$g_{HB} = \frac{\gamma_{R,h}\, \sigma_h}{f_h} - 1 \leq 0 \tag{3.15}$$

where $\sigma_h$ is the hoop stress $\frac{p\, D}{2\, t}$ with $p$ the hydrostatic pressure and $f_h$ is the hoop buckling strength given by:

$$f_h = \begin{cases} fy & ; \quad f_{he} > 2.44 f_y \\ 0.7 \left(\dfrac{f_{he}}{fy}\right)^{0.4} f_y & ; \quad 0.55 f_y < f_{he} \leq 2.44 f_y \\ f_{he} & ; \quad f_{he} \leq 0.55 f_y \end{cases} \tag{3.16}$$

$$f_{he} = 2\, C_h\, E\, \frac{t}{D} \tag{3.17}$$

$$C_h = \begin{cases} 0.80 & ; & & & \mu & < & 1.5 \\ \dfrac{0.737}{(\mu - 0.579)} & ; & 1.5 & \leq & \mu & < & 0.825D/t \\ 0.44t/D + 0.21\dfrac{(D/t)^3}{\mu^4} & ; & 0.825D/t & \leq & \mu & < & 1.6D/t \\ 0.44t/D & ; & & & \mu & \geq & 1.6D/t \end{cases} \tag{3.18}$$

$$\mu = \frac{L}{D}\sqrt{\frac{2D}{t}} \tag{3.19}$$

being $f_{he}$ the representative elastic critical hoop buckling strength, $C_h$ the elastic critical hoop buckling coefficient, and $\mu$ a geometric parameter depending on the length of the tubular between stiffening rings or end connections $L$.

*b*) Axial tension, bending moment and hydrostatic pressure: The expression is similar to (3.5) but changing the representative strengths.

$$g_{TBS} = \frac{\gamma_{R,t}\, N}{f_{t,h}\, A} + \frac{\gamma_{R,b}\, \sqrt{{M_y}^2 + {M_z}^2}}{f_{b,h}\, W_e} - 1 \leq 0 \tag{3.20}$$

where those new resistances are computed as:

$$f_{t,h} = \left(\sqrt{1 + 0.09B^2 - B^{2\eta}} - 0.3B\right) f_y \tag{3.21}$$

$$f_{b,h} = \left(\sqrt{1 + 0.09B^2 - B^{2\eta}} - 0.3B\right) f_b \tag{3.22}$$

$$B = \frac{\gamma_{R,h}\, \sigma_h}{f_h} \quad ; \quad \mu = 5.4\frac{f_h}{f_y} \tag{3.23}$$

*c*) Axial compression, bending moment and hydrostatic pressure: In this case, three constraints need to be imposed where the first two are identical to the non-submerged case but substituting the resistances.

$$g_{CBS} = \frac{\gamma_{R,c}\, N}{f_c\, A} + \frac{\gamma_{R,b}}{f_{b,h}\, W_e}\sqrt{\frac{C_{m,y}\, {M_y}^2}{1 - \frac{N}{N_{e,y}}} + \frac{C_{m,z}\, {M_z}^2}{1 - \frac{N}{N_{e,z}}}} - 1 \leq 0 \tag{3.24}$$

$$g_{CBS2} = \frac{\gamma_{R,c}\, N}{f_{yc}\, A} + \frac{\gamma_{R,b}\, \sqrt{{M_y}^2 + {M_z}^2}}{f_{b,h}\, W_e} - 1 \leq 0 \tag{3.25}$$

The third constraint is imposed if the following conditions are satisfied:

$$\text{if } \sigma_c > 0.5\frac{f_{he}}{\gamma_{R,h}} \quad \text{and} \quad \frac{f_{xe}}{\gamma_{R,c}} > 0.5\frac{f_{he}}{\gamma_{R,h}} \tag{3.26}$$

then:

$$g_{CBS3} = \frac{\frac{N}{A} + \frac{\sqrt{M_y^2 + M_z^2}}{W_e} - 0.5\frac{f_{he}}{\gamma_{R,h}}}{\frac{f_{xe}}{\gamma_{R,c}} - 0.5\frac{f_{he}}{\gamma_{R,h}}} + \left(\frac{\gamma_{R,h}\sigma_h}{f_{he}}\right)^2 - 1 \leq 0 \tag{3.27}$$

The latter combines the effects of compressive stress due to axial and bending loading and the hoop stress from the surrounding hydrostatic pressure.

3. Combined actions for both, submerged and non-submerged elements.

*a*) Shear, bending moment and torsional moment ($y$ axis):

$$g_{SBTy} = \begin{cases} \frac{\gamma_{R,b}M_z}{W_e f_{m,Red}} - \sqrt{1.4 - \frac{2\sqrt{3}\gamma_{R,v}V_y}{f_y A}} - 1 \leq 0; & \frac{2\sqrt{3}\gamma_{R,v}V_y}{f_y A} \geq 0.4 \\ \frac{\gamma_{R,b}M_z}{W_e f_{m,Red}} - 1 \leq 0; & \frac{2\sqrt{3}\gamma_{R,v}V_y}{f_y A} < 0.4 \end{cases} \tag{3.28}$$

*b*) Shear, bending moment and torsional moment ($z$ axis):

$$g_{SBTz} = \begin{cases} \frac{\gamma_{R,b}M_y}{W_e f_{m,Red}} - \sqrt{1.4 - \frac{2\sqrt{3}\gamma_{R,v}V_z}{f_y A}} - 1 \leq 0; & \frac{2\sqrt{3}\gamma_{R,v}V_z}{f_y A} \geq 0.4 \\ \frac{\gamma_{R,b}M_y}{W_e f_{m,Red}} - 1 \leq 0; & \frac{2\sqrt{3}\gamma_{R,v}V_z}{f_y A} < 0.4 \end{cases} \tag{3.29}$$

where:

$$f_{m,Red} = f_b\sqrt{1 - 3\left(\frac{\tau_t}{f_d}\right)^2} \quad ; \quad \tau_t = \frac{M_x}{2\pi(D/2)^2\, t} \quad ; \quad f_d = \frac{f_y}{\gamma_{R,v}} \tag{3.30}$$

A summary of the decision tree for the ULS constraints is shown in figure 3.1.

**Fatigue Limit State constraints**

The previous chapter already explained the fatigue phenomena and how it is modeled and accounted for in this thesis. Equation (2.79) represents the damage associated with a particular point of the structure subject to a certain record of stresses. Fatigue limit state (FLS) checks the feasibility of the design during its design life under normal state operational conditions, thereby, a range of possible states have to be considered to compute the total damage on the structure. Then equation (2.79) is modified as:

$$D = \sum_{l=1}^{N_p} P_l \frac{1}{\overline{a}} \sum_{i_1}^{k} n_i \left(\frac{t}{t_r}\right)^{k'm} (\Delta\sigma_i)^m \tag{3.31}$$

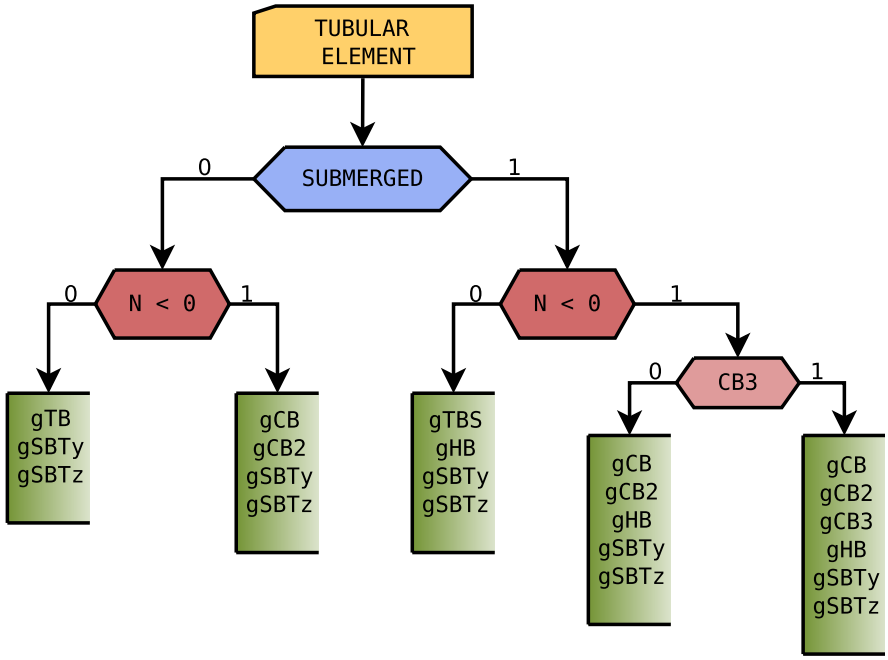


**Figure 3.1. Decision tree for ULS constraints.**

Equation (2.79) has been transformed into another summation affected by a factor $P_l$ that represents the probability of appearance of a particular load case. $N_p$ is the total number of load cases considered. As explained in the previous chapter, the damage is computed for each hot-spot in each load case and during the whole design life, from 300 and 600 seconds simulations. Affecting the damage of each load case by the probability of appearance accounts for the estimated time that load case is impacting the structure.

For offshore wind turbines the particular load cases under normal conditions include wind and wave specific situations which are normally related between them. For short-term simulations it is common to use power spectrum functions to determine the wave conditions, usually as a Pierson-Moskowitz or a JONSWAP. However, for long-term simulations wave and wind conditions can again be modeled with generic distributions or in terms of scatter diagrams. Scatter diagrams provide the occurrence of a given state, for example for wave loading it represents the frequency in which a given $(H, T)$ pair appears. There are as well directional scatter diagrams that account for the direction of the wind and waves.

Even though the scatter diagram of figure 3.2 is relatively small, it would be extremely demanding, in terms of memory and storage, to compute the fatigue life damage for every $(H, T)$ pair. This issue comes from the fact that the stress ranges are counted with the rainflow counting algorithm, thus the whole stress record at each hot spot has

| Significant wave height m | Peak period s | | | | | | | | | | | | | |
|---|---|---|---|---|---|---|---|---|---|---|---|---|---|---|
| | 0 to 1,99 | 2 to 3,99 | 4 to 5,99 | 6 to 7,99 | 8 to 9,99 | 10 to 11,99 | 12 to 13,99 | 14 to 15,99 | 16 to 17,99 | 18 to 19,99 | 20 to 21,99 | 22 to 23,99 | >24 | Total |
| 0,00 to 0,49 | | | | 0,02 | | 0,03 | 0,02 | 0,03 | | | | | | 0,10 |
| 0,50 to 0,99 | | | 0,50 | 5,37 | 2,55 | 3,48 | 3,14 | 2,46 | 0,64 | 0,13 | 0,05 | 0,02 | | 18,34 |
| 1,00 to 1,49 | | | 0,34 | 11,01 | 16,65 | 9,40 | 11,01 | 8,76 | 2,74 | 0,88 | 0,24 | 0,04 | | 61,07 |
| 1,50 to 1,99 | | | | 0,08 | 5,85 | 4,67 | 2,76 | 2,95 | 1,19 | 0,33 | 0,09 | 0,03 | | 17,95 |
| 2,00 to 2,49 | | | | | 0,17 | 0,79 | 0,58 | 0,41 | 0,19 | 0,07 | 0,03 | | | 2,24 |
| 2,50 to 2,99 | | | | | | 0,06 | 0,08 | 0,04 | 0,05 | 0,02 | | | | 0,25 |
| >3,00 | | | | | | | 0,02 | 0,03 | | | | | | 0,05 |
| **Total** | | | 0,84 | 16,48 | 25,22 | 18,43 | 17,61 | 14,68 | 4,81 | 1,43 | 0,41 | 0,09 | 0 | 100,00 |

**Figure 3.2. Wave scatter diagram from [API-RP-2A-LRFD, 1993].**

to be stored[3].

A scatter diagram can easily have 50 or 100 $(H, T)$ pairs, and that only for one wave's direction. Thus, it is undeniable that using a full directional scatter diagram to assess as accurate as possible the fatigue damage of the structure and additionally include it in an optimization loop and computing the sensitivity analysis is completely out of the question right now. The methodology developed in this thesis is applied in upcoming chapters to application examples in which the load cases considered are described. For the sake of simplicity and computing efficiency wind and waves states are considered related so in terms of fatigue each pair wave height-period is associated with a particular wind speed.

Back to the fatigue life constraint, (3.31) represents the normalized damage which is indeed limited by what is called a usage factor. That usage factor is calculated as a ratio $1/DFF$ where $DFF$ stands for Design Fatigue Factor. According to the standards [DNV-OS-C101, 2014] different $DFFs$ are applied depending on the significance and availability for inspection of the structural component. In this thesis a $DFF$ of 3 will be considered almost for every hot-spot considering that it is a non-accessible area and not planned for inspection or repair. Note that there are cases in which the $DFF$ can take a value of 10.

The structural constraint for fatigue life is then

$$g_F = \sum_{l=1}^{N_p} P_l \frac{1}{a} \sum_{i_1}^{k} n_i \left(\frac{t}{t_r}\right)^{k'm} (\Delta\sigma_i)^m - \frac{1}{DFF} \leq 0 \tag{3.32}$$

There is also a group of dimensional constraints that limit geometric characteristics of the joints of the tubular elements. Equation (A.2) of Appendix A shows the limits for these geometrical parameters that guarantee the validity of the expressions used for

[3]Given a jacket made by 124 elements with 2 nodes each and 8 hot spots at each chord and each brace, for a 600 seconds simulation with a time step of 0.1 seconds; the size of the stresses record is 190.464 MB of memory for one single load case.

the SCFs. Those limits are normalized to match the shape of the structural constraints and included as dimensional constraints for every joint:

$$\left\{\begin{array}{c} g_{\beta m} = 0.2 - \dfrac{d}{D} \leq 0 \\ \\ g_{\beta M} = \dfrac{d}{D} - 1.0 \leq 0 \end{array}\right\} \left\{\begin{array}{c} g_{\tau m} = 0.2 - \dfrac{t}{T} \leq 0 \\ \\ g_{\tau M} = \dfrac{t}{T} - 1.0 \leq 0 \end{array}\right\}$$

$$\left\{\begin{array}{c} g_{\gamma m} = \dfrac{1}{4} - \dfrac{D}{64T} \leq 0 \\ \\ g_{\gamma M} = \dfrac{D}{64T} - 1.0 \leq 0 \end{array}\right\} \left\{\begin{array}{c} g_{\alpha m} = \dfrac{1}{10} - \dfrac{L}{20D} \leq 0 \\ \\ g_{\alpha M} = \dfrac{L}{20D} - 1.0 \leq 0 \end{array}\right\} \tag{3.33}$$

$$\left\{\begin{array}{c} g_{\theta m} = \dfrac{4}{9} - \dfrac{4\theta}{\pi} \leq 0 \\ \\ g_{\theta M} = \dfrac{4\theta}{\pi} - 1.0 \leq 0 \end{array}\right\}$$

where $d$ and $t$ are the diameter and thickness of the brace and $D$ and $T$ of the chord that converge at the joint. The length of the chord is $L$ and the angle between chord and brace is $\theta$.

**Frequency constraints**

Offshore wind turbines are particularly dynamic sensitive due to the multiple cyclic loading and forcing frequencies. There are two typical forcing frequencies, the first is the rotational frequency of the rotor usually called 1P. In addition, the tower dam and shadow effect of the blade passing in front of the tower causes a drop in the upstream wind velocity, as seen in the previous chapter, generating another excitation frequency called the blade-passing frequency or 3P.

The design recommendation is to keep the first natural frequencies of the structure between the 1P and the 3P frequencies with a 10% margin. Figure 3.3a draws the Campbell diagram for a 5MW offshore wind turbine that represents the 1P and 3P frequencies with respect to the rotor speed and the allowable natural frequencies for the structure. There are three valid regions (soft-soft, soft-stiff, stiff-stiff) and jacket's designs are usually conceived to fall in the soft-stiff region. The soft-soft and stiff-stiff regions are typically avoided as one is close to the wave's peak frequencies and the other implies an over-stiffed structure.

Thereby if the structure needs to be designed to fall into the soft-stiff region its first natural frequencies need to be limited by the upper 1P frequency and by the lower 3P frequency plus the 10% margin, $(\omega_{1P}, \omega_{3P})$. The common practice is to limit the first two natural frequencies, thus:

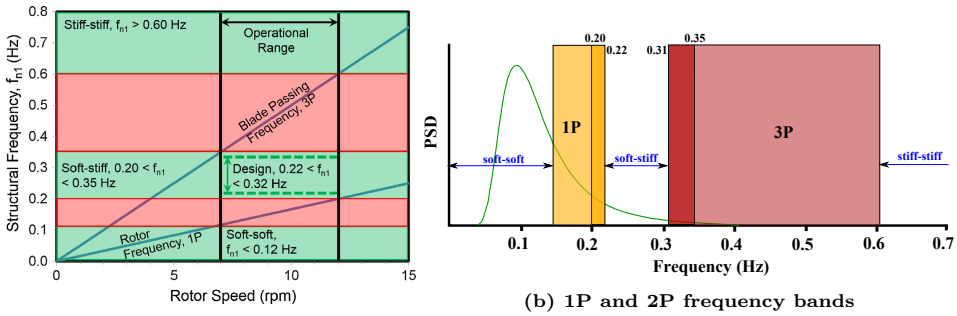


(a) Campbell diagram.

(b) 1P and 2P frequency bands

**Figure 3.3. Campbell diagram for the NREL 5MW turbine [Myers et al., 2015] and 1P and 2P frequency bands.**

$$\begin{aligned} \omega_{1P} \leq \omega_1 \leq \omega_{3P} \\ \omega_{1P} \leq \omega_2 \leq \omega_{3P} \end{aligned} \tag{3.34}$$

Once again, to express restrictions of (3.34) as constraints they are normalized. Thus:

$$\left\{ \begin{array}{l} g_{\omega 1m} = 1.0 - \dfrac{\omega_1}{\omega_{1P}} \leq 0 \\ g_{\omega 1M} = \dfrac{\omega_1}{\omega_{3P}} - 1.0 \leq 0 \end{array} \right\} \qquad \left\{ \begin{array}{l} g_{\omega 2m} = 1.0 - \dfrac{\omega_2}{\omega_{1P}} \leq 0 \\ g_{\omega 2M} = \dfrac{\omega_2}{\omega_{3P}} - 1.0 \leq 0 \end{array} \right\} \tag{3.35}$$

### 3.2.3. Design variables

The optimization variables or design variables are the properties of the structure allowed to change seeking to improve the design. Structural optimization problems are often classified according to the particular property described by these design variables as Size, Shape or Topology optimization. In sizing optimization the overall geometry of the structure is held constant and the design variables are dimensions of specific elements or particular parts of the structure. In shape optimization the contour or some geometric parameters of the structure are the design variables although the connectivity is kept constant. Finally, topology optimization is the most general form where the complete distribution of material in the structure is optimized.

Even though the ideal would be to perform a topology optimization to achieve the best typology and shape of the structure, we are far from being able to apply or even pose the until now described problem in terms of a topology optimization problem.

Leaving topology optimization behind we could still perform a size or shape optimization or a combined size and shape optimization. The latter is the approach proposed in this thesis.

For the size optimization of the jacket structure the dimensions of the cross-sections of the tubular elements are chosen as design variables. In this case there are two separated design variables for each element, $D_i$ and $t_i$, diameter and thickness respectively.

For the shape optimization part one could think that, since jackets are framed type structures conformed by discrete bars connected at joints, the reasonable approach could be to use the three dimensional coordinates of the joints as design variables. While this might be partially true and actually feasible, that strategy would probably lead to conceptually complicated structures and harder to construct in practice. So, a more restricted approach where the geometrical design variables are still able to change the overall geometry of the structure needs to be proposed. In this thesis the design variables for the shape optimization of the jacket are chosen similar to those of [Martínez, 2012]. The work is focused on the optimization of truss structures for power transmission towers. The towers are described by a finite number of blocks of bars and the horizontal dimensions of those blocks are taken as shape design variables.

However, that formulation is not directly applied here as changing the horizontal dimensions of each block independently destroys the straight profile of the main legs of the structure. While this could be assumed in [Martínez, 2012], it is unsuited for jackets since the rigid joints between tubular elements would tremendously increase its complexity. It would be harder to define which bars act as chords and which as braces. In fact, there would be no chord as there would be no continuous element in the joint. Furthermore, one joint could change its classification due to the changes in the angles[4].

Based on those reasons, in this thesis only the horizontal dimensions of the bottom and the top of the jacket ($\mu_B, \mu_T$) are considered as shape design variables. This surely limits the scope of the proposed formulation but guarantees constructional simplicity.

This thesis considers four-legged jackets which have rotational symmetry of 90° with respect to the vertical axis. Thus, bottom and top base are square-shaped and elements of the same type at the same height share cross-section. In summary, the proposed optimization problem has $2 \times$ number of different elements $+ 2$ design variables.

A typical size optimization problem for truss or framed steel structures, if intended to be realistic, needs to take under consideration the fact that steel profiles are delivered according to a certain catalog, so only specific dimensions of the profile can be acquired. However, the tubular elements that conform the support structures of wind turbines do not respond to that kind of catalog, but rather are fabricated on demand from steel plates of the required thickness to be then bent and welded to form the shape of the circular cross-section. Thereby the $D$ and $t$ design variables can be considered continuous as well as the geometrical design variables, which simplifies the handling of the optimization problem and opens the range of possible optimization algorithms to be applied.

[4]For example, a K joint in which the angle between the two sides of the chord decreases could end up being an X joint. Joint classification can be consulted in Appendix A.

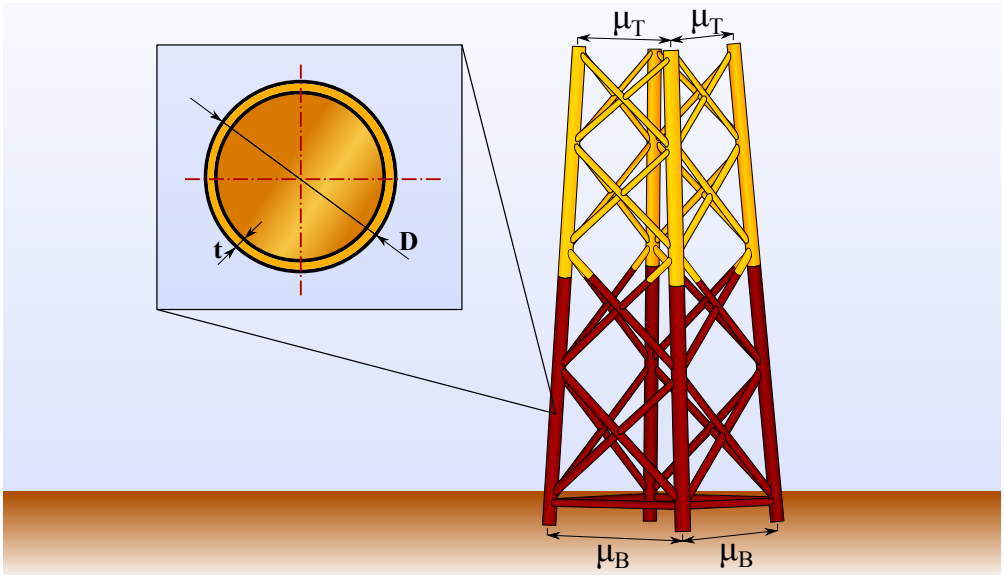


**Figure 3.4. Optimization design variables.**

## 3.3. Time-dependent constraints handling

So far we have been stealthily keeping ourselves away from a key issue. The fact that we are dealing with a structural dynamics problem and thus the response of the structure is computed at each time step. That means that the stresses and by consequence the constraints that depend on those stresses are time-dependent. It represents no change to the fatigue limit state constraint and the frequency constraint, but the ultimate limit state constraints have to be treated differently as we have different responses of the structure for each time step.

This is one of the three major topics in dynamic structural optimization, that are:

- The treatment of the time-dependent constraints.
- The sensitivity analysis.
- The approximation, which tries to avoid the computational effort of computing the dynamic response by approximating it.

This section is intended to deal with the first of the above points. The second will be treated in the next chapter and the third is not included in this thesis as the response of the jacket structure will not be approximated but directly computed.

### 3.3.1. Short review of time-dependent constraints treatment

Regarding the treatment of the time-dependent constraints there are a set of strategies each of them with their advantages and drawbacks. The following is an attempt

to summarize the main techniques, for further reading one can consult the extensive works of J.S. Arora [Wang & Arora, 2005; Kang et al., 2006; Wang & Arora, 2009].

### Pointwise constraints

The simplest option to handle time-dependent constraints is to consider all the constraints at all the time steps with an active strategy. A threshold value is set to define if a constraint is active or not. The constraints are then computed at every time step and added to the active constraints set if they exceed the threshold value. This methodology can result efficient for designs not strongly constrained but is completely beyond application for problems with countless active constraints.

### Worst case approach

The worst case approach reduces the number of constraints from the number of time steps to one by only considering the point at which each constraint reaches its maximum value. The main drawback of this method is that it does not consider that the time instant at which the maximum occurs can change between iterations.

The methodology can be improved by considering not only the maximum of the constraint but all the local maximums values in time, or even considering the points near those local maximums. The absolute maximum can move between designs but it can be expected to belong to the group of local maximums or points near them.

### Equivalent functional

Each constraint is reduced again to one but by considering an equivalent functional that integrates all the time record of the constraint. The functional is:

$$\int_0^T < g(\boldsymbol{x},t) > dt \leq 0 \quad \text{with} \quad < g(\boldsymbol{x},t) >= \begin{cases} 0 & \text{if} \quad g < 0 \\ g & \text{if} \quad g \geq 0 \end{cases} \tag{3.36}$$

The satisfaction of equation (3.36) is equivalent to the fulfillment of the constraints, however, the equivalent functional is not smooth with respect to the design variables and it is often unstable [Hsieh & Arora, 1984].

### Transformation method

Another completely different approach is to transform the constrained optimization problem to an unconstrained one. There are a few ways to do so but one of the most spread ones is the Augmented Lagrangian Method (ALM) [Rockafellar, 1973]. The ALM is less efficient compared to the above mentioned methods, which are classified as direct methods, when dealing with large scale problems since the augmented function of the unconstrained problem is formed by an integrate of all the constraints.

### 3.3.2. Constraint aggregation functions and proposed method

The pointwise constraint strategy is directly rejected, not only by its main drawback but because we have to remember that the simulation for the jacket is 600 seconds long with $\Delta t$ around 0.1 seconds. The former means that, for each bar of the jacket the model ends up with 6000 constraint values just for one ULS constraint and a single load case. Not all the values are considered since only the active constraints do, but one single constraint may be active at many time steps or even during the whole simulation. If we add that up to the fatigue life constraint that is computed for 8 spots of every node of every bar, the problem can easily grow beyond manageability.

Moreover, most of the above formulations have a major issue and it is how to combine its use with sensitivity analysis and the computation of the gradients.

Alternatively, there is actually a known technique to deal with large-scale constrained mass optimization problems which has never been used to simplify the treatment of time-dependent constraints in dynamic structural optimization: Constraint aggregation functions.

Constraint aggregation is typically applied in topology optimization for weight minimization under stress constraints. The behavior of the tensional constraints is evaluated over a finite region of the structure by smooth estimating functions to guarantee that they can be used with gradient-based optimization [París, 2007; Lambe et al., 2017]. Nevertheless, the problem is obviously being changed and the design region for optimization can differ from that of the original problem.

From all the aggregation strategies, there are two classical functionals preferred, the Kreisselmeier-Steinhauser aggregation (KS) [Kreisselmeier & Steinhauser, 1979] and the $p$-norm aggregation [Duysinx & Sigmund, 1998]. In this work the use of the Kreisselmeier-Steinhauser function is proposed to aggregate the Ultimate Limit State constraints in time.

The original continuous formulation of the KS function was:

$$KS(g,\rho) = \frac{1}{\rho}\ln\left(\int_{\Omega} e^{\rho g} d\Omega\right) \tag{3.37}$$

where $g$ is the constraint being aggregated, $\Omega$ is the domain and $\rho$ is a parameter of the KS function.

The discrete approach of (3.37) is analogous:

$$KS(g,\rho) = \frac{1}{\rho}\ln\left(\sum_{i=1}^{n_g} e^{\rho g_i}\right) \tag{3.38}$$

being $n_g$ the number of constraints $g_i$ being aggregated.

The selection of $\Omega$, or $n_g$ in the finite approach, allows the aggregation of constraints separated in different locations of the structure in typical topology optimization. Thus the structure can be divided in subdomains where the local constraints are treated by blocks or semi-globally [París et al., 2009, 2010]. However, in this thesis the KS function is intended to aggregate constraints in the time domain and the aggregation

by blocks losses sense. Thus, the aggregation of the constraints is extended over the whole time domain.

The global constraint using the KS function for the total number of time steps ($N_T = T/\Delta t$) is then:

$$G^j_{KS} = \frac{1}{\rho} \ln \left( \sum_{i=1}^{N_T} e^{\rho g_j(\boldsymbol{x}, t_i)} \right) - \frac{1}{\rho} \ln(N_T) \tag{3.39}$$

The main advantages of using the constraint aggregation function are:

- Large-scale constrained optimization problems are reduced.
- The global constraints introduced are continuously differentiable and suitable for gradient-based optimization.
- The global constraint retains information about all the constraints, active or not.

In essence, the KS function contains information about all the constraints but weighting them and giving more importance to the most violated or active constraints. The greater the value of $\rho$ the greater the influence of the violated constraints compared to others. In the limit $\rho \to \infty \Leftrightarrow \frac{1}{\rho} \to 0$, the function is equivalent to the worst case methodology. However it still holds information about other constraints while the worst case approach can not.

Actually, the value of $\rho$ has major influence on the optimized design and the behavior of the aggregated constraint and how accurately it represents the information of all the constraints. There are approaches where the values of $\rho$ are calculated with an adaptive approach and it is increased during the optimization process in order to get close to the function $max\{g_i\}$ [James et al., 2009]. The increase can also be performed unconditionally or based on the sensitivity of the KS function with respect to the parameter $\rho$.

In order to select $\rho$ the behavior of $G_{KS}$ is studied. Taking an example model with a number of constraints similar to that of the problem we are dealing with and forcing a 10% of them to be violated while the rest remains inactive. Figure 3.5 shows how the $G_{KS}$ function responds when a certain value for the violation of the constraints is imposed.

As mentioned, the greater the value of $\rho$ the closest the function is to the maximum value of $g_i$. For low values it is also perceived that the KS function does not represent accurately the behavior of the constraints as there are a 10% violated and the function does not dictate so. Expecting a reasonable allowance of 2% for each local constraint at least values of $\rho = 150$ have to be taken. Recall that we need to choose values of the parameter sufficiently large to detect the violations of the constraints but not too much that the KS function is excessively nonlinear and could produce unstable convergence.

In figure 3.6 it is shown how as the number of violated constraints increases the requisites for $\rho$ relax since those violated constraints begin to gain importance in the design by themselves without the need for an artificial exponential function.

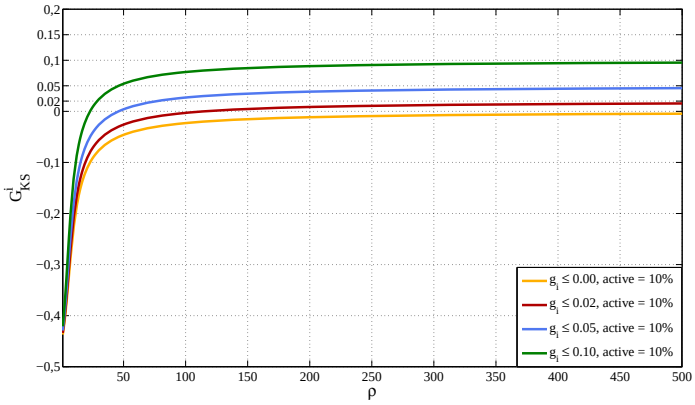


**Figure 3.5.** $\rho$ **influence with 10% constraints active.**

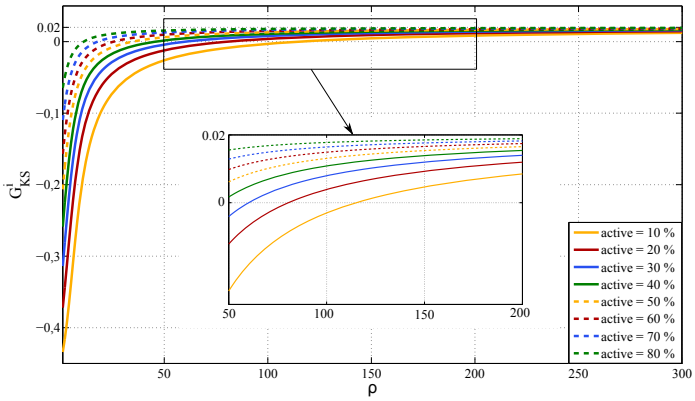


**Figure 3.6.** $\rho$ **influence allowing 2% violation of the constraints.**

## 3.4. Summary and conclusions

Structural optimization is meant to give the best fitted response to a particular structural problem. In order to reach the perfectly suited design, the mathematical problem has to be flawlessly defined and matched with the actual requisites the structure needs to meet. The field of offshore structures optimization is yet to be deeply explored and many works start to arise.

This chapter reflects the mathematical definition of the optimization problem of jacket structures for offshore wind turbines. The optimization is focused on a combined size and shape weight minimization. For doing so, the design variables represent the overall geometry of the substructure and the dimensions that determine the cross-section of the members.

The requirements upon the structure are translated to optimization constraints of three main types. The ULS constraints are imposed to limit the stress level of the bars specially under maximum loading. The combined action of forces is taken into account as well as buckling effects in compressed members. The FLS constraint is devoted to keep the fatigue damage of the welded joints due to cyclic loading under safety margins. The fatigue constraint comes with additional dimensional restrictions which limit particular geometrical parameters of the joints to guarantee the validity of the SCFs. Last but not least, there are four frequency constraints that impose minimum and maximum values for the first two natural frequencies of the structure to avoid specific known excitation frequencies of the rotor and the rotation of the blades.

There is one major problem with all that. There is one fatigue life constraint for each hot-spot of the welded joints. There are 4 frequency constraints. And there are from 3 to 6 ULS constraints for each tubular element and for each load case but, more important, for each time step. That is one of the key aspects in dynamic response optimization of structures. Several techniques are available to handle time-dependent constraints but none seem to be adequate for the proposed problem.

In this thesis a new approach for the treatment of time-dependent constraints in dynamic response optimization of structures is proposed based on constraint aggregation functions typically used in topology optimization. Particularly, the Kreisselmeier-Steinhauser aggregation function is used to transform the individual per step constraints to global constraints over the whole time domain. The proposed method allows to reduce the optimization problem without loosing too much information about the behavior of the constraints and also being compatible with sensitivity analysis.

Making the numbers for an average jacket formed by 124 elements we have 3968 fatigue constraints, 1392 dimensional constraints from the SCFs limitations and 4 frequency constraints. If we consider the 10 min minimum simulation required with a time step of 0.1 s we end up with 8 928 000 ULS constraints for each load case. Reducing the number of ULS constraints with the aggregation function leads to only 744 restrictions for each load case making the solution of the optimization problem available and reachable.

The differentiation of the constraints for sensitivity analysis purposes, explained in the following chapter, would be completely unaffordable in terms of memory storage if it was not for the implementation of the constraint aggregation technique.

Chapter 4

# Sensitivity analysis

*"The pessimist looks down and hits his head. The optimist looks up and loses his footing. The realist looks forward and adjusts his path accordingly."*
**Robert Kirkman**, The Walking Dead.

## 4.1. Introduction

Sensitivity analysis is common in structural optimization methods. Not only is needed due to the non-convex and nonlinear character of the design region to apply the most common algorithms but it gives quantitative measure of how the functions, that define and control the problem, depend on the design variables and parameters of the problem. In our case, the sensitivity analysis means computing the derivatives of the objective function and the constraints with respect to the design variables. There are a few ways of computing these derivatives but one thing is clear, the sensitivity analysis represents a significant (if not predominant) part of the computational time involved and a huge amount of storage needed for all the derivatives with respect to each variable.

We will get back to that later.

The chapter is organized sequentially in the sense that, the first derivatives presented may seem unjustified but upcoming sections will need those expressions.

It is important to remember that the design variables defined in the statement of the optimization problem are the dimensions that define the cross-sections of the bars $(D_i, t_i)$ and the bottom and top widths of the jacket $(\mu_B, \mu_T)$.

## 4.2. Notation

Before starting to explicit the sensitivities of all the functions involved in the optimization problem we have to introduce a few things. First, the notation in the following

sections will be as follows:

Let $\boldsymbol{\xi}$ be the vector of design variables:

$$\boldsymbol{\xi} = \left\{ \begin{array}{c} \xi_1 \\ \xi_2 \\ \vdots \\ \xi_n \end{array} \right\} \tag{4.1}$$

And let $f(\boldsymbol{\xi}) = f(\xi_1, \xi_2, \ldots, \xi_n)$ be any function that depends on the design variables. Then its sensitivity or derivative with respect to the design variables can be expressed as:

$$\frac{df}{d\boldsymbol{\xi}} = \nabla f = \left\{ \frac{\partial f}{\partial \xi_1}, \frac{\partial f}{\partial \xi_2}, \ldots, \frac{\partial f}{\partial \xi_n} \right\} \tag{4.2}$$

Let $\boldsymbol{s}$ be any direction of modification of the design variables so that:

$$\boldsymbol{\xi}^{k+1} = \boldsymbol{\xi}^k + \theta^k \boldsymbol{s}^k \tag{4.3}$$

Then, we define the directional derivative [Navarrina & Casteleiro, 1991] of any function $f(\boldsymbol{\xi})$ as:

$$D_s f = \frac{df}{d\boldsymbol{\xi}} \frac{d\boldsymbol{\xi}}{d\theta} = \frac{df}{d\boldsymbol{\xi}} \boldsymbol{s} \tag{4.4}$$

Similarly, for any $\boldsymbol{F}(\boldsymbol{\xi})$ like:

$$\boldsymbol{F}(\boldsymbol{\xi}) = \left\{ \begin{array}{c} F_1(\xi_1, \xi_2, \ldots, \xi_n) \\ F_2(\xi_1, \xi_2, \ldots, \xi_n) \\ \vdots \\ F_m(\xi_1, \xi_2, \ldots, \xi_n) \end{array} \right\} \tag{4.5}$$

Its sensitivity and thus its directional derivative:

$$\frac{d\boldsymbol{F}}{d\boldsymbol{\xi}} = \nabla \boldsymbol{F} = \left( \begin{array}{cccc} \frac{\partial F_1}{\partial \xi_1} & \frac{\partial F_1}{\partial \xi_2} & \cdots & \frac{\partial F_1}{\partial \xi_n} \\ \frac{\partial F_2}{\partial \xi_1} & \frac{\partial F_2}{\partial \xi_2} & \cdots & \frac{\partial F_2}{\partial \xi_n} \\ \vdots & \vdots & \ddots & \vdots \\ \frac{\partial F_m}{\partial \xi_1} & \frac{\partial F_m}{\partial \xi_2} & \cdots & \frac{\partial F_m}{\partial \xi_n} \end{array} \right) \rightarrow D_s \boldsymbol{F} = \left\{ \begin{array}{c} D_s F_1 \\ D_s F_2 \\ \vdots \\ D_s F_m \end{array} \right\} = \frac{d\boldsymbol{F}}{d\boldsymbol{\xi}} \frac{d\boldsymbol{\xi}}{d\theta} = \frac{d\boldsymbol{F}}{d\boldsymbol{\xi}} \boldsymbol{s} \tag{4.6}$$

The directional derivative represents the derivative of any given function with respect to a particular design variable represented by the direction $\boldsymbol{s}$. Note that, the

problem has as many possible directions of derivation as design variables, and the components of the full gradient of the function are all the directional derivatives.

In this chapter elemental derivatives, say those of the lowest level of derivation, are expressed simply as a derivative with respect to any design variable $\xi$ unspecified, whereas derivatives in the general formulation of the sensitivities are expressed with the most general notation using the concept of directional derivatives of (4.4).

## 4.3. Differentiation method

When facing the solution of the sensitivities of the problem, two possibilities arise: Direct Differentiation and the Adjoint State Method. In order to decide which of the methods is best here let us first introduce the general statement of the analysis and optimization problem which is depicted in figure 4.1.

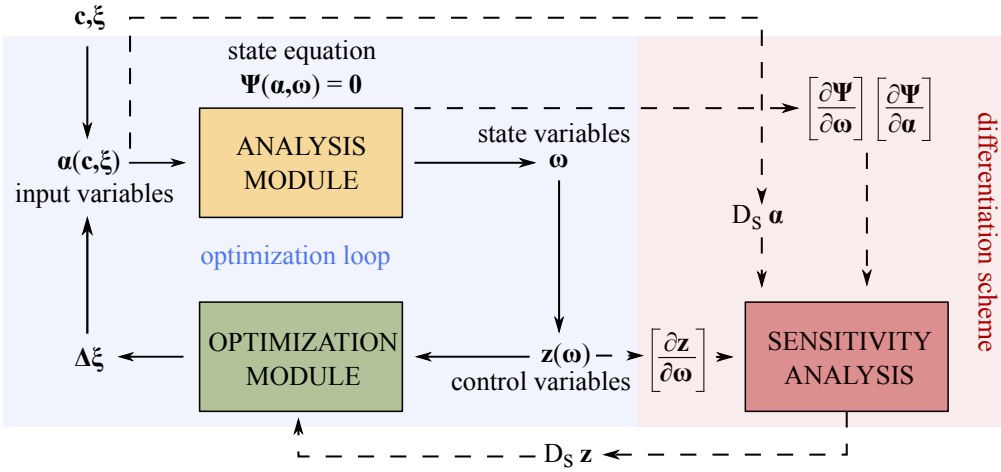


**Figure 4.1. General data flow in an analysis and design optimization numerical implementation.**

For any optimization problem we can separate the variables that define the design between design constants $\boldsymbol{c}$ and design variables $\boldsymbol{\xi}$. However, the analysis module usually requires the information to be supplied in a certain shape $\boldsymbol{\alpha}(\boldsymbol{c},\boldsymbol{\xi})$. The outputs of the analysis are usually called state variables $\boldsymbol{\omega}$ although, they do not have to match those needed by the optimization module. Those are called control variables $\boldsymbol{z}(\boldsymbol{\omega})$ and constitute the magnitudes that allow to measure the betterness or validity of the design. Then, the optimization methodology finds a direction of modification of the design variables $\boldsymbol{\Delta\xi}$, the input variables are recalculated and the whole process start right over. This is called optimization loop.

Many optimization algorithms need information about the sensitivities of the control variables so they can decide which direction to take. Generally, the first order sensitivities help finding the direction of modification of the design variables and the

second order sensitivities are computed to achieve the amplitude of variation, or length of modification of the variables along the obtained direction. That information is provided by what is called sensitivity analysis.

So, in summary, we need the sensitivities or derivatives of the control variables $D_s\boldsymbol{z}$, which are derived as:

$$D_s\boldsymbol{z} = \frac{\partial \boldsymbol{z}}{\partial \boldsymbol{\omega}}\, D_s\boldsymbol{\omega} \tag{4.7}$$

Derivatives of the control variables with respect to the state variables $\boldsymbol{\omega}$ are straightforward however, we need the directional derivative of those state variables coming out of the analysis module. For that, we need to differentiate the state equation as [Navarrina et al., 2012]:

$$D_s\boldsymbol{\Psi} = \mathbf{0} \Leftrightarrow \left[\frac{\partial \boldsymbol{\Psi}}{\partial \boldsymbol{\alpha}}\right] D_s\,\boldsymbol{\alpha} + \left[\frac{\partial \boldsymbol{\Psi}}{\partial \boldsymbol{\omega}}\right] D_s\boldsymbol{\omega} = \mathbf{0} \tag{4.8}$$

which means solving the following systems of equations:

$$\left[\frac{\partial \boldsymbol{\Psi}}{\partial \boldsymbol{\omega}}\right] D_s\boldsymbol{\omega} = -\left[\frac{\partial \boldsymbol{\Psi}}{\partial \boldsymbol{\alpha}}\right] D_s\,\boldsymbol{\alpha} \tag{4.9}$$

Thus, to solve the above systems we have to derive the input variables $D_s\boldsymbol{\alpha}$. Then the arranged process would be:

1. Compute the derivative of the input variables. $\longrightarrow D_s\boldsymbol{\alpha}$
2. Solve the derivatives of the state variables of (4.8) for each possible direction of sensitivity $\boldsymbol{s}$. $\longrightarrow D_s\boldsymbol{\omega}$
3. Obtain the sensitivities of the control variables from (4.7). $\longrightarrow D_s\boldsymbol{z}$

The above methodology of differentiation is known as Direct Differentiation and it involves the solution of as many systems of equations as directions of sensitivities or design variables $n$.

However, we can slightly modify the above process. We can in fact, express the derivative of the state variables as:

$$D_s\boldsymbol{\omega} = -\left[\frac{\partial \boldsymbol{\Psi}}{\partial \boldsymbol{\omega}}\right]^{-1} \left[\frac{\partial \boldsymbol{\Psi}}{\partial \boldsymbol{\alpha}}\right] D_s\,\boldsymbol{\alpha} \tag{4.10}$$

and then, directly introduce it in (4.7) to obtain:

$$D_s\boldsymbol{z} = -\underbrace{\frac{\partial \boldsymbol{z}}{\partial \boldsymbol{\omega}}\left[\frac{\partial \boldsymbol{\Psi}}{\partial \boldsymbol{\omega}}\right]^{-1}}_{\boldsymbol{\mu}_z^t} \left[\frac{\partial \boldsymbol{\Psi}}{\partial \boldsymbol{\alpha}}\right] D_s\,\boldsymbol{\alpha} \tag{4.11}$$

Finally, the sensitivities of the control variables would be:

$$D_s \boldsymbol{z} = \boldsymbol{\mu}_z^t \left[\frac{\partial \boldsymbol{\Psi}}{\partial \boldsymbol{\alpha}}\right] D_s\, \boldsymbol{\alpha} \tag{4.12}$$

where $\boldsymbol{\mu}_z^t$ is called the adjoint state and is obtained solving:

$$\left[\frac{\partial \boldsymbol{\Psi}}{\partial \boldsymbol{\omega}}\right]^t \boldsymbol{\mu}_z = -\left(\frac{\partial \boldsymbol{z}}{\partial \boldsymbol{\omega}}\right)^t \tag{4.13}$$

In summary, the rearranged process would be:

1. Compute the derivative of the input variables. $\longrightarrow D_s\boldsymbol{\alpha}$
2. Solve the adjoint state of (4.13) for each control variable $z$. $\longrightarrow \boldsymbol{\mu}_z^t$
3. Obtain the sensitivities of the control variables from (4.12). $\longrightarrow D_s\boldsymbol{z}$

The latter is called the Adjoint State Method and it involves the solution of as many systems of equations as control variables the optimization problem has $(m)$.

Both methods are quite similar in terms of actual derivatives to compute and the major difference between them is the number of systems of equations to solve. So the decision of which method is best suited for a particular problem lies on the comparison between the number of design variables $n$ and the number of control variables $m$ [Navarrina et al., 2000]. The number of control variables is related to the number of constraints of the problem. While there are optimization problems where the number of constraints might be lower than the number of design variables, that is not usual at all in structural optimization. Particularly, our problem, as it has been described in chapter 3, has a very limited number of design variables while thousands of constraints. So in this case, Direct Differentiation is clearly advantageous before the Adjoint State Method by far.

## 4.4. Elemental derivatives

This section describes the derivatives of the most basic expressions that depend on the design variables, which are: the mechanical properties of the cross-sections, the length of the elements and the structural matrices whose coefficients are functions of those properties.

All the elemental derivatives are analytically differentiated as they are explicit expressions of the design variables.

In the following $\xi$ will represent any design variable, then:

$$\frac{\partial D_i}{\partial \xi} = \begin{cases} 0 & \text{if} \quad \xi \neq D_i \\ 1 & \text{if} \quad \xi = D_i \end{cases} \qquad \frac{\partial t_i}{\partial \xi} = \begin{cases} 0 & \text{if} \quad \xi \neq t_i \\ 1 & \text{if} \quad \xi = t_i \end{cases} \tag{4.14}$$

where $D_i$ and $t_i$ represent the diameter and thickness of i-$th$ element.

### 4.4.1. Mechanical properties derivatives

The mechanical properties of the elements are the cross-sectional area and moments of inertia of the tubular members ($A_i, I_i^y = I_i^z, J_i$)

$$A_i = \frac{\pi}{4}\left(D_i^2 - (D_i - 2t_i)^2\right) \tag{4.15}$$

$$I_i^y = I_i^z = \frac{\pi}{64}\left(D_i^4 - (D_i - 2t_i)^4\right) \tag{4.16}$$

$$J_i = \frac{\pi}{128}\left(D_i^4 - (D_i - 2t_i)^4\right) \tag{4.17}$$

Their corresponding derivatives are:

$$\frac{\partial A_i}{\partial \xi} = \pi\left(t\frac{\partial D_i}{\partial \xi} + (D_i - 2t_i)\frac{\partial t_i}{\partial \xi}\right) = \begin{cases} \pi t_i & \text{if} \quad \xi = D_i \\ \pi(D_i - 2t_i) & \text{if} \quad \xi = t_i \\ 0 & \text{if} \quad \xi \neq D_i, t_i \end{cases} \tag{4.18}$$

$$\begin{aligned} \frac{\partial I_i^y}{\partial \xi} = \frac{\partial I_i^z}{\partial \xi} &= \frac{\pi}{16}\left(D_i^3\frac{\partial D_i}{\partial \xi} - (D_i - 2t_i)^3\left(\frac{\partial D_i}{\partial \xi} - 2\frac{\partial t_i}{\partial \xi}\right)\right) \\ &= \begin{cases} \frac{\pi}{16}\left(D_i^3 - (D_i - 2t_i)^3\right) & \text{if} \quad \xi = D_i \\ \frac{\pi}{8}(D_i - 2t_i)^3 & \text{if} \quad \xi = t_i \\ 0 & \text{if} \quad \xi \neq D_i, t_i \end{cases} \end{aligned} \tag{4.19}$$

$$\begin{aligned} \frac{\partial J_i}{\partial \xi} &= \frac{\pi}{32}\left(D_i^3\frac{\partial D_i}{\partial \xi} - (D_i - 2t_i)^3\left(\frac{\partial D_i}{\partial \xi} - 2\frac{\partial t_i}{\partial \xi}\right)\right) \\ &= \begin{cases} \frac{\pi}{32}\left(D_i^3 - (D_i - 2t_i)^3\right) & \text{if} \quad \xi = D_i \\ \frac{\pi}{16}(D_i - 2t_i)^3 & \text{if} \quad \xi = t_i \\ 0 & \text{if} \quad \xi \neq D_i, t_i \end{cases} \end{aligned} \tag{4.20}$$

### 4.4.2. Length derivative

The length of the elements depends directly on the coordinates of the nodes of the structure that depend on the shape design variables ($\mu_B, \mu_T$).

Any element's length can be obtained from the coordinates of its nodes as:

$$L_i = \sqrt{(X_{i,2} - X_{i,1})^2 + (Y_{i,2} - Y_{i,1})^2 + (Z_{i,2} - Z_{i,1})^2} \tag{4.21}$$

We can differentiate the above expression as:

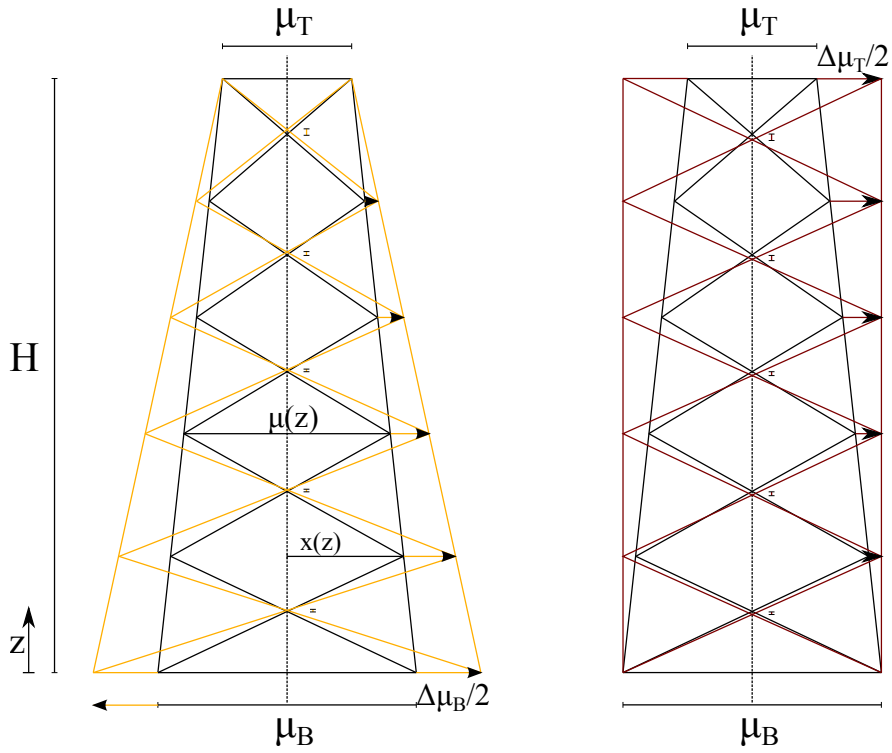


**Figure 4.2. Variation of the coordinates with respect to the geometrical design variables.**

$$\begin{aligned}\frac{\partial L_i}{\partial \xi} = \; & \frac{1}{2}\left((X_{i,2}-X_{i,1})^2+(Y_{i,2}-Y_{i,1})^2+(Z_{i,2}-Z_{i,1})^2\right)^{-1/2} \\ & \left[2(X_{i,2}-X_{i,1})\left(\frac{\partial X_{i,2}}{\partial \xi}-\frac{\partial X_{i,1}}{\partial \xi}\right)+2(Y_{i,2}-Y_{i,1})\left(\frac{\partial Y_{i,2}}{\partial \xi}-\frac{\partial Y_{i,1}}{\partial \xi}\right)\right. \\ & \left.+2(Z_{i,2}-Z_{i,1})\left(\frac{\partial Z_{i,2}}{\partial \xi}-\frac{\partial Z_{i,1}}{\partial \xi}\right)\right] = \\ & \frac{1}{L_i}\left[(X_{i,2}-X_{i,1})\left(\frac{\partial X_{i,2}}{\partial \xi}-\frac{\partial X_{i,1}}{\partial \xi}\right)+(Y_{i,2}-Y_{i,1})\left(\frac{\partial Y_{i,2}}{\partial \xi}-\frac{\partial Y_{i,1}}{\partial \xi}\right)\right. \\ & \left.+(Z_{i,2}-Z_{i,1})\left(\frac{\partial Z_{i,2}}{\partial \xi}-\frac{\partial Z_{i,1}}{\partial \xi}\right)\right]\end{aligned} \tag{4.22}$$

Thus, we need the derivatives of the coordinates with respect to the design variables. We can then analyze how the coordinates change with the modification of the widths of the top and bottom bases. Figure 4.2 shows the geometrical changes with each modification of the variables. It is worth saying that the modification of the dimensions does not affect the height of the intersections between the X braces and the legs. However, the central intersection between the two braces forming the X does change its vertical coordinate in order to keep the straight alignment of the bars.

If we also want to keep the straight line of the legs of the jacket we can define the equation of the $X$ coordinate of the legs at any height $Z$. Also, the origin is set in the center of the jacket then $X(Z) = \mu(Z)/2$.

$$\mu(Z) = \frac{\mu_B - \mu_T}{H} + \mu_B \longrightarrow X(Z) = \frac{Z}{2}\frac{\mu_B - \mu_T}{H} + \frac{\mu_B}{2} \tag{4.23}$$

In this work we consider the jacket completely symmetric. Then the same can be applied to the $Y$ coordinate:

$$Y(Z) = \frac{Z}{2}\frac{\mu_B - \mu_T}{H} + \frac{\mu_B}{2} \tag{4.24}$$

We can now differentiate the above expressions with respect to the geometrical variables:

$$\frac{\partial X_i}{\partial \xi} = \begin{cases} \frac{1}{2}\left(1 - \frac{Z}{H}\right) & \text{if} \quad \xi = \mu_B \\ \frac{1}{2}\frac{Z}{H} & \text{if} \quad \xi = \mu_T \\ 0 & \text{otherwise} \end{cases} \qquad \frac{\partial Y_i}{\partial \xi} = \begin{cases} \frac{1}{2}\left(1 - \frac{Z}{H}\right) & \text{if} \quad \xi = \mu_B \\ \frac{1}{2}\frac{Z}{H} & \text{if} \quad \xi = \mu_T \\ 0 & \text{otherwise} \end{cases} \tag{4.25}$$

We need as well the derivative of the $Z$ coordinates. Recall that the height of the nodes of the legs does not change with the design variables but the intersection joints of the X braces do. Thus, we need to express the $Z$ coordinate of those nodes as functions of the design variables.

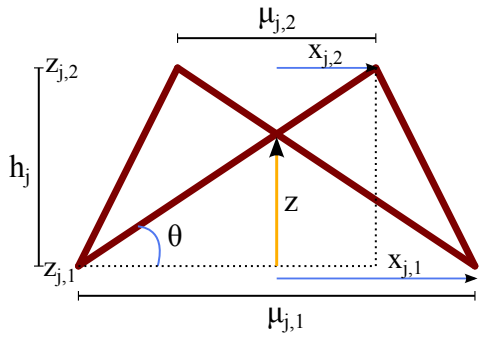


**Figure 4.3.** $Z$ **coordinate of the intersection in X joints.**

Given any block of the jacket as drawn in figure 4.3, the height of the central node can be expressed in terms of the angle $\theta$, that is:

$$\tan(\theta) = \frac{h_j}{\frac{\mu_{j,1}}{2} + \frac{\mu_{j,2}}{2}} \longrightarrow Z = Z_{j,1} + \tan(\theta)(X - X_0) \tag{4.26}$$

where $X$ is the coordinate of the center of the block and $X_0 = -\mu_{k,l}/2$

Then we can define the local coordinate $Z$ of the joint as:

$$Z = Z_{j,1} + \frac{h_j\ \mu_{j,1}}{\mu_{j,1} + \mu_{j,2}} \tag{4.27}$$

The widths of the block $\mu_{j,1}$ and $\mu_{j,2}$ can be expressed as twice the coordinate $X$ of their corresponding node on the leg then:

$$Z = Z_{j,1} + \frac{h_j\ 2X_{j,1}}{2X_{j,1} + 2X_{j,2}} \tag{4.28}$$

And those coordinates can also be derived with respect to the design variables according to (4.25), so finally, the derivative of the $z$ coordinate of the intersection nodes can be obtained as:

$$\left\{ \begin{array}{l} \dfrac{dZ}{d\mu_B} = \dfrac{\partial Z}{\partial X_{j,1}}\dfrac{dX_{j,1}}{d\mu_B} + \dfrac{\partial Z}{\partial X_{j,2}}\dfrac{dX_{j,2}}{d\mu_B} \\ \dfrac{dZ}{d\mu_T} = \dfrac{\partial Z}{\partial X_{j,1}}\dfrac{dX_{j,1}}{d\mu_T} + \dfrac{\partial Z}{\partial X_{j,2}}\dfrac{dX_{j,2}}{d\mu_T} \end{array} \right\} \Leftrightarrow$$

$$\left\{ \begin{array}{l} \dfrac{dZ}{d\mu_B} = \dfrac{h_j(X_{j,1}+X_{j,2}) - h_j X_{j,1}}{(X_{j,1}+X_{j,2})^2}\dfrac{1}{2}\left(1 - \dfrac{Z_{j,1}}{H}\right) - \dfrac{h_j X_{j,1}}{(X_{j,1}+X_{j,2})^2}\dfrac{1}{2}\left(1 - \dfrac{Z_{j,2}}{H}\right) \\ \dfrac{dZ}{d\mu_T} = \dfrac{h_j(X_{j,1}+X_{j,2}) - h_j X_{j,1}}{(X_{j,1}+X_{j,2})^2}\dfrac{1}{2}\dfrac{Z_{j,1}}{H} - \dfrac{h_j X_{j,1}}{(X_{j,1}+X_{j,2})^2}\dfrac{1}{2} - \dfrac{Z_{j,2}}{H} \end{array} \right\} \tag{4.29}$$

### 4.4.3. Structural matrices derivatives

The derivatives of the structural matrices (mass, damping and stiffness) will be later needed. In section 2.3 of chapter 2 $\boldsymbol{M}$, $\boldsymbol{C}$ and $\boldsymbol{K}$ were described and fully explained. Some of the parts may have seem unnecessary but they are referred in the chapter so now we can take use of them to differentiate all the expressions.

#### Stiffness matrix derivative

Considering the constitutive, compatibility and equilibrium equation, the elemental structural stiffness matrix could be formed and differentiated from:

$$\boldsymbol{K} = \boldsymbol{B}^t\boldsymbol{D}\boldsymbol{B} \tag{4.30}$$

or more conveniently like:

$$\left.\begin{array}{l} \boldsymbol{K} = \boldsymbol{B}^t\boldsymbol{S} \\ \\ \boldsymbol{S} = \boldsymbol{D}\boldsymbol{B} \\ \\ \boldsymbol{B} = \boldsymbol{E}\boldsymbol{T} \end{array}\right\} \Rightarrow \begin{array}{l} D_s\boldsymbol{K} = D_s\boldsymbol{B}^t\boldsymbol{S} + \boldsymbol{B}^t \quad D_s\boldsymbol{S} \\ \qquad\qquad\qquad\qquad\quad \swarrow \\ D_s\boldsymbol{S} \quad = D_s\boldsymbol{D}\boldsymbol{B} + \boldsymbol{D} \quad D_s\boldsymbol{B} \\ \qquad\qquad\qquad\qquad\quad \swarrow \\ D_s\boldsymbol{B} \quad = D_s\boldsymbol{E}\boldsymbol{T} + \boldsymbol{E}D_s\boldsymbol{T} \end{array} \tag{4.31}$$

So, from bottom up, we only need $D_s\boldsymbol{E}$, $D_s\boldsymbol{T}$ and $D_s\boldsymbol{D}$ to construct the derivative of the elemental stiffness matrix.

The derivative of $\boldsymbol{E}$ (2.15) with respect to a given design variable $\xi$ is:

$$\frac{\partial \boldsymbol{E}}{\partial \xi} = \frac{1}{L^2}\frac{\partial L}{\partial \xi}\begin{pmatrix} 0 & 0 & 0 & 0 & 0 & 0 & 0 & 0 & 0 & 0 & 0 & 0 \\ 0 & 0 & 1 & 0 & 0 & 0 & 0 & 0 & -1 & 0 & 0 & 0 \\ 0 & 0 & 1 & 0 & 0 & 0 & 0 & 0 & -1 & 0 & 0 & 0 \\ 0 & 0 & 0 & 0 & 0 & 0 & 0 & 0 & 0 & 0 & 0 & 0 \\ 0 & -1 & 0 & 0 & 0 & 0 & 0 & 1 & 0 & 0 & 0 & 0 \\ 0 & -1 & 0 & 0 & 0 & 0 & 0 & 1 & 0 & 0 & 0 & 0 \end{pmatrix} \tag{4.32}$$

The above derivative has only components with respect to the geometrical variables as it only depends on the length of the elements.

In order to differentiate the transformation matrix $\boldsymbol{T}$ (2.16) we need to differentiate matrix $\boldsymbol{R'}$, for which we have two expressions, (2.7) and (2.10). However, (2.10) is used only for the rotating elements of the turbine blades that do not depend on the design variables and so have null derivative. Additionally, (2.7) considers an angle of roll $\varphi$ that is irrelevant when dealing with tubular cross-sections. So the angle of roll can be neglected and we only need to differentiate the simplest transformation matrix given by (2.4).

The derivatives needed for each component of the matrix are:

$$\frac{\partial r_{xX}}{\partial \xi} = \frac{1}{L^2}\left(\left(\frac{\partial X_2}{\partial \xi} - \frac{\partial X_1}{\partial \xi}\right)L - (X_2 - X_1)\frac{\partial L}{\partial \xi}\right) \tag{4.33}$$

$$\frac{\partial r_{xY}}{\partial \xi} = \frac{1}{L^2}\left(\left(\frac{\partial Y_2}{\partial \xi} - \frac{\partial Y_1}{\partial \xi}\right)L - (Y_2 - Y_1)\frac{\partial L}{\partial \xi}\right) \tag{4.34}$$

$$\frac{\partial r_{xZ}}{\partial \xi} = \frac{1}{L^2}\left(\left(\frac{\partial Z_2}{\partial \xi} - \frac{\partial Z_1}{\partial \xi}\right)L - (Z_2 - Z_1)\frac{\partial L}{\partial \xi}\right) \tag{4.35}$$

where $(X_1, Y_1, Z_1)$ and $(X_2, Y_2, Z_2)$ are the global coordinates of the nodes of the element.

A common term in the matrix is $\sqrt{r_{xX}^2 + r_{xY}^2}$, if we call it $\Upsilon$ for the sake of simplicity in the expressions and derive it:

$$\frac{\partial \Upsilon}{\partial \xi} = \frac{r_{xX}\dfrac{\partial r_{xX}}{\partial \xi} + r_{xY}\dfrac{\partial r_{xY}}{\partial \xi}}{\Upsilon} \tag{4.36}$$

Then the rest of the derivatives are:

$$\frac{\partial}{\partial \xi}\left(\frac{-r_{xY}}{\Upsilon}\right) = -\frac{\dfrac{\partial r_{xY}}{\partial \xi}\Upsilon - r_{xY}\dfrac{\partial \Upsilon}{\partial \xi}}{r_{xX}^2 + r_{xY}^2} \tag{4.37}$$

$$\frac{\partial}{\partial \xi}\left(\frac{r_{xX}}{\Upsilon}\right) = \frac{\dfrac{\partial r_{xX}}{\partial \xi}\Upsilon - r_{xX}\dfrac{\partial \Upsilon}{\partial \xi}}{r_{xX}^2 + r_{xY}^2} \tag{4.38}$$

$$\frac{\partial}{\partial \xi}\left(-\frac{r_{xX}r_{xZ}}{\Upsilon}\right) = -\frac{\left(\dfrac{\partial r_{xX}}{\partial \xi}r_{xZ} + r_{xX}\dfrac{\partial r_{xZ}}{\partial \xi}\right)\Upsilon - r_{xX}r_{xZ}\dfrac{\partial \Upsilon}{\partial \xi}}{r_{xX}^2 + r_{xY}^2} \tag{4.39}$$

$$\frac{\partial}{\partial \xi}\left(-\frac{r_{xY}r_{xZ}}{\Upsilon}\right) = -\frac{\left(\dfrac{\partial r_{xY}}{\partial \xi}r_{xZ} + r_{xY}\dfrac{\partial r_{xZ}}{\partial \xi}\right)\Upsilon - r_{xY}r_{xZ}\dfrac{\partial \Upsilon}{\partial \xi}}{r_{xX}^2 + r_{xY}^2} \tag{4.40}$$

We can now assemble the derivative of the transformation matrix as:

$$\frac{\partial \boldsymbol{R}}{\partial \xi} = \begin{pmatrix} \dfrac{\partial r_{xX}}{\partial \xi} & \dfrac{\partial r_{xY}}{\partial \xi} & \dfrac{\partial r_{xZ}}{\partial \xi} \\ \dfrac{\partial}{\partial \xi}\left(\dfrac{-r_{xY}}{\Upsilon}\right) & \dfrac{\partial}{\partial \xi}\left(\dfrac{r_{xX}}{\Upsilon}\right) & 0 \\ \dfrac{\partial}{\partial \xi}\left(-\dfrac{r_{xX}r_{xZ}}{\Upsilon}\right) & \dfrac{\partial}{\partial \xi}\left(-\dfrac{r_{xY}r_{xZ}}{\Upsilon}\right) & \dfrac{\partial \Upsilon}{\partial \xi} \end{pmatrix} \tag{4.41}$$

and

$$\frac{\partial \boldsymbol{T}}{\partial \xi} = \begin{pmatrix} \dfrac{\partial \boldsymbol{R}}{\partial \xi} & \boldsymbol{\Omega} & \boldsymbol{\Omega} & \boldsymbol{\Omega} \\ \boldsymbol{\Omega} & \dfrac{\partial \boldsymbol{R}}{\partial \xi} & \boldsymbol{\Omega} & \boldsymbol{\Omega} \\ \boldsymbol{\Omega} & \boldsymbol{\Omega} & \dfrac{\partial \boldsymbol{R}}{\partial \xi} & \boldsymbol{\Omega} \\ \boldsymbol{\Omega} & \boldsymbol{\Omega} & \boldsymbol{\Omega} & \dfrac{\partial \boldsymbol{R}}{\partial \xi} \end{pmatrix} \tag{4.42}$$

The above derivative depends again only on the geometric design variables thus, the derivative of $\boldsymbol{B}$ depends only on $(\mu_B, \mu_T)$ and has null derivative with respect to the size variables.

The only matrix left to differentiate is $\boldsymbol{D}$ (2.15). Differentiating each of its terms:

$$\frac{\partial}{\partial\xi}\left(\frac{EA}{L}\right) = E\left(\frac{\frac{\partial A}{\partial\xi}L - A\frac{\partial L}{\partial\xi}}{L^2}\right) \quad (4.43) \qquad \frac{\partial}{\partial\xi}\left(\frac{GJ}{L}\right) = G\left(\frac{\frac{\partial J}{\partial\xi}L - J\frac{\partial L}{\partial\xi}}{L^2}\right) \quad (4.44)$$

$$\frac{\partial}{\partial\xi}\left(\frac{4EI_y}{e}\right) = 4E\left(\frac{\frac{\partial I_y}{\partial\xi}L - I_y\frac{\partial L}{\partial\xi}}{L^2}\right) \quad (4.45) \qquad \frac{\partial}{\partial\xi}\left(\frac{2EI_y}{L}\right) = 2E\left(\frac{\frac{\partial I_y}{\partial\xi}L - I_y\frac{\partial L}{\partial\xi}}{L^2}\right) \quad (4.46)$$

$$\frac{\partial}{\partial\xi}\left(\frac{4EI_z}{L}\right) = 4E\left(\frac{\frac{\partial I_z}{\partial\xi}L - I_z\frac{\partial L}{\partial\xi}}{L^2}\right) \quad (4.47) \qquad \frac{\partial}{\partial\xi}\left(\frac{2EI_z}{L}\right) = 2E\left(\frac{\frac{\partial I_z}{\partial\xi}L - I_z\frac{\partial L}{\partial\xi}}{L^2}\right) \quad (4.48)$$

With these three matrices derivatives and the matrices already described in chapter 2 we can assemble the derivative of the elemental stiffness matrix.

### Mass matrix derivative

The consistent mass matrix (2.25) can be derived easily. However we have to take into account that the expression in (2.25) is referred to local axes so the global mass matrix for each element is computed as:

$$\boldsymbol{M} = \boldsymbol{T}^t\,\boldsymbol{M'}\,\boldsymbol{T} \quad \longrightarrow \quad D_s\boldsymbol{M} = D_s\boldsymbol{T}^t\,\boldsymbol{M'}\,\boldsymbol{T} + \boldsymbol{T}^t\,D_s\boldsymbol{M'}\,\boldsymbol{T} + \boldsymbol{T}^t\,\boldsymbol{M'}\,D_s\boldsymbol{T} \quad (4.49)$$

where we need the derivative of $\boldsymbol{M'}$ which contains 4 types of elements affected by different constants. For clarity those 4 types of elements and its derivative can be expressed as:

$$\begin{aligned}
&1.\quad M_{ij} = \beta_1\rho\,A\,L \quad \rightarrow \quad \frac{\partial M_{ij}}{\partial\xi} = \beta_1\rho\left(\frac{\partial A}{\partial\xi}L + A\frac{\partial L}{\partial\xi}\right)\\
&2.\quad M_{ij} = \beta_2\rho\,A\,L^2 \quad \rightarrow \quad \frac{\partial M_{ij}}{\partial\xi} = \beta_2\rho\left(\frac{\partial A}{\partial\xi}L^2 + 2\,A\,L\frac{\partial L}{\partial\xi}\right)\\
&3.\quad M_{ij} = \beta_3\rho\,A\,L^3 \quad \rightarrow \quad \frac{\partial M_{ij}}{\partial\xi} = \beta_3\rho\left(\frac{\partial A}{\partial\xi}L^3 + 3\,A\,L^2\frac{\partial L}{\partial\xi}\right)\\
&4.\quad M_{ij} = \beta_4\rho\,J\,L \quad \rightarrow \quad \frac{\partial M_{ij}}{\partial\xi} = \beta_4\rho\left(\frac{\partial J}{\partial\xi}L + J\frac{\partial L}{\partial\xi}\right)
\end{aligned} \quad (4.50)$$

Additionally, the terms of the hydrodynamic added mass (2.26) that affect the translation degrees of freedom can be differentiated as:

$$\frac{\partial m_a}{\partial \xi} = \rho \frac{\pi}{4} \left( 2D \frac{\partial D}{\partial \xi} L + D^2 \frac{\partial L}{\partial \xi} \right) \tag{4.51}$$

**Damping matrix derivative**

The damping mass matrix used in this work corresponds to the classical Rayleigh damping where the matrix is obtained as an aggregation of the mass and stiffness matrices. Thus,

$$\boldsymbol{C} = \alpha_1 \boldsymbol{M} + \alpha_2 \boldsymbol{K} \quad \rightarrow \quad D_s \boldsymbol{C} = D_s \alpha_1 \boldsymbol{M} + \alpha_1 D_s \boldsymbol{M} + D_s \alpha_2 \boldsymbol{K} + \alpha_2 D_s \boldsymbol{K} \tag{4.52}$$

However, $\alpha_1$ and $\alpha_2$ are implicit functions of the design variables through the natural frequencies of the structure. Although their sensitivities can be computed using the sensitivities of the eigenfrequencies (as it will be seen in 4.5.7) their weight can be neglected before the values of the sensitivities of the mass and stiffness matrices. In particular, the derivatives of those matrices are more than 6 orders of magnitude higher.

Then, the sensitivity of the damping matrix is approximated just as:

$$D_s \boldsymbol{C} \approx \alpha_1 D_s \boldsymbol{M} + \alpha_2 D_s \boldsymbol{K} \tag{4.53}$$

## 4.5. Constraints sensitivities

The computation of the sensitivities and therefore, the derivatives of the structural constraints of the optimization problem, constitutes the most important and costly branch of the sensitivity analysis. In essence they give quantitative measure on the sensitivity of the structural response with respect to the design variables. That information is essential in the optimization process and it must be as accurate as possible. The three types of constraints described in the previous chapter call for a particular approach described in the following.

### 4.5.1. Constraints sensitivities handling

The constraints imposed to the optimization problem, and more particularly the ULS constraints, are explicit functions of the design variables but they also depend on the forces acting on the elements, being also implicit functions of those design variables through the displacements experienced by the structure.

$$G_i(\boldsymbol{\xi}) = \tilde{G}_i(\boldsymbol{\xi}, \boldsymbol{\sigma}(\boldsymbol{u}))\big|_{\boldsymbol{u}(\boldsymbol{\xi})} \tag{4.54}$$

The above issue can be easily differentiated as:

$$D_s G_i = \frac{d\tilde{G}_i}{d\boldsymbol{\xi}} \boldsymbol{s} \rightarrow D_s G_i = D_s \tilde{G}_i + \frac{\partial \tilde{G}_i}{\partial \boldsymbol{\sigma}} D_s \boldsymbol{\sigma} \qquad \downarrow \qquad D_s \boldsymbol{\sigma} = D_s \tilde{\boldsymbol{\sigma}} + \frac{\partial \tilde{\boldsymbol{\sigma}}}{\partial \boldsymbol{u}} D_s \boldsymbol{u} \tag{4.55}$$

where $\boldsymbol{\sigma}$ is the vector of structural stresses directly computed from the direct stiffness method depicted in equation (2.18).

However, from the constitutive and compatibility equation we have that:

$$\boldsymbol{\sigma} = \boldsymbol{S}\,\boldsymbol{u} \quad \longrightarrow \quad D_s\,\boldsymbol{\sigma} = D_s\,\boldsymbol{S}\,\boldsymbol{u} + \boldsymbol{S}\,D_s\,\boldsymbol{u} \tag{4.56}$$

Thereby we could insert (4.56) in (4.55) to obtain:

$$D_s G_i = D_s \tilde{G}_i + \frac{\partial \tilde{G}_i}{\partial \boldsymbol{\sigma}} \left( D_s \boldsymbol{S} \boldsymbol{u} + \boldsymbol{S} D_s \boldsymbol{u} \right) \tag{4.57}$$

The so far described formulation is strictly correct. Nevertheless it does not account for some key facts. The fact that the actual forces or stresses upon the structure are not those of (4.56) but the member end forces due to distributed loads along the span of the elements have to be added. And also the fact that the optimization constraints do not depend only on the components of (2.18) but on all the three forces and three moments per node of the member in local axis:

$$\boldsymbol{f'} = \{N_1, Vy_1, Vz_1, Mx_1, My_1, Mz_1, N_2, Vy_2, Vz_2, Mx_2, My_2, Mz_2\} \tag{4.58}$$

That vector of forces accounts for the forces obtained directly from the solution of the equations of motion and for the equivalent forces due to distributed loads. Using the equilibrium equation those forces in local axis are:

$$\boldsymbol{f'} = \boldsymbol{E}^t\,\boldsymbol{\sigma} + \boldsymbol{f'}_{eq} = \boldsymbol{E}^t\,\boldsymbol{S}\,\boldsymbol{u} + \boldsymbol{T}\,\boldsymbol{f}_{eq} \tag{4.59}$$

where the equivalent forces are transformed from the global reference frame since it is where they usually are computed in the implementation.

Consequently, we can modify the described formulation from (4.54) to introduce all the forces. Then the constraints and their derivatives could be formulated as:

$$G_i(\boldsymbol{\xi}) = \tilde{G}_i(\boldsymbol{\xi}, \boldsymbol{f'}(\boldsymbol{u}))\big|_{\boldsymbol{u}(\boldsymbol{\xi})} \tag{4.60}$$

$$D_s G_i = D_s \tilde{G}_i + \frac{\partial \tilde{G}_i}{\partial \boldsymbol{f'}} D_s \boldsymbol{f'} \qquad \downarrow \qquad D_s \boldsymbol{f'} = D_s \boldsymbol{E}^t\,\boldsymbol{S}\,\boldsymbol{u} + \boldsymbol{E}^t\,D_s \boldsymbol{S}\,\boldsymbol{u} + \boldsymbol{E}^t\,\boldsymbol{S}\,D_s \boldsymbol{u} + D_s \boldsymbol{T}\,\boldsymbol{f}_{eq} + \boldsymbol{T}\,D_s \boldsymbol{f}_{eq} \tag{4.61}$$

The derivatives of $\boldsymbol{E}$, $\boldsymbol{S}$ and $\boldsymbol{T}$ were already obtained in the current chapter so in order to attain the derivatives of the constraints we need the terms:

- $D_s\tilde{G}_i \rightarrow$ Directional derivative of the expression of the constraint with respect to the design variables.
- $\dfrac{\partial \tilde{G}_j}{\partial \boldsymbol{f'}} \rightarrow$ Derivative of the expression of the constraint with respect to the local member-end forces of (4.58).
- $D_s\boldsymbol{u} \rightarrow$ Directional derivative of the movements of the degrees of freedom with respect to the design variables.
- $D_s\boldsymbol{f}_{eq} \rightarrow$ Directional derivative of the equivalent member-end forces due to distributed loads with respect to the design variables.

The proposed formulation is applicable to the ULS constraints of the structural problem. The above terms are fully described in the next sections.

### 4.5.2. ULS constraints derivatives

Regarding the first two terms, the explicit expressions of the derivatives of the ULS structural constraints described in 3.2.2 with respect to both, the design variables and the member-end forces, were analytically obtained in this work.

All the expressions are fully detailed in section B.2 of Appendix B including the derivatives of every additional parameter. They are set aside as they are just analytic derivatives of, in many cases, long and entangled functions and it would make no sense to fill the current chapter with such a tedious read.

### 4.5.3. Differentiation of the dynamic equation

The third term reflects the behavior of the structural movements with respect to changes in the design variables or in other words, their sensitivities. We now have to remind the reader that we are dealing with a structural dynamics problem and so, we are integrating the dynamic equation of motion in the time domain. This particular aspect was fully described in 2.5.

Given the dynamic equation of motion (2.61), we can differentiate the expression with respect to the design variables as:

$$\boldsymbol{M}\,\ddot{\boldsymbol{u}}+\boldsymbol{C}\,\dot{\boldsymbol{u}}+\boldsymbol{K}\,\boldsymbol{u}=\boldsymbol{f} \rightarrow D_s\boldsymbol{M}\,\ddot{\boldsymbol{u}}+\boldsymbol{M}\,D_s\ddot{\boldsymbol{u}}+D_s\boldsymbol{C}\,\dot{\boldsymbol{u}}+\boldsymbol{C}\,D_s\dot{\boldsymbol{u}}+D_s\boldsymbol{K}\,\boldsymbol{u}+\boldsymbol{K}\,D_s\boldsymbol{u}=D_s\boldsymbol{f} \Leftrightarrow \tag{4.62}$$

$$\Leftrightarrow \boldsymbol{M}\,D_s\ddot{\boldsymbol{u}}+\boldsymbol{C}\,D_s\dot{\boldsymbol{u}}+\boldsymbol{K}\,D_s\boldsymbol{u}=\underbrace{[D_s\boldsymbol{f}-D_s\boldsymbol{M}\,\ddot{\boldsymbol{u}}-D_s\boldsymbol{C}\,\dot{\boldsymbol{u}}-D_s\boldsymbol{K}\,\boldsymbol{u}]}_{\boldsymbol{f^*}} \tag{4.63}$$

Which gives us $n$ systems of equations to solve at each time step, being $n$ the number of design variables. In the Direct Differentiation scheme, the above is the differentiation

of the state equation and the solution of the systems given by (4.9). That means that for each time instant we have to solve $n+1$ systems of equations, one to obtain the movements of the structure and $n$ to solve the sensitivities of those movements with respect to each design variable. That is obviously not for free and the fee is payed in computational time. Figure 4.4 draws the CPU time involved in the solution of the dynamic system in the linear and non-linear case compared with those shown in figure 2.18. However, this scheme is more efficient compared to an Adjoint State Method proposed for example in [Oest et al., 2017]

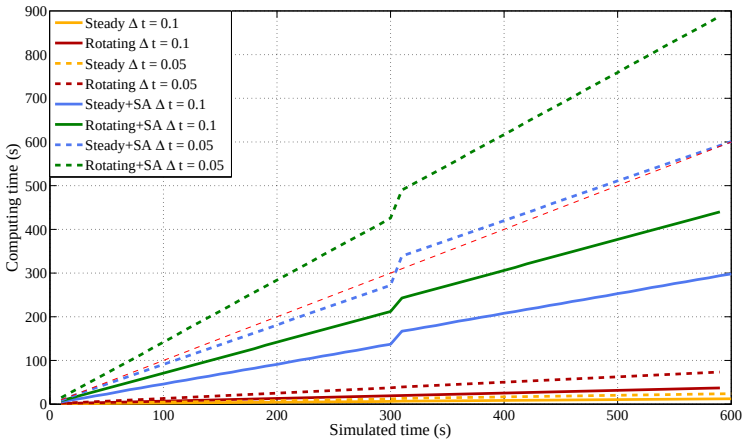


**Figure 4.4. Computing time for the steady and rotating case for different time steps including the sensitivity analysis with 22 design variables.**

We were in ratios 1/10 computing time to simulated time but now the ratio is 1/2 for the linear case with $\Delta t = 0.1$ and greater than one if we decrease the time step. That is more than undesirable and conceptually means that it takes more time to simulate the phenomenon than for it to happen. The $n+1$ systems are again integrated using the Newmark method and the Non-linear Newmark method. In the rotating scheme we have to remember that the structural matrices were recalculated at each time step. However, luckily their derivatives do not need to be recalculated as the parts of them that changes with the rotation of the blades do not depend on the design variables.

### 4.5.4. External forces derivatives

In (4.61) we saw the need for the derivatives of the equivalent forces due to distributed loads. Additionally because of (4.63) we also need the derivatives of the bare forces acting on the structure. Chapter 2 describes the loads considered in this work and how they are treated (self weight, buoyancy, wind and waves). However, the wind aerodynamic load has not to be treated here as its influence is only considered on the

tower and blades and they do not change with the design variables of the jacket. In other words, the sensitivity of the wind load with respect to the design variables is null.

Nevertheless, self weight, buoyancy and waves do change with the design variables, in fact they are extremely sensitive to them.

### Self weight and buoyancy

According to (2.30) the generic load due to self weight and buoyancy can be computed using the marine method as:

$$W_e = g\,L\,(\rho_s\,A_s + \rho_{mg}\,A_{mg} + \rho_w\,A_w - \rho_w\,A_t)$$

$$= \frac{g\pi\,L}{4}\underbrace{\left(\left(D^2-(D-2t)^2\right)\rho_s + \left((D+2t_{mg})^2 - D^2\right)\rho_{mg} + (D-2t)^2\,\rho_w - D^2\rho_w\right)}_{A^*} \tag{4.64}$$

we can differentiate the above expression simply as:

$$\frac{\partial W}{\partial \xi} = \frac{g\pi}{4}\left(\frac{\partial L}{\partial \xi}\,A^* + L\frac{\partial A^*}{\partial \xi}\right) \tag{4.65}$$

What we deal with is the vector of nodal forces arising from the distributed weight and buoyancy load. That vector in global axes and its derivative are:

$$\boldsymbol{f}_{wb} = \begin{Bmatrix} 0 \\ 0 \\ -\frac{W}{2} \\ -\frac{W}{12}\Delta Y \\ \frac{W}{12}\Delta X \\ 0 \\ 0 \\ 0 \\ -\frac{W}{2} \\ \frac{W}{12}\Delta Y \\ -\frac{W}{12}\Delta X \\ 0 \end{Bmatrix} \quad \Rightarrow \quad \frac{\partial \boldsymbol{f}_{wb}}{\partial \xi} = \begin{Bmatrix} 0 \\ 0 \\ -\frac{1}{2}\frac{\partial W_e}{\partial \xi} \\ -\frac{1}{12}\left(\frac{\partial W}{\partial \xi}\Delta Y + W\frac{\partial \Delta Y}{\partial \xi}\right) \\ \frac{1}{12}\left(\frac{\partial W}{\partial \xi}\Delta X + W\frac{\partial \Delta X}{\partial \xi}\right) \\ 0 \\ 0 \\ 0 \\ -\frac{1}{2}\frac{\partial W}{\partial \xi} \\ \frac{1}{12}\left(\frac{\partial W}{\partial \xi}\Delta Y + W\frac{\partial \Delta Y}{\partial \xi}\right) \\ -\frac{1}{12}\left(\frac{\partial W}{\partial \xi}\Delta X + W\frac{\partial \Delta X}{\partial \xi}\right) \\ 0 \end{Bmatrix} \tag{4.66}$$

with $\Delta X = X_2 - X_1 \rightarrow \dfrac{\partial \Delta X}{\partial \xi} = \dfrac{\partial X_2}{\partial \xi} - \dfrac{\partial X_1}{\partial \xi}$ and $\Delta Y = Y_2 - Y_1 \rightarrow \dfrac{\partial \Delta Y}{\partial \xi} = \dfrac{\partial Y_2}{\partial \xi} - \dfrac{\partial Y_1}{\partial \xi}$

The vector of equivalent forces ($\boldsymbol{f}_{eq}$) and its derivative are exactly the opposite of the above.

**Waves**

Wave loading one of the most important loads acting on an offshore structure together with wind. The forces on the submerged elements of the structure due to waves and current have a strong dependency on the dimensions of the elements and their positions. And thus a high sensitivity with respect to the design variables of the proposed optimization problem. Thereby, their derivatives or the variation of that load with the designs could not in any case be neglected.

In order to differentiate the wave loads we will use everything described in section 2.4.4, and particularly the steps depicted to compute the forces on inclined submerged or partially submerged elements.

1. Derivatives of the discretized coordinates in which each element is divided.

$$\left\{ \begin{array}{l} X_i = X_1 + (i-1)\dfrac{\Delta X}{nd} \\ Y_i = Y_1 + (i-1)\dfrac{\Delta Y}{nd} \\ Z_i = Z_1 + (i-1)\dfrac{\Delta Z}{nd} \end{array} \right\} \quad \Rightarrow \quad \left\{ \begin{array}{l} \dfrac{\partial X_i}{\partial \xi} = \dfrac{\partial X_1}{\partial \xi} + (i-1)\dfrac{1}{nd}\dfrac{\partial \Delta X}{\partial \xi} \\ \dfrac{\partial Y_i}{\partial \xi} = \dfrac{\partial Y_1}{\partial \xi} + (i-1)\dfrac{1}{nd}\dfrac{\partial \Delta Y}{\partial \xi} \\ \dfrac{\partial Z_i}{\partial \xi} = \dfrac{\partial Z_1}{\partial \xi} + (i-1)\dfrac{1}{nd}\dfrac{\partial \Delta Z}{\partial \xi} \end{array} \right\} \tag{4.67}$$

However the wave can come from any given direction $S$ with components in $X$ and $Y$, thus:

$$\delta_i = X_i \cos(\theta) + Y_i \sin(\theta) \qquad \rightarrow \qquad \frac{\partial \delta}{\partial \xi} = \frac{\partial X_i}{\partial \xi}\cos(\theta) + \frac{\partial Y_i}{\partial \xi}\sin(\theta) \tag{4.68}$$

being $\delta_i$ the coordinate in $S$ direction of the discretized point $i$ and $\theta$ the angle of the waves with respect to the global $X$ axis.

Also the surface of the wave can be differentiated as:

$$\eta(\delta, t) = \frac{H}{2}\cos(k\delta - \omega t) \qquad \rightarrow \qquad \frac{\partial \eta}{\partial \xi} = -k\frac{H}{2}\sin(k\delta - \omega t)\frac{\partial \delta}{\partial \xi} \tag{4.69}$$

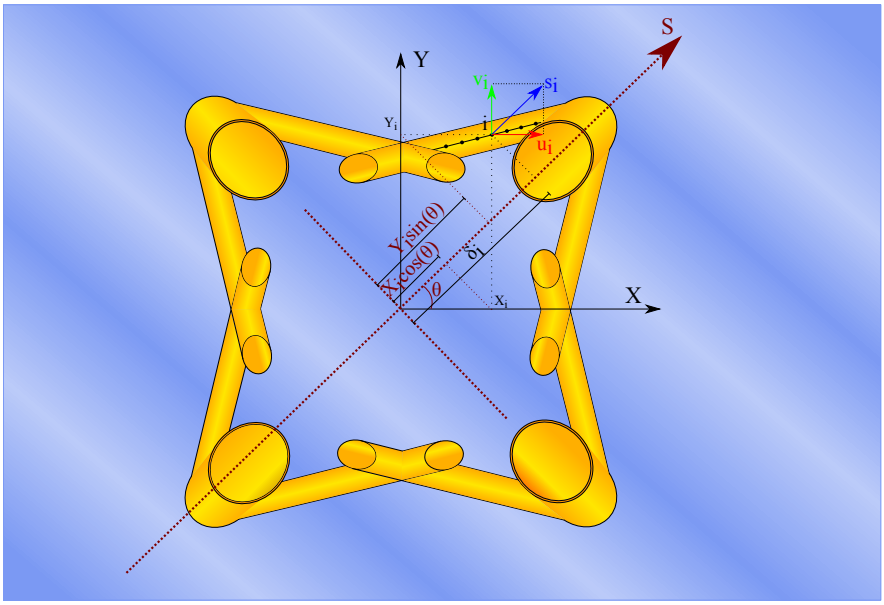


**Figure 4.5. Wave direction and global axes.**

2. Derivatives of the velocity and acceleration of the particles in the direction of the waves $s_i$, $\dot{s}_i$ and in vertical direction $w_i$, $\dot{w}_i$.

$$\frac{\partial s_i}{\partial \xi} = \frac{gkH}{2\omega \cosh^2(k(d+\eta)} \left[\left(k\frac{\partial Z_i}{\partial \xi}\sinh(kZ_i)\cos(k\delta_i - \omega t) - \cosh(kZ_i)\left(k\frac{\partial \delta}{\partial \xi}\right)\sin(k\delta_i - \omega t)\right) \cosh(k(d+\eta)) - [\cosh(kZ_i)\cos(k\delta_i - \omega t)]\, k\frac{\partial \eta}{\partial \xi}\sinh(k(d+\eta))\right] \tag{4.70}$$

$$\frac{\partial \dot{s}_i}{\partial \xi} = \frac{gkH}{2\cosh^2(k(d+\eta)} \left[\left(k\frac{\partial Z_i}{\partial \xi}\sinh(kZ_i)\sin(k\delta_i - \omega t) + \cosh(kZ_i)\left(k\frac{\partial \delta}{\partial \xi}\right)\cos(k\delta_i - \omega t)\right) \cosh(k(d+\eta)) - [\cosh(kZ_i)\sin(k\delta_i - \omega t)]\, k\frac{\partial \eta}{\partial \xi}\sinh(k(d+\eta))\right] \tag{4.71}$$

$$\begin{aligned}\frac{\partial w_i}{\partial \xi} &= \frac{gkH}{2\omega\cosh^2(k(d+\eta)} \\ &\left[\left(k\frac{\partial Z_i}{\partial \xi}\cosh\left(kZ_i\right)\sin\left(k\delta_i-\omega t\right)+\sinh\left(kZ_i\right)\left(k\frac{\partial \delta}{\partial \xi}\right)\cos\left(k\delta_i-\omega t\right)\right)\right. \\ &\left.\cosh\left(k(d+\eta)\right)-\left[\sinh(kZ_i)\sin(k\delta_i-\omega t)\right]k\frac{\partial \eta}{\partial \xi}\sinh\left(k(d+\eta)\right)\right]\end{aligned} \tag{4.72}$$

$$\begin{aligned}\frac{\partial \dot{w}_i}{\partial \xi} &= -\frac{gkH}{2\cosh^2(k(d+\eta)} \\ &\left[\left(k\frac{\partial Z_i}{\partial \xi}\cosh\left(kZ_i\right)\cos\left(k\delta_i-\omega t\right)-\sinh\left(kZ_i\right)\left(k\frac{\partial \delta}{\partial \xi}\right)\sin\left(k\delta_i-\omega t\right)\right)\right. \\ &\left.\cosh\left(k(d+\eta)\right)-\left[\sinh(kZ_i)\cos(k\delta_i-\omega t)\right]k\frac{\partial \eta}{\partial \xi}\sinh\left(k(d+\eta)\right)\right]\end{aligned} \tag{4.73}$$

3. Derivatives of the velocities and accelerations of the particles in the local axes of the element.

$$\left\{\begin{array}{c} u_i' \\ v_i' \\ w_i' \end{array}\right\} = \boldsymbol{T}\left\{\begin{array}{c} u_i \\ v_i \\ w_i \end{array}\right\} = \boldsymbol{T}\left\{\begin{array}{c} s_i\ \cos(\theta) \\ s_i\ \sin(\theta) \\ w_i \end{array}\right\}; \left\{\begin{array}{c} \dot{u_i}' \\ \dot{v_i}' \\ \dot{w_i}' \end{array}\right\} = \boldsymbol{T}\left\{\begin{array}{c} \dot{s}_i\ \cos(\theta) \\ \dot{s}_i\ \sin(\theta) \\ \dot{w}_i \end{array}\right\} \Rightarrow \tag{4.74}$$

$$\left\{\begin{array}{c} \dfrac{\partial u_i'}{\partial \xi} \\ \dfrac{\partial v_i'}{\partial \xi} \\ \dfrac{\partial w_i'}{\partial \xi} \end{array}\right\} = \frac{\partial \boldsymbol{T}}{\partial \xi}\left\{\begin{array}{c} s_i\ \cos(\theta) \\ s_i\ \sin(\theta) \\ w_i \end{array}\right\} + \boldsymbol{T}\left\{\begin{array}{c} \dfrac{\partial s_i}{\partial \xi}\ \cos(\theta) \\ \dfrac{\partial s_i}{\partial \xi}\ \sin(\theta) \\ \dfrac{\partial w_i}{\partial \xi} \end{array}\right\} \tag{4.75}$$

$$\left\{\begin{array}{c} \dfrac{\partial \dot{u_i}'}{\partial \xi} \\ \dfrac{\partial \dot{v_i}'}{\partial \xi} \\ \dfrac{\partial \dot{w_i}'}{\partial \xi} \end{array}\right\} = \frac{\partial \boldsymbol{T}}{\partial \xi}\left\{\begin{array}{c} \dot{s}_i\ \cos(\theta) \\ \dot{s}_i\ \sin(\theta) \\ \dot{w}_i \end{array}\right\} + \boldsymbol{T}\left\{\begin{array}{c} \dfrac{\partial \dot{s}_i}{\partial \xi}\ \cos(\theta) \\ \dfrac{\partial \dot{s}_i}{\partial \xi}\ \sin(\theta) \\ \dfrac{\partial \dot{w}_i}{\partial \xi} \end{array}\right\} \tag{4.76}$$

4. Derivative of the Morison's formula to obtain the derivative of the local forces.

$$\begin{aligned}\frac{\partial f_{y,i}'}{\partial \xi} &= \frac{\pi}{4}\,\rho\,C_M\left[2\,D\,\frac{\partial D}{\partial \xi}\,\dot{v_i'} + D^2\,\frac{\partial \dot{v_i'}}{\partial \xi}\right] \\ &+\frac{1}{2}\,\rho\,C_D\left[\frac{\partial D}{\partial \xi}\,v_i'\,|v_i'| + D\,\frac{\partial v_i'}{\partial \xi}\,|v_i'| + D\,v_i'\,\frac{v_i'}{|v_i'|}\,\frac{\partial v_i'}{\partial \xi}\right]\end{aligned} \tag{4.77}$$

$$\begin{aligned}\frac{\partial f'_{z,i}}{\partial \xi} &= \frac{\pi}{4}\,\rho\,C_M\left[2\,D\,\frac{\partial D}{\partial \xi}\,\dot{w'_i}+D^2\,\frac{\partial \dot{w'_i}}{\partial \xi}\right]\\ &+\frac{1}{2}\,\rho\,C_D\left[\frac{\partial D}{\partial \xi}\,w'_i\,|w'_i|+D\,\frac{\partial w'_i}{\partial \xi}\,|w'_i|+D\,w'_i\,\frac{w'_i}{|w'_i|}\,\frac{\partial w'_i}{\partial \xi}\right]\end{aligned} \tag{4.78}$$

5. Derivative of the total forces acting along the length of the discretized element.

$$F'_{y,i}=f'_{y,i}\delta l_i \quad\rightarrow\quad \frac{\partial F'_{y,i}}{\partial \xi}=\frac{\partial f'_y}{\partial \xi}\delta l_i+f'_y\frac{\partial \delta l_i}{\partial \xi} \tag{4.79}$$

$$F'_{z,i}=f'_{z,i}\delta l_i \quad\rightarrow\quad \frac{\partial F'_{z,i}}{\partial \xi}=\frac{\partial f'_z}{\partial \xi}\delta l_i+f'_z\frac{\partial \delta l_i}{\partial \xi} \tag{4.80}$$

where $\dfrac{\partial \delta l_i}{\partial \xi}=\dfrac{1}{nd}\,\dfrac{\partial L}{\partial \xi}$

6. Derivative of the point of application of the force.

$$\frac{\partial x_{F'_i}}{\partial \xi}=\frac{i-1}{nd}\,\frac{\partial L}{\partial \xi} \tag{4.81}$$

We can now obtain the derivative of the vector of member-end forces due to the distributed wave loading in the local reference frame:

$$\frac{\partial \boldsymbol{f'}}{\partial \xi}=\left\{\frac{\partial f'_{x,1}}{\partial \xi},\frac{\partial f'_{y,1}}{\partial \xi},\frac{\partial f'_{z,1}}{\partial \xi},\frac{\partial m'_{x,1}}{\partial \xi},\frac{\partial m'_{y,1}}{\partial \xi},\frac{\partial m'_{z,1}}{\partial \xi},\frac{\partial f'_{x,2}}{\partial \xi},\frac{\partial f'_{y,2}}{\partial \xi},\frac{\partial f'_{z,2}}{\partial \xi},\frac{\partial m'_{x,2}}{\partial \xi},\frac{\partial m'_{y,2}}{\partial \xi},\frac{\partial m'_{z,2}}{\partial \xi},\right\} \tag{4.82}$$

$$\frac{\partial f'_{x,1}}{\partial \xi}=\frac{\partial f'_{x,2}}{\partial \xi}=\frac{\partial m'_{x,1}}{\partial \xi}=\frac{\partial m'_{x,2}}{\partial \xi} \;=\; 0 \tag{4.83}$$

$$\begin{aligned}\frac{\partial f'_{y,1}}{\partial \xi}=\;&\sum_{i=1}^{nd+1}\left[\frac{1}{L^3}\left(\frac{\partial F'_{y,i}}{\partial \xi}(L-x_{F'_{y,i}})^2(L+2x_{F'_{y,i}})+\right.\right.\\ &F'_{y,i}\,2(L-x_{F'_{y,i}})\left(\frac{\partial L}{\partial \xi}-\frac{\partial x_{F'_{y,i}}}{\partial \xi}\right)(L+2x_{F'_{y,i}})\;+\\ &\left.\left.F'_{y,i}(L-x_{F'_{y,i}})^2\left(\frac{\partial L}{\partial \xi}+2\frac{\partial x_{F'_{y,i}}}{\partial \xi}\right)\right)-F'_{y,i}(L-x_{F'_{y,i}})^2(L+2x_{F'_{y,i}})\frac{3}{L^4}\frac{\partial L}{\partial \xi}\right]\end{aligned} \tag{4.84}$$

$$\begin{aligned}\frac{\partial f'_{z,1}}{\partial \xi} = \sum_{i=1}^{nd+1} \Bigg[ \frac{1}{L^3} \Bigg( & \frac{\partial F'_{z,i}}{\partial \xi}(L - x_{F'_{z,i}})^2(L + 2x_{F'_{z,i}}) + \\ & F'_{z,i}\, 2(L - x_{F'_{z,i}}) \left( \frac{\partial L}{\partial \xi} - \frac{\partial x_{F'_{z,i}}}{\partial \xi} \right) (L + 2x_{F'_{z,i}}) + \\ & F'_{z,i}(L - x_{F'_{z,i}})^2 \left( \frac{\partial L}{\partial \xi} + 2\frac{\partial x_{F'_{z,i}}}{\partial \xi} \right) \Bigg) - F'_{z,i}(L - x_{F'_{z,i}})^2(L + 2x_{F'_{z,i}}) \frac{3}{L^4} \frac{\partial L}{\partial \xi} \Bigg]\end{aligned} \tag{4.85}$$

$$\begin{aligned}\frac{\partial m'_{y,1}}{\partial \xi} = - \sum_{i=1}^{nd+1} \Bigg[ \frac{1}{L^2} \Bigg( & \frac{\partial F'_{z,i}}{\partial \xi} x_{F'_{z,i}}(L - x_{F'_{z,i}})^2 + F'_{z,i} \frac{\partial x_{F'_{z,i}}}{\partial \xi}(L - x_{F'_{z,i}})^2 + \\ & F'_{z,i} x_{F'_{z,i}}\, 2(L - x_{F'_{z,i}}) \left( \frac{\partial L}{\partial \xi} - \frac{\partial x_{F'_{z,i}}}{\partial \xi} \right) \Bigg) - F'_{z,i} x_{F'_{z,i}}(L - x_{F'_{z,i}})^2 \frac{2}{L^3} \frac{\partial L}{\partial \xi} \Bigg]\end{aligned} \tag{4.86}$$

$$\begin{aligned}\frac{\partial m'_{z,1}}{\partial \xi} = \sum_{i=1}^{nd+1} \Bigg[ \frac{1}{L^2} \Bigg( & \frac{\partial F'_{y,i}}{\partial \xi} x_{F'_{y,i}}(L - x_{F'_{y,i}})^2 + F'_{y,i} \frac{\partial x_{F'_{y,i}}}{\partial \xi}(L - x_{F'_{y,i}})^2 \\ & + F'_{y,i} x_{F'_{y,i}} 2(L - x_{F'_{y,i}}) \left( \frac{\partial L}{\partial \xi} - \frac{\partial x_{F'_{y,i}}}{\partial \xi} \right) \Bigg) - F'_{y,i} x_{F'_{y,i}}(L - x_{F'_{y,i}})^2 \frac{2}{L^3} \frac{\partial L}{\partial \xi} \Bigg]\end{aligned} \tag{4.87}$$

$$\begin{aligned}\frac{\partial f'_{y,2}}{\partial \xi} = \sum_{i=1}^{nd+1} \Bigg[ \frac{1}{L^3} \Bigg( & \frac{\partial F'_{y,i}}{\partial \xi} x^2_{F'_{y,i}} \left( L + 2(L - x_{F'_{y,i}}) \right) + \\ & F'_{y,i}\, 2x_{F'_{y,i}} \frac{\partial x_{F'_{y,i}}}{\partial \xi} \left( L + 2(L - x_{F'_{y,i}}) \right) \\ & F'_{y,i} x^2_{F'_{y,i}} \left( \frac{\partial L}{\partial \xi} + 2 \left( \frac{\partial L}{\partial \xi} - \frac{\partial x_{F'_{y,i}}}{\partial \xi} \right) \right) \Bigg) - \\ & F'_{y,i} x^2_{F'_{y,i}} \left( L + 2(L - x_{F'_{y,i}}) \right) \frac{3}{L^4} \frac{\partial L}{\partial \xi} \Bigg]\end{aligned} \tag{4.88}$$

$$\begin{aligned}\frac{\partial f'_{z,2}}{\partial \xi} = \sum_{i=1}^{nd+1} \Bigg[ \frac{1}{L^3} \Bigg( & \frac{\partial F'_{z,i}}{\partial \xi} x^2_{F'_{z,i}} \left( L + 2(L - x_{F'_{z,i}}) \right) + \\ & F'_{z,i}\, 2x_{F'_{z,i}} \frac{\partial x_{F'_{z,i}}}{\partial \xi} \left( L + 2(L - x_{F'_{z,i}}) \right) + \\ & F'_{z,i} x^2_{F'_{z,i}} \left( \frac{\partial L}{\partial \xi} + 2 \left( \frac{\partial L}{\partial \xi} - \frac{\partial x_{F'_{z,i}}}{\partial \xi} \right) \right) \Bigg) - \\ & F'_{z,i} x^2_{F'_{z,i}} \left( L + 2(L - x_{F'_{z,i}}) \right) \frac{3}{L^4} \frac{\partial L}{\partial \xi} \Bigg]\end{aligned} \tag{4.89}$$

$$\frac{\partial m'_{y,2}}{\partial \xi} = \sum_{i=1}^{nd+1} \left[ \frac{1}{L^2} \left( \frac{\partial F'_{z,i}}{\partial \xi} x^2_{F'_{z,i}} (L - x_{F'_{z,i}}) + F'_{z,i}\, 2 x_{F'_{z,i}} \frac{\partial x_{F'_{z,i}}}{\partial \xi} (L - x_{F'_{z,i}}) + F'_{z,i} x^2_{F'_{z,i}} \left( \frac{\partial L}{\partial \xi} - \frac{\partial x_{F'_{z,i}}}{\partial \xi} \right) \right) L^2 - F'_{z,i} x^2_{F'_{z,i}} (L - x_{F'_{z,i}}) \frac{2}{L^3} \frac{\partial L}{\partial \xi} \right] \tag{4.90}$$

$$\frac{\partial m'_{z,2}}{\partial \xi} = -\sum_{i=1}^{nd+1} \left[ \frac{1}{L^2} \left( \frac{\partial F'_{y,i}}{\partial \xi} x^2_{F'_{y,i}} (L - x_{F'_{y,i}}) + F'_{y,i}\, 2 x_{F'_{y,i}} \frac{\partial x_{F'_{y,i}}}{\partial \xi} (L - x_{F'_{y,i}}) + F'_{y,i} x^2_{F'_{y,i}} \left( \frac{\partial L}{\partial \xi} - \frac{\partial x_{F'_{y,i}}}{\partial \xi} \right) \right) L^2 - F'_{y,i} x^2_{F'_{y,i}} (L - x_{F'_{y,i}}) \frac{2}{L^3} \frac{\partial L}{\partial \xi} \right] \tag{4.91}$$

The above overloaded expressions constitute the components of the derivative of the vector of nodal forces and moments due to wave loading on an element with respect to its local axes. The equivalent member-end forces are exactly the opposite and to reference them in global axes we only need to apply the transformation matrix we have been using so far.

With this the information needed to compute the derivatives of the structural constraints is complete, although there is one step left. The ULS constraints were treated using constraint aggregation functions (3.3) thus, the sensitivities of the actual constraints applied to the problem are the sensitivities of those aggregated functions.

### 4.5.5. Aggregated constraints derivatives

In this thesis the use of constraint aggregation functions is proposed to aggregate the ULS constraints in the time domain. The methodology allows an enormous reduction of the size of the problem still being differentiable and retaining information about all the constraints, active or not.

We have defined the aggregated constraint for a given ULS restriction $g_j$ as:

$$G^j_{KS}(\boldsymbol{x}) = \tilde{G}^j_{KS}(\boldsymbol{x}, \boldsymbol{\sigma}(\boldsymbol{u}))\Big|_{\boldsymbol{u}(\boldsymbol{x})} = \frac{1}{\rho} \ln \left( \sum_{i=1}^{N_T} e^{\rho\, g_j(\boldsymbol{x}, t_i)} \right) - \frac{1}{\rho} \ln(N_T) \tag{4.92}$$

The formulation allows to transform a very large set of discrete values of constraints into a continuously differentiable function.

$$D_s G^j_{KS}(\boldsymbol{x}) = \frac{\sum_{i=1}^{N_T} e^{\rho\, g_j(\boldsymbol{x}, t_i)} D_s g_j(\boldsymbol{x}, t_i)}{\sum_{i=1}^{N_T} e^{\rho\, g_j(\boldsymbol{x}, t_i)}} \tag{4.93}$$

Note that, even though the constraint aggregation strategy reduces significantly the problem, we still have to compute at every time instant all the values of the constraints ($g_j(\boldsymbol{x}, t_i)$) and their respective derivatives ($D_s g_j(\boldsymbol{x}, t_i)$).

### 4.5.6. FLS constraints sensitivities

It will be seen in later chapters but, most of the designs of steel jackets for offshore wind turbines are fatigue driven. Not only the fatigue damage limits the design but the fatigue constraint is active in many of the hot-spots of the structure. So, it is essential to catch the behavior of these constraints through the sensitivity analysis and be as accurate as possible.

First, we have seen in 3.2.2 that the SCFs used in this work are limited by some requirements for the dimensions of the elements. Those requirements were included in the formulation as constraints according to (3.33), whose derivatives are easily acquired.

Second, the SCFs are used to scale the nominal stresses at the tubular welded joints based on the member-end forces. The SCFs' formulas depend basically on the dimensions and orientations of the joint members and thereby, are strongly dependent on the design variables defined in our optimization problem. In fact, those coefficients have major impact on the fatigue damage computed. In conclusion, it is mandatory to include the SCFs' formulas in the sensitivity analysis and so, to compute their derivatives with respect to the design variables. This issue is shown in [Chew et al., 2015] presenting the results for the sensitivity analysis of fatigue damage with and without differentiating the SCFs.

In Appendix B, sections B.3.1 through B.3.5 fully describe the analytical derivatives of the geometrical constraints and all the expressions of the Stress Concentration Factors. It all with the purpose of obtaining the derivative of the fatigue damage constraint (3.32):

$$D_s g_F = \sum_{l=1}^{N_p} P_l \frac{1}{\overline{a}} \sum_{i=1}^{k} n_i \left[ k' m \frac{1}{t_r} \left( \frac{t}{t_r} \right)^{k'm} D_s t (\Delta\sigma_i)^m + \left( \frac{t}{t_r} \right)^{k'm} m (\Delta\sigma_i)^{m-1} D_s \Delta\sigma_i \right] \tag{4.94}$$

In the above equation, the hypothesis that the number of stress blocks counted by the Rainflow $n_i$ are not affected by changes in the design variables is taken. This hypothesis is essentially true for the stress blocks that rule the fatigue damage.

The problem is that (4.94) needs $D_s \Delta\sigma_i$, which is the derivative of the amplitude of the stress cycles counted by the rainflow. In [Choi & Kim, 2005] authors postulate that an analytical approach to obtain the derivatives of the fatigue life is barely impossible due to the fact that the damage is calculated counting the peaks and valleys of the stresses record. They also stand up for the use of a finite difference scheme to compute the sensitivities.

In [Chew et al., 2013, 2016] authors propose an analytical formulation to differentiate the stress ranges by considering that:

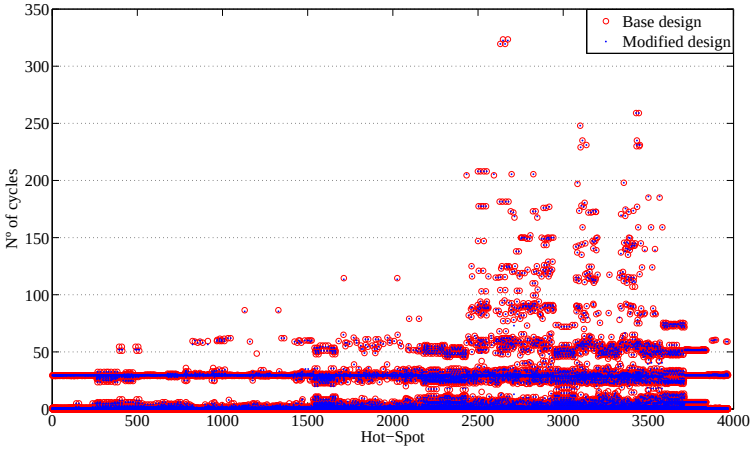


**Figure 4.6. Number of stress blocks for each hot-spot in a base design and a design modifying the design variables.**

$$\frac{\partial \Delta\sigma_i}{\partial \xi} = \begin{cases} \left.\frac{d\sigma_i(t)}{d\xi}\right|_{t=t_{i,1}} - \left.\frac{d\sigma_i(t)}{d\xi}\right|_{t=t_{i,2}} & \text{if } \sigma_i(t_i,1) > \sigma_i(t_i,2) \\ \left.\frac{d\sigma_i(t)}{d\xi}\right|_{t=t_{i,2}} - \left.\frac{d\sigma_i(t)}{d\xi}\right|_{t=t_{i,1}} & \text{if } \sigma_i(t_i,1) < \sigma_i(t_i,2) \end{cases} \tag{4.95}$$

where $t_{i,1}$ and $t_{i,2}$ are the times of initial and reversal points measured on the time history of stresses that give $\Delta\sigma_i$.

However this presents some issues. Firstly, the stress ranges $\Delta\sigma_i$ are arranged in bins $i$ that arise from various stress cycles of the same amplitude occurring at different times. So it is unclear which one of the many $t_i$ for the peaks and the valleys would give the proper derivative ( figure 4.7).

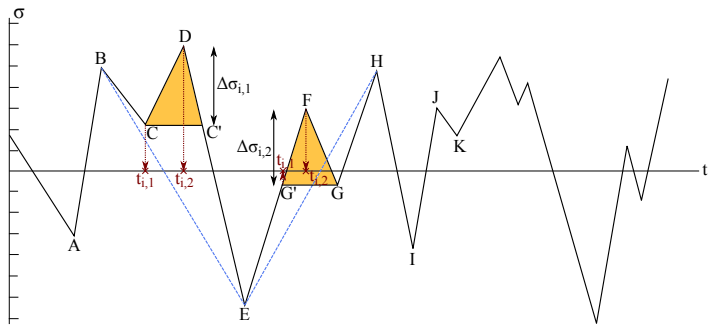


**Figure 4.7. Initial and reversal points for two different cycles of the same amplitude counted by the rainflow.**

Secondly, given a design variable change, two cycles of the same amplitude could be different afterwards and that would not be captured by (4.95) as they would be represented by the same derivative.

In summary, there is no analytical derivative for the stress cycles counted by the rainflow algorithm. Thereby the sensitivity of the damage and so, of the fatigue constraint, have to be assessed otherwise. In the absence of analytical gradients, finite differences is the common methodology used. However, using a pure finite difference approach would mean to perturb every single design variable at least once, solve the simulation and damage for each perturbation and then find the sensitivities for each variable (4.8a). The former would carry a tremendous amount of CPU time and memory while we can take advantage of the fact that we already have some of the analytical derivatives needed.

In previous sections we saw the formulation to obtain the sensitivities of the ULS constraints. Those derivatives involved the computation of the derivatives of the stresses and movements. So, if we already have the analytical derivatives of the stresses we can use them to compute the derivatives of the fatigue damage.

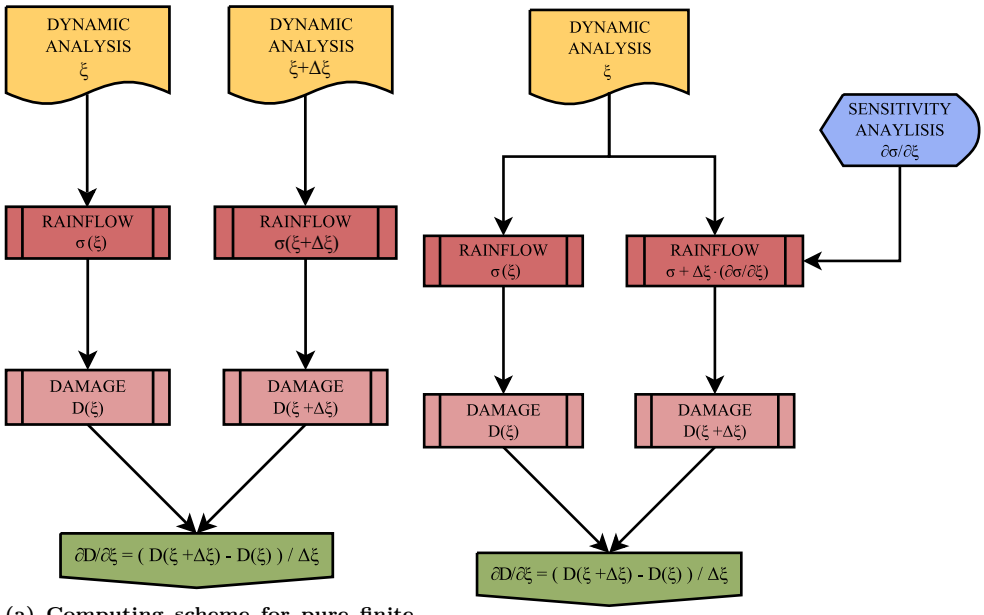


**(a) Computing scheme for pure finite differences.**

**(b) Computing scheme for combined approach.**

**Figure 4.8. Flowchart comparison between sensitivity analysis approaches for fatigue damage.**

Given the analytical derivative of the stresses $\frac{\partial \sigma}{\partial \xi}$ we can approximate the stresses for a given perturbation of the design variables $\Delta\xi$ as:

$$\sigma(\xi + \Delta\xi) \approx \sigma(\xi) + \Delta\xi \frac{\partial \sigma}{\partial \xi} \tag{4.96}$$

keeping in mind that the derivatives of the hot-spot stresses are obtained as:

$$\frac{\partial \sigma_1}{\partial \xi} = \frac{\partial SCF_{AC}}{\partial \xi}\,\sigma_x + SCF_{AC}\,\frac{\partial \sigma_x}{\partial \xi} + \frac{\partial SCF_{MIP}}{\partial \xi}\,\sigma_{my} + SCF_{MIP}\,\frac{\partial \sigma_{my}}{\partial \xi} \tag{4.97}$$

$$\begin{aligned}\frac{\partial \sigma_2}{\partial \xi} =& \frac{1}{2}\left(\frac{\partial SCF_{AC}}{\partial \xi} + \frac{\partial SCF_{AS}}{\partial \xi}\right)\sigma_x + \frac{1}{2}\left(SCF_{AC} + SCF_{AS}\right)\frac{\partial \sigma_x}{\partial \xi} + \\ & \frac{1}{2}\sqrt{2}\,\frac{\partial SCF_{MIP}}{\partial \xi}\,\sigma_{my} + \frac{1}{2}\sqrt{2}\,SCF_{MIP}\,\frac{\partial \sigma_{my}}{\partial \xi} - \frac{1}{2}\sqrt{2}\,\frac{\partial SCF_{MOP}}{\partial \xi}\,\sigma_{mz} - \\ & \frac{1}{2}\sqrt{2}\,SCF_{MOP}\,\frac{\partial \sigma_{mz}}{\partial \xi}\end{aligned} \tag{4.98}$$

$$\frac{\partial \sigma_3}{\partial \xi} = \frac{\partial SCF_{AS}}{\partial \xi}\,\sigma_x + SCF_{AS}\,\frac{\partial \sigma_x}{\partial \xi} - \frac{\partial SCF_{MOP}}{\partial \xi}\,\sigma_{mz} - SCF_{MOP}\,\frac{\partial \sigma_{mz}}{\partial \xi} \tag{4.99}$$

$$\begin{aligned}\frac{\partial \sigma_4}{\partial \xi} =& \frac{1}{2}\left(\frac{\partial SCF_{AC}}{\partial \xi} + \frac{\partial SCF_{AS}}{\partial \xi}\right)\sigma_x + \frac{1}{2}\left(SCF_{AC} + SCF_{AS}\right)\frac{\partial \sigma_x}{\partial \xi} - \\ & \frac{1}{2}\sqrt{2}\,\frac{\partial SCF_{MIP}}{\partial \xi}\,\sigma_{my} - \frac{1}{2}\sqrt{2}\,SCF_{MIP}\,\frac{\partial \sigma_{my}}{\partial \xi} - \frac{1}{2}\sqrt{2}\,\frac{\partial SCF_{MOP}}{\partial \xi}\,\sigma_{mz} - \\ & \frac{1}{2}\sqrt{2}\,SCF_{MOP}\,\frac{\partial \sigma_{mz}}{\partial \xi}\end{aligned} \tag{4.100}$$

$$\frac{\partial \sigma_5}{\partial \xi} = \frac{\partial SCF_{AC}}{\partial \xi}\,\sigma_x + SCF_{AC}\,\frac{\partial \sigma_x}{\partial \xi} - \frac{\partial SCF_{MIP}}{\partial \xi}\,\sigma_{my} - SCF_{MIP}\,\frac{\partial \sigma_{my}}{\partial \xi} \tag{4.101}$$

$$\begin{aligned}\frac{\partial \sigma_6}{\partial \xi} =& \frac{1}{2}\left(\frac{\partial SCF_{AC}}{\partial \xi} + \frac{\partial SCF_{AS}}{\partial \xi}\right)\sigma_x + \frac{1}{2}\left(SCF_{AC} + SCF_{AS}\right)\frac{\partial \sigma_x}{\partial \xi} - \\ & \frac{1}{2}\sqrt{2}\,\frac{\partial SCF_{MIP}}{\partial \xi}\,\sigma_{my} - \frac{1}{2}\sqrt{2}\,SCF_{MIP}\,\frac{\partial \sigma_{my}}{\partial \xi} + \frac{1}{2}\sqrt{2}\,\frac{\partial SCF_{MOP}}{\partial \xi}\,\sigma_{mz} + \\ & \frac{1}{2}\sqrt{2}\,SCF_{MOP}\,\frac{\partial \sigma_{mz}}{\partial \xi}\end{aligned} \tag{4.102}$$

$$\frac{\partial \sigma_7}{\partial \xi} = \frac{\partial SCF_{AS}}{\partial \xi}\,\sigma_x + SCF_{AS}\,\frac{\partial \sigma_x}{\partial \xi} + \frac{\partial SCF_{MOP}}{\partial \xi}\,\sigma_{mz} + SCF_{MOP}\,\frac{\partial \sigma_{mz}}{\partial \xi} \tag{4.103}$$

$$\begin{aligned}\frac{\partial \sigma_8}{\partial \xi} =& \frac{1}{2}\left(\frac{\partial SCF_{AC}}{\partial \xi} + \frac{\partial SCF_{AS}}{\partial \xi}\right)\sigma_x + \frac{1}{2}\left(SCF_{AC} + SCF_{AS}\right)\frac{\partial \sigma_x}{\partial \xi} + \\ & \frac{1}{2}\sqrt{2}\,\frac{\partial SCF_{MIP}}{\partial \xi}\,\sigma_{my} + \frac{1}{2}\sqrt{2}\,SCF_{MIP}\,\frac{\partial \sigma_{my}}{\partial \xi} + \frac{1}{2}\sqrt{2}\,\frac{\partial SCF_{MOP}}{\partial \xi}\,\sigma_{mz} + \\ & \frac{1}{2}\sqrt{2}\,SCF_{MOP}\,\frac{\partial \sigma_{mz}}{\partial \xi}\end{aligned} \tag{4.104}$$

Now we can run the rainflow algorithm through all those perturbed stresses at the hot-spots to obtain the damage of those modified designs $D(\xi + \Delta\xi)$. Then, we can reverse the finite differences to obtain the numerical derivative of the damage for each design variable as:

$$\frac{\partial D}{\partial \xi} \approx \frac{D(\xi + \Delta\xi) - D(\xi)}{\Delta\xi} \tag{4.105}$$

Figure 4.8 shows the comparison between a pure finite differences approach and the proposed combined approach. The savings may seem low but we avoid as many solutions of the dynamic equation as design variables we define, with the associated cost each solution has, particularly for the rotating case. Even though, the cost for this analysis is still extremely high, not only in CPU time as we have to run the rainflow algorithm through all the modified stresses, but also in storage[1].

An additional advantage is that, as we are actually counting again, we can actually consider the possible variation in the number of cycles $n_i$ if any, that was neglected by (4.94).

### 4.5.7. Frequency constraints sensitivities

Last but not least, we have the constraints limiting the first natural frequencies of the structure. As stated in section 3.2.2 we have an upper and lower limit for the first two natural frequencies of the system giving 4 optimization constraints (3.35). The expressions are readily derivable although we have to obtain the sensitivities of the natural frequencies with respect to the design variables for which we will use what was explained in previous chapters (2.5.1).

To get the natural frequencies we posed the generalized inverse eigenvalue problem to acquire the eigenvalues $\rho_i = 1/\lambda_i$ as:

$$\boldsymbol{M}\,\boldsymbol{\phi}_i = \rho_i\,\boldsymbol{K}\,\boldsymbol{\phi}_i \tag{4.106}$$

We can derive the above expression as:

[1] We saw in chapter 3 that the size of the stresses record for all the hot-spots for a 600s simulation could reach 190.464 MB. Using simple math it means that for 22 design variables the additional space to storage the derivatives of the hot-spots stresses would be 4190.208 MB. 4 GB of memory for just one single load case.

$$
\begin{aligned}
D_s \quad &\rightarrow \quad D_s\boldsymbol{M}\,\boldsymbol{\phi}_i + \boldsymbol{M}\,D_s\boldsymbol{\phi}_i = D_s\rho_i\,\boldsymbol{K}\,\boldsymbol{\phi}_i + \rho_i\,D_s\boldsymbol{K}\,\boldsymbol{\phi}_i + \rho_i\,\boldsymbol{K}\,D_s\boldsymbol{\phi}_i \Leftrightarrow \\
&\Leftrightarrow \quad D_s\boldsymbol{M}\,\boldsymbol{\phi}_i + (\boldsymbol{M} - \rho_i\boldsymbol{K})\;D_s\phi_i = D_s\rho_i\,\boldsymbol{K}\,\boldsymbol{\phi}_i + \rho_i\,D_s\boldsymbol{K}\,\boldsymbol{\phi}_i \Leftrightarrow \\
&\Leftrightarrow \quad \boldsymbol{\phi}_i^t\,D_s\boldsymbol{M}\,\boldsymbol{\phi}_i + \underbrace{\boldsymbol{\phi}_i^t\,(\boldsymbol{M} - \rho_i\,\boldsymbol{K})}_{=0}\,D_s\phi_i = \underbrace{\boldsymbol{\phi}_i^t\,D_s\rho_i\,\boldsymbol{K}\,\boldsymbol{\phi}_i}_{D_s\rho_i\,\underbrace{\boldsymbol{\phi}_i^t\,\boldsymbol{K}\,\boldsymbol{\phi}_i}_{=1^*}} + \boldsymbol{\phi}_i^t\,\rho_i\,D_s\boldsymbol{K}\,\boldsymbol{\phi}_i \Leftrightarrow \\
&\Leftrightarrow \quad \boldsymbol{\phi}_i^t D_s\boldsymbol{M}\,\boldsymbol{\phi}_i = D_s\rho_i + \boldsymbol{\phi}_i^t\,\rho_i\,D_s\boldsymbol{K}\,\boldsymbol{\phi}_i \Leftrightarrow \\
&\Leftrightarrow \quad D_s\rho_i = \boldsymbol{\phi}_i^t\;(D_s\boldsymbol{M} - \rho_i\,D_s\boldsymbol{K})\,\boldsymbol{\phi}_i
\end{aligned}
\tag{4.107}
$$

We can not forget that the natural frequencies are:

$$
\omega_i = \frac{1}{2\pi}\sqrt{\frac{1}{\rho_i}} \qquad \rightarrow \qquad D_s\omega_i = -\frac{1}{4\pi}\rho_i^{-3/2}D_s\rho_i \tag{4.108}
$$

Thereby, we can simply get the sensitivities of the natural frequencies using the eigenvalues, the eigenvectors and the sensitivities of the mass and stiffness matrix. The derivatives of the frequency constraints are then:

$$
\left\{ \begin{array}{c} D_s g_{\omega 1m} = -\dfrac{1}{\omega_{1P}} D_s\omega_1 \\ \\ D_s g_{\omega 1M} = \dfrac{1}{\omega_{3P}} D_s\omega_1 \end{array} \right\} \qquad \left\{ \begin{array}{c} D_s g_{\omega 2m} = -\dfrac{1}{\omega_{1P}} D_s\omega_2 \\ \\ D_s g_{\omega 2M} = \dfrac{1}{\omega_{3P}} D_s\omega_2 \end{array} \right\} \tag{4.109}
$$

## 4.6. Objective function sensitivity

At this point, the only thing left to derive in the optimization problem is the objective function. Compared to everything written so far in the chapter it is completely straightforward. The sensitivity clears the behavior of the objective function, it means the betterness of the design, with respect to changes in the variables or parameters that define the optimization problem.

Given the derivatives of the cross-sectional area (4.18) and length of each element (4.22), the derivative of the objective function or weight or the structure (3.3) is:

$$
\frac{\partial W}{\partial \xi} = \rho \sum_{i=1}^{n} \frac{\partial A_i}{\partial \xi}\, l_i + A_i \frac{\partial l_i}{\partial \xi} \tag{4.110}
$$

*the eigenvectors or natural modes are $\boldsymbol{K}$ orthogonals.

## 4.7. Summary and conclusions

Sensitivity analysis gives quantitative measure on the behavior of the optimization problem with respect to the design variables or parameters of the problem. Also, the derivatives of the functions are required to apply many of the mathematical optimization algorithms and in particular the one used and described in the next chapter. The main functions to derive are the objective function and the constraints. The differentiation of the objective function is straightforward while the thick of the sensitivity analysis is the differentiation of the constraints.

Direct Differentiation is chosen before Adjoint State Method since for this particular optimization problem it is clearly advantageous in terms of computational effort.

The ULS constraints are explicit functions of the design variables and stresses which are implicit functions of the design variables through the movements of the structure. Thus stresses, or forces, and movements have to be also derived which gives us $n$ additional dynamic systems of equations to solve, one for each design variable. After all, what has to be derived are the actual constraints imposed to the optimization problem, in this case, the aggregated functions. All those derivatives are obtained through analytic differentiation. For the FLS constraints, an analytical approach is to the date unreachable due to the counting method used. The proposed formulation combines analytical derivatives with finite differences to obtain the sensitivities of fatigue damage of each hot-spot. The last constraint of natural frequencies is easy to derive analytically.

The sensitivity core of the computational code is probably the most expensive part in terms of CPU time and storage. All the additional systems of equations to solve, the derivatives of the full time stress record with respect to all the variables and moreover the process of counting them, demand a large amount of resources. This fact is extremely limiting as that flood of information comes for every one of the load cases considered. This imposes a narrow frontier between what we can and what we can not face in terms of optimization.

Chapter 5

# Optimization method

*"This is how humans are: We question all our beliefs, except for the ones that we really believe in, and those we never think to question."*
**Orson Scott Card**, Speaker for the Dead.

## 5.1. Introduction

Chapter 3 laid the foundation of the proposed optimization problem. It also said that one of the most important steps (maybe the most important) was the establishment and definition of the optimization problem itself. The selection of a proper optimization algorithm is another fundamental pillar on which the acquisition of a valid optimized solution rests. In fact, sometimes the algorithm choice might be more important at the computational and mathematical level than the algorithm itself.

For better or worse, the definition of the optimization problem already imposes or restricts the use of certain algorithms (see the shape of the objective function, the imposition of constraints and their shape, the type of design variables, etc). In our case, the objective function and constraints are highly non-linear and the design variables are continuous.

Also, there are categories of optimization algorithms that are directly rejected, for example, heuristic and stochastic algorithms. That is mainly because those algorithms typically involve a high number of structural reanalysis to evaluate the swarm of test designs they generate[1], which is far from efficient given the computational cost of solving the proposed structural dynamics problem and particularly the evaluation of the fatigue damage.

[1]This is not strictly true because that drawback can be wisely bypassed using the information gained with the sensitivity analysis [Martínez, 2012]. Although they still require a lot of reanalysis of the structure.

Chapter 4 contains a detailed description of the first order sensitivity analysis carried out. There is a number of optimization algorithms and methodologies that require the information of the sensitivities, but up to second order. So they need the second derivatives of the objective function and constraints. While the first order derivatives give information about the path or direction to take, the second order derivatives tell us "how far" we should go in that particular direction or, what is called, the step size. However, the second order derivatives or the hessian of the system is often highly computational demanding although there are techniques to approximate it. High order sensitivity analysis could also be used to reduce non-linear problems.

In summary, choosing the optimization algorithm to use in the specific structural optimization problem is almost completely determined by the characteristics of the problem itself. This chapter is intended to choose and describe a suitable optimization algorithm to solve the problem of optimizing jacket substructures for offshore wind turbines.

## 5.2. Optimization algorithms and offshore engineering

This section is not intended to be a full review of optimization methods nor serve as a handbook of optimization. For extensive study in mathematical programming and optimization one can consult [Hernández, 1990; Fletcher, 2000; Chong & Zak, 2001; Lee & El-Sharkawi, 2008] among others. The scheme of figure 5.1 is a quick glimpse on a possible classification of optimization problems according to their properties and some of the most known algorithms.

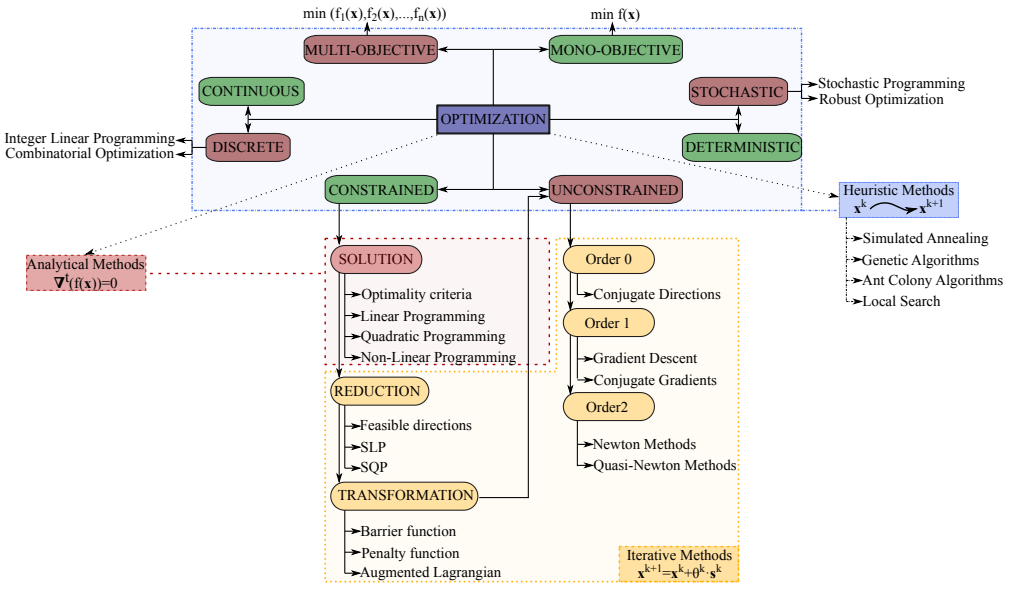


**Figure 5.1. General simplified scheme of optimization methods.**

See that the optimization problem we have defined falls always on the green branch of the four classifying properties depicted (Mono-objective, deterministic, continuous and constrained). That is not surprising as most of the structural optimization problems share those particularities. Luckily, those are also the most deeply studied problems and for which there are more available algorithms.

Under those terms there are three paths to follow. There are a few problems for which analytical and exact optimization methods have been developed, unfortunately the one in our hands is not one of them, so there are two paths left. Either we reduce or approximate the problem iteratively to one that has solution or we transform the problem to an unconstrained optimization problem.[2]

As said, transformation methods try to modify the constrained problem to get an equivalent unconstrained problem. Penalty Methods change the objective function adding a term that considers the imposed constraints. However, the subproblem created may be defective as it may be unbounded below which can be quite troublesome for the unconstrained algorithms [Gill et al., 1989]. Barrier Function Methods, also known as Interior Point methods, arise from the penalty function concept to prevent unfeasible iterations. The method generates "barriers" that bound the equivalent unconstrained problem to generate strictly feasible iterations. However, typical barrier functions tend to have singularities that make line search procedures inefficient or end up being ill conditioned. In addition, Penalty and Barrier Function Methods are not recommended for highly constrained problems.

One famous approach is the set of Augmented Lagrangian Methods (ALM). ALM are based on the Karush-Kuhn-Tucker conditions and the Lagrange Multipliers [Birgin & Martínez, 2014]. Given the problem defined in 3.2, the Lagrangian function will be defined by:

$$\mathscr{L}(\boldsymbol{x}, \boldsymbol{\lambda}, \boldsymbol{\mu}) = f(\boldsymbol{x}) + \sum_{i=1}^{l} \lambda_i \, h_i(\boldsymbol{x}) + \sum_{j=1}^{m} \mu_i \, g_i(\boldsymbol{x}) \tag{5.1}$$

whereas the Augmented Lagrangian will be :

$$\mathscr{L}_\rho(\boldsymbol{x}, \boldsymbol{\lambda}, \boldsymbol{\mu}) = f(\boldsymbol{x}) + \frac{\rho}{2} \left[ \sum_{i=1}^{l} \left( h_i(\boldsymbol{x}) + \frac{\lambda_i}{\rho} \right)^2 + \sum_{j=1}^{m} \left( \max\left(0, g_i(\boldsymbol{x}) + \frac{\mu_i}{\rho}\right) \right)^2 \right] \tag{5.2}$$

with $\rho > 0$ a penalty parameter, $\lambda \in \mathbb{R}^l$ and $\mu \in \mathbb{R}^m_+$ the Lagrange multipliers [Rockafellar, 1973].

At each iteration of the ALM, the function $\mathscr{L}_{\rho_k}$ has to bee minimized using one method for unconstrained optimization. Nevertheless, the role of the multipliers is extremely relevant and the convergence of the ALM depends critically on the multipliers estimation. The performance of the procedure is very sensitive to the choice of

[2]There are more options however we already rejected the possibility of using heuristic algorithms.

the penalty parameter and multipliers and it can be a waste of computational effort especially in early stages of the algorithm. In fact, the use of Lagrange Multipliers methods was shadowed by the Barrier Functions already mentioned and reduction methods described in the following. Nowadays the use of ALM seems to be gaining renewed attention [Curtis et al., 2015; Bai et al., 2016; Dentcheva et al., 2016]

The group of methods that has attracted more focus on the last decades are the ones under the title reduction methods in figure 5.1. These methods share the feature that they do not transform the problem into an unconstrained one rather they treat it directly either by approximating it or reducing it to a simpler problem. They also share the scheme of iterative methods where the optimum design is addressed as a series of discrete points related as:

$$\boldsymbol{x}^{k+1} = \boldsymbol{x}^k + \theta^k \, \boldsymbol{s}^k \tag{5.3}$$

where $\boldsymbol{s}^k$ is the vector or direction of modification and $\theta^k$ a scale factor also called step size. The selection of the direction is particular of each method for example, the Feasible Directions method bases the direction of each iteration on a few simple rules [Zoutendijk, 1960].

In many occasions it is sufficient with approximating the problem to one with analytic solution. The solution of the new problem obviously differs from the one sought so the solution of the approximated problem is performed iteratively until convergence. Those methods are Sequential Linear Programming (SLP) and Sequential Quadratic Programming (SQP). They both reduce the problem but with different order of approximation.

Given the constrained optimization problem:

$$\min F(\boldsymbol{x}) \tag{5.4}$$

subject to:

$$g_j(\boldsymbol{x}) \leq 0 \qquad\qquad j = 1, m \tag{5.5}$$

The solution of the problem is approached iteratively as (5.3) with $\theta^k \, \boldsymbol{s}^k = \Delta \boldsymbol{x}^k$, then the objective function and the constraints can be approximated as:

$$\begin{aligned} F(\boldsymbol{x}^{k+1}) &\approx \underbrace{\overbrace{F(\boldsymbol{x}^k) + \frac{dF(\boldsymbol{x}^k)}{d\boldsymbol{x}} \Delta \boldsymbol{x}^k}^{SLP} + \frac{1}{2} \left(\Delta \boldsymbol{x}^k\right)^t \, \boldsymbol{H} \left(F(\boldsymbol{x}^k)\right) \, \Delta \boldsymbol{x}^k}_{SQP} \\ g_j(\boldsymbol{x}^{k+1}) &\approx \underbrace{g_j(\boldsymbol{x}^k) + \frac{dF(\boldsymbol{x}^k)}{d\boldsymbol{x}} \Delta \boldsymbol{x}^k}_{SLP \,\&\, SQP} \end{aligned} \tag{5.6}$$

The SLP method approximates the optimization problem as a sequence of linear problems whereas the SQP simply has a higher order of approximation for the objective function. Each sub-problem is then solved using linear programming for the SLP

method and second order methods as Newton methods for SQP formulations or methods that approximate the Hessian matrix (Quasi-Newton Methods). The computation or approximation of the Hessian matrix and thus, the second derivatives, its an obvious disadvantage of the SQP method.

In this work, Sequential Linear Programming is proposed for the optimization of steel jacket substructures for offshore wind turbines. The approach is described in upcoming sections along with its strengths and weaknesses.

The proposed method is neither unique nor absolute. In section 1.2 of this thesis, some of the most relevant works in optimization of jackets for offshore wind turbines were briefly discussed. The algorithms used in each case are far from agreement and authors justify and highlight the pros and cons of their methods. For example [Yoshida, 2006; Nasseri et al., 2014] utilize genetic algorithms despite the immense computational effort involved, the latter using at least 1000 generations. [Karadeniz et al., 2010] and [Chew et al., 2016], both use SQP. The first uses algorithm of the commercial IMSL library (International Mathematical and Statistics Library) where the second uses a toolbox of Matlab. [Chew et al., 2016] then uses a Quasi-Newton algorithm with a Broyden-Fletcher-Goldbarg-Shanno (BFGS) approximation of the Hessian matrix. [Oest et al., 2017] employees the SLP of the commercial IBM ILOG CPLEX optimizer, a large-scale optimization solver. Finally, there are other approaches as the one of [Zwick et al., 2012] and [Schafhirt et al., 2016] where authors solve just a sizing equation for each element independently considering that small changes in singular elements of the structure do not influence the global behavior of the structure.

## 5.3. Optimization algorithm

### 5.3.1. Sequential Linear Programming

The SLP method bases its performance in the linearization of the objective function and constraints. This approximation can be seen in the conceptual figure 5.2. Clearly, the optimum design obtained with the linearized problem does not have to match that of the original non-linear problem. In fact, the SLP carries some drawbacks worth keeping in mind. The linearization may trim the feasible design region leaving valid designs out. Also, if the optimum design activates only one constraint, the sequence of linear problems may oscillate between vertex[3].

Given the linear approximation of the optimization problem:

$$\begin{aligned} F(\boldsymbol{x}^{k+1}) = F(\boldsymbol{x}^k + \Delta\boldsymbol{x}^k) &\approx F(\boldsymbol{x}^k) + \frac{dF(\boldsymbol{x}^k)}{d\boldsymbol{x}}\Delta\boldsymbol{x}^k \\ g_j(\boldsymbol{x}^{k+1}) = g_j(\boldsymbol{x}^k + \Delta\boldsymbol{x}^k) &\approx g_j(\boldsymbol{x}^k) + \frac{dg_j(\boldsymbol{x}^k)}{d\boldsymbol{x}}\Delta\boldsymbol{x}^k \end{aligned} \tag{5.7}$$

[3]The reason is the solution of the linear problem as seen in section 5.3.3

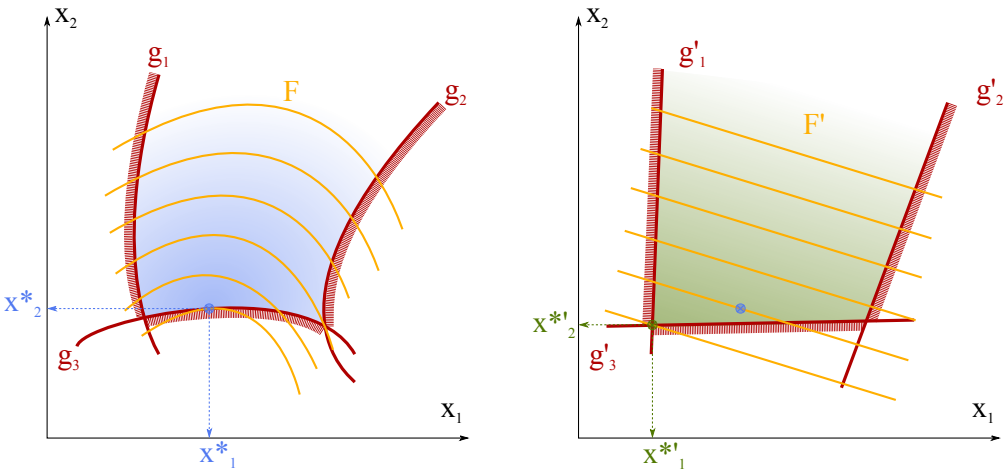


**Figure 5.2. Linearization of the objective function and constraints.**

we are seeking the design variables $\boldsymbol{x}^*$ that minimize the functional $F(\boldsymbol{x})$ still subject to the constraints $g_j(\boldsymbol{x}) \leq 0$. So, in each step the aim is to reduce the value of the objective function. In order to do so, the factor added each time has to be minimized. Then the new objective function of the linearized problem becomes:

$$\min\{F(\boldsymbol{x})\} \rightarrow \min\left\{F(\boldsymbol{x}^k + \Delta\boldsymbol{x}^k) \approx F(\boldsymbol{x}^k) + \frac{dF(\boldsymbol{x}^k)}{d\boldsymbol{x}}\Delta\boldsymbol{x}^k\right\} \rightarrow \min\left\{\frac{dF(\boldsymbol{x}^k)}{d\boldsymbol{x}}\Delta\boldsymbol{x}^k\right\} \tag{5.8}$$

Right now we are interested only in acquiring the direction of minimization so we can ignore the step size and formulate the new objective of the approximated linear problem as:

$$\min\left\{\frac{dF(\boldsymbol{x}^k)}{d\boldsymbol{x}}\boldsymbol{s}^k\right\} \tag{5.9}$$

With regard to the constraints:

$$g_j(\boldsymbol{x}) \leq 0 \rightarrow g_j(\boldsymbol{x}^k + \Delta\boldsymbol{x}^k) \approx g_j(\boldsymbol{x}^k) + \frac{dg_j(\boldsymbol{x}^k)}{d\boldsymbol{x}}\Delta\boldsymbol{x}^k \leq 0 \quad \Leftrightarrow \quad \frac{dg_j(\boldsymbol{x}^k)}{d\boldsymbol{x}}\Delta\boldsymbol{x}^k \leq -\,g_j(\boldsymbol{x}^k) \tag{5.10}$$

Once again, we are interested just in the minimization direction thus, the new constraints can be stated as:

$$\frac{dg_j(\boldsymbol{x}^k)}{d\boldsymbol{x}}\boldsymbol{s}^k \leq -\,g_j(\boldsymbol{x}^k) \qquad j = 1, m \tag{5.11}$$

In summary, the original problem is lineariazed and sequentially solved as:

$$\left\{\begin{array}{l} \min\{F(\boldsymbol{x})\} \\ \text{subject to:} \\ \quad g_j(\boldsymbol{x}) \leq 0 \qquad j=1,m \end{array}\right\} \approx \left\{\begin{array}{l} \min\left\{\dfrac{dF(\boldsymbol{x}^k)}{d\boldsymbol{x}}\boldsymbol{s}^k\right\} \\ \text{subject to:} \\ \quad \dfrac{dg_j(\boldsymbol{x}^k)}{d\boldsymbol{x}}\boldsymbol{s}^k \leq -\,g_j(\boldsymbol{x}^k) \qquad j=1,m \end{array}\right\} k=1,\ldots \tag{5.12}$$

Each of the $k$ sub-problems is then solved using linear programming. Obviously this is where all the described in chapter 4 grows in importance as the accuracy of the sensitivity analysis directly affects the accuracy of the linear approximation of the optimization problem.

### 5.3.2. Moving limits

Again, the approximation of the original problem and linearization of the non-linear objective and constraint functions carries inherent disadvantages. There have been several modified approaches proposed according to [Hernández, 1990]. One of the most successful was the one devised by [Griffith & Stewart, 1961] illustrated in figure 5.3.

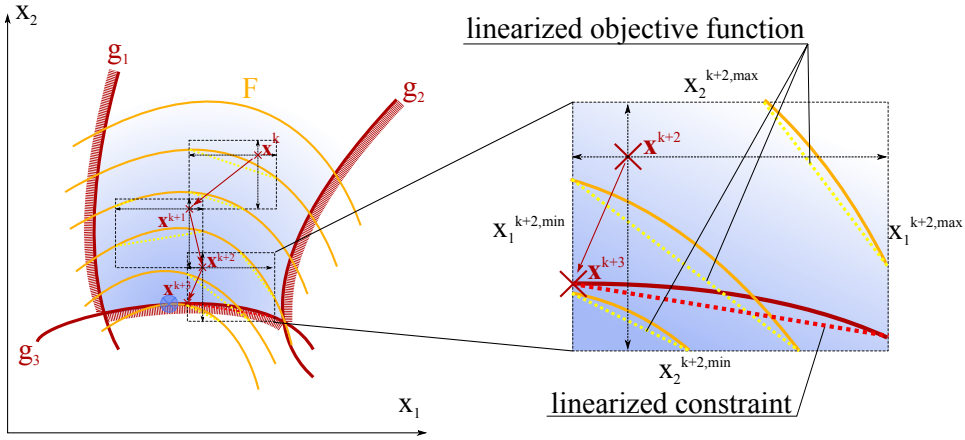


**Figure 5.3. Moving limits in the SLP method.**

The approach introduces at each iteration what are called moving limits which are lower and upper limits to the variation of the design variables at each step. So, when solving each sub-linearized problem, the design region is bounded by these lower and upper limits and by the linearized constraints if any of them intersects the space defined by the moving limits. The methodology has been proved effective and solves some of the convergence issues of SLP. For example, it is possible now to detect those minima

located at intersections with only one constraint and not a vertex of the domain. It is worth saying that the moving limits can be different for every point.

In [Chen, 1993] one can find a comparison between 6 methods for computing the moving limits, the results are assorted and, exceptions apart, there are not big discrepancies between methods. In [Lamberti & Pappalettere, 2000] the authors compare again 7 different moving limit approaches. It is shown how distinct methods present different optimization results as well as computational costs although the SLP method is very robust and the differences are more noticeable in CPU time than in the optimized solution.[Lamberti & Pappalettere, 2003] contains a review of the development of moving limits within SLP method and also proposes a method to compute the limits based on predicting the difference between the non-linear problem and the linear approximation at each iteration.

Even though, one of the most extended approaches is still the establishment of the moving limits as a percentage of the current value of the design variables or even fixed values that can be adjusted (increased or decreased) during the optimization process given the direction of modification for each variable [Hafka et al., 1990; Arora, 1989].

### 5.3.3. Simplex

So far we have depicted how do we transform or approach the non-linear optimization problem stated. We have concluded that the problem could be reduced to a series of approximated linear problems, but we also have to define a method to solve those linear programming problems which have analytic solution. From the set of techniques available the Simplex seems to be the most accepted one. There is an extensive literature on the Simplex method, however [Dantzig & Thapa, 1997a] and [Dantzig & Thapa, 1997b] are specially recommended references from the inventor of the algorithm himself. Also, the reader is encouraged to consult [París, 2007] as the developed algorithm in that work is the one implemented in the current methodology. The following is an attempt to briefly describe the procedure of the algorithm and the main factors that may influence our problem.

Any linear programming problem can be stated in mathematical form as:

$$\begin{aligned} & \min \boldsymbol{c}^t \boldsymbol{x} = f \\ \text{subject to:} \quad & \\ & \boldsymbol{A}\boldsymbol{x} = \boldsymbol{b} \\ & \boldsymbol{l} \geq 0 \quad ; \quad \boldsymbol{l} \leq \boldsymbol{x} \leq \boldsymbol{u} \end{aligned} \tag{5.13}$$

the above is called the standard form of a linear program where $\boldsymbol{l}$ and $\boldsymbol{u}$ represent the lower and upper values of the design variables or bound constraints. The original algorithm of Dantzig was not prepared to deal with bounds for the variables although it only considered non-negative design variables. A version to account for these limits was developed later [Dantzig, 1987].

The Simplex Method works in two phases: Phase I seeks for a canonical basic feasible solution and Phase II is the application of the Simplex Algorithm. Note that

there is a difference between what constitutes the Simplex Method and the Simplex Algorithm. Note also that the Simplex is defined to work only with non-negative design variables and equality constraints.

The canonical basic feasible solution is the starting point of the Simplex Algorithm. It is obtained by pivot operations over the system in (5.13) similar to those of a Gaussian elimination. The canonical form separates the variables in dependent and independent (or basic and non-basic variables), so the system is reduced to:

$$\boldsymbol{I}\,\boldsymbol{x}_B + \boldsymbol{A'}\,\boldsymbol{x}_N = \boldsymbol{b'} \tag{5.14}$$

where $\boldsymbol{x}_B$ and $\boldsymbol{x}_N$ represent the set of basic and non-basic variables.

Given the canonical basic feasible solution the Phase II of the methodology, the Simplex Algorithm, is able to reach the optimum solution. In essence, the Simplex Algorithms finds the optimum solution by moving over the contour of the feasible design region from vertex to vertex. The example of figures 5.2 and 5.3 and the importance of the moving limits is now clearer.

### Application to SLP

In summary, first we approximate the non-linear optimization problem to a linear program using (5.12) and second we apply the Simplex Method to that sub-problem to solve the direction of modification of the design variables $\boldsymbol{s}^k$. The problem in (5.12) is equivalent to that of (5.13) with:

$$\begin{aligned} \frac{dF(\boldsymbol{x}^k)}{d\boldsymbol{x}}\boldsymbol{s}^k &\equiv \boldsymbol{c}^t\,\boldsymbol{x} \\ \frac{dg_j(\boldsymbol{x}^k)}{d\boldsymbol{x}}\boldsymbol{s}^k \leq -\,g_j(\boldsymbol{x}^k) &\equiv \boldsymbol{A}\,\boldsymbol{x} = \boldsymbol{b} \end{aligned} \tag{5.15}$$

Still, it is easy to see that there are some aspects of the above equivalence and the Simplex Method that have to be treated.

Firstly, we have said that the Simplex Method deals only with non-negative design variables. Our design variables are non-negative, remember that they are the diameter and thickness of the cross-sections of the bars and the bottom and top base widths of the jacket. However, we are not solving the optimization problem directly. In the SLP method, the variables for each sub-problem to solve are the components of the direction of modification of the design variables in each iteration. And they can be positive or negative as any design variable can increase or decrease its value. To adapt the problem to be solvable with the Simplex we just need to do a translation of the variables using the lower bound of the moving limits.

$$\boldsymbol{s'}_i = \boldsymbol{s}_i - \boldsymbol{l}_i \qquad i = 1, n \tag{5.16}$$

being $n$ the number of design variables.

Once solved, the sub-problem has to be translated back.

Secondly, the Simplex Method is not prepared to deal with inequality constraints. In order to transform our inequality ($\leq$0) constraints to equality functions we have to introduce positive slack variables.

With both modifications we can rewrite (5.11) as:

$$\frac{dg_j(\boldsymbol{x}^k)}{d\boldsymbol{x}}\boldsymbol{s}^k \pm h_j = -\,g_j(\boldsymbol{x}^k) - \sum_{i=1}^{n} l_i\, g_{j,i} \qquad j = 1, m \tag{5.17}$$

where $h_j$ are the slack variables for each constraint and $g_{j,i}$ are the components of each constraint $j$ that affect each design variable $i$.

Now the linearized sub-problem is ready to be solved using the Simplex Method described earlier.

#### Dependencies

It may seem strange but in most cases finding the canonical basic solution can be harder that the application of the Simplex Algorithm to achieve the optimal solution. There are many issues that can compromise the acquisition of a basic solution and unfortunately one of them appears in the proposed optimization problem almost always.

The four legged jacket substructures objective of this work have 90º rotational symmetry with respect to the $Z$ axis. So, symmetric elements share exactly the same properties (cross-section, length) and so, depend on the same design variables. And when they are subject to loads coming from a principal direction (for example waves), they also experience the same forces. This leads to repeated constraints through all the structure that then appear in the matrix system of the linear program generating a dependent system that can produce vacuous equations when pivoting.

The repeated equations add no information to the system and can simply be deleted. The implementation of the optimization method includes an algorithm to delete those constraint equations from the system. That small action can seem meaningless but it also importantly reduces the number of constraints of the system and works in pursuit of computational efficiency.

### 5.3.4. Steepest descent

The Simplex Method within the SLP algorithm has been proved robust and reliable. However it requires the information of the active constraints set. Given the situation where no constraints are active, the Simplex Method can not be applied. Under this circumstance the optimization iteration is performed using the Steepest Descent method. The direction of modification of the design is computed using just the gradient of the objective function.

$$\boldsymbol{s}^k = -\boldsymbol{\nabla} F(\boldsymbol{x}^k) \tag{5.18}$$

The direction is bounded by the moving limits of the design variables in order to prevent sudden and too large changes in the design that could easily take it out of the feasible region given the non-linearity of the structural constraints.

## 5.4. Optimization methodology and numerical implementation

At this point, the whole proposed methodology for the optimization of steel jacket substructures for offshore wind turbines has been exposed. There might be specific details that were not deeply explained as they make more sense when describing the particular application examples.

Figure 5.4 is an attempt to summarize every programmed algorithm and the flow of the computational code. Obviously and unfortunately not everything fits in the flowchart and there are many aspects that have been obviated. For example, sensitivity analysis implementation is far more complicated than that shown in the flowchart but it is impossible to even try to draw it without messing the whole chart. The non-linear Newmark algorithm performs inner iterations within each time step that are not reflected. Not a single thing is said about the dimensional constraints or about the bound constraints. Loads are merely mentioned when each of them has its own and arduous subroutine for which an specific flowchart could be drawn. And many more.

In any case, it can be seen that the code is principally divided in three main cores: Modeling, Analysis and Optimization. Here follows a short summary of what do those cores do and how do they work. Note that the Sensitivity Analysis is divided in 5 kernels (from 0 to 4) where the level 0 represents the most basic derivatives that are then used through all the code, and level 4 are the last derivatives computed.

1. **Modeling:** The first core builds up the computational model of the offshore wind turbine from the jacket to the blades. It is basically formed by two pieces, data reading and model generation. It also calls to three of the Sensitivity kernels.

    - Data reading: Simply reads a data file containing the main geometry of the structure and sections of the elements.
    - Model generation: Is the heavy part of the first core. It generates the computational model from the data assembling all the structural matrices and computing all the required properties of the model. It computes the natural frequencies and modes of vibration and it also computes the static loads and the first step or initial condition of the dynamic loading. It calls to three differentiating kernels to compute the derivatives of the main properties of the system, the derivatives of the structural matrices and the derivative of the forces.

2. **Analysis:** The second core performs a single yet determining phase, the dynamic analysis of the structure. It uses the third level of the sensitivity analysis. It is by far the more expensive task of the code in computational terms.

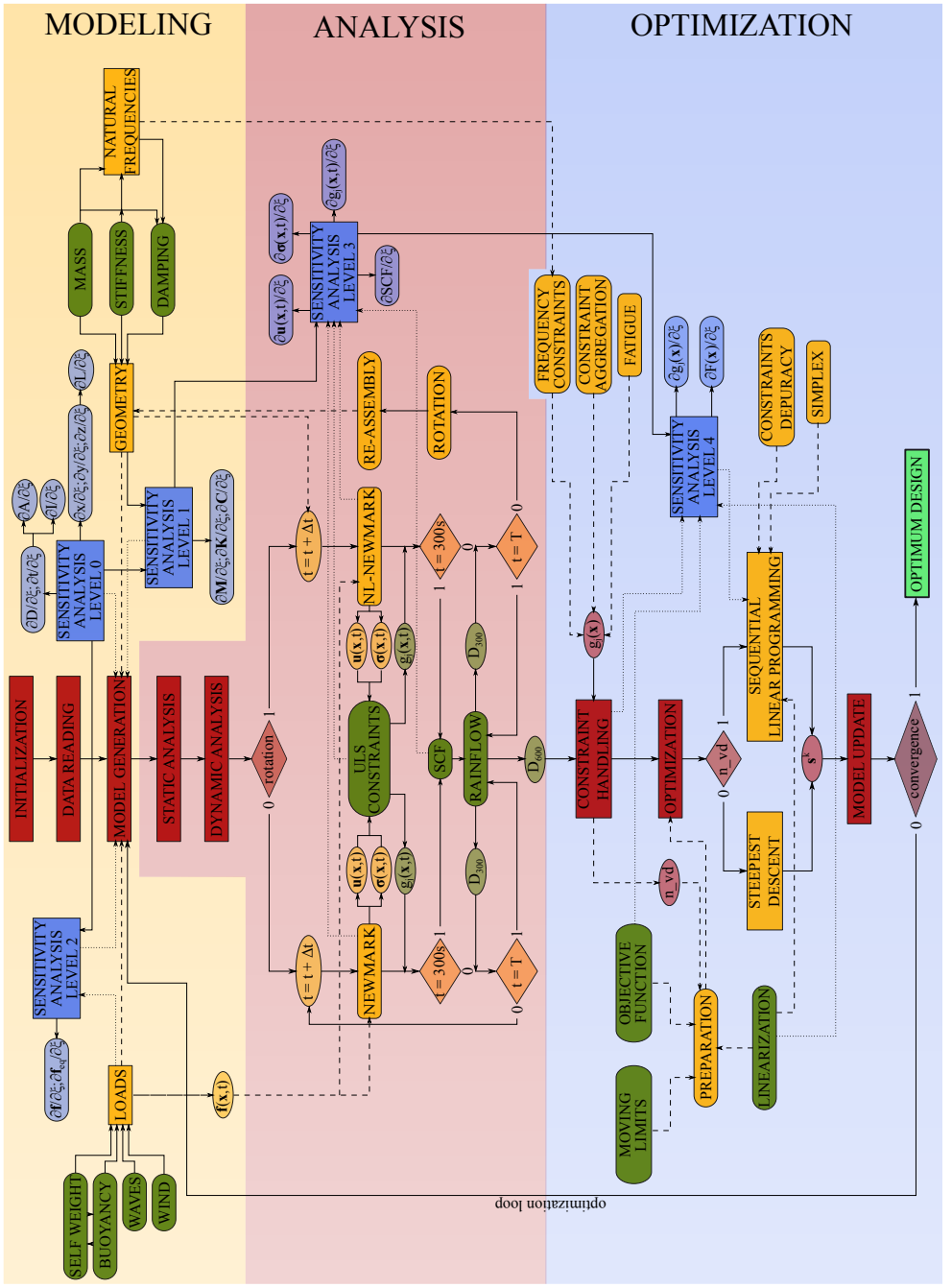


**Figure 5.4. Numerical implementation scheme.**

- Static analysis: Firstly, a static analysis is performed. The results serve as initial condition for the following dynamic analysis.
- Dynamic analysis: The structural dynamic analysis is the central pillar of the code on which the results of the subsequent optimization process relies. The analysis is divided whether the model is allowed to rotate or not. Both sides call to the loading process to compute the time-dependent loads. The rotating branch integrates the dynamic equation of motion using the non-linear Newmark algorithm and between time steps needs to rotate the blades and call to the re-assembly of the geometry of the turbine to recalculate the structural matrices. At 300s and 600s there are checkpoints in the algorithm to run the rainflow counting process to achieve the fatigue damage at those ages. The computation of the SCFs is included in this loop. Also, all the ULS structural constraints are computed at each time step, they will be aggregated in the next and last core of the implementation. The third Sensitivity kernel is devoted to solve the differentiated dynamic system in order to acquire the sensitivities of movements and stresses and therefore of the ULS constraints, as well as the derivatives of the SCFs.

3. **Optimization:** The third and last core tries to achieve the main objective of the whole code and optimize the jacket design. The fourth level of the sensitivity analysis is required in this process.

   - Constraint handling: This sub-process manages all the information of the constraints as it comes from the dynamic analysis and generates the constraints themselves. The Kreisselmeier-Steinhauser aggregation is computed here as well as the generation of the fatigue damage expected at design life and the corresponding constraint. Every constraint is assembled and numbered in one array. The sensitivities of the constraints are computed and stored.
   - Optimization: Previous to enter the optimization process and after the constraint handling all the variables are prepared. The objective function and its derivative are computed, the moving limits established and the linearization of the optimization problem is carried out using the information cast by the fourth sensitivity level. Two branches appear when entering the optimization process whether there are active constraints or not. If not, the direction of optimization is obtained through a Steepest Descent method with the gradient of the objective function and considering the moving limits of the design variables. This path is rarely followed as in most cases at least dimensional constraints are active in the initial design. Otherwise, the Sequential Linear Programming method begins firstly by eliminating the repeated constraints and then applying the Simplex Method already described. The result of the optimization process is the modification of the design variables.

- Model update: The design variables are modified according to the result of the optimization process and the structural model is updated with the new data. Convergence is checked, if positive the optimized design has been achieved, if not, the optimization loop carries the process all up to the model generation process of the Modeling core to recalculate the necessary properties of the new design and restart the analysis and optimization.

## 5.5. Summary and conclusions

This chapter describes the optimization method and algorithms used in this work. The proposed optimization problem is clearly non-linear in both the objective function and the structural constraints. The solution is based on the application of Sequential Linear Programming to reduce the non-linear structure to a series of approximated linear problems that will be later solved using linear programming. In these approximations the accuracy of the first order sensitivity analysis performed takes special relevance. Moving limits are used to restrict the step of the optimization iterations in order to improve the convergence of the algorithm and also keep the linear approximation as close as possible. The arising linear programs at each iteration are then solved using the Simplex Method, particularly the implementation developed in [París, 2007]. Some adjustments of the SLP formulation have to be touched to be solvable by the Simplex like the incorporation of lower and upper bounds for the design variables and the fact that the structural constraints are formulated as inequalities.

Finally, the whole computing scheme of the implemented methodology is presented and outlined comprising chapters 2 through the present one. The next chapter applies the developed technique to several application examples comparing the performance of the algorithm for different parameters and under different situations to expose its strengths and weaknesses.

Chapter 6

# Application examples

*"A person may be only practical but then he realizes routinely. A person may be only theoretical but then what he conceives of is often unrealizable"*
**Georges Politzer**, Elementary principles of philosophy.

*"What cannot be settled by experiment is not worth debating"*
**Newton's Flaming Laser Sword**

## 6.1. Introduction

Even though the number of offshore wind farms is rapidly increasing and jacket substructures are being installed more and more often, jacket designs are not easily available. That is mainly a result of an "offshore race"[1] between companies trying to monopolize new energy sources while keeping their technologies secret and protected by patents. So, laying your hands on a real jacket design for offshore wind turbines is quite a challenge.

Luckily and wisely, the International Energy Agency (IEA) has a Wind Agreement to exchange information and research progress on large-scale wind projects. The 30th task of the agreement is the "Comparison of Dynamic Computer Codes and Models for Offshore Wind Energy". Under this task, one of the projects was the Offshore Code Comparison Collaboration and the Offshore Code Comparison Collaboration Continuation, called OC3 and OC4 respectively. The interesting part of these projects is the full definition of an offshore jacket and wind turbine and the comparison of the structural analysis by different commercial and custom codes. All the work can be consulted in the specific documentation of the project, although all the needed data can

[1] We could make an analogy to the Space Race during the Cold War, although now the race is taking place in the seas and between private companies. We could go farther and call it the "Warm War" referring to the undeniable global warming.

be found in [Jonkman et al., 2009; Vorpahl & Popko, 2012; Vorpahl et al., 2012; Popko et al., 2014]. At the same time, the jacket described is taken from the UpWind project of the European Wind Energy Association [de Vries, 2011]. The main optimization works focused on jacket structures referenced in this work obviously use the UpWind jacket.

Given the lack of available designs, the UpWind jacket is the reference structure used in this work although, some discrete modifications of the base jacket are proposed in this chapter and optimized using the developed methodology. The chapter first describes the particularities and characterizes the basic OWT model. Then, a few parameters of the optimization algorithm and methodology are studied. The extent of the formulation including the rotation of the blades is analyzed from its impact on the initial design to the optimization process and the different optimum designs. Finally a design considering a more accurate approximation of the environmental conditions and several modifications of the basic UpWind jacket is proposed, optimized and evaluated.

## 6.2. Model description

The following is a brief description of all the parts that integrate the full offshore wind turbine and a detailed description of the jacket.

### Turbine tower

The turbine tower is a 68.00 m tall steel conical cylinder which diameter and thickness decreases with height until 4/5 of the total height where it increases again. The profile of the tower is defined by 9 different cross sections. However the structural model is built up with elements of constant section using the averaged properties as shown in table 6.1

Additionally, three point masses are included in the tower to consider the flanges, bolts and other equipment. The point masses are located at 0.00 m, 34.00 m and 68.00 m weighting 1.9 t, 1.4 t and 1.0 t respectively. This point masses are accounted in the model as lumped masses at those nodal points considering only the traslational inertia as said in 2.4.1 .

### Rotor-nacelle assembly

The rotor-nacelle assembly is modeled using beam elements as well. The location and geometry of the members is depicted in figure 6.1. The properties of each cross-section are defined to match those of the real nacelle, specially mass. Figure 6.1 points out the centers of gravity of the hub and the nacelle, although, in the model the hub elements are considered massless and the weight is introduced again as a point mass. On the other side, the center of gravity of the nacelle is positioned by balancing the masses of the four bars that build the model. The hub mass is 56.78 t and the nacelle 240.00 t.

| | Height | $D$ (m) | $t$ (mm) | N° | $A$ (mm$^2$) | $I$ (mm$^4$) | $J$ (mm$^4$) |
|---|---|---|---|---|---|---|---|
| 70.15+ | 0.00 | 5.500 | 32 | | | | |
| | | | | 1 | 0.55860 | 2.15593 | 1.07797 |
| | 1.00 | 5.777 | 32 | | | | |
| | | | | 2 | 0.52791 | 1.94232 | 0.97116 |
| | 12.00 | 5.318 | 30 | | | | |
| | | | | 3 | 0.47146 | 1.5808 | 0.79040 |
| | 22.00 | 5.082 | 28 | | | | |
| | | | | 4 | 0.40234 | 1.22314 | 0.61157 |
| | 34.00 | 4.800 | 24 | | | | |
| | | | | 5 | 0.33705 | 0.91842 | 0.45921 |
| | 44.00 | 4.565 | 22 | | | | |
| | | | | 6 | 0.29237 | 0.71923 | 0.35962 |
| | 54.00 | 4.329 | 20 | | | | |
| | | | | 7 | 0.32802 | 0.71664 | 0.35832 |
| | 63.00 | 4.118 | 30 | | | | |
| | | | | 8 | 0.37973 | 0.77104 | 0.38552 |
| | 68.00 | 4.000 | 30 | | | | |

**Table 6.1. Cross-sectional properties of the tower elements**

### Blades

Blades are also formed by discrete beams. The glasfiber blades are 61.5 meters long and their airfoil sections are detailed in [Jonkman et al., 2009] along with the structural properties. Again, the variable cross-sections are modeled with constant elements with the averaged properties between sections giving 50 different elements per blade. Each blade weights 17.74 t distributed along the blade's span with the mass of each averaged element.

### Transition piece

The transition piece of the OWT is a particularly critical part of the structure, specially when the submerged substructure is a jacket type. It is commended to be a transition between the four-legged geometry of the jacket and the singular mono-pile of the tower and carry the stresses from one structure to the other. Designs are diverse and, as mentioned, strongly subjected to specific patents. Though, one of the most used designs consists of a squared horizontal plate with a central pipe that receives the base of the tower and braced by four smaller tubular elements towards the legs of the jacket 6.2

Nevertheless, the current interest is the modelization and analysis of the jacket structure for which the transition piece relatively lacks of importance, at least its geometry. So, in [Vorpahl et al., 2012] the transition piece is considered just a rigid concrete block 9.6 x 9.6 x 4 m with a mass of 666 t. The purpose of this model is

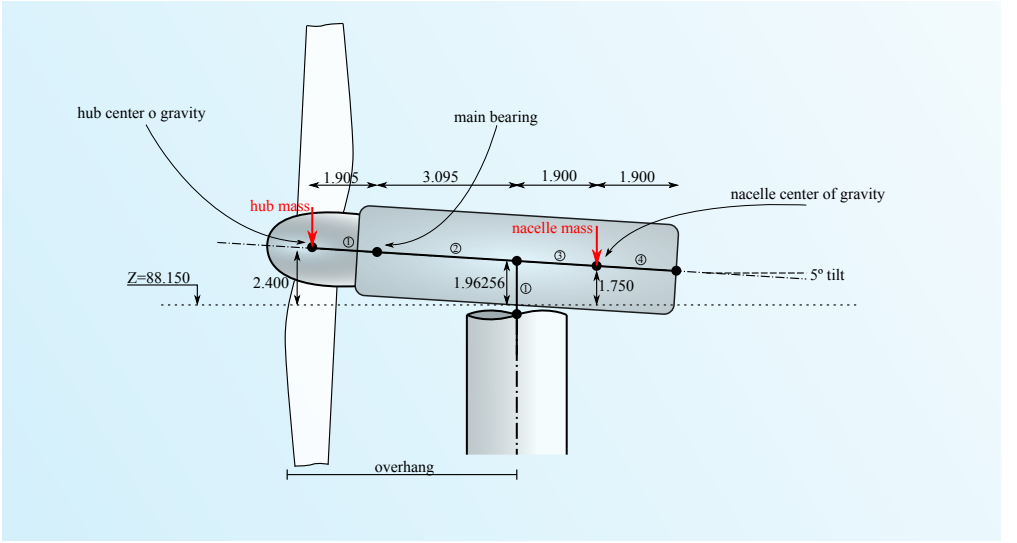


**Figure 6.1. Rotor-nacelle assembly model.**


**Figure 6.2. Examples of transition pieces [Lee et al., 2016].**

to guarantee a sufficiently rigid connection between the jacket piles and the turbine tower. Recall that the model proposed in these works uses only beam elements thus, in order to represent the concrete block, the whole mass and stiffness of the block is condensed in a set of discrete bars with the corresponding cross-section, inertia and material properties to match the mass and stiffness of the concrete structure.

Figure 6.3 shows the three models initially proposed in the development of this thesis. The requisites for the model are again, the representation of the global properties of the block, the definition of four bottom and on centered top nodes to join the jacket legs with the tower base, and the creation of a sufficiently rigid connection between them. Model a) was selected as it is a better representation of the distributed properties of the block and its overall geometry. The mass of the model can be easily matched

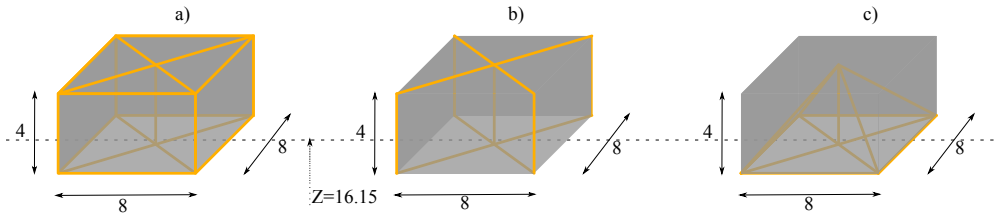


**Figure 6.3. Transition piece modeling options.**

with the cross-sections and an equivalent density and then the stiffness or inertia of the elements can be adjusted by the natural frequencies of the system. The vertical elements of the geometry are part of the jacket, as described in the following section, and thus, can not contribute neither to the transition piece's mass nor stiffness.

### 6.2.1. Jacket

The steel jacket substructure is a three-dimensional framed structure made by tubular cross-sections. The geometry and characteristics of the members are described in figure 6.4 and tables 6.2,6.3, 6.4 and 6.5. The tubular structure is 65.65 meters high being its bottom and top widths 12 and 8 meters respectively. The structure is clamped at 50 meters deep. It is formed by 4 levels of X sections and a horizontal bracing bar at the bottom. There are 4 different cross-sections, two for the legs, one for the braces and the last one for the 4 vertical bars embedded in the transition piece. However, considering the flooded legs (F) under the Mean Sea Level and the marine growth (MG) on elements between -2.0 and -40.0 m it leads to 8 different cross sections shown in table 6.3. Note that this is the initial configuration defined by the UpWind Reference jacket, the optimization design variables are not limited to that classification of the structural elements although they do have to respect the structural symmetry.

Between -45.500 and -50.000 m the jacket legs intersect the part of the piles over the mudline. The tubular legs are grouted inside the piles and embed until -49.50. The grouting material weights 2 t/m$^3$ and the dimensions of the pile are $D = 2.082$ m and $t$ =0.060 m. The last 0.5 m till the mudline are just the pile without grouting or jacket leg inside.

The first step of the validation is the verification of the modeled mass. The jacket modeled is 673.810 t where the references state that its mass is 673.718 t, it means a deviation of 92 kg, a 0.014 %. The total mass of the whole offshore wind turbine system is 2295.146 t.

The verification of the accuracy of the coupled model and the dynamic analysis is scattered in chapter 2. Figure 2.12 shows that the torque and thrust forces exerted to the blades and therefore to the structure for a range of wind and rotational speeds are in good agreement with the analysis carried out under the OC4 project. The same goes for figures 2.16 and 2.17 where in the first one the first five natural vibration modes

are drawn and the second plots the shear force at the mudline in global X direction under wave loading.

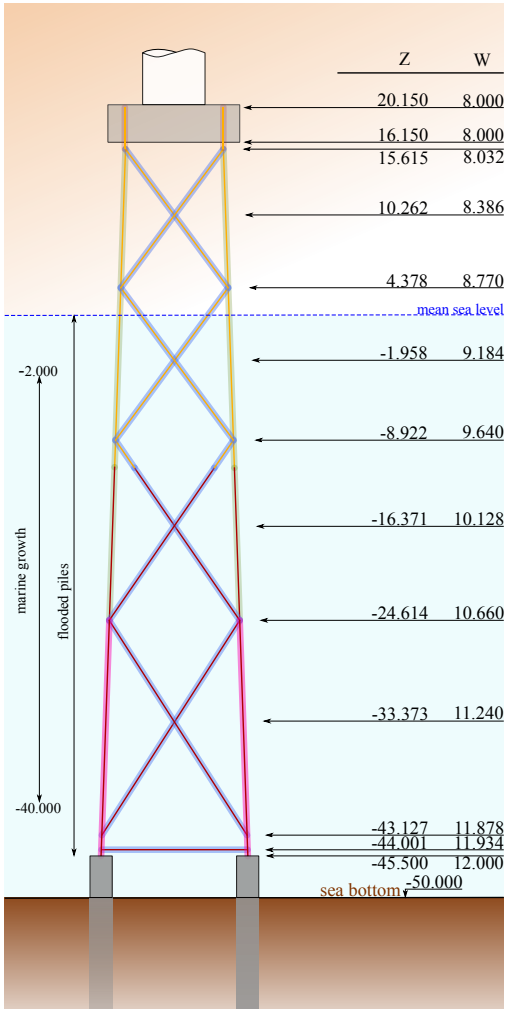


**Figure 6.4. OC4 jacket geometry.**

| | $D$ | $t$ | $A$ | $I$ | $J$ |
|---|---|---|---|---|---|
| 1 | 0.800 | 0.020 | 0.04901 | 0.00373 | 0.00187 |
| 2 | 1.200 | 0.050 | 0.18064 | 0.02992 | 0.01496 |
| 3 | 1.200 | 0.035 | 0.12810 | 0.02175 | 0.01088 |
| 4 | 1.200 | 0.040 | 0.14577 | 0.00246 | 0.01227 |

**Table 6.2. Cross sections of the members.**

| | S | F | MG | F+MG |
|---|---|---|---|---|
| 1 | X | | X | |
| 2 | | X | | X |
| 3 | X | X | | X |
| 4 | X | | | |

**Table 6.3. Combinations of cross-sections circumstances.**

Material : $\rho = 7.85$ t/m$^3$
$E = 2.1\ 10^8$ kN/m$^2$
$\nu = 0.3$

**Table 6.4. Material properties.**

| Additional masses: | | |
|---|---|---|
| 1 | Marine Growth: | -40 $\leq z \leq$ -2 |
| | | t= 0.100 |
| | | $\rho$ =1.1 t/m$^3$ |
| 2 | Flooded Piles: | $z \leq MSL$ |
| | | $\rho$ =1.025 t/m$^3$ |

**Table 6.5. Additional masses.**

## 6.3. Performance and efficiency

In chapter 2 the computational cost of the solution of the dynamic equations of motion for the non-rotating and the rotating case were brought out. The subject was resumed in chapter 4 incorporating the additional cost and memory storage due to the first order sensitivity analysis. While the dynamic analysis per se was not an issue, the sensitivity analysis introduced an enormous extra cost and space required, giving ratios of computing time to simulated time close to 1 or even greater for the variable geometry scheme. That being said, its merely for one single load case. The size of the

analysis and optimization problem has to be multiplied by the number of loading cases we want to consider in the design.

The main problem is that the number of load cases usually considered in offshore wind turbines is not short but extremely large. There are different ways of dealing with the environmental conditions uncertainty. One of the most famous is to describe the environmental offshore actions in a scatter diagram that sets the probability of a given sea state $(H, T)$ which can be related to a wind speed $(V)$, and we are already simplifying things. Moreover, those loads are exerted in a particular direction, so the scatter diagram could be a directional scatter diagram also expressing the dispersion of the incoming directions of the loads.

At this point it is already clear that the proposed methodology is not remotely capable of dealing with the huge size of the complete problem. A full scatter diagram can not in anyway be tackled with the optimization method proposed and so, the number of load cases has to be strongly reduced.

This is specially pronounced in the rotating case due to the nonlinear solving and the continuous update of the structural matrices. And there is one fact that was not mentioned in the previous chapters. We have stated that the rotation of the blades is imposed on the model, given a fixed rotational speed. That speed is nothing but a result of the wind speed action upon the aerodynamic section of the blades. Which means that, for different wind speeds, the turbine rotates at different angular velocities. Which also means that the structural matrices do not change only between time steps but also between load cases, as for a same time step, the blades will be at different positions for different wind speeds. This adds even more computational effort and space to store the different matrices at each time step.

So here is the wall right now. Some of the upcoming application examples of the chapter can seem simple or lacking some aspects of the reality in offshore structures, but the reason is that it is unmanageable at this moment. Of course there is always room for improvement, and the last chapter of this thesis summarizes some of the improvements and future developments of interest, where the increase of the computational efficiency holds significant weight.

## 6.4. Optimization parameters

This section is intended to measure the influence of the parameters of the optimization algorithm described in 5. Actually, the SLP method implemented and the Simplex algorithm do not have numerous parameters or variables and the methodology is considerably straightforward. The main details that can be adjusted may be: the moving limits that restrict the advance in the design variables to keep the error in the linearization controlled and improve the convergence of the method, and the threshold value that defines whether a constraint is considered active or not.

### 6.4.1. Moving limits for the SLP Method

The moving limits concept within the SLP have been explained in section 5.3.2. The approaches to define these boundaries can be distinguished between methods that manually fix the values (constant or variable) and methods that determine the values using the information of the optimization constraints and objective function.

Some of the techniques proposed in [Lamberti & Pappalettere, 2000] were considered in the development of this work, however they were rejected for the following reasons. The first of the best working methods proposed is to define the moving limits as:

$$\Delta x_i \leq \frac{\left|b_i - g_i(\boldsymbol{x}^k)\right|}{\sum_{j=1}^{m} \frac{\partial g_i}{\partial x_j}} \tag{6.1}$$

where $b_i$ represents the limit value for each optimization constraint.

The largest value is taken as the moving limit. However, it presents the inherent drawback that the moving limits are the same for all design variables, which makes no sense in the problem in hands since the design variables represent different physical magnitudes and have different orders of magnitude.

Another formulation that does not present the above problem is:

$$||\nabla g_i|| = \sqrt{\sum_{j=1}^{n} \left(\frac{\partial g_i}{\partial x_j}\right)^2} \quad ; \quad d_i = \frac{\left|b_i - g_i(\boldsymbol{x}^k)\right|}{||\nabla g_i||} \quad i = 1, m \tag{6.2}$$

$$\Delta x_j = \frac{\left|\frac{\partial g_i}{\partial x_j}\right|}{||\nabla g_i||} d_i \tag{6.3}$$

which gives $m$ moving limits for each design variable, where $m$ is the number of active constraints. Then, for each variable, again the largest value is taken as moving limit.

The method has been tried in the proposed formulation with poor results. The reasons were: first, that the moving limits computed were initially very different even for design variables with close values; and second, some of the limits computed were too large that the designs rapidly changed from feasible to unfeasible. Many of the optimization constraints went from non-active to strongly violated in one single iteration.

In light of the discouraging results a step back was taken to simpler formulations. The moving limits of the design variables are manually fixed without considering the proximity of the constraints or the influence of the objective function. Firstly, fixed margins were imposed for each design variable, being different for each design variable type (diameters, thicknesses and geometry variables) but equal for every variable of the same type, say 0.01, 0.001 and 0.50 meters respectively. However that does not take into account the stage of the optimization process and the fact that the designs grow in number of active constraints. The more constrained a design is, the more care has to be taken in the step to make, so it makes sense to progressively reduce the moving

limits throughout the optimization process. It also makes sense not to modify every variable the same fixed amount but the same proportion. Then, the moving limits can be defined as a percentage of the current design variable.

Table 6.6 shows a few discrete results with different percentages of moving limits for the non-rotating and the rotating case. The results shown are for the OC4 jacket subject to a single load case of 8 m/s wind speed at the hub and a 6 m high wave of 10 seconds period.

| | Non-rotating | | | | Rotating | | | |
|---|---|---|---|---|---|---|---|---|
| ML | W | itera | t | active | W | itera | t | active |
| 1.00% | 277.906 | 112 | 21826 | 173 | 293.380 | 196 | 109368 | 205 |
| 2.00% | 269.959 | 107 | 18965 | 217 | 297.415 | 55 | 30902 | 218 |
| 5.00% | 268.664 | 76 | 11790 | 154 | 298.361 | 23 | 13113 | 166 |
| 7.00% | 333.336 | 7 | 1253 | 60 | 299.122 | 23 | 13201 | 183 |

**Table 6.6. Optimized results for different moving limits (ML).**

Even though there is not a clear tendency in the results some careful assertions can be made.

- Too large limits can be dangerous and while they reduce the objective function significantly in few iterations the algorithm can soon be unable to improve the design.
- Smaller limits tend to achieve better designs although the cost in iterations and thus computing time is higher.

Therefore, although it is not desirable, it seems that there is not a specific value for the moving limits that guarantees the best performance of the algorithm. They can be relatively bounded between the values shown in the table and there is still a window where the algorithm is robust enough.

### 6.4.2. Activation limit

Obviously, of the 6108 constraints of the problem for each load case, not all of them affect or condition the design to the same extent. The activation limit is the decision value that defines if a constraint is considered in the optimization algorithm or not. As all the constraints are normalized in values from -1 to 0 we can set the same percentage of activation for every constraint. The common practice is to define this value around an 80%. The impact on the algorithm is that, higher values mean less active constraints and the direction of modification is easily found at each step. That has the risk of taking a step too far that could make a constraint go from inactive to violated. In the opposite case of a lower value, it means introducing more constraints in the optimization process, gaining information about the design, though it could also

introduce “noise”, understood as vacuous information of constraints that even though are active do not increase their value and do not condition the design.

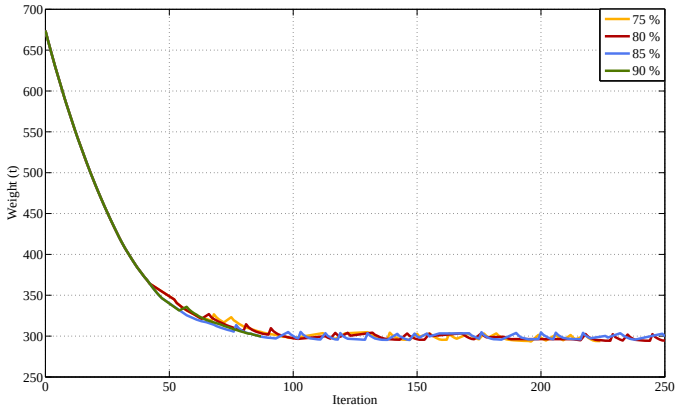


**Figure 6.5. Optimization evolution for different activation limits.**

Figure 6.5 plots the evolution of the objective function for the jacket structure considering 75%, 80%, 85% and 90% activation limits. The setup of the case study is the rotating structure with the same single load case used in the previous section and moving limits of 1%. The optimized designs achieved show again the robustness of the algorithm where for 75 to 85%, the weight is 293.380, 293.956 and 293.749 t respectively. It is worth notice that there is an increase in the iterations needed as we increase the activation limit, needing 196, 257 and 288 iterations respectively. The 90% activation case reaches 299.662 t in 87 iterations but leaves the feasible design region in iteration 88 by violating fatigue constraints.

### 6.4.3. Design variables influence

In 3.2.3 the selection of which characteristics of the jacket are used as design variables is explained. Thus, this work differs from the main optimization works carried out so far in jacket structures by introducing two additional variables that partially control the general geometry of the structure. Although the influence of those variables is not individually significant, combined with the typical size optimization approach, it constitutes a step forward in the acquisition of new optimum designs.

The following shows the results for the jacket example used so far considering only the sizing design variables and the shape design variables separately.

Figure 6.6 draws the two optimum designs. The size optimization reaches an optimum weight of 302.92 t in 121 iterations, very close to the optimum design achieved using both design variables, while the design using only the shape variables reaches only 643 tons. It is clear which of the characteristics has greater influence on the design. It is also worth noticing how the shape design variables follow a path of decreasing the

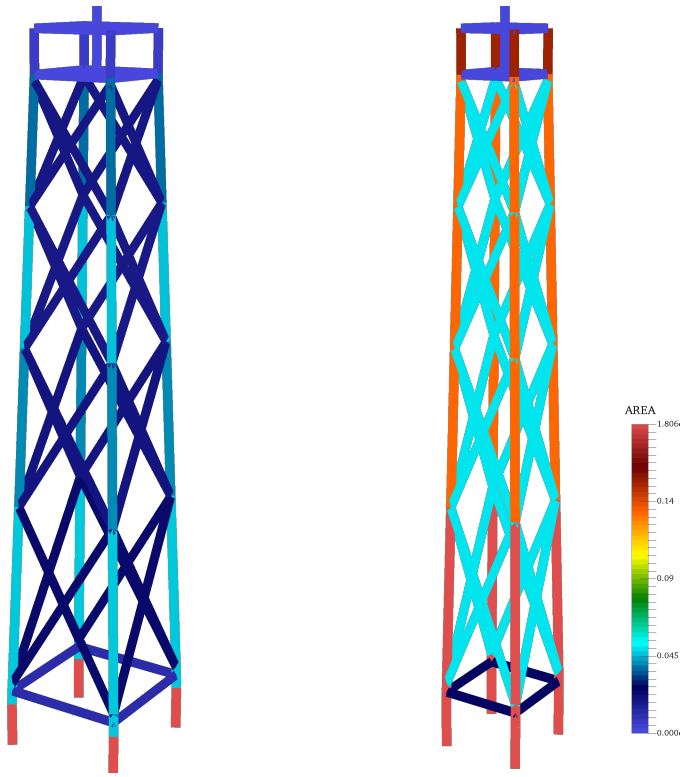


**(a) Optimum design using only size optimization.** **(b) Optimum design using only shape optimization.**

**Figure 6.6. Comparison between shape and size optimization performed separately.**

width of the jacket while, using both variables the design tends to augment the width of both bases and get an optimum design with greater global inertia. Even though it is prove that the importance relies mostly on the size design variables, adding just two variables for the geometry allows the optimization process to achieve a better design with 293.380 t.

## 6.5. Rotation influence

In previous chapters, the influence of the rotating blades in the structural model has been analyzed from the computational and numerical point of view. This section is mainly focused in analyzing how does considering the rotation of the blades affects the design and by extent the optimization process and optimum solution. The initial setup will be the same used so far, since the load case used represents fairly a typical offshore environmental situation. At the wind speed of 8 m/s at the hub, the rotational speed of the blades is set to 9 rpm.

### 6.5.1. Initial design

At a 75% activation limit, the initial design of the jacket does not have any active constraint related to stresses or fatigue. The only constraints active are the dimensional and the frequency constraints which are near the upper limit. So, the differences in the behavior of the model are easily perceived when analyzing the movements and stress level of certain nodes and bars.

Figure 6.7 shows the displacements of the initial design under the described load case for the non-rotating and the rotating case. In 6.7a the displacement in the global X axis for the central node of the second X brace of the jacket is plotted. The differences are quite visible. Not only there is a substantial increment of the movements but their periodicity is completely changed. In the 60 seconds simulation, the non-rotating case shows 6 full cycles of movements that are motivated by the wave loading of 10 s period. However, the rotating case shows two periods; the period between maxima remains 10 s but additional cycles of 2.222 s appear related to the blade passing frequency. The same happens in 6.7b where now the magnitude drawn is the rotation around the X axis of the turbine head. Here the differences are more pronounced as in the non-rotating case the nacelle lateral oscillation is practically null and the rotating case exhibits again the 2.222 seconds periodicity in the displacement.

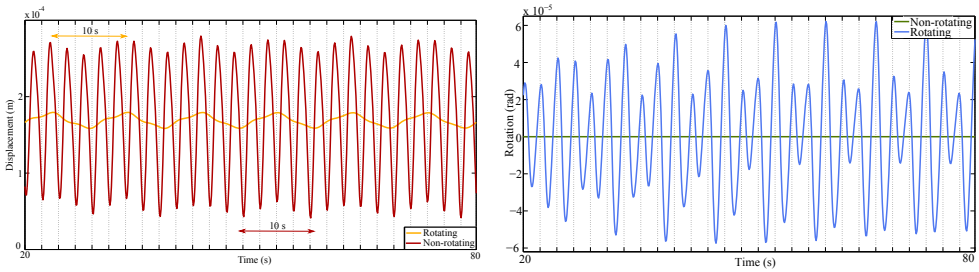


**(a) X movement at the second X-brace central node in the upwind face of the jacket.**

**(b) Rotation of node that represents the nacelle around X axis.**

**Figure 6.7. Comparison of displacements between the non-rotating and the rotating case.**

The impact of the above phenomenon is not related only to the increment of displacements and rotations, which imply an increase of stresses on the elements, but to the change in the number of cycles each element undergoes. Remember that the fatigue damage is proportional to the amplitude of the stress cycles and to the number of cycles. Here it has been proved that not only the amplitude of the stress cycles changes but the number of cycles does too.

Table 6.7 shows an example of the great impact the increment in number of cycles and amplitude of the stresses has on the structure and the associated fatigue damage. It represents the ratio between the damage computed in the rotating model and that of the non-rotating case for 4 legs of the jacket. Obviously, the impact on the different hot-spots differs as they do not depend on the stresses due to the same forces.

| | Hot-spot | | | | | | | |
|---|---|---|---|---|---|---|---|---|
| Leg | 1 | 2 | 3 | 4 | 5 | 6 | 7 | 8 |
| 1 | 1394.27 | 68.37 | 114.33 | 352.99 | 12.22 | 7.45 | 10.52 | 62.31 |
| 2 | 800.86 | 45.69 | 11.55 | 7.03 | 14.46 | 659.96 | 70.46 | 31.25 |
| 3 | 816.58 | 49.99 | 88.85 | 589.57 | 15.46 | 8.15 | 12.59 | 69.46 |
| 4 | 1420.93 | 66.43 | 10.77 | 7.52 | 12.19 | 379.74 | 108.64 | 66.46 |

**Table 6.7. Ratio between the rotating and non-rotating total fatigue damage at design life for the 4 legs of the jacket at the third level.**

Whereas the magnitude of the ratios could seem exaggerated, recall that the stress range is affected by an exponent $m$ according to [DNV-RP-C203, 2011] which can be either 3 or 5. If we take for example the stress at the first hot-spot for leg 1 (figure 6.8), see that the pattern of increasing amplitude and number of cycles is repeated. We can make a quick number using the plot: we can take the $\Delta\sigma$ as 0.05 and 0.20 approximately for the non-rotating and rotating case respectively. Now if we count the number of cycles just as the number of maxima for each case we have 19 and 27. The proportion of cycles is 1.455 and of stress amplitude 4. The stress ratio to the power of 5 gives 1024 and multiplied by 1.455 is $\approx$ 1490. See that the magnitude is similar to the first cell of table 6.7.

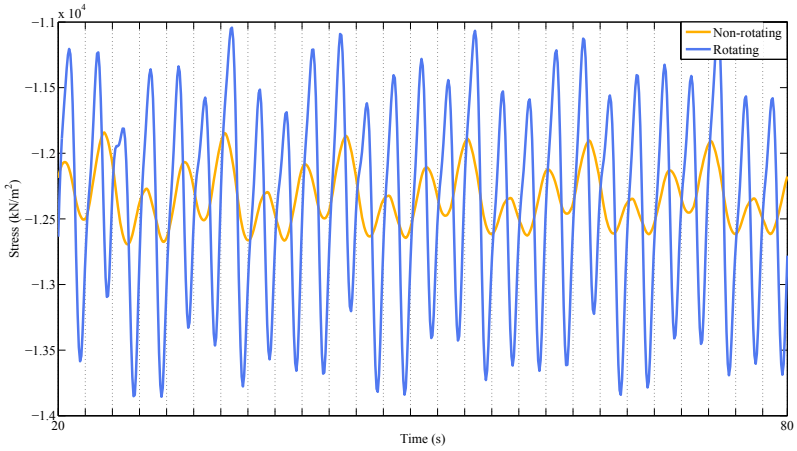


**Figure 6.8. Stresses at leg 1 and hot-spot 1 in the non-rotating and rotating case.**

### 6.5.2. Optimization process

Reasonably, even though the initial design is the same for both cases, the above demonstrated that the initial condition for the optimization process is not the same as the state of the structure is different and the constraints are at distinct levels. At the first optimization steps the processes run near but soon they start to separate as the

number of active constraints increases in the rotating model. More active constraints mean more vertex generated with the linearization of the problem by the SLP and thus, more intersections to check by the Simplex algorithm. A single different decision at a given point is enough to deviate one design from another.

We are going to compare the best results so far for the non-rotating and rotating case which are achieved using a 5% and a 1% for the moving limits of the non-rotating and rotating case respectively.

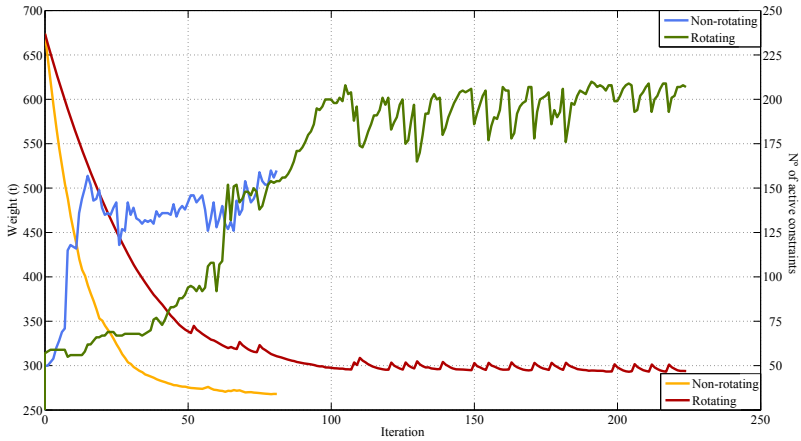


**Figure 6.9. Evolution of the objective function and the number of active constraints for the non-rotating and the rotating case.**

Figure 6.9 plots the evolution of the weight of the jacket and the number of active constraints of each design during the optimization process with and without rotation. The first thing to notice is the greater slope of the non-rotating case as the moving limits imposed are larger than those of the rotating case. The convergence of the non-rotating case is relatively quick requiring only 76 iterations. Note as well that, the first steps of the algorithm rapidly decrease the weight of the jacket and increase the number of active constraints of the design. However, the optimization runs different for the rotating case. Firstly, the ratio of descent of the weight is smaller due to the 1% moving limits. The greater difference comes in the convergence of the algorithm. Where the non-rotating case converges in few iterations, the rotating structure reaches the horizontal asymptote but oscillates in weights around 300.0 t. It has been checked and it is not a result of the small moving limits but of the linearization of a more non-linear problem. From iteration 100 it is seen how the pattern repeats and the solution is oscillating between vertex found by the Simplex and defined by the SLP formulation described. The optimum design is reached in iteration 196 with 293.38 t whereas in iteration 100 the objective function is 297.61. It is certainly possible that in the 150 next iterations the global optimum is not reached and the algorithm keeps oscillating around it.

### 6.5.3. Optimum design

Finally, all the differences in the status of the initial design and the path of the optimization process are reflected in the acquisition of distinct optimized designs. The optimization has been carried out considering 22 design variables, it means 10 different cross-sections, one for each level of leg and X braces, another for the horizontal braces at the bottom and an additional one for the bars embed in the transition piece. The last two variables are the geometrical variables.

Figure 6.10 shows the overall geometry and the distribution of the cross-sections of the elements in the optimized designs. The optimized weights for the non-rotating and rotating structure are 268.66 t and 293.38 t respectively, discussion about the designs apart, it means an 8.5% less for the non-rotating scheme. The differences can be qualitatively seen in figure 6.10. The rotating structure tends to gain bending inertia by increasing the bottom base width still reducing the section of the legs. However, in the non-rotating case, the profile of the jacket tends to a prism shape and does not reduce to the same extent the section of the legs. The specific results for the design variables are in table 6.8. Many of the design variables for the diameters of the tubular members are at their minimum bound of 0.5 m.

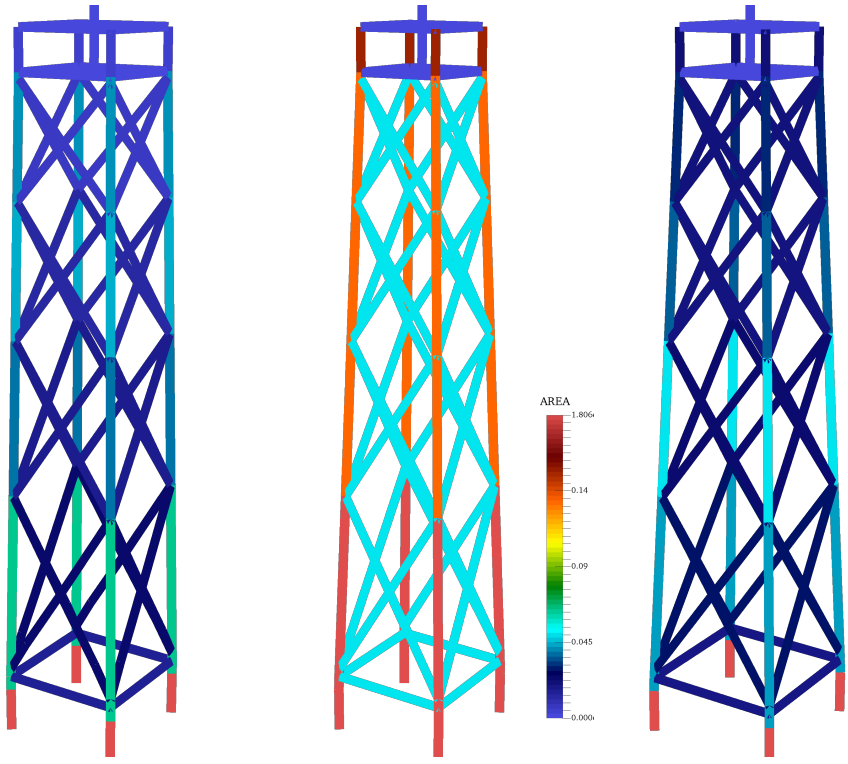


(a) Non-rotating. (b) Initial. (c) Rotating.

**Figure 6.10. Comparison of optimized designs between non-rotating and rotating case.**

| | $D_1$ | $D_2$ | $D_3$ | $D_4$ | $D_5$ | $D_6$ | $D_7$ | $D_8$ | $D_9$ | $D_{10}$ |
|---|---|---|---|---|---|---|---|---|---|---|
| **Non-rotating** | 0.562 | 0.500 | 0.500 | 0.500 | 0.501 | 0.760 | 0.777 | 0.798 | 0.768 | 0.687 |
| **Rotating** | 0.500 | 0.500 | 0.500 | 0.500 | 0.500 | 0.500 | 0.778 | 0.616 | 0.563 | 0.500 |
| | $t_1$ | $t_2$ | $t_3$ | $t_4$ | $t_5$ | $t_6$ | $t_7$ | $t_8$ | $t_9$ | $t_{10}$ |
| **Non-rotating** | 7.0 | 12.5 | 8.4 | 6.1 | 2.4 | 20.6 | 13.3 | 12.5 | 12.0 | 1.0 |
| **Rotating** | 9.4 | 15.0 | 11.7 | 9.9 | 10.3 | 22.5 | 16.6 | 15.2 | 14.1 | 11.0 |
| | | | | | | | | | $W_b$ | $W_t$ |
| **Non-rotating** | | | | | | | | | 12.273 | 10.141 |
| **Rotating** | | | | | | | | | 13.862 | 9.153 |

**Table 6.8. Design variables comparison between the rotating and the non-rotating model (dimensions in meters for diameters and widths and millimeters for thicknesses).**

The biggest differences are:

- In diameters: Sections 6 and 9 which correspond to the lower and upper legs.
- In thicknesses: There is an order of magnitude of difference in sections 5 and 10 that define the upper X brace elements and the members embed in the transition piece.
- In geometry: As mentioned, in the rotating case the bottom base is significantly increased approximately and the shape of the jacket is more conical.

Regarding the state of the optimum designs, both structures are at the lower limit imposed for the natural frequencies of the system. The number of active constraints at the optimum is 154 for the non-rotating rotor and 205 for the moving structure. The rotating case has 19 more active fatigue constraints than the non-rotating case (56). Figure 6.11 shows which joints of the jacket have any fatigue constraint active.

For this case, the fatigue is concentrated mostly in the X type joints of the jacket where, obviously, the rotating case pushes further the structure and more constraints are active. The increment in the thickness of section 5 is motivated by the increment in the fatigue level experienced by the X braces at the top of the jacket.

In light of the results, it seems obvious that the rotation of the blades its a phenomenon that needs to be included in the model and of course in the design and optimization process. Most of the cited works of analysis and optimization referenced in this work perform static analysis, quasi-static or do not introduce the rotation of the blades in the optimization loop. From now on, the upcoming examples of this thesis have all of them been analyzed considering the rotation of the blades.

## 6.6. Approximation of real environmental conditions

In the previous examples only one single load case was considered. While it is not realistic and does not represent accurately the environmental conditions any offshore structure is subjected to, introducing multiple load cases implies a considerably increase in the computational effort needed. However, to actually test the performance of the

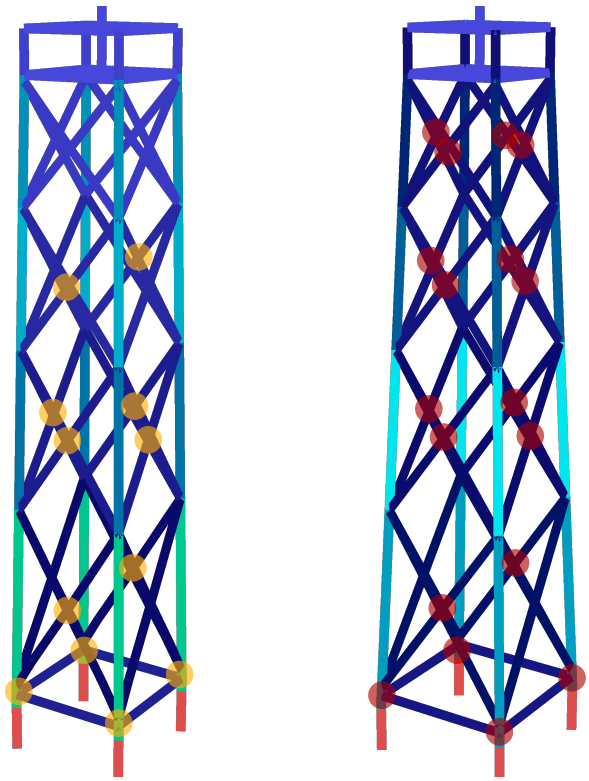

**Figure 6.11. Comparison of active fatigue constraints for the non-rotating (left) and rotating (right) optimum designs.**

optimization algorithm developed it has to be faced against a real problem, or at least one that reflects the actual environmental conditions and the forces acting upon the structure. For example, in [Chew et al., 2016] the OC4 jacket is optimized considering 14 load cases, of which 1 corresponds to a ULS case, and the rest to FLS cases.

Having said that, the developed analysis and optimization methodology is still incapable of dealing with that number of load cases, specially when the rotation of the blades is considered. The reason is that, even though the rotation of the blades is geometrically imposed, the speed of rotation has to match the actual input of the wind speed, since the rotation is a consequence of that incoming wind force. It means that if the wind speed is different for each load case, the speed of rotation is different for each load case and what is most important, the rate of change of the structural characteristics is different for each load case. Thus, the mass, damping and stiffness matrices are not the same for distinct load cases at the same time step. Then, we have to compute and store multiple structural matrices at each time step. This is a consequence of performing the dynamic analysis on the full coupled model of the offshore wind turbine while other approaches just compute the loads in the isolated aerodynamic part and

| Case | $H_s$ [m] | $T$ [s] | $V_{hub}$ [m/s] | $P$ [%] |
|---|---|---|---|---|
| ULS | 9.40 | 13.70 | 42.73 | - |
| FLS 1 | 1.07 | 6.03 | 2.00 | 19.163 |
| FLS 2 | 1.31 | 5.67 | 8.00 | 52.143 |
| FLS 3 | 2.47 | 6.71 | 18.00 | 22.120 |
| FLS 4 | 4.46 | 8.86 | 30.00 | 6.574 |

**Table 6.9. Description of the lumped load cases for ULS and FLS.**

then apply them to the support structure as a loads time history.

Bearing that in mind, the load cases used in [Chew et al., 2016] had to be reduced. In order to resemble the environmental conditions imposed by the 14 load cases, they are merged in only 5 load cases. The single ULS case remains equal and the 13 left FLS cases are lumped in 4 representative cases. The loads hypotheses are presented in table 6.9. Note that the ULS case is not affected by any probability as the probability of occurrence of the load cases influences only the accumulated fatigue damage as expressed in (3.32). The different speeds of rotation for each wind speed for the UpWind wind turbine are defined in [Jonkman et al., 2009].

The increment in computing resources is significant. In figure 4.4 it is shown that it took approximately 500 seconds for the algorithm to perform the 600 s simulation including the sensitivity analysis and a $\Delta t = 0.1$s. That was considering a single load case. However, in the current example with 5 load cases it takes 2950 s to perform the analysis and 20.6 Gb of memory usage on runtime. It means nearly 50 minutes of computing time per optimization iteration.

The optimum design is reached in 284 iterations (804155 s or ∼223 hours) with an objective function of 302.554 tones. 448 constraints are active at the optimum design, corresponding 2 to natural frequency constraints, 128 dimensional, 266 ULS and 52 FLS constraints. Figures 6.12 and 6.13 plot the evolution of the optimization process and the shape and size of the design as well as the full process for each of the 22 design variables.

The design variables are limited by bound constraints. While the variables are never close to the upper limits, some of them are close to or even at the minimum value. The minimum bound limits established for the design variables was 0.5 m for the diameters and 3.2 mm for the thicknesses. The ratio $D/t$ was set according to tables in [DIN EN 10220:2002, 2002]. Top and bottom widths were both limited by 5.8 meters considering that the base of the tower has a diameter 5.6 m.

While 284 iterations might seem too many structural reanalysis, the optimization methodology already reaches a weight of 305.974 tones at iteration 78. From that point the algorithm oscillates around the optimum. As explained in chapter 5 this is caused by the linearization of the constraints and the first order information. The methodology could indeed be sped up by the implementation of a second order sensitivity analysis.

The optimum design clearly tends to a wider bottom and top bases. While in the

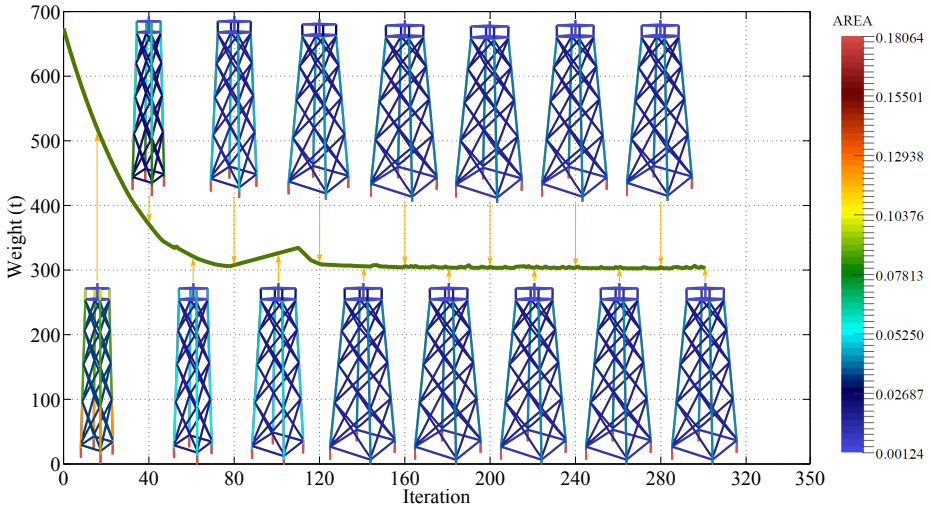


**Figure 6.12. Evolution of the design during the optimization process.**

first stage of the optimization process, corresponding to a fast reduction of the objective function, almost every design variables is decreased, from iteration 30 on, most of the variables keep descending while the shape of the structure starts to increase. The reason is the natural frequency constraints. Since the cross-sections have greater impact on the weight of the structure, the algorithm keeps decreasing them while increasing the width of the jacket to increase its inertia and satisfy the lower limit of the frequency constraints. Following sections will further study and explain this behavior.

## 6.7. Changes in the design

Given the OC4 jacket basic design, we could try to discretely modify the design adding or removing elements of the structure and changing the height of the bracing X blocks. We could then, optimize them with the proposed formulation to conclude which of the altered structures behaves best structurally. In this section, several modifications of the topology of the structure are proposed and optimized, although the suitable approach would be to consider the reformulation of the algorithm to perform a topology optimization of the jacket with the coordinates of the nodes and the connectivity of the elements as design variables.

### 6.7.1. Number of X bracing blocks

The first property we can change at first sight is the number of X bracing blocks the jacket is formed by. In this regard, the designs proposed are formed by 3, 4, 5 and 6 blocks as seen in figure 6.14, being 4 the basic OC4 jacket. There is no design

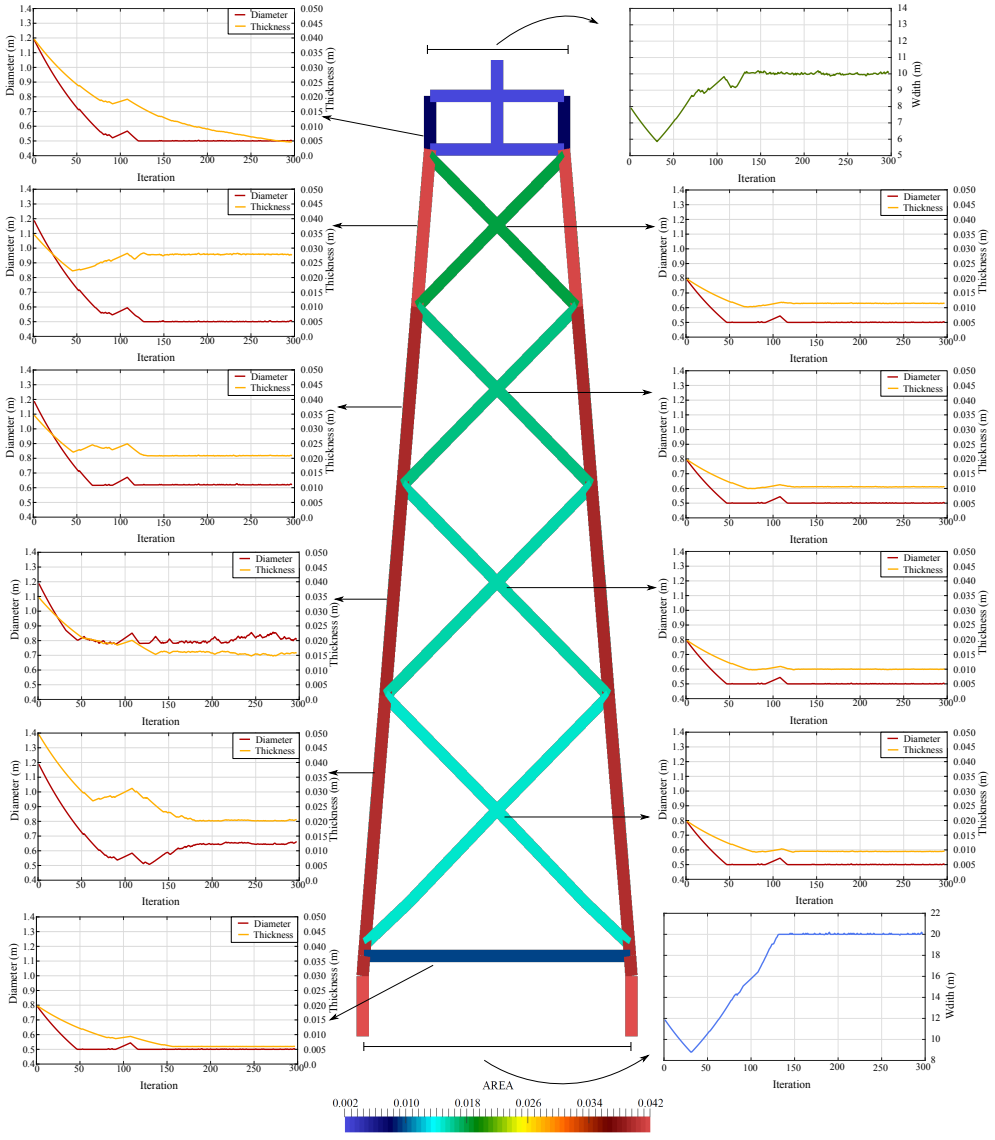


**Figure 6.13. Design variables optimization process.**

with less than 3 blocks since the length of the brace elements would be excessive and dimensional constraints (3.33) would be hard to satisfy, also the forces borne by each element and thereby the stresses would be too much. Table 6.10 shows blocks height for each design and their initial weight.

| | $H_1$ | $H_2$ | $H_3$ | $H_4$ | $H_5$ | $H_6$ | $W_{ini}$ |
|---|---|---|---|---|---|---|---|
| 3x | 22.892 | 20.235 | 15.615 | - | - | - | 666.04 |
| 4x | 18.513 | 15.692 | 13.3 | 11.237 | - | - | 673.81 |
| 5x | 18.701 | 13.978 | 10.448 | 7.809 | 7.806 | - | 715.23 |
| 6x | 9.351 | 9.351 | 13.978 | 10.448 | 7.809 | 7.806 | 737.88 |

**Table 6.10. Height of the X bracing blocks in the modified designs.**

Note that all the modified designs keep the mean sea level between two different blocks. Additionally, the 6x jacket is similar to the 5x jacket just dividing the first block into two of the same height. Each block of the structures has its own 4 design variables, separating the section $(D, t)$ of the legs and the section of the braces except the 6X jacket, where the two bottom blocks share the same 4 design variables.

The structures are subjected to a 6 meter height wave with 10 seconds of period and a shear wind of 8 m/s at the hub. The Design Fatigue Factor is 3 for all the joints of the jacket. Also, a 2% of violation is allowed in the designs in order to give the SLP algorithm and the Simplex a bit of clearance to handle the constraints and its first order approximation.

It is interesting to note that the best optimized design is still the basic OC4 jacket. The 3X jacket is the worst of the proposed designs while the one closer to the optimized OC4 is the 6X jacket. Figure 6.15 plots the value of the objective function through the optimization process for the four designs and also draws their optimum designs. The exact values of the design variables as well as the optimum weight are displayed in tables 6.11, 6.12 and 6.13.

| | $W_{op}$ | itera | active | $W_b$ | $W_t$ |
|---|---|---|---|---|---|
| 3X | 327.165 | 263 | 170 | 14.778 | 5.663 |
| 4X | 293.380 | 196 | 205 | 13.862 | 9.153 |
| 5X | 309.708 | 250 | 304 | 16.416 | 6.679 |
| 6X | 298.874 | 221 | 282 | 12.948 | 10.967 |

**Table 6.11. Weight, iterations, active constraints and shape design variables at the optimum changing the height of the blocks.**

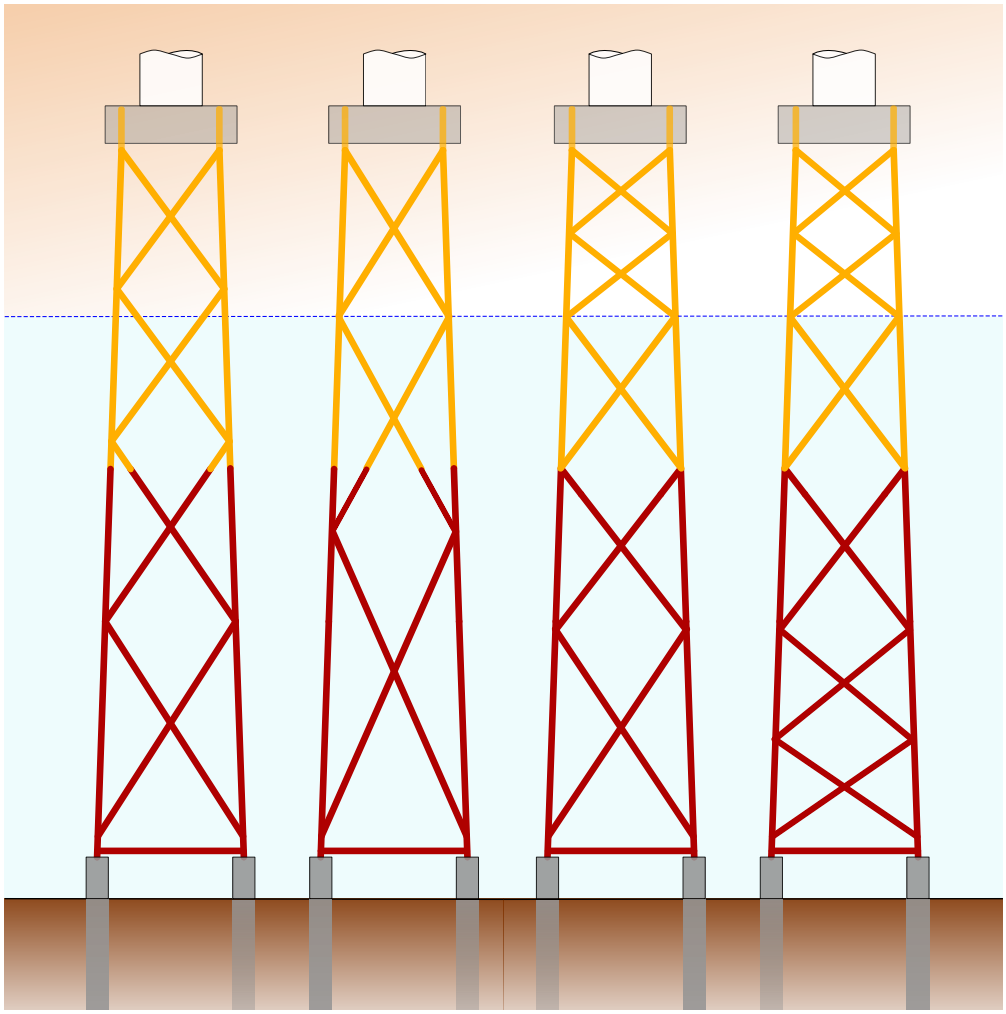

**Figure 6.14. Design variations by adding or removing X bracing blocks on the basic OC4 jacket.**

| | 3X | 4X | 5X | 6X |
|---|---|---|---|---|
| $D_1$ | 0.725 | 0.500 | 0.607 | 0.500 |
| $D_2$ | 0.500 | 0.500 | 0.500 | 0.500 |
| $D_3$ | 0.500 | 0.500 | 0.500 | 0.500 |
| $D_4$ | 0.500 | 0.500 | 0.500 | 0.500 |
| $D_5$ | 0.866 | 0.500 | 0.500 | 0.500 |
| $D_6$ | 1.084 | 0.500 | 0.500 | 0.500 |
| $D_7$ | 0.901 | 0.778 | 0.645 | 0.547 |
| $D_8$ | 0.500 | 0.616 | 0.822 | 0.583 |
| $D_9$ | - | 0.563 | 0.615 | 0.612 |
| $D_{10}$ | - | 0.500 | 0.673 | 0.501 |
| $D_{11}$ | - | - | 0.530 | 0.544 |
| $D_{12}$ | - | - | 0.500 | 0.500 |

**Table 6.12. Diameter in meters of the designs changing the height of the blocks.**

| | 3X | 4X | 5X | 6X |
|---|---|---|---|---|
| $t_1$ | 8.6 | 9.4 | 7.2 | 5.9 |
| $t_2$ | 15.8 | 15.0 | 16.6 | 13.4 |
| $t_3$ | 10.3 | 11.7 | 10.8 | 10.8 |
| $t_4$ | 9.8 | 9.9 | 9.7 | 9.4 |
| $t_5$ | 21.2 | 10.3 | 10.1 | 8.0 |
| $t_6$ | 16.9 | 22.5 | 11.3 | 8.2 |
| $t_7$ | 14.9 | 16.6 | 23.7 | 23.9 |
| $t_8$ | 4.1 | 15.2 | 17.1 | 19.2 |
| $t_9$ | - | 14.1 | 13.0 | 13.3 |
| $t_{10}$ | - | 11.0 | 10.7 | 16.2 |
| $t_{11}$ | - | - | 16.9 | 14.3 |
| $t_{12}$ | - | - | 5.4 | 6.5 |

**Table 6.13. Thickness in millimeters of the designs changing the height of the blocks.**

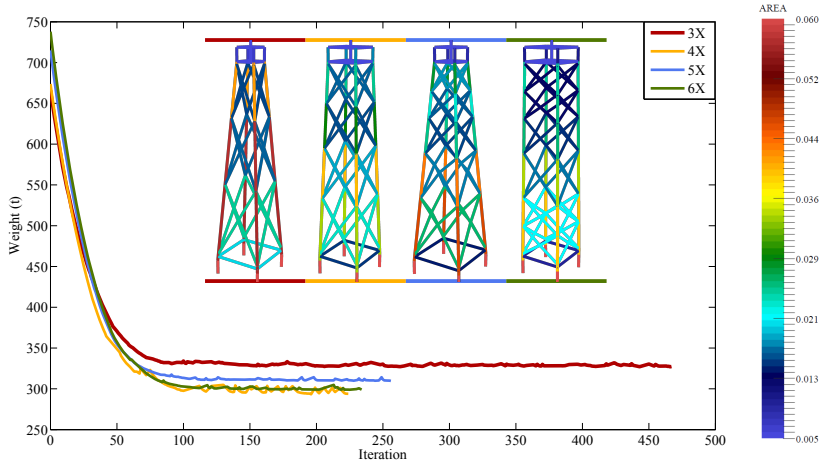


**Figure 6.15. Evolution of the objective function for the modified designs and optimum geometry and sections.**

It can be seen in table 6.12 that all the diameters for the X braces are at the inferior bound limit of the design variable (0.5 m) which means that there is still room for improvement if we reduce the side constraint for those variables. The main perceivable difference between optimum designs is in the geometrical design variables. The 3X and 5X designs tend to a conical shape where the 4X and the 6X designs are more rectangular shaped. The main reason for this tendency in the optimum designs is again the lower limit for the natural frequency constraint (3.35). As the sizing design variables decrease, so do the stiffness and the mass of the structure. Although, the

reduction is more pronounced in stiffness than mass and the frequency of the first natural modes of vibration is lowered. Since those first natural modes correspond to global modes of vibration and they are limited by the frequency constraints, the global inertia of the jackets is increased by expanding its bottom base, as shown in figure 6.16.

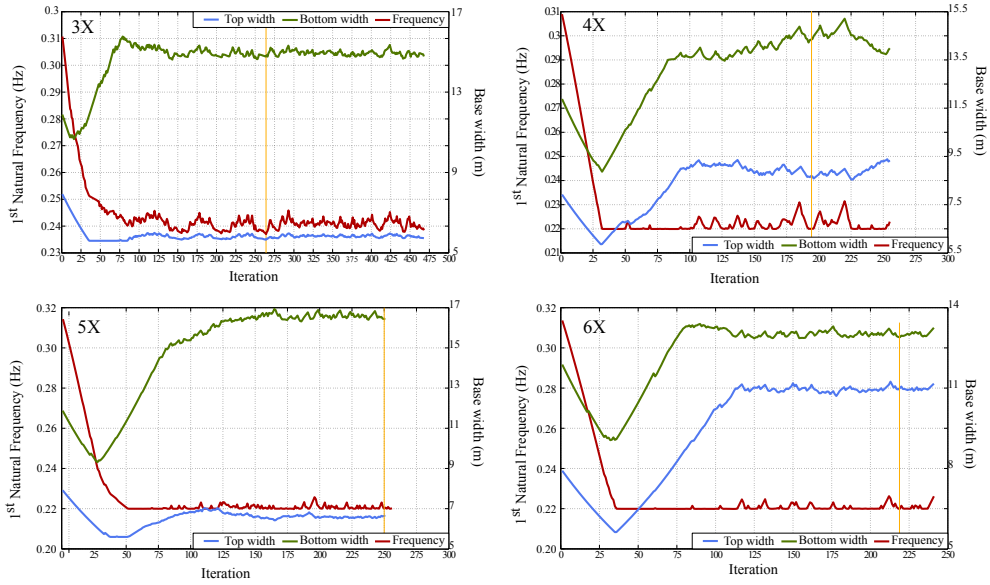


**Figure 6.16. First natural frequency of the designs and evolution of the geometrical design variables.**

However, that is not the only cause. Figure 6.16 shows that the relation (natural frequency - bottom width - top width) is not the same for the four structures and their design evolution. Designs 3X and 5X are able to manage the natural frequency by widening the base of the jacket while keeping the top approximately equal. Notwithstanding, designs 4X and 6X increase both bases exactly at the iteration when the first natural frequency touches its lower limit. One of the dimensional constraints, specifically the one that controls the relation between the length of the chord and its diameter (3.33), plays a significant role in the designs. Figure 6.17a shows the design region for that particular constraint and the position of the nodes of the four optimum designs.

Jacket 3X has the longest chords of the designs and thus, the design variables controlling the diameter of the bars are greater compared to those of the other optimum designs since the mentioned dimensional constraint restricts the length to diameter ratio. Once those cross-sections have the minimum diameter reachable, the only way left for the algorithm to keep decreasing the weight of the structure is to reduce the thickness of the sections and the width of the jacket. But it cannot reduce both at the same time as doing so would end up violating the frequency constraint. Since the

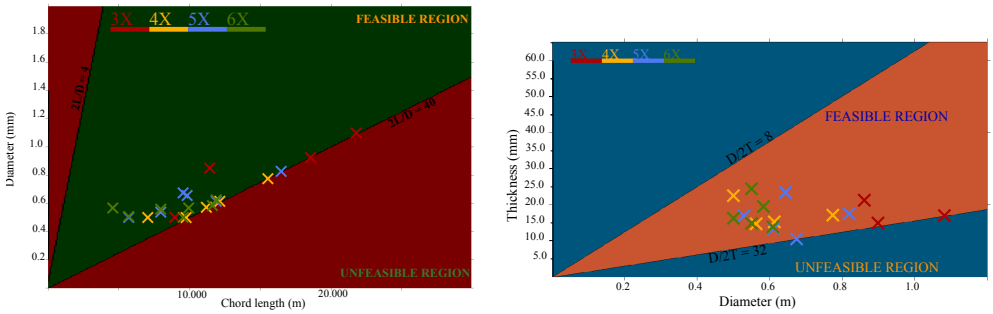


(a) (b)

**Figure 6.17. Feasible region for dimensional constraints (3.33) limiting $\alpha$ and $\gamma$ in T and K joints, and location/values of the constraints for the 4 modified designs.**

sensitivity of the weight of the structure is greater with respect to the thickness than with respect to the length of the elements, the algorithm chooses to reduce thickness and increase the size of the whole jacket. However, there is another dimensional constraint that limits the ratio of the diameter of the chord over its thickness (figure 6.17b), which affects specially design 3X. The length of the legs is the greatest of all designs thus, to fulfill the $\alpha$ constraint the elements have bigger diameters. And finally, to satisfy the $\gamma$ constraint they need to have bigger thicknesses as well. That is also the reason of design 3X being the heaviest.

### 6.7.2. Number of X bracing blocks avoiding complex joints

The optimum designs of the previous section define different sections for each block of the structure. While this is conceptually correct, we have to recall that the legs of the jacket are continuous elements, moreover, the geometrical design variables that control the shape of the structure were specifically selected to keep the straight alignment of the legs. Thus, if the size of the tubular element changes between blocks some kind of transition between sections has to be introduced. Differences in diameter are made with what is called a conical transition (figure 6.18). Figure 6.18 also draws the usual weld in thickness transitions.

Both situations produce additional stress concentrations, for example, in butt weld connections due to thickness differences, the stress concentrations are a consequence of eccentricities ($\delta$). In these cases the transition is preferably placed outside since the S-N curve for the outside weld toe is less severe than for the inside weld root [DNV-RP-C203, 2011]. Nevertheless, what is never desirable is to locate the transition between sections at the frontier between blocks of the jacket as that is where the K joints are and there is no need to make even more complicated the multiplanar K joint or to introduce additional stress concentrations.

One solution, apart from using cast or forged joints, is to locate the transition between sections, not at the frontier between blocks but at the middle of them as

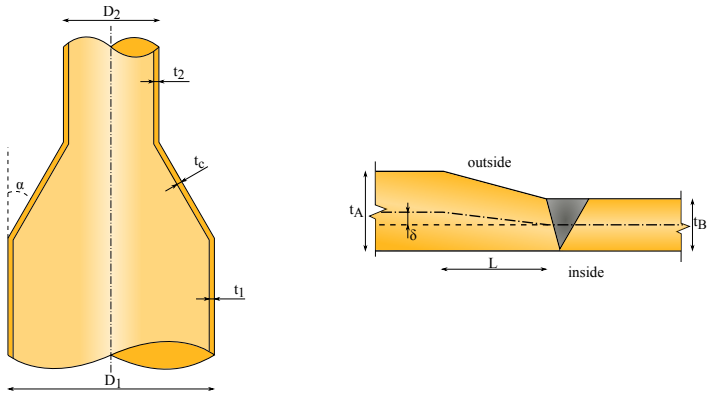


**Figure 6.18. Conical transition between tubular sections and changes in thickness. Adapted from [DNV-RP-C203, 2011].**

shown in figure 6.19. It would be necessary only to define new nodes in the structural model at the middle of the blocks to connect the elements and assign the material properties. The strategy would isolate the transition between sections and avoid the additional stress concentrations at the K joints. Note that even the use of cast nodes would necessary require for the transition to be out of the joint.

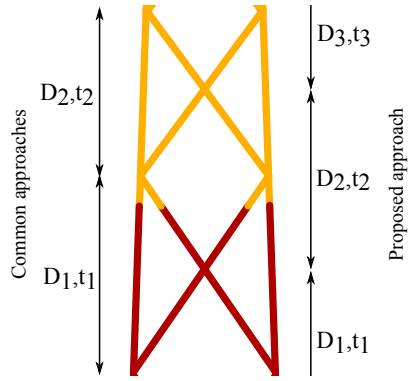


**Figure 6.19. Section transition location avoiding the generation of complex joints (Color change is just a representation of the actual paint of the structure).**

Thereby, the same four proposed designs of jackets are optimized moving the transition between sections from the K joints to the middle of the blocks. Based on the optimized design variables shown in 6.12, the side constraints or bounds for the design variables were decreased to 0.2 m for the diameters and 2 mm for the thickness of the tubular elements. Additionally, the elements of bottom blocks of the 6X jacket were divided into 8 design variables. The concentration of stresses of the conical transitions, ever better placed now, is neglected. It does not affect the comparison with the previous results since it was not considered in them neither. However, in further

developments it would be necessary to accurately reproduce that type of connection and include their SCFs. The results and values of the optimized design variables are shown in tables 6.14, 6.15 and 6.16. Note that most of the weight reduction of the optimum designs compared to those of the previous section comes from the lower bound constraints imposed.

Figure 6.20 plots the objective function of the four optimized designs. In this case, 3XM is still the design that performs worst since the leg elements are still the longest and the dimensional constraints strongly limit the improvement of the design. However there is a change. Designs 4XM and 5XM achieve similar optimized results with 255.283 and 253.856 tones respectively and comparable values for the design variables, and even similar overall shape. It is design 6XM the one that achieves the lowest weight of the optimum designs. As explained in the previous section, 6XM design takes advantage of the fact that it has shorter legs between joints and therefore shorter chords. That allows a further reduction of the diameters and thicknesses of the leg's sections without violating the dimensional constraints.

| | $W_{op}$ | itera | active | $W_b$ | $W_t$ |
|---|---|---|---|---|---|
| 3XM | 307.494 | 158 | 286 | 18.328 | 5.600 |
| 4XM | 255.283 | 240 | 363 | 14.634 | 7.524 |
| 5XM | 253.856 | 176 | 406 | 15.133 | 7.947 |
| 6XM | 235.544 | 171 | 522 | 14.357 | 10.686 |

**Table 6.14. Weight, iterations, active constraints and shape design variables at the optimum changing the location of the transition between sections.**

| | 3XM | 4XM | 5XM | 6XM |
|---|---|---|---|---|
| $D_1$ | 0.642 | 0.528 | 0.531 | 0.441 |
| $D_2$ | 0.332 | 0.276 | 0.275 | 0.205 |
| $D_3$ | 0.217 | 0.200 | 0.201 | 0.201 |
| $D_4$ | 0.202 | 0.200 | 0.200 | 0.204 |
| $D_5$ | 0.661 | 0.200 | 0.200 | 0.200 |
| $D_6$ | 1.086 | 0.582 | 0.200 | 0.200 |
| $D_7$ | 0.895 | 0.853 | 0.576 | 0.752 |
| $D_8$ | 0.434 | 0.723 | 0.810 | 0.435 |
| $D_9$ | - | 0.515 | 0.607 | 0.468 |
| $D_{10}$ | - | 0.358 | 0.454 | 0.593 |
| $D_{11}$ | - | - | 0.454 | 0.605 |
| $D_{12}$ | - | - | 0.363 | 0.546 |
| $D_{13}$ | - | - | - | 0.398 |
| $D_{14}$ | - | - | - | 0.371 |

**Table 6.15. Diameter in meters of the designs changing the location of the transition between sections.**

| | 3XM | 4XM | 5XM | 6XM |
|---|---|---|---|---|
| $t_1$ | 7.7 | 6.3 | 6.5 | 6.5 |
| $t_2$ | 17.3 | 15.3 | 15.9 | 12.7 |
| $t_3$ | 8.4 | 9.2 | 9.5 | 9.7 |
| $t_4$ | 8.7 | 8.5 | 8.5 | 8.0 |
| $t_5$ | 35.2 | 9.1 | 8.5 | 7.1 |
| $t_6$ | 23.6 | 30.4 | 9.2 | 7.3 |
| $t_7$ | 14.0 | 20.5 | 29.0 | 18.8 |
| $t_8$ | 22.1 | 13.4 | 20.9 | 24.3 |
| $t_9$ | - | 15.0 | 14.0 | 24.1 |
| $t_{10}$ | - | 21.4 | 16.1 | 21.0 |
| $t_{11}$ | - | - | 16.2 | 14.0 |
| $t_{12}$ | - | - | 22.7 | 14.4 |
| $t_{13}$ | - | - | - | 19.6 |
| $t_{14}$ | - | - | - | 21.1 |

**Table 6.16. Thickness in millimeters of the designs changing the location of the transition between sections.**

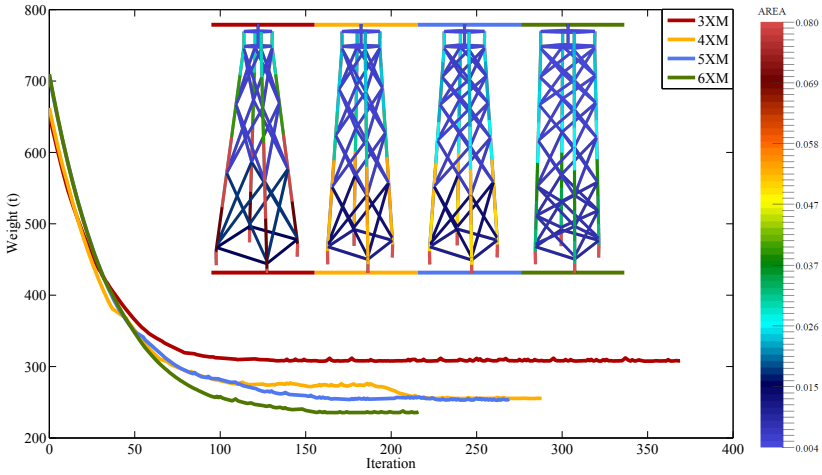


**Figure 6.20. Evolution of the objective function for the modified designs with intermediate joints and optimum geometry and sections.**

In spite of the results, we can not fall into the wrong conclusion that the more divisions we make in the structure the better the design we achieve. When separating blocks in two we are adding brace elements to the jacket. To reach a lower weight in the optimum design implies reducing an extra weight introduced by the additional bars. For example, if we were to divide the third block of the 6XM jacket, the 8 braces would be split in 16. In design 6XM those braces are approximately 17 meters long and their section has a diameter of 0.2 m and 8.0 mm of thickness, which can not be reduced much longer. The 16 resultant elements would be around 12 meters long. Assuming they would have the same cross section, their total weight would be more than 7 tones, while the weight of the initial configuration is nearly 5 tones. Their thickness would have to be reduced to 5.0 mm, which would violate the constraint that relates the thicknesses between chords and braces. Moreover, the section would not be able to hold the stresses produced by the forces acting upon the structure.

Figure 6.21 plots the displacements of the head of the jacket in the global X direction for the optimized jackets. Displacements somehow reflect the level of optimization acquired since the lighter the structure, the larger the displacements. It is worth saying that, even though the peak displacement varies from design to design, the amplitude of the cyclic movements (at least those of greater wave length) coincides. However, for the cyclic displacements exhibiting higher frequencies of vibration there is a change in the pattern of movements in design 6XM. Some of the amplitudes of the cycles are slightly attenuated.

For the 8 m/s wind speed at the hub, the rotation of the blades is settled as 9 rpm or 0.9425 rad/s [Jonkman et al., 2009], which means that the structure, more particularly the blades, repeat their position each 2.22 seconds. Notwithstanding, the tower damn

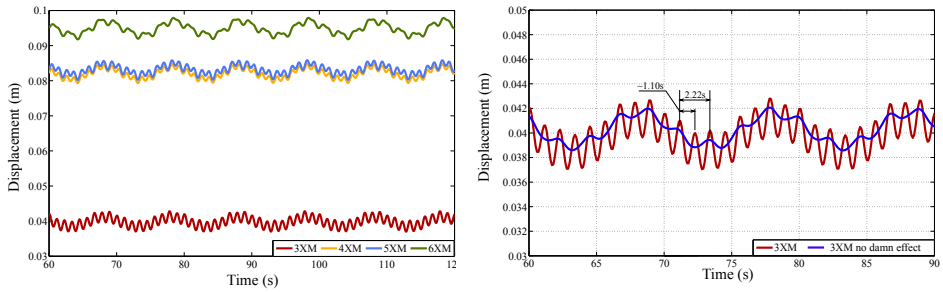


**Figure 6.21. Displacement in the global X axis of the head center of the optimized jackets and comparison for the 3XM design with and without considering the tower dam effect.**

effect has an even shorter period. Imagine the blades at the position where one of the blades is completely vertical (position A) and the other two are at +120° and -120° (positions B and C respectively). At 9 rpm it takes approximately 2.22 seconds for blade at B to reach C. However, the tower damn effect has more influence upon the blades forming 30° with the tower (as reflected in figure 2.13b). Thus, the tower damn effect affects blades passing in front of the tower from position B' at 150° to position C' at -150°. And it takes half the time to make it from B' to C' than B to C. Figure 6.21 also shows that if the tower damn effect is removed from the model the structure does not undergoes the ≈1.10 seconds periodic vibration.

Design 6XM is somehow capable of attenuating the vibration of the structure induced by the tower damn effect. The displacements cycles are a reflection of the stress cycles supported by the structure consequently, design 6XM is subjected to less cycles of stresses and therefore less susceptible to fatigue damage.

### 6.7.3. Horizontal braces

Since one of the most restrictive constraints is the lower natural frequency limit we can try to augment the stiffness of the jackets so when the size of the sections descends the ratio stiffness/mass keeps between the boundaries. In order to do so we can add supplementary bracing bars between the K joints. Note that the addition of bars implies an extra weight, so the algorithm will have to reduce the other sections to compensate the additional weight introduced.

It is worth mention that the results for these proposed designs are a first approximation. The additional brace elements generate a different type of joints at the locations of the old K joints. The new nodes can be classified as KT joints according to [DNV-RP-C203, 2011]. However, in this work they have been treated separately, meaning that, the new central brace is considered forming a T/Y joint with the legs while the other bars form the previous K joint. The formulas of the SCFs for KT joints are mostly modifications and adaptations of the K and T/Y joint's SCFs so the proposed approximation is adequate as a first glimpse on how the modified designs would behave.

The results for the optimum designs are shown in figure 6.22 and tables 6.19, 6.17 and 6.18.

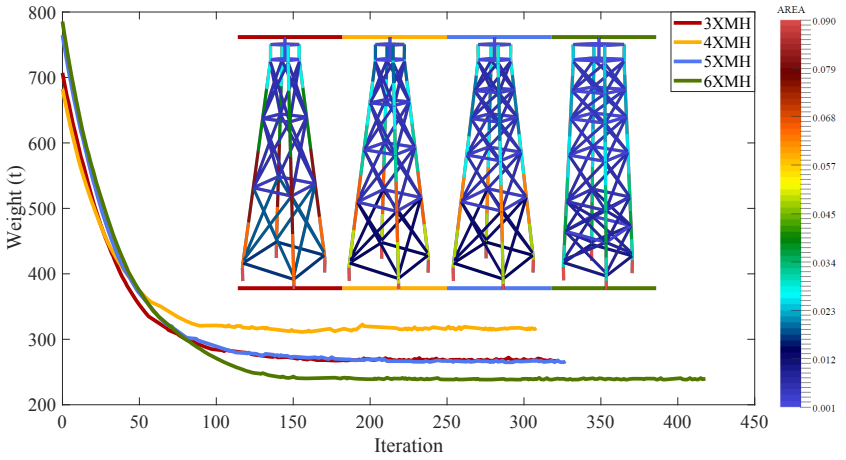


**Figure 6.22. Evolution of the objective function for the modified designs with intermediate joints and horizontal braces, and optimum geometry and sections.**

| | 3XMH | 4XMH | 5XMH | 6XMH |
|---|---|---|---|---|
| $D_1$ | 0.667 | 0.592 | 0.555 | 0.407 |
| $D_2$ | 0.339 | 0.251 | 0.240 | 0.200 |
| $D_3$ | 0.217 | 0.200 | 0.200 | 0.200 |
| $D_4$ | 0.224 | 0.200 | 0.200 | 0.200 |
| $D_5$ | 0.716 | 0.202 | 0.200 | 0.200 |
| $D_6$ | 1.085 | 0.592 | 0.200 | 0.200 |
| $D_7$ | 0.894 | 0.858 | 0.555 | 0.808 |
| $D_8$ | 0.583 | 0.727 | 0.814 | 0.407 |
| $D_9$ | 0.215 | 0.650 | 0.610 | 0.469 |
| $D_{10}$ | 0.234 | 0.349 | 0.471 | 0.594 |
| $D_{11}$ | - | 0.200 | 0.457 | 0.606 |
| $D_{12}$ | - | 0.200 | 0.464 | 0.455 |
| $D_{13}$ | - | 0.200 | 0.200 | 0.479 |
| $D_{14}$ | - | - | 0.200 | 0.472 |
| $D_{15}$ | - | - | 0.202 | 0.200 |
| $D_{16}$ | - | - | 0.200 | 0.400 |
| $D_{17}$ | - | - | - | 0.200 |
| $D_{18}$ | - | - | - | 0.200 |
| $D_{19}$ | - | - | - | 0.200 |

**Table 6.17. Diameter in meters of the designs adding horizontal braces.**

| | 3XMH | 4XMH | 5XMH | 6XMH |
|---|---|---|---|---|
| $t_1$ | 8.0 | 7.1 | 7.9 | 7.6 |
| $t_2$ | 17.9 | 16.6 | 17.1 | 12.9 |
| $t_3$ | 8.4 | 8.9 | 9.3 | 9.5 |
| $t_4$ | 8.4 | 8.4 | 8.5 | 7.9 |
| $t_5$ | 29.7 | 9.7 | 9.1 | 7.2 |
| $t_6$ | 24.1 | 27.3 | 10.4 | 7.6 |
| $t_7$ | 14.0 | 24.8 | 28.7 | 20.6 |
| $t_8$ | 15.5 | 14.1 | 25.0 | 25.4 |
| $t_9$ | 5.7 | 13.8 | 14.8 | 25.9 |
| $t_{10}$ | 5.5 | 18.1 | 14.0 | 18.1 |
| $t_{11}$ | - | 5.0 | 14.3 | 13.3 |
| $t_{12}$ | - | 4.3 | 20.1 | 16.0 |
| $t_{13}$ | - | 4.8 | 5.0 | 15.0 |
| $t_{14}$ | - | - | 4.2 | 16.6 |
| $t_{15}$ | - | - | 4.8 | 3.1 |
| $t_{16}$ | - | - | 4.4 | 3.9 |
| $t_{17}$ | - | - | - | 3.3 |
| $t_{18}$ | - | - | - | 2.4 |
| $t_{19}$ | - | - | - | 2.3 |

**Table 6.18. Thickness in millimeters of the designs adding horizontal braces.**

| | $W_{op}$ | itera | active | $W_b$ | $W_t$ |
|---|---|---|---|---|---|
| 3XMH | 311.016 | 156 | 393 | 18.189 | 5.600 |
| 4XMH | 266.842 | 268 | 484 | 17.510 | 5.636 |
| 5XMH | 264.930 | 293 | 574 | 17.864 | 6.400 |
| 6XMH | 238.375 | 288 | 615 | 15.215 | 9.916 |

**Table 6.19. Weight, iterations, active constraints and shape design variables at the optimum adding horizontal braces.**

None of the additionally braced optimum designs improves the designs of the previous section. Moreover, tables 6.17 and 6.18 reflect that those bars are unnecessary since in most cases they end up near the minimum diameter and thickness imposed in the methodology. The strategy also did not work for the control of the natural frequencies and, at the optimum, they are again at the lower constraint.

## 6.8. Summary and conclusions

As a general conclusion, the optimization algorithm developed is quite robust and exhibits a reliable behavior when facing different jackets under different external and internal conditions. The convergence curves show two extremely differentiated phases: A first one where a fast drop of the objective function takes place (high slope), and a second one, where with minor changes of the design variables, the algorithm explore the surroundings of the optimum design thoroughly (quasi horizontal). In the second phase the algorithm shows certain signs of oscillation around the optimum design due to the construction of the SLP method.

Particularly, the UpWind model of an offshore jacket [de Vries, 2011] was used in this chapter as main design to test the performance of the optimization algorithm. This thesis proposes a formulation where not only the size of the jacket is optimized but also its shape. For that purpose, the bottom and top widths of the jacket are considered design variables. While the influence of those two design variables alone is quite low, the combined shape and size optimization is able to reach optimum designs unachievable using size optimization alone. Nevertheless, it has been proved that the sections of the elements play a decisive role in the weight reduction of the jacket.

The rotation of the blades in the fully coupled model of the OWT is proved necessary or essential to an accurate representation of the phenomena involved and the structural behavior. Specially, the jacket changes drastically its dynamic response when introducing the rotation, experiencing new and larger stress cycles. Which is determinant to the fatigue damage undergone by the welded joints of the structure.

Since the target of this thesis is a very specific type of real structures, the methodology developed should be able to handle and solve practical examples as real as possible. Nevertheless, the intrinsic computational cost required, explained in chapters 3 and 4, is enormous. Not only the inherent cost of the algorithm itself is high but a correct

modelization of the actual environmental conditions suffered by the structure implies hundreds of load cases, each one with a probability of appearance, in order to represent precisely the offshore weather and its consequences upon the structure. In this chapter a problem with 5 load cases lumping normal conditions in an offshore location is solved. The mentioned cost is reflected in the fact that one single iteration took nearly 1 hour of computational time and the optimization run for more than 9 days. This issue is one of the most susceptible to be improved about the developed methodology in further researches.

Several modifications of the basic UpWind jacket design have been proposed and optimized. The proposed configurations are based on different connectivities between the elements of the structure and on the addition or removal of some of them. Also, there is a proposal for changing the way the jackets are traditionally modeled. The transition between different cross-sections is moved from the joints to the middle point of the legs between nodes. It avoids an additional and excessive concentration of stresses that can derive in fatigue failure.

It has been confirmed that the design of the jackets is strongly fatigue driven but, the restraints for the values of the natural frequencies of vibration of the system and the dimensional constraints imposed for the SCFs to be valid [DNV-RP-C203, 2011], are determinant in the optimum solution reached and the evolution of the design through the optimization. The optimized designs have active constraints from all types.

With respect to the algorithm's parameters: The threshold value to decide whether a given constraint is considered active or not, the activation limit, has a slight impact on the performance of the optimization algorithm. Choosing higher activation limits may drive more easily the design at early stages but might fail when approaching the optimum design since small changes could take a constraint directly from inactive to violated. This is in close relation with the establishment of the moving limits for the SLP algorithm. They seem to be determinant to a reliable function of the optimization since they clearly affect the accuracy of the first order approximation taken and the linearization of the feasible design region. While presenting slow convergence ratios, small moving limits appear to make the algorithm more robust and give consistent results.

Chapter 7

# Remarks, conclusions and further developments

*"What if the future's just to remind me that my past was my only blessing?"*
**Hotel Books**, Every day, the same.

## 7.1. Introduction

If you have come this far, that could only mean two things: either you have read everything until here or skipped everything. In case of the latter, a brief summary of the work developed in this thesis is presented in this chapter along with the most relevant concluding remarks and some possible targets for the continuation of this work in future researches.

## 7.2. Remarks and conclusions

The remarks and conclusions are organized similarly to the document in relation to the structural model, the optimization model and the results.

### 7.2.1. Structural model

The structural model is based on a non-linear dynamic analysis of three dimensional framed structures with rigid joints of what constitutes the whole model of an offshore wind turbine upon a jacket substructure. The non-linear analysis is used to perform a time domain integration of the structure considering a constant change in geometry over time due to the rotation of the blades.

The structural model is subjected to the most important loads acting on an offshore structure which are self weight, buoyancy, wind and waves. Wind force on the blades

is computed using the Blade Element Momentum Theory and the aerodynamic characteristics of each segment of the blades. Wind acting on the tower is considered just a drag force but taking into account the dam effect of the passing blade. First order Airy and second order Stokes directional waves are considered and their forces upon the structure are calculated using Morison's formula.

One of the most relevant and yet hardest to assess effects on typical offshore structures is fatigue. In this thesis the damage on the joints of the jacket is estimated using the Palmgren-Miner rule using the Rainflow method to count the stress cycles. The stresses are also computed at the hot-spots of the joints affected by Stress Concentration Factors. Then, the damage expected at design life for the structure is linearly extrapolated from shorter simulations of 300 and 600 seconds with high accuracy.

From the structural model developed the following conclusions can be drawn:

- Even though the tubular members conforming the structure could be expected to show shell behavior due to their length to thickness ratio, the representation using beam elements is proved accurate enough to catch the dynamic behavior of the jacket and OWT model.
- The incorporation of the rotating blades required the time integration to be performed by a non-linear algorithm since the mass, stiffness and damping matrices change between time steps. It is absolutely necessary to include the rotation of the blades in order to capture the whole coupled dynamic behavior of the jacket under an operating turbine.
- The results of the time domain analysis agree with those of the references in terms of the response of the structure under typical offshore loading conditions.
- The damage at the hot-spots estimated by linear extrapolation has been checked against much larger simulations with good agreement and accuracy. The average error is under 10% although the overall error is significantly lower and the 10% comes from particular hot-spots ($< 5\%$) where the extrapolation fails significantly. Additionally, the extrapolated damage is always higher than the computed in larger simulations so the structure would be in any case over-designed and reliable.

### 7.2.2. Optimization model

The optimization model is presented as a weight minimization of the steel jacket under Ultimate Limit Stress, Fatigue Limit State and frequency constraints as well as side constraints for the design variables and dimensional constraints that keep the size of the elements under certain limits. Cross-sections of the tubular elements and bottom and top widths of the jacket are chosen as design variables to perform a shape and size optimization.

Since the dynamic response of the structure is to be optimized, ULS constraints have to be imposed for every time-step of the time history analysis. There are several formulations to deal with time-dependent constraints in the literature. However,

they present a set of issues and none is able to guarantee a strict fulfillment of all the constraints while being computationally manageable. In this thesis a novel approach where the time-dependent constraints are merged using constraint aggregation functions is proposed.

Sequential Linear Programming is used to tackle the proposed non-linear optimization problem, on which each linear sub-problem is solved using the Simplex algorithm. A first order sensitivity analysis is computed as required for the SLP methodology. Direct differentiation and analytic derivatives are used to obtain the sensitivities except for the fatigue constraint, which are obtained combining the information of the analytic derivatives with finite differences.

The following conclusions can be extracted from the optimization model presented:

- The design variables selected allow the optimization of the cross-sections of the members (size) and the overall geometry of the jacket (shape) while preserving the initial structure's configuration, connectivity and construction feasibility.
- The use of aggregation constraint functions for the time-dependent constraints allowed an efficient treatment of the transient response optimization problem, solving one of the major issues within optimization of offshore structures.
- The Kreisselmeier-Steinhauser function was used and its parameters calibrated to keep the violation of the constraints under a 2%. The K-S function also allows analytic derivatives to be used in the sensitivity analysis.
- The sensitivity analysis is by far the most expensive part of the code in terms of CPU time and storage. The use of Direct Differentiation over Adjoint State Method is clearly advantageous since there are fewer design variables than constraints.
- All the derivatives of the SCFs had to be implemented in order for the sensitivity of the fatigue constraint to be precise.
- Since the fatigue constraint has no analytic derivative a combined approach with finite differences for the damage values had to be used. The formulation proved to be accurate for design modifications within the moving limits defined in the SLP method for the design variables.

### 7.2.3. Optimization results

From the application examples shown in chapter 6 some conclusions can be finally brought up:

- Significant weight reductions of the jackets are obtained under typical offshore environmental loading conditions and constraints involving stresses, fatigue and natural frequencies.

- The optimized designs keep the general shape of the structure thanks to how the design variables that control the shape optimization are selected.
- The developed algorithm exhibits fair robustness in its performance when dealing with different structures and conditions.
- The optimized designs have many active constraints from all of the implemented types.
- Considering the rotation of the blades is absolutely necessary and it affects deeply the optimum designs obtained since it makes the designs more susceptible to fatigue.
- It has been found that the natural frequency constraints are particularly relevant, during the optimization process, to determine the direction of optimization for the design variables, specially the shape design variables.
- The transitions between different cross-sections have been relocated from the joints of the structure to the middle of the blocks in order to avoid excessively complex joints and additional concentration of stresses.

## 7.3. Further developments

The work developed in this thesis constitutes a reliable and effective methodology for the optimization of jackets for offshore wind turbines under real conditions. However, it establishes the foundation for future developments that could be build upon the current formulation or opens the gate for the arrival of brand new approaches.

For the sake of symmetry and consistency with everything written so far, future lines of work can be organized whether they belong to the structural model or to the optimization approach.

### 7.3.1. Structural model

Further developments of the structural model are related mainly to aspects still missing in this work's model and associated with specific details beyond the general description of an offshore wind turbine model. Those most relevant are described below.

- **Soil-structure interaction:** This work took the hypothesis of the jacket being clamped at its bottom. However, experimental results show that the natural frequencies and the damping factors change significantly with the type of soil they are built upon . Thus, the soil-foundation interaction affects the dynamic behavior of the structure.

Jacket's legs lay over piles. Traditionally, pile-soil interaction is modeled using dynamic $p - y$ curves that simulate the soil resistance to movement. While pile-soil interaction is relatively easy to asses and model, jackets do not lay over one pile but over close piles or even clusters of piles. Therefore the response is affected by the so called pile-soil-pile interaction. Pile-soil interaction has been extensively studied for monopile type foundations however there is fewer works on pile-soil-pile interaction for offshore jackets.

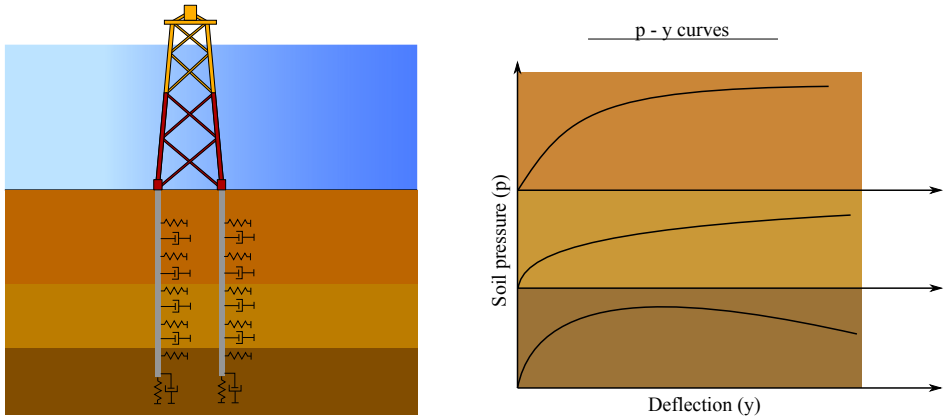


**Figure 7.1. Soil-structure interaction model and dynamic $p - y$ curves.**

- **Complete SCFs library:** This thesis accounts for the Stress Concentration Factors of joints present in almost every offshore jacket (T/Y, X and K). But those three types do not cover every possible kind of joint and also there are SCFs for parts of the structure which are not technically joints, for example: transitions between different thicknesses, transitions between different diameters, changes of orientation, and others.

  The importance of fatigue in the optimum design of the steel jackets has been already pointed out. For that reason, it would be crucial in future works to account for every possible SFC for every part of the structure subject of stress concentration and susceptible of fatigue failure.

- **Nonlinear effects:** While jackets constitute quite stiff structures and they can be analyzed under linear hypothesis, the carbon-fiber blades actually experiment considerably large displacements. In an operating wind turbine, blades can undergo a bending deflection of a 10% of their radius and significant torsional angles, specially near the tip.

  Wind loads are computed using the aerodynamic properties of discrete sections of the blades. Thus, large deformations of the blades, especially torsional angles that would modify the pitch angle, would derive in considerably different acting forces from those considered in the undeformed shape.

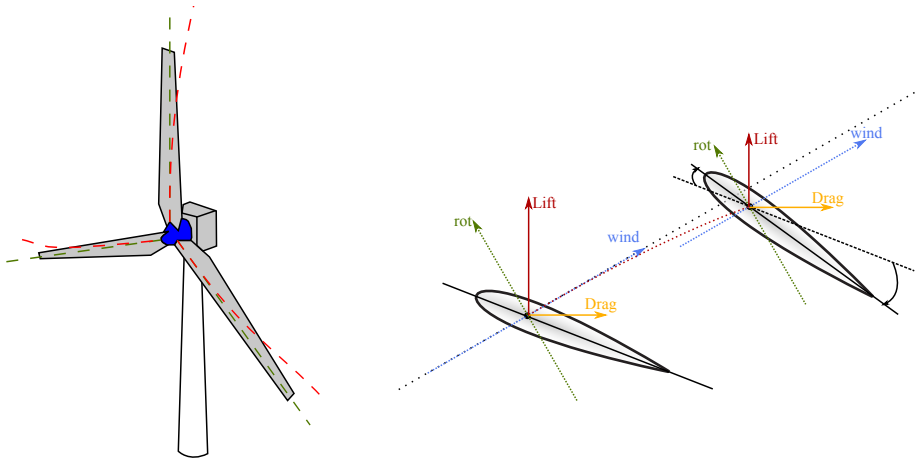


**Figure 7.2. Large deformations of wind turbine blades.**

- **Loading conditions:** In this thesis loads from self weight, buoyancy, wind and waves have been considered. However, jackets are subjected to a wider range of loads during its design life. For example, loads from the shipment process or from the jacket launch are not accounted for. The weight of appurtenances is also not considered. Additionally, it will be interesting in further developments to include more types of waves than the linear Airy and the second order Stokes wave to be able to adapt the loading condition to more environments. Finally, the wind profile included in this thesis does not considers turbulence which is an important issue for the fatigue assessment of the structure. Future works need to account for different turbulent models to accurately predict the dynamic loading of the wind.
- **Multibody dynamics:** Flexible multibody dynamics formulation is able to account for large deformations. It can model the motion of elements and couple it with the structural behavior using joints and kinematical constraints. It would be interesting to integrate the solution of flexible multibody dynamics within the optimization loop as efficient as possible.

### 7.3.2. Optimization approach

Regarding the optimization part of the developed work in this thesis, there are a few key factors identified as important for future works.

- **Second order sensitivity analysis:** Second order sensitivity of objective function and constraints would open a series of possibilities for the optimization. They would allow to use second order optimization algorithms.

  It could also be use to provide information on how to obtain the best suited scale factor (5.3) to measure how far we go in the direction of optimization given by

the linear programming algorithm. The latter would prevent oscillations of the designs due to the linearization of the problem near the optimum.

- **Additional design variables:** Even though topology optimization might still be too far given the size of the proposed problem, there are still several options on how to define the design variables and thereby how to allow designs to be modified. For example, the so called method Growing Ground Structure could be used. This method constitutes a truss topology optimization procedure where bars and nodes are iteratively added or removed from an initial ground structure.

  The next reasonable step from the formulation developed in this thesis could be introduce the height of the blocks of the jacket as design variables. It could be easily implemented and the results would offer a view and objective judgment on how many blocks are necessary in the optimum design.

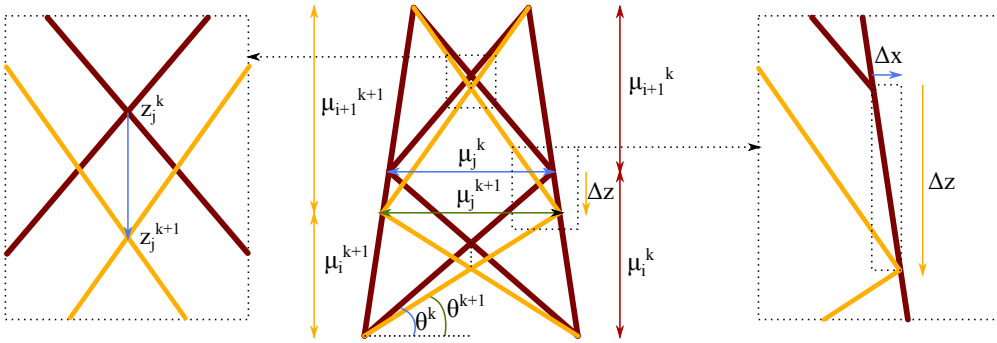


**Figure 7.3. Height of jacket's blocks as design variables schematics.**

### 7.3.3. Others

Last but not least, there is one future improvement which could not fall into any of the above groups.

- **Computational efficiency:** As stated in numerous parts of this document, the complete optimization of the offshore jacket coupled with the dynamic movement of the tower and blades, the assessment of fatigue and the first order sensitivity analysis is extremely demanding in terms of computational resources, both storage and time.

  In this sense, a thoroughly optimization of the code through intensive parallelization could not only improve the performance of the analysis and optimization process but would allow to address completely real environmental conditions.

Appendix A

# Stress concentration factors for fatigue life design

*"Never let your sense of morals prevent you from doing what is right."*

**Isaac Asimov**, Foundation.

## A.1. Introduction

In previous chapters a full description of the strategy to obtain the fatigue life damage for the structure has been exposed. As stated, this fatigue failure is based on the stress calculations at the so called hot-spots at the welded joints between tubular bars of the structure. This hot-spot areas represent the locations where exceptional concentration of stresses appear due to the geometrical characteristics of the connection itself.

From the first experimental works in SCFs [Toprac & Beale, 1967], in the past 30 years there has been an extensive study, through different techniques, of the parametric expressions for the concentration factors; each of them arriving to slightly different parametric equations in some cases or even considerable discrepancy in others. Thus, it seems obvious that there is not an agreed solution for the level of stress concentration at welded joints.

In the scope of this work, the offshore recommendations and standards, and in particular the standards for offshore steel structures, have been taken as guidance in many steps. Thereby, the SCF formulas used are taken from the DNV standard [DNV-RP-C203, 2011] which have been validated.

## A.2. Previous considerations and hypothesis

According to their geometry, there are several types of planar and multiplanar tubular joints, some of which can be seen in figure A.1. Nevertheless, most common jacket structures include only a few number of them, specially, T, Y, X and K joints are present in every design and less often TY and KT joints. This work includes only the SCFs for those more usual type of nodes.

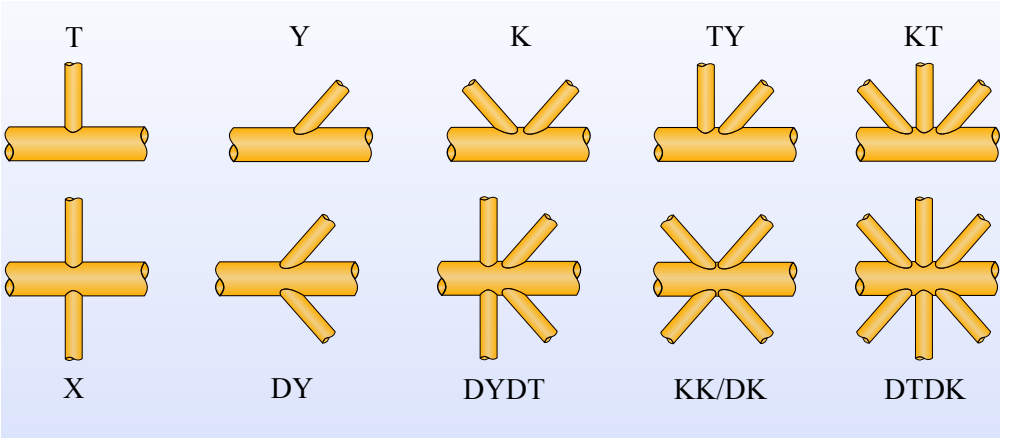


**Figure A.1. Types of tubular joints (adapted from [Saini et al., 2016]).**

While the former classifies each joint based on its geometry, the final categorization of the intersection can be different from its shape class due to the forces acting on each brace and the balance or proportion between them. That being so, a particular joint can be classified for example as 50% K and 50% Y if the axial load in one of the braces is 50% of the axial load on the other (figure A.2). Thus, each joint needs to be classified according to its geometry and loading balance.

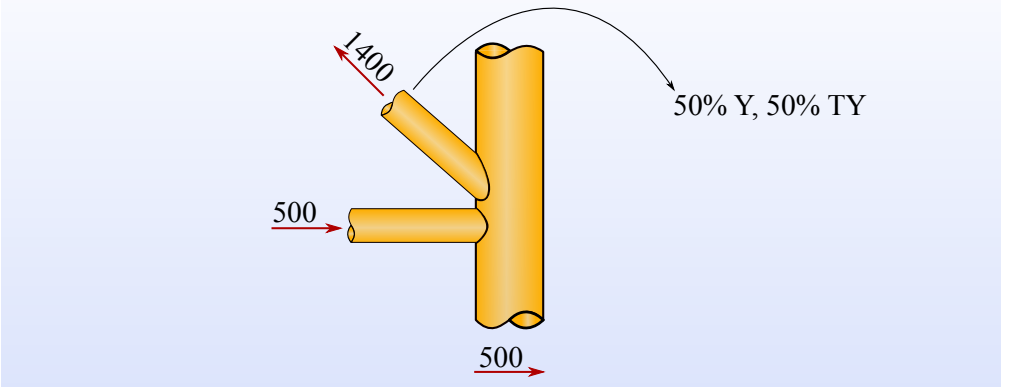


**Figure A.2. Joint classiffication according to forces balance (adapted from[DNV-RP-C203, 2011]).**

The implications of this statement are more important than it may seem. As it has already been said many times along this document, this work performs a full dynamic analysis in the time domain; meaning that, for each time step, an instant response of the structure is obtained including, of course, forces on the elements. Due to the time-dependent loading conditions, the forces on the elements change at each time step. Taking into account the joint classification method exposed leads to joints that change its classification at each time step. This would not only complicate the analysis itself but the optimization process. The sensitivity analysis of the Stress Concentration Factors and thereby of the fatigue failure constraint would not only depend on the design variables and the stress level but in the possibility of one joint changing its classification and so its hot-spot stresses between iterations. Thereby, the SCFs functions for each node, for each time step would become non continuous and non continuously differentiable. To avoid this issue the classification of joints according to the forces balance has been neglected in this work and they are only classified according to geometry reasons. It has also been checked that for most cases, and during the time simulation, the stress level on the structural joints for different braces is reasonably similar to take this assumption.

Getting back to the geometry of the joints one can easily see that every joint of a jacket is a multi-planar joint. The studies on SCFs for multi-planar joints has increased in the past years with the extensive work of Ahmadi [Ahmadi et al., 2011; Ahmadi & Lotfollahi-Yaghin, 2012; Ahmadi et al., 2012] and others [Karamanos et al., 1999; Chiew et al., 1999; Woghiren & Brennan, 2009]. The results of these studies show that differences are found between the values of the SCF for uni-planar and multi-planar joints. In some cases using the uni-planar formulation under-predicts the SCF and others over-predicts them. The derivation of specific three-dimensional SCF formulations requires for detailed study of each type of joint under strict conditions and the formulas have not yet been extensively validated. Thereby and since the specific standard [DNV-RP-C203, 2011] shows only SCFs for uni-planar tubular joints, in this work it is assumed the hypothesis that different planes of a common joint do not interact between them and so they are treated as simple planar joints, this is also stated in [ABS, 2003].

As well as the three-dimensional multi-planar effects are not considered, the possibility of overlapping joints is also neglected as the SCFs for that type of joints are not validated [ABS, 2003]. The formulation developed can account for gaped joints or with no gap.

Not only intersections between multiple tubular elements develop concentration of stresses at their welds. Also conical transitions connecting tubular members with different diameters or cross-sections need to consider that effect. Even though this work proposes the optimization of the cross-sections of the bars leading to connections where those type of joints would be needed, they are not considered as the dimensions and characteristics of the conical transition are not defined and not included in the design optimization problem.

## A.3. Geometrical properties

Some geometrical parameters are needed to determine the values of the SCFs for each type of joint. These parameters are mostly ratios of the dimensions of the connected elements. Figure A.3 which is a simple T/Y joint (based on the value of the $\theta$ angle) represents the principal variables required.

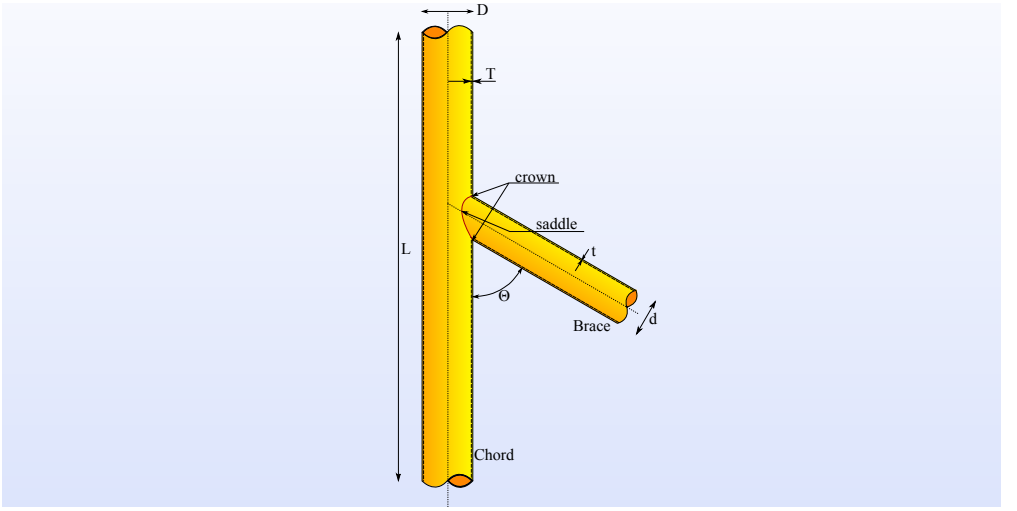


**Figure A.3. Geometrical definition for tubular joints. T/Y joint.**

The main parameters to compute the SCFs are:

$$\beta = \frac{d}{D} \qquad \tau = \frac{t}{T} \qquad \alpha = \frac{2\,L}{D} \qquad \gamma = \frac{D}{2\,T} \qquad \zeta = \frac{g}{D} \tag{A.1}$$

where $d$, $t$, $D$ and $T$ are the diameter and thickness of the brace and chord respectively. $L$ is the length of the particular chord the brace is attached to and $g$ is the gap between adjacent braces.

## A.4. SCFs formulas

The Stress Concentration Factors used in this work are extracted from [DNV-RP-C203, 2011] which takes the coefficients from [Efthymiou, 1988], which constitute the most used parametric equations for tubular joints, and were derived using finite element methods. Efthymiou's equations are some of the best fitting parametric equations due to the greater correlation with steel models by the Efthymiou FE models and the fewer conservative assumptions made. These equations tend to be nearest to a mean fit [UK-HSE, 1997].

There are 8 SCFs for each node type, 4 for the brace and 4 for the chord. In each bar, 2 for stresses due to axial load, one concentrated on the saddle and one on the

crown, and 2 for bending moments, one for in-plane bending and one for out-of-plane bending.

The validity of the following expressions is guaranteed for the following limits of the geometrical parameters defined in equation (A.1)

$$\begin{array}{rcccl} 0.2 & \leq & \beta & \leq & 1.0 \\ 0.2 & \leq & \tau & \leq & 1.0 \\ 8 & \leq & \gamma & \leq & 32 \\ 4 & \leq & \alpha & \leq & 40 \\ 20^{\text{o}} & \leq & \theta & \leq & 90^{\text{o}} \\ \frac{-0.6\beta}{\sin\theta} & \leq & \zeta & \leq & 1.0 \end{array} \tag{A.2}$$

### A.4.1. T/Y joints

Figure A.3 draws a schematic example of a simple tubular T/Y joint. The Stress Concentration Factors for this type of joints are:

$$SCF_{T,AC,C} = \gamma^{0.2}\,\tau\left(2.65 + 5\,(\beta - 0.65)^2\right) + \tau\,\beta\,(0.25\,\alpha - 3)\,\sin(\theta) \tag{A.3}$$

$$SCF_{T,AS,C} = \gamma\,\tau^{1.11}\left(1.11 - 3\,(\beta - 0.52)^2\right)(\sin(\theta))^{1.6} \tag{A.4}$$

$$SCF_{T,MIP,C} = 1.45\,\beta\,\tau^{0.85}\,\gamma^{(1-0.68\beta)(\sin(\theta))^{0.7}} \tag{A.5}$$

$$SCF_{T,MOP,C} = \gamma\,\tau\,\beta\left(1.7 - 1.05\,\beta^3\right)(\sin(\theta))^{1.6} \tag{A.6}$$

$$SCF_{T,AC,B} = 3 + \gamma^{1.2}\left(0.12\,e^{-4\beta} + 0.011\,\beta^2 - 0.045\right) + \beta\,\tau\,(0.1\alpha - 1.2) \tag{A.7}$$

$$SCF_{T,AS,B} = 1.3 + \gamma\,\tau^{0.52}\,\alpha^{0.1}\left(0.187 - 1.25\beta^{1.1}\,(\beta - 0.96)\right)(\sin(\theta))^{(2.7-0.01\alpha)} \tag{A.8}$$

$$SCF_{T,MIP,B} = 1 + 0.65\,\beta\,\tau^{0.4}\,\gamma^{(1.09-0.77\beta)}\,(\sin(\theta))^{(0.06\gamma-1.16)} \tag{A.9}$$

$$SCF_{T,MOP,B} = \tau^{-0.54}\,\gamma^{-0.05}\left(0.99 - 0.47\beta + 0.08\beta^4\right)\,SCF_{T,MIP,B} \tag{A.10}$$

For joints with short chords ($\alpha < 12$) some of the factors need to be corrected by factors:

$$f_{T,1} = 1 - \left(0.83\,\beta - 0.56\,\beta^2 - 0.02\right)\,\gamma^{0.23}\,e^{\left(-0.21\,\gamma^{-1.16}\,\alpha^{2.5}\right)} \tag{A.11}$$

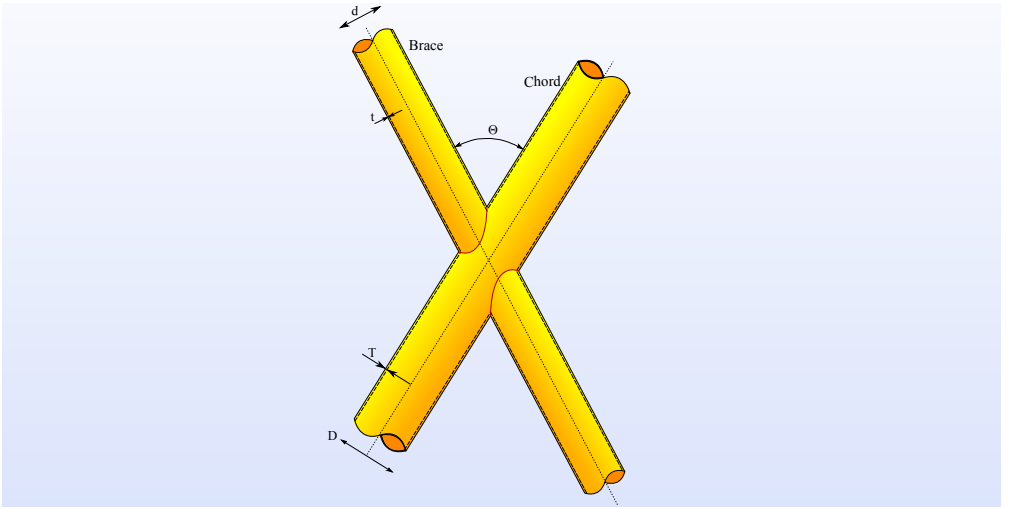


**Figure A.4. Geometrical definition of an X joint.**

$$f_{T,3} = 1 - 0.55\,\beta^{1.8}\,\gamma^{0.16}\,e^{\left(-0.49\,\gamma^{-0.89}\,\alpha^{1.8}\right)} \tag{A.12}$$

Factor $f_{T,1}$ affects equations (A.4) and (A.8) while factor $f_{T,3}$ corrects the values of (A.6) and (A.10).

### A.4.2. X joints

X joints are characterized for their symmetrical geometry often joining two elements with the same dimensions. Thus the selection of which one is the chord is based on which element is continuous and which does not. The continuous element takes the chord role while the element broken in two makes two braces. It can be taken as a T/Y joint with two opposite braces, then the SCFs are similar to those of T/Y joints in some cases and equal in others.

$$SCF_{X,AC,C} = \gamma^{0.2}\,\tau\left(2.65 + 5(\beta - 0.65)^2\right) - 3\,\tau\,\beta\,\sin(\theta) \tag{A.13}$$

$$SCF_{X,AS,C} = 3.87\,\gamma\,\tau\,\beta\left(1.10 - \beta^1.8\right)(\sin(\theta))^{1.7} \tag{A.14}$$

$$SCF_{X,MIP,C} = 1.45\,\beta\,\tau^{0.85}\,\gamma^{(1-0.68\beta)(\sin(\theta))^{0.7}} \tag{A.15}$$

$$SCF_{X,MOP,C} = \gamma\,\tau\,\beta\left(1.56 - 1.34\,\beta^4\right)(\sin(\theta))^{1.6} \tag{A.16}$$

$$SCF_{X,AC,B} = 3 + \gamma^{1.2}\left(0.12\,e^{-4\beta} + 0.011\beta^2 - 0.045\right) \tag{A.17}$$

$$SCF_{X,AS,B} = 1 + 1.9\,\gamma\,\tau^{0.5}\beta^{0.9}\left(1.09 - \beta^{1.7}\right)\left(\sin(\theta)\right)^{2.5} \tag{A.18}$$

$$SCF_{X,MIP,B} = 1 + 0.65\,\beta\,\tau^{0.4}\,\gamma^{(1.09-0.77\beta)}\left(\sin(\theta)\right)^{(0.06\gamma-1.16)} \tag{A.19}$$

$$SCF_{X,MOP,B} = \tau^{-0.54}\,\gamma^{-0.05}\left(0.99 - 0.47\beta + 0.08\beta^4\right)\ SCF_{X,MIP,B} \tag{A.20}$$

### A.4.3. K joints

K joints appear in almost every intersection of braces with the main legs of the jackets, thereby in common designs it is the most repeated connection.

$$\begin{aligned} SCF_{K,AC,C} \;=\; & \tau^{0.9}\,\gamma^{0.5}\left(0.67 - \beta^2 + 1.16\beta\right)\sin(\theta)\left(\tfrac{\sin(\theta_{max})}{\sin(\theta_{min})}\right)^{0.3}\left(\tfrac{\beta_{max}}{\beta_{min}}\right)^{0.3} \\ & \left(1.64 + 0.29\beta^{-0.38}\arctan(8\zeta)\right) \end{aligned} \tag{A.21}$$

$$\begin{aligned} SCF_{K,AS,C} \;=\; & \tau^{0.9}\,\gamma^{0.5}\left(0.67 - \beta^2 + 1.16\beta\right)\sin(\theta)\left(\tfrac{\sin(\theta_{max})}{\sin(\theta_{min})}\right)^{0.3}\left(\tfrac{\beta_{max}}{\beta_{min}}\right)^{0.3} \\ & \left(1.64 + 0.29\beta^{-0.38}\arctan(8\zeta)\right) \end{aligned} \tag{A.22}$$

$$SCF_{K,MIP,C} = 1.45\,\beta\,\tau^{0.85}\,\gamma^{(1-0.68\beta)(\sin(\theta))^{0.7}} \tag{A.23}$$

$$\begin{aligned} SCF_{K,MOP,C} \;=\; & \gamma\,\tau_a\,\beta_a\left(1.7 - 1.05\,\beta_a^3\right)\left(\sin(\theta_a)\right)^{1.6}\left(1 - 0.08(\beta_b\,\gamma)^{0.5}e^{-0.8x}\right) + \\ & \gamma\,\tau_b\,\beta_b\left(1.7 - 1.05\,\beta_b^3\right)\left(\sin(\theta_b)\right)^{1.6}\left(1 - 0.08(\beta_a\,\gamma)^{0.5}e^{-0.8x}\right) \\ & \left(2.05\,\beta_{max}^{0.5}\,e^{-1.3x}\right) \end{aligned} \tag{A.24}$$

$$\begin{aligned} SCF_{K,AC,B} = & 1 + \tau^{0.9}\,\gamma^{0.5}\left(0.67 - \beta^2 + 1.16\beta\right)\sin(\theta)\left(\tfrac{\sin(\theta_{max})}{\sin(\theta_{min})}\right)^{0.3}\left(\tfrac{\beta_{max}}{\beta_{min}}\right)^{0.3} \\ & \left(1.64 + 0.29\beta^{-0.38}\arctan(8\zeta)\right)\left(1.97 - 1.57\beta^{0.25}\right)\tau^{-0.14}\left(\sin(\theta)\right)^{0.7} + \\ & (\sin\theta)^{1.8}\left(\theta_{max} + \theta_{min}\right)\left(0.131 - 0.084\arctan(14\zeta + 4.2\beta)\right) \\ & C\,\beta^{1.5}\,\gamma^{0.5}\,\tau^{-1.22} \end{aligned} \tag{A.25}$$

$$\begin{aligned} SCF_{K,AS,B} = & 1 + \tau^{0.9}\,\gamma^{0.5}\left(0.67 - \beta^2 + 1.16\beta\right)\sin(\theta)\left(\tfrac{\sin(\theta_{max})}{\sin(\theta_{min})}\right)^{0.3}\left(\tfrac{\beta_{max}}{\beta_{min}}\right)^{0.3} \\ & \left(1.64 + 0.29\beta^{-0.38}\arctan(8\zeta)\right)\left(1.97 - 1.57\beta^{0.25}\right)\tau^{-0.14}\left(\sin(\theta)\right)^{0.7} + \\ & (\sin\theta)^{1.8}\left(\theta_{max} + \theta_{min}\right)\left(0.131 - 0.084\arctan(14\zeta + 4.2\beta)\right) \\ & C\,\beta^{1.5}\,\gamma^{0.5}\,\tau^{-1.22} \end{aligned} \tag{A.26}$$

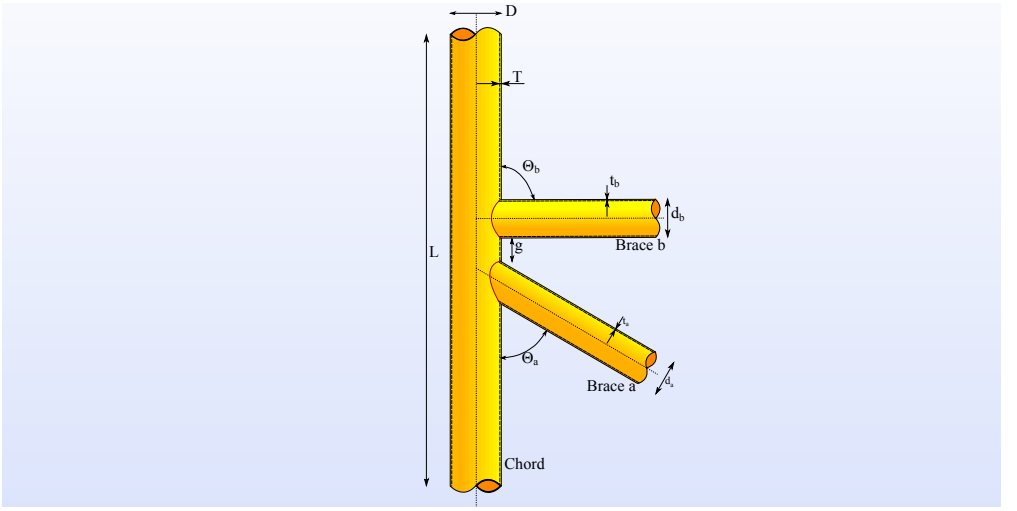


**Figure A.5. Geometrical definition of an K joint.**

$$SCF_{K,MIP,B} = 1 + 0.65\,\beta\,\tau^{0.4}\,\gamma^{(1.09-0.77\beta)}\,(\sin(\theta))^{(0.06\gamma-1.16)} \tag{A.27}$$

$$\begin{aligned} SCF_{K,MOP,B} \;=\; & \gamma\,\tau_a\,\beta_a\left(1.7-1.05\,\beta_a^3\right)(\sin(\theta_a))^{1.6}\left(1-0.08(\beta_b\,\gamma)^{0.5}e^{-0.8x}\right)+ \\ & \gamma\,\tau_b\,\beta_b\left(1.7-1.05\,\beta_b^3\right)(\sin(\theta_b))^{1.6}\left(1-0.08(\beta_a\,\gamma)^{0.5}e^{-0.8x}\right) \\ & \left(2.05\,\beta_{max}^{0.5}\,e^{-1.3x}\right)\left(\tau^{-0.54}\,\gamma^{-0.05}\left(0.99-0.47\beta+0.08\beta^4\right)\right) \end{aligned} \tag{A.28}$$

where $x = 1 + \frac{\zeta\sin(\theta)}{\beta}$ and $C$ is a coefficient that takes the values: 0 for gap joints, 1 for the through brace and 0.5 for overlapping joints (not considered in this work).

The short chord correction factor in K joints that affects factors $SCF_{K,MOP,C}$ and $SCF_{K,MOP,B}$ is:

$$f_{K,4} = 1 - 1.07\,\beta^{1.88}\,e^{\left(-0.16\gamma^{1.06}\alpha^{2.4}\right)} \tag{A.29}$$

Appendix B

# Constraints Sensitivities

*"The saddest aspect of life right now is that science gathers knowledge faster than society gathers wisdom."*
**Isaac Asimov**

## B.1. Introduction

This appendix shows the full derivation of the first order sensitivity analysis of the structural constraints used in the optimization problem and described in chapter 3.

Chapter 4 also explains how the derivatives of the expressions stated by [Norsok, 2004] and [DNV-RP-C203, 2011] are obtained. The constraints derivatives with respect to the design variables are obtained as follows:

$$\frac{dG_i}{d\boldsymbol{\xi}} = \frac{\partial \tilde{G}_i}{\partial \boldsymbol{\xi}} + \frac{\partial \tilde{G}_i}{\partial \boldsymbol{f'}} \frac{d\boldsymbol{f'}}{d\boldsymbol{\xi}} \tag{B.1}$$

where $G_i(\boldsymbol{\xi}) = \tilde{G}_i(\boldsymbol{\xi}, \boldsymbol{f'}(\boldsymbol{u}))\big|_{\boldsymbol{u}(\boldsymbol{\xi})}$ is the $i-th$ structural constraint of any element, $\xi$ is the design variable with respect we are differentiating and $\boldsymbol{f'}(\xi)$ is the vector of nodal forces at the ends of the elements in local axis.

In this appendix the expressions for $\frac{\partial \tilde{G}_i}{\partial \xi}$ and $\frac{\partial \tilde{G}_i}{\partial \boldsymbol{f'}}$ will be fully derived, where

$$\frac{\partial \tilde{G}_i}{\partial \boldsymbol{f'}} = \left\{ \frac{\partial \tilde{G}_i}{N_1}, \frac{\partial \tilde{G}_i}{Vy_1}, \frac{\partial \tilde{G}_i}{Vz_1}, \frac{\partial \tilde{G}_i}{Mx_1}, \frac{\partial \tilde{G}_i}{My_1}, \frac{\partial \tilde{G}_i}{Mz_1}, \frac{\partial \tilde{G}_i}{N_2}, \frac{\partial \tilde{G}_i}{Vy_2}, \frac{\partial \tilde{G}_i}{Vz_2}, \frac{\partial \tilde{G}_i}{Mx_2}, \frac{\partial \tilde{G}_i}{My_2}, \frac{\partial \tilde{G}_i}{Mz_2} \right\} \tag{B.2}$$

being $N$, $Vy$, $Vz$, $Mx$, $My$ and $Mz$ are the element forces. The subscript (1-2) indicates the first or second node of the element.

## B.2. Ultimate Limit State constraints

In chapter 3, a full description of the structural constraints and all their parameters can be found. Therefore the already described parameters will not be redefined here. Nevertheless, their derivatives will.

For the sake of simplicity in the notation of the derivatives all the properties are implicitly referred to each structural element.

Regarding the derivative of the constraint equation with respect to the forces on the element, only the nonzero components of the vector $\frac{\partial \tilde{G}_i}{\partial \boldsymbol{f}'}$ will be written. The subscript for the node will be also neglected.

### B.2.1. Axial tension and bending without hydrostatic pressure

The structural constraint for unsubmerged elements subject to axial tension and bending reads:

$$g_{TB} = \frac{\gamma_{R,t}\, N}{f_t\, A} + \frac{\gamma_{R,b}\, \sqrt{{M_y}^2 + {M_z}^2}}{f_b\, W_e} - 1 \leq 0 \tag{B.3}$$

Thus, the derivative of the tension and bending constraint with respect to a design variable $\xi$ would be:

$$\frac{\partial g_{TB}}{\partial \xi} = \frac{\gamma_{R,t}\, N}{f_t} \frac{\left(-\frac{\partial A}{\partial \xi}\right)}{A^2} + \gamma_{R,b} \sqrt{{M_y}^2 + {M_z}^2} \left( \frac{-\frac{\partial f_b}{\partial \xi}\, W_e - \frac{\partial W_e}{\partial \xi}\, f_b}{(f_b\, W_e)^2} \right) \tag{B.4}$$

The derivative of the representative bending strength is:

$$\frac{\partial f_b}{\partial \xi} = \begin{cases} \frac{\frac{\partial W_p}{\partial \xi}\, W_e - W_p \frac{\partial W_e}{\partial \xi}}{W_e^2}\, f_y & , \quad \frac{f_y\, d}{E\, t} \leq 0.0517 \\ \left\{ \begin{array}{l} \left[ -2.58 \frac{f_y}{E} \frac{\frac{\partial d}{\partial \xi}\, t - d\, \frac{\partial t}{\partial \xi}}{t^2} \right] \frac{W_p}{W_e}\, f_y + \\ \left[ 1.13 - 2.58 \frac{f_y\, d}{E\, t} \right] \frac{\frac{\partial W_p}{\partial \xi}\, W_e - W_p \frac{\partial W_e}{\partial \xi}}{W_e^2}\, f_y \end{array} \right\} & , \quad 0.0517 < \frac{f_y\, d}{E\, t} \leq 0.1034 \\ \left\{ \begin{array}{l} \left[ -0.76 \frac{f_y}{E} \frac{\frac{\partial d}{\partial \xi}\, t - d\, \frac{\partial t}{\partial \xi}}{t^2} \right] \frac{W_p}{W_e}\, f_y + \\ \left[ 0.94 - 0.76 \frac{f_y\, d}{E\, t} \right] \frac{\frac{\partial W_p}{\partial \xi}\, W_e - W_p \frac{\partial W_e}{\partial \xi}}{W_e^2}\, f_y \end{array} \right\} & , \quad 0.1034 < \frac{f_y\, d}{E\, t} \leq 120 \frac{f_y}{E} \end{cases} \tag{B.5}$$

The nonzero components of the derivative of the constraint with respect to the element forces are:

$$\frac{\partial g_{TB}}{\partial N} = \frac{\gamma_{R,t}}{f_t\, A} \tag{B.6}$$

$$\frac{\partial g_{TB}}{\partial My} = \frac{1}{2}\frac{\gamma_{R,b}}{f_b\, W_e}\frac{2\, M_y}{\sqrt{{M_y}^2 + {M_z}^2}} \tag{B.7}$$

$$\frac{\partial g_{TB}}{\partial Mz} = \frac{1}{2}\frac{\gamma_{R,b}}{f_b\, W_e}\frac{2\, M_z}{\sqrt{{M_y}^2 + {M_z}^2}} \tag{B.8}$$

### B.2.2. Axial compression and bending without hydrostatic pressure

Unsubmerged elements subject to axial compression and bending need to satisfy equations (B.9) and (B.10):

$$g_{CB} = \frac{\gamma_{R,c}\, N}{f_c\, A} + \frac{\gamma_{R,b}}{f_b\, W_e}\sqrt{\frac{C_{m,y}\, {M_y}^2}{1-\frac{N}{N_{e,y}}} + \frac{C_{m,z}\, {M_z}^2}{1-\frac{N}{N_{e,z}}}} - 1 \leq 0 \tag{B.9}$$

$$g_{CB2} = \frac{\gamma_{R,c}\, N}{f_{yc}\, A} + \frac{\gamma_{R,b}\sqrt{{M_y}^2 + {M_z}^2}}{f_b\, W_e} - 1 \leq 0 \tag{B.10}$$

Derivative of equation (B.9) with respect to the design variables is:

$$\begin{aligned}\frac{\partial g_{CB}}{\partial \xi} = {} & \gamma_{R,c}\, N\left(-\frac{\frac{\partial f_c}{\partial \xi}\, A + f_c\frac{\partial A}{\partial \xi}}{(f_c\, A)^2}\right) + \gamma_{R,b}\left\{\left(-\frac{\frac{\partial f_b}{\partial \xi}\, W_e + f_b\frac{\partial W_e}{\partial \xi}}{(f_b\, W_e)^2}\right)\sqrt{\frac{C_{m,y}\, {M_y}^2}{1-\frac{N}{N_{e,y}}} + \frac{C_{m,z}\, {M_z}^2}{1-\frac{N}{N_{e,z}}}} + \right. \\ & \frac{1}{f_b\, W_e}\left[\left(\frac{C_{m,y}\, M_y}{1-\frac{N}{N_{e,y}}}\right)\left(\frac{\frac{\partial C_{m,y}}{\partial \xi} M_y\left(1-\frac{N}{N_{e,y}}\right) + C_{m,y} M_y\left(\frac{N\frac{\partial N_{e,y}}{\partial \xi}}{N_{e,y}^2}\right)}{\left(1-\frac{N}{N_{e,y}}\right)^2}\right) + \right. \\ & \left.\left.\left(\frac{C_{m,z}\, M_z}{1-\frac{N}{N_{e,z}}}\right)\left(\frac{\frac{\partial C_{m,z}}{\partial \xi} M_z\left(1-\frac{N}{N_{e,z}}\right) + C_{m,z} M_z\left(\frac{N\frac{\partial N_{e,z}}{\partial \xi}}{N_{e,z}^2}\right)}{\left(1-\frac{N}{N_{e,z}}\right)^2}\right)\right] \frac{1}{\sqrt{\frac{C_{m,y}\, {M_y}^2}{1-\frac{N}{N_{e,y}}} + \frac{C_{m,z}\, {M_z}^2}{1-\frac{N}{N_{e,z}}}}}\right\}\end{aligned} \tag{B.11}$$

where the derivatives of the required parameters are in order of appearance:

$$\frac{\partial f_c}{\partial \xi} = \begin{cases} \dfrac{\partial f_{yc}}{\partial \xi} - 0.278\left(2\lambda\dfrac{\partial \lambda}{\partial \xi} f_{yc} + \lambda^2\dfrac{\partial f_{yc}}{\partial \xi}\right) & ; \quad \lambda \leq 1.34 \\ 0.9\dfrac{\frac{\partial f_{yc}}{\partial \xi}\lambda^2 - 2 f_{yc}\lambda\frac{\partial \lambda}{\partial \xi}}{\lambda^4} & ; \quad \lambda > 1.34 \end{cases} \tag{B.12}$$

$$\frac{\partial f_{yc}}{\partial \xi} = \begin{cases} 0 & ; \quad \frac{f_y}{f_{xe}} \leq 0.170 \\ 0.274 f_y^2 \dfrac{\frac{\partial f_{xe}}{\partial \xi}}{f_{xe}^2} & ; \quad \frac{f_y}{f_{xe}} > 0.170 \end{cases} \tag{B.13}$$

$$\frac{\partial f_{xe}}{\partial \xi} = 2\, C_x\, E \frac{\frac{\partial t}{\partial \xi}\, d - t\, \frac{\partial d}{\partial \xi}}{d^2} \tag{B.14}$$

$$\frac{\partial \lambda}{\partial \xi} = \frac{K\, L}{\pi \sqrt{E}} \frac{\frac{\frac{\partial f_{yc}}{\partial \xi}}{2\sqrt{f_{yc}}}\, r - \sqrt{f_{yc}} \frac{\partial r}{\partial \xi}}{r^2} + \frac{K}{\pi\, r} \sqrt{\frac{f_{yc}}{E}} \frac{\partial L}{\partial \xi} \tag{B.15}$$

$$\frac{\partial C_{m,y}}{\partial \xi} = \frac{0.4\, N}{N_{e,y}^2}\, \frac{\partial N_{e,y}}{\partial \xi} \tag{B.16}$$

$$\frac{\partial C_{m,z}}{\partial \xi} = \frac{0.4\, N}{N_{e,z}^2}\, \frac{\partial N_{e,z}}{\partial \xi} \tag{B.17}$$

$$\frac{\partial N_{e,y}}{\partial \xi} = \frac{\pi^2\, E}{K_y^2} \frac{\frac{\partial A}{\partial \xi} \left(\frac{L}{r}\right)^2 - 2\, A \left(\frac{L}{r}\right) \left(\frac{\frac{\partial L}{\partial \xi}\, r - L\, \frac{\partial r}{\partial \xi}}{r^2}\right)}{\left(\frac{L}{r}\right)^4} \tag{B.18}$$

$$\frac{\partial N_{e,z}}{\partial \xi} = \frac{\pi^2\, E}{K_z^2} \frac{\frac{\partial A}{\partial \xi} \left(\frac{L}{r}\right)^2 - 2\, A \left(\frac{L}{r}\right) \left(\frac{\frac{\partial L}{\partial \xi}\, r - L\, \frac{\partial r}{\partial \xi}}{r^2}\right)}{\left(\frac{L}{r}\right)^4} \tag{B.19}$$

While the derivative of equation (B.10) is quite similar to the derivative of the axial tension and bending constraint:

$$\frac{\partial g_{CB2}}{\partial \xi} = \gamma_{R,c}\, N \left(-\frac{\frac{\partial f_{yc}}{\partial \xi}\, A + f_{yc}\, \frac{\partial A}{\partial \xi}}{(f_{yc}\, A)^2}\right) + \gamma_{R,b} \sqrt{{M_y}^2 + {M_z}^2} \left(\frac{-\frac{\partial f_b}{\partial \xi}\, W_e - \frac{\partial W_e}{\partial \xi}\, f_b}{(f_b\, W_e)^2}\right) \tag{B.20}$$

Again, the nonzero derivatives of equations (B.9) and (B.10) with respect to the element forces are:

$$\begin{aligned} \frac{\partial g_{CB}}{\partial N} = {} & \frac{\gamma_{R,c}}{f_c\, A} + \\ & \frac{\gamma_{R,b}}{f_b\, W_e} \frac{1}{\sqrt{\frac{C_{m,y}\, M_y}{1 - \frac{N}{N_{e,y}}}^2 + \frac{C_{m,z}\, M_z}{1 - \frac{N}{N_{e,z}}}^2}} \left[ \left(\frac{C_{m,y}\, M_y}{1 - \frac{N}{N_{e,y}}}\right) \left(\frac{My \frac{\partial C_{m,y}}{\partial N} \left(1 - \frac{N}{N_{e,y}}\right) - C_{m,y}\, M_y \left(\frac{-1}{N_{e,y}}\right)}{\left(1 - \frac{N}{N_{e,y}}\right)^1}\right) + \right. \\ & \left. \left(\frac{C_{m,z}\, M_z}{1 - \frac{N}{N_{e,z}}}\right) \left(\frac{Mz \frac{\partial C_{m,z}}{\partial N} \left(1 - \frac{N}{N_{e,z}}\right) - C_{m,z}\, M_z \left(\frac{-1}{N_{e,z}}\right)}{\left(1 - \frac{N}{N_{e,z}}\right)^1}\right) \right] \end{aligned} \tag{B.21}$$

$$\frac{\partial g_{CB}}{\partial M_y} = \frac{\gamma_{R,b}}{f_b W_e} \frac{\left(\frac{C_{m,y}}{1-\frac{N}{N_{e,y}}}\right)^2 M_y}{\sqrt{\frac{C_{m,y}\,{M_y}^2}{1-\frac{N}{N_{e,y}}} + \frac{C_{m,z}\,{M_z}^2}{1-\frac{N}{N_{e,z}}}}} \tag{B.22}$$

$$\frac{\partial g_{CB}}{\partial M_z} = \frac{\gamma_{R,b}}{f_b W_e} \frac{\left(\frac{C_{m,z}}{1-\frac{N}{N_{e,z}}}\right)^2 M_z}{\sqrt{\frac{C_{m,y}\,{M_y}^2}{1-\frac{N}{N_{e,y}}} + \frac{C_{m,z}\,{M_z}^2}{1-\frac{N}{N_{e,z}}}}} \tag{B.23}$$

$$\frac{\partial g_{CB2}}{\partial N} = \frac{\gamma_{R,c}}{f_{yc}\,A} \tag{B.24}$$

$$\frac{\partial g_{CB2}}{\partial My} = \frac{1}{2} \frac{\gamma_{R,b}}{f_b\,W_e} \frac{2\,M_y}{\sqrt{{M_y}^2 + {M_z}^2}} \tag{B.25}$$

$$\frac{\partial g_{CB2}}{\partial Mz} = \frac{1}{2} \frac{\gamma_{R,b}}{f_b\,W_e} \frac{2\,M_z}{\sqrt{{M_y}^2 + {M_z}^2}} \tag{B.26}$$

with:

$$\frac{\partial C_{m,y}}{\partial N} = -0.4/N_{e,y} \tag{B.27}$$

$$\frac{\partial C_{m,z}}{\partial N} = -0.4/N_{e,z} \tag{B.28}$$

### B.2.3. Axial tension and bending with hydrostatic pressure

For tubular members below the water line that are not flooded, the requirement for axial tension combined with bending is:

$$g_{TBS} = \frac{\gamma_{R,t}\,N}{f_{t,h}\,A} + \frac{\gamma_{R,b}\,\sqrt{{M_y}^2 + {M_z}^2}}{f_{b,h}\,W_e} - 1 \leq 0 \tag{B.29}$$

where the only changes with respect to the axial tension and bending constraint for nonsubmerged elements ((B.3)) are the axial tension and bending strengths $f_{t,h}$ and $f_{b,h}$.

Thus, the sensitivity of the constraint can be written:

$$\frac{\partial g_{TBS}}{\partial \xi} = \gamma_{R,t}\,N \left(-\frac{\frac{\partial f_{t,h}}{\partial \xi}\,A + f_{t,h}\,\frac{\partial A}{\partial \xi}}{(f_{t,h}\,A)^2}\right) + \gamma_{R,b}\,\sqrt{{M_y}^2 + {M_z}^2} \left(\frac{-\frac{\partial f_{b,h}}{\partial \xi}\,W_e - \frac{\partial W_e}{\partial \xi}\,f_{b,h}}{(f_{b,h}\,W_e)^2}\right) \tag{B.30}$$

Where the derivative of all the parameters needed to obtain the strengths are:

$$\frac{\partial f_{t,h}}{\partial \xi} = \frac{0.09\, B \frac{\partial B}{\partial \xi} - \left(2\eta B^{2\eta-1}\frac{\partial B}{\partial \xi} + B^{2\eta} ln(B) 2 \frac{\partial \eta}{\partial \xi}\right)}{\sqrt{1 + 0.09B2 - B^{2\eta}}} f_y - 0.3 \frac{\partial B}{\partial \xi} f_y \tag{B.31}$$

$$\begin{aligned} \frac{\partial f_{b,h}}{\partial \xi} \quad = \quad & \frac{0.09\, B \frac{\partial B}{\partial \xi} - \left(2\eta B^{2\eta-1}\frac{\partial B}{\partial \xi} + B^{2\eta} ln(B) 2 \frac{\partial \eta}{\partial \xi}\right)}{\sqrt{1 + 0.09B^2 - B^{2\eta}}} f_b - 0.3 \frac{\partial B}{\partial \xi} f_b + \\ & \left(\sqrt{1 + 0.09B2 - B^{2\eta}} - 0.3\, B\right) \frac{\partial f_b}{\partial \xi} \end{aligned} \tag{B.32}$$

$$\frac{\partial \eta}{\partial \xi} = -\frac{4}{f_y} \frac{\partial f_h}{\partial \xi} \tag{B.33}$$

$$\frac{\partial B}{\partial \xi} = \gamma_{R,h} \frac{\frac{\partial \sigma_h}{\partial \xi} f_h - \sigma_h \frac{\partial f_h}{\partial \xi}}{f_h^2} \tag{B.34}$$

$$\frac{\partial \sigma_h}{\partial \xi} = \frac{\rho\, g\, h}{2} \frac{\frac{\partial d}{\partial \xi} t - d \frac{\partial t}{\partial \xi}}{t^2} \tag{B.35}$$

$$\frac{\partial f_h}{\partial \xi} = \begin{cases} \frac{\partial f_{he}}{\partial \xi} & ; \quad f_{he} \leq 0.55 f_y \\ 0.7\, 0.4 \left(\frac{f_{he}}{f_y}\right)^{-0.6} \frac{\partial f_{he}}{\partial \xi} & ; \quad 0.55 f_h < f_{he} \leq 2.44 f_y \\ 0 & ; \quad 2.44 f_y < f_{he} \end{cases} \tag{B.36}$$

$$\frac{\partial f_{he}}{\partial \xi} = 2\, E \frac{\left(\frac{\partial C_h}{\partial \xi}\, t + C_h \frac{\partial t}{\partial \xi}\right) d - C_h\, t\, \frac{\partial d}{\partial \xi}}{d^2} \tag{B.37}$$

$$\frac{\partial C_h}{\partial \xi} = \begin{cases} 0 & ; \quad \mu < 1.5 \\ -0.737 \frac{\frac{\partial \mu}{\partial \xi}}{(\mu - 0.579)^2} & ; \quad 1.5 \leq \mu < 0.825 d/t \\ 0.44 \frac{\frac{\partial t}{\partial \xi} d - t \frac{\partial d}{\partial \xi}}{d^2} + 0.21 \frac{2\left(\frac{d}{t}\right)^2 \left(\frac{\frac{\partial d}{\partial \xi} t - d \frac{\partial t}{\partial \xi}}{t^2}\right) \mu^4 - \left(\frac{d}{t}\right)^3 4\mu^3 \frac{\partial \mu}{\partial \xi}}{\mu^8} & ; \quad 0.825 d/t \leq \mu < 1.6 d/t \\ 0.44 \frac{\frac{\partial t}{\partial \xi} d - t \frac{\partial d}{\partial \xi}}{d^2} & ; \quad 1.6 d/t \leq \mu \end{cases} \tag{B.38}$$

$$\frac{\partial \mu}{\partial \xi} = \sqrt{2} \frac{\frac{\partial L}{\partial \xi} \sqrt{dt} - L \left(\frac{\frac{\partial d}{\partial \xi} t + d \frac{\partial t}{\partial \xi}}{2\sqrt{dt}}\right)}{dt} \tag{B.39}$$

Again, the nonzero derivatives of equation (B.29) with respect to the forces of the element are:

$$\frac{\partial g_{TBS}}{\partial N} = \frac{\gamma_{R,t}}{f_{t,h}\, A} \tag{B.40}$$

$$\frac{\partial g_{TBS}}{\partial My} = \frac{1}{2}\frac{\gamma_{R,b}}{f_{b,h}\, W_e}\frac{2\, M_y}{\sqrt{{M_y}^2 + {M_z}^2}} \tag{B.41}$$

$$\frac{\partial g_{TBS}}{\partial Mz} = \frac{1}{2}\frac{\gamma_{R,b}}{f_{b,h}\, W_e}\frac{2\, M_z}{\sqrt{{M_y}^2 + {M_z}^2}} \tag{B.42}$$

### B.2.4. Axial compression and bending with hydrostatic pressure

Submerged elements subject to combined compression, bending and hydrostatic pressure need to fulfill:

$$g_{CBS} = \frac{\gamma_{R,c}\, N}{f_c\, A} + \frac{\gamma_{R,b}}{f_{b,h}\, W_e}\sqrt{\frac{C_{m,y}\, {M_y}^2}{1-\frac{N}{N_{e,y}}} + \frac{C_{m,z}\, {M_z}^2}{1-\frac{N}{N_{e,z}}}} - 1 \leq 0 \tag{B.43}$$

$$g_{CBS2} = \frac{\gamma_{R,c}\, N}{f_{yc}\, A} + \frac{\gamma_{R,b}\sqrt{{M_y}^2 + {M_z}^2}}{f_{b,h}\, W_e} - 1 \leq 0 \tag{B.44}$$

$$g_{CBS3} = \frac{\frac{N}{A} + \frac{\sqrt{M_y^2+M_z^2}}{W_e} - 0.5\frac{f_{he}}{\gamma_{R,h}}}{\frac{f_{xe}}{\gamma_{R,c}} - 0.5\frac{f_{he}}{\gamma_{R,h}}} + \left(\frac{\gamma_{R,h}\sigma_h}{f_{he}}\right)^2 - 1 \leq 0 \tag{B.45}$$

Equation (B.45) needs to be checked only when $\frac{N}{A} + \frac{\sqrt{M_y^2+M_z^2}}{W_e} > 0.5\frac{f_{he}}{\gamma_{R,h}}$ and $\frac{f_{xe}}{\gamma_{R,c}} > 0.5\frac{f_{he}}{\gamma_{R,h}}$.

The first two constraints are equivalent to those for axial compression and bending without hydrostatic pressure but again changing the strength factors. Thus, their derivatives with respect to the optimization design variables read:

$$\begin{aligned}\frac{\partial g_{CBS}}{\partial \xi} = {} & \gamma_{R,c}\, N \left( -\frac{\frac{\partial f_{c,h}}{\partial \xi}\, A + f_{c,h}\, \frac{\partial A}{\partial \xi}}{(f_{c,h}\, A)^2} \right) + \\ & \gamma_{R,b} \left\{ \left( -\frac{\frac{\partial f_{b,h}}{\partial \xi}\, W_e + f_{b,h}\, \frac{\partial W_e}{\partial \xi}}{(f_{b,h}\, W_e)^2} \right) \sqrt{\frac{C_{m,y}\, M_y}{1-\frac{N}{N_{e,y}}}^2 + \frac{C_{m,z}\, M_z}{1-\frac{N}{N_{e,z}}}^2} + \right. \\ & \frac{1}{f_{b,h}\, W_e} \left[ \left( \frac{C_{m,y}\, M_y}{1-\frac{N}{N_{e,y}}} \right) \left( \frac{\frac{\partial C_{m,y}}{\partial \xi} M_y \left(1-\frac{N}{N_{e,y}}\right) + C_{m,y} M_y \left( \frac{N \frac{\partial N_{e,y}}{\partial \xi}}{N_{e,y}^2} \right)}{\left(1-\frac{N}{N_{e,y}}\right)^2} \right) + \right. \\ & \left. \left( \frac{C_{m,z}\, M_z}{1-\frac{N}{N_{e,z}}} \right) \left( \frac{\frac{\partial C_{m,z}}{\partial \xi} M_z \left(1-\frac{N}{N_{e,z}}\right) + C_{m,z} M_z \left( \frac{N \frac{\partial N_{e,z}}{\partial \xi}}{N_{e,z}^2} \right)}{\left(1-\frac{N}{N_{e,z}}\right)^2} \right) \right] \\ & \left. \frac{1}{\sqrt{\frac{C_{m,y}\, M_y}{1-\frac{N}{N_{e,y}}}^2 + \frac{C_{m,z}\, M_z}{1-\frac{N}{N_{e,z}}}^2}} \right\} \end{aligned} \tag{B.46}$$

$$\frac{\partial g_{CBS2}}{\partial \xi} = \gamma_{R,c} N \left( -\frac{\frac{\partial f_{yc}}{\partial \xi}\, A + f_{yc}\, \frac{\partial A}{\partial \xi}}{(f_{yc}\, A)^2} \right) + \gamma_{R,b} \sqrt{M_y{}^2 + M_z{}^2} \left( \frac{-\frac{\partial f_{b,h}}{\partial \xi}\, W_e - \frac{\partial W_e}{\partial \xi}\, f_{b,h}}{(f_{b,h}\, W_e)^2} \right) \tag{B.47}$$

$$\begin{aligned}\frac{\partial g_{CBS3}}{\partial \xi} = {} & \frac{1}{\left( \frac{f_{xe}}{\gamma_{R,c}} - 0.5 \frac{f_{he}}{\gamma_{R,h}} \right)^2} \left[ \left( -\frac{N}{A^2} \frac{\partial A}{\partial \xi} - \frac{1}{W_e^2} \frac{\partial W_e}{\partial \xi} \sqrt{M_y^2 + M_z^2} - \frac{0.5}{\gamma_{R,h}} \frac{\partial f_{he}}{\partial \xi} \right) \right. \\ & \left. \left( \frac{f_{xe}}{\gamma_{R,c}} - 0.5 \frac{f_{he}}{\gamma_{R,h}} \right) - \left( \frac{N}{A} + \frac{\sqrt{M_y^2 + M_z^2}}{W_e} - 0.5 \frac{f_{he}}{\gamma_{R,h}} \right) \left( \frac{\frac{\partial f_{xe}}{\partial \xi}}{\gamma_{R,c}} - 0.5 \frac{\frac{\partial f_{he}}{\partial \xi}}{\gamma_{R,h}} \right) \right] + \\ & 2\gamma_{R,h} \left( \frac{\gamma_{R,h} \sigma_h}{f_{he}} \right) \left( \frac{\frac{\partial \sigma_h}{\partial \xi} f_{he} - \sigma_h \frac{\partial f_{he}}{\partial \xi}}{f_{he}^2} \right) \end{aligned} \tag{B.48}$$

Derivatives with respect to the forces are:

$$\begin{aligned}\frac{\partial g_{CBS}}{\partial N} = {} & \frac{\gamma_{R,c}}{f_{c,h}\, A} + \frac{\gamma_{R,b}}{f_{b,h}\, W_e} \frac{1}{\sqrt{\frac{C_{m,y}\, M_y}{1-\frac{N}{N_{e,y}}}^2 + \frac{C_{m,z}\, M_z}{1-\frac{N}{N_{e,z}}}^2}} \\ & \left[ \left( \frac{C_{m,y}\, M_y}{1-\frac{N}{N_{e,y}}} \right) \left( \frac{M_y \frac{\partial C_{m,y}}{\partial N} \left(1-\frac{N}{N_{e,y}}\right) - C_{m,y}\, M_y \left(\frac{-1}{N_{e,y}}\right)}{\left(1-\frac{N}{N_{e,y}}\right)^1} \right) + \right. \\ & \left. \left( \frac{C_{m,z}\, M_z}{1-\frac{N}{N_{e,z}}} \right) \left( \frac{M_z \frac{\partial C_{m,z}}{\partial N} \left(1-\frac{N}{N_{e,z}}\right) - C_{m,z}\, M_z \left(\frac{-1}{N_{e,z}}\right)}{\left(1-\frac{N}{N_{e,z}}\right)^1} \right) \right] \end{aligned} \tag{B.49}$$

$$\frac{\partial g_{CBS}}{\partial M_y} = \frac{\gamma_{R,b}}{f_{b,h} W_e} \frac{\left(\frac{C_{m,y}}{1-\frac{N}{N_{e,y}}}\right)^2 M_y}{\sqrt{\frac{C_{m,y}\, M_y}{1-\frac{N}{N_{e,y}}}^2 + \frac{C_{m,z}\, M_z}{1-\frac{N}{N_{e,z}}}^2}} \tag{B.50}$$

$$\frac{\partial g_{CBS}}{\partial M_z} = \frac{\gamma_{R,b}}{f_{b,h} W_e} \frac{\left(\frac{C_{m,z}}{1-\frac{N}{N_{e,z}}}\right)^2 M_z}{\sqrt{\frac{C_{m,y}\, M_y}{1-\frac{N}{N_{e,y}}}^2 + \frac{C_{m,z}\, M_z}{1-\frac{N}{N_{e,z}}}^2}} \tag{B.51}$$

$$\frac{\partial g_{CBS2}}{\partial N} = \frac{\gamma_{R,c}}{f_{yc}\, A} \tag{B.52}$$

$$\frac{\partial g_{CBS2}}{\partial My} = \frac{1}{2} \frac{\gamma_{R,b}}{f_{b,h}\, W_e} \frac{2\, M_y}{\sqrt{M_y{}^2 + M_z{}^2}} \tag{B.53}$$

$$\frac{\partial g_{CBS2}}{\partial Mz} = \frac{1}{2} \frac{\gamma_{R,b}}{f_{b,h}\, W_e} \frac{2\, M_z}{\sqrt{M_y{}^2 + M_z{}^2}} \tag{B.54}$$

$$\frac{\partial g_{CBS3}}{\partial N} = \frac{\frac{1}{A}}{\frac{f_{xe}}{\gamma_{R,c}} - 0.5\frac{f_{he}}{\gamma_{R,h}}} \tag{B.55}$$

$$\frac{\partial g_{CBS3}}{\partial My} = \frac{\frac{M_y}{\sqrt{M_y^2+M_z^2}}}{\frac{f_{xe}}{\gamma_{R,c}} - 0.5\frac{f_{he}}{\gamma_{R,h}}} \tag{B.56}$$

$$\frac{\partial g_{CBS3}}{\partial Mz} = \frac{\frac{M_z}{\sqrt{M_y^2+M_z^2}}}{\frac{f_{xe}}{\gamma_{R,c}} - 0.5\frac{f_{he}}{\gamma_{R,h}}} \tag{B.57}$$

### B.2.5. Shear, bending and torsional moment

The requirement for tubular members subjected to interaction between shear, bending and torsional moment for both $y$ and $z$ local axis are:

$$g_{SBTy} = \begin{cases} \frac{\gamma_{R,b} M_z}{W_e f_{m,Red}} - \sqrt{1.4 - \frac{2\sqrt{3}\gamma_{R,v} V_y}{f_y A}} - 1 \leq 0 & ; \quad \frac{2\sqrt{3}\gamma_{R,v} V_y}{f_y A} \geq 0.4 \\ \frac{\gamma_{R,b} M_z}{W_e f_{m,Red}} - 1 \leq 0 & ; \quad \frac{2\sqrt{3}\gamma_{R,v} V_y}{f_y A} < 0.4 \end{cases} \tag{B.58}$$

$$g_{SBTz} = \begin{cases} \frac{\gamma_{R,b} M_y}{W_e f_{m,Red}} - \sqrt{1.4 - \frac{2\sqrt{3}\gamma_{R,v} V_z}{f_y A}} - 1 \leq 0 & ; \quad \frac{2\sqrt{3}\gamma_{R,v} V_z}{f_y A} \geq 0.4 \\ \frac{\gamma_{R,b} M_y}{W_e f_{m,Red}} - 1 \leq 0 & ; \quad \frac{2\sqrt{3}\gamma_{R,v} V_z}{f_y A} < 0.4 \end{cases} \tag{B.59}$$

Consequently:

$$\frac{\partial g_{SBTy}}{\partial \xi} = \begin{cases} -\frac{\gamma_{R,b} M_z}{(W_e f_{m,Red})^2}\left(\frac{\partial W_e}{\partial \xi} f_{m,Red} + W_e \frac{\partial f_{m,Red}}{\partial \xi}\right) - \frac{1}{2}\frac{\frac{2\sqrt{3}\gamma_{R,v} V_y}{f_y A^2}\frac{\partial A}{\partial \xi}}{\sqrt{1.4 - \frac{2\sqrt{3}\gamma_{R,v} V_y}{f_y A}}} & ; \frac{2\sqrt{3}\gamma_{R,v} V_y}{f_y A} \geq 0.4 \\ -\frac{\gamma_{R,b} M_z}{(W_e f_{m,Red})^2}\left(\frac{\partial W_e}{\partial \xi} f_{m,Red} + W_e \frac{\partial f_{m,Red}}{\partial \xi}\right) & ; \frac{2\sqrt{3}\gamma_{R,v} V_y}{f_y A} < 0.4 \end{cases} \tag{B.60}$$

$$\frac{\partial g_{SBTz}}{\partial \xi} = \begin{cases} -\frac{\gamma_{R,b} M_y}{(W_e f_{m,Red})^2}\left(\frac{\partial W_e}{\partial \xi} f_{m,Red} + W_e \frac{\partial f_{m,Red}}{\partial \xi}\right) - \frac{1}{2}\frac{\frac{2\sqrt{3}\gamma_{R,v} V_z}{f_y A^2}\frac{\partial A}{\partial \xi}}{\sqrt{1.4 - \frac{2\sqrt{3}\gamma_{R,v} V_z}{f_y A}}} & ; \frac{2\sqrt{3}\gamma_{R,v} V_z}{f_y A} \geq 0.4 \\ -\frac{\gamma_{R,b} M_y}{(W_e f_{m,Red})^2}\left(\frac{\partial W_e}{\partial \xi} f_{m,Red} + W_e \frac{\partial f_{m,Red}}{\partial \xi}\right) & ; \frac{2\sqrt{3}\gamma_{R,v} V_z}{f_y A} < 0.4 \end{cases} \tag{B.61}$$

where the derivatives of the parameters are:

$$\frac{\partial f_{m,Red}}{\partial \xi} = \sqrt{1 - 3\left(\frac{\gamma_{R,t}\tau_t}{f_y}\right)^2}\frac{\partial f_b}{\partial \xi} - \frac{f_b}{2}\frac{6\left(\frac{\gamma_{R,t}^2 \tau_t}{f_y^2}\right)\frac{\partial \tau_t}{\partial \xi}}{\sqrt{1 - 3\left(\frac{\gamma_{R,t}\tau_t}{f_y}\right)^2}} \tag{B.62}$$

$$\frac{\partial \tau_t}{\partial \xi} = -\frac{M_x}{\pi/2}\frac{2d\frac{\partial d}{\partial \xi}t + d^2\frac{\partial t}{\partial \xi}}{d^4 t^2} \tag{B.63}$$

As for the other constraints we have to get the derivatives with respect to the forces.

$$\frac{\partial g_{SBTy}}{\partial V_y} = \begin{cases} \frac{1}{2}\frac{\frac{2\sqrt{3}\gamma_{R,v}}{f_y A}}{\sqrt{1.4 - \frac{2\sqrt{3}\gamma_{R,v} V_y}{f_y A}}} & ; \frac{2\sqrt{3}\gamma_{R,v} V_y}{f_y A} \geq 0.4 \\ 0 & ; \frac{2\sqrt{3}\gamma_{R,v} V_y}{f_y A} < 0.4 \end{cases} \tag{B.64}$$

$$\frac{\partial g_{SBTy}}{\partial M_x} = \begin{cases} -\frac{\gamma_{R,b} M_z}{W e f_{m,Red}^2}\frac{\partial f_{m,Red}}{\partial M_x} & ; \frac{2\sqrt{3}\gamma_{R,v} V_y}{f_y A} \geq 0.4 \\ -\frac{\gamma_{R,b} M_z}{W e f_{m,Red}^2}\frac{\partial f_{m,Red}}{\partial M_x} & ; \frac{2\sqrt{3}\gamma_{R,v} V_y}{f_y A} < 0.4 \end{cases} \tag{B.65}$$

$$\frac{\partial g_{SBTy}}{\partial M_z} = \begin{cases} \frac{\gamma_{R,b}}{W e f_{m,Red}} & ; \frac{2\sqrt{3}\gamma_{R,v} V_y}{f_y A} \geq 0.4 \\ \frac{\gamma_{R,b}}{W e f_{m,Red}} & ; \frac{2\sqrt{3}\gamma_{R,v} V_y}{f_y A} < 0.4 \end{cases} \tag{B.66}$$

$$\frac{\partial g_{SBTz}}{\partial V_z} = \begin{cases} \frac{1}{2}\frac{\frac{2\sqrt{3}\gamma_{R,v}}{f_y A}}{\sqrt{1.4-\frac{2\sqrt{3}\gamma_{R,v}V_z}{f_y A}}} & ; \quad \frac{2\sqrt{3}\gamma_{R,v}V_z}{f_y A} \geq 0.4 \\ 0 & ; \quad \frac{2\sqrt{3}\gamma_{R,v}V_z}{f_y A} < 0.4 \end{cases} \tag{B.67}$$

$$\frac{\partial g_{SBTz}}{\partial M_x} = \begin{cases} -\frac{\gamma_{R,b}M_y}{Wef^2_{m,Red}}\frac{\partial f_{m,Red}}{\partial M_x} & ; \quad \frac{2\sqrt{3}\gamma_{R,v}V_z}{f_y A} \geq 0.4 \\ -\frac{\gamma_{R,b}M_y}{Wef^2_{m,Red}}\frac{\partial f_{m,Red}}{\partial M_x} & ; \quad \frac{2\sqrt{3}\gamma_{R,v}V_z}{f_y A} < 0.4 \end{cases} \tag{B.68}$$

$$\frac{\partial g_{SBTz}}{\partial M_y} = \begin{cases} \frac{\gamma_{R,b}}{Wef_{m,Red}} & ; \quad \frac{2\sqrt{3}\gamma_{R,v}V_z}{f_y A} \geq 0.4 \\ \frac{\gamma_{R,b}}{Wef_{m,Red}} & ; \quad \frac{2\sqrt{3}\gamma_{R,v}V_z}{f_y A} < 0.4 \end{cases} \tag{B.69}$$

where

$$\frac{\partial f_{m,Red}}{\partial M_x} = -\frac{f_b}{2}\frac{6\left(\frac{\gamma^2_{R,t}\tau_t}{f^2_y}\right)\frac{\partial \tau_t}{\partial M_x}}{\sqrt{1-3\left(\frac{\gamma_{R,t}\tau_t}{f_y}\right)^2}} \tag{B.70}$$

$$\frac{\partial \tau_t}{\partial M_x} = \frac{2}{\pi\, d^2\, t} \tag{B.71}$$

### B.2.6. Hoop Buckling

The hoop buckling constraint for submerged elements is:

$$g_{HB} = \frac{\gamma_{R,h}\sigma_h}{f_h} - 1 \leq 0 \tag{B.72}$$

Thereby:

$$\frac{\partial g_{HB}}{\partial \xi} = \gamma_{R,h}\frac{\frac{\partial \sigma_h}{\partial \xi} f_h - \sigma_h \frac{\partial f_h}{\partial \xi}}{f_h^2} \tag{B.73}$$

## B.3. Fatigue Limit State constraints

The fatigue life constraint defined in this work takes the shape:

$$g_f = \sum_{j=1}^{N_c} P_j \frac{1}{a}\sum_{i=1}^{n_b} n_i \left(\frac{t}{t_{ref}}\right)^{k\,m} (\Delta\sigma_i)^m - \frac{1}{DFF} \leq 0 \tag{B.74}$$

The explanation of this expression as well as the strategy for the computation of its sensitivity has already been explained in chapters 2, 3 and 4. That strategy to

achieve the sensitivity for the non-analytically differentiable equation (B.74) involves the computation of the analytic derivatives of the stresses $\sigma$ which, as seen in chapter 4, are computed through the Stress Concentration Factors (SCF). This chapter provides the expressions for the sensitivities of the SCFs needed to compute the derivatives of the stresses with respect to the design variables.

### B.3.1. Derivative of the geometrical parameters of the joint

The derivatives of the geometrical parameters that are common to all the joints are:

$$\frac{\partial \beta}{\partial \xi} = \frac{\frac{\partial d}{\partial \xi} D - d \frac{\partial D}{\partial \xi}}{D^2} \tag{B.75}$$

$$\frac{\partial \tau}{\partial \xi} = \frac{\frac{\partial t}{\partial \xi} T - t \frac{\partial T}{\partial \xi}}{T^2} \tag{B.76}$$

$$\frac{\partial \gamma}{\partial \xi} = \frac{\frac{\partial D}{\partial \xi} T - D \frac{\partial T}{\partial \xi}}{2\, T^2} \tag{B.77}$$

$$\frac{\partial \alpha}{\partial \xi} = 2\, \frac{\frac{\partial L}{\partial \xi} D - L \frac{\partial D}{\partial \xi}}{D^2} \tag{B.78}$$

Some of the factors depend also on the angle by the tubular elements converging at the joint denoted by $\theta$. Let $\boldsymbol{b}_1$ and $\boldsymbol{b}_2$ be the vectors that define the spacial orientation of two bars at the joint. Then, the angle between them is:

$$\theta = \arccos \frac{\boldsymbol{b}_1 \boldsymbol{b}_2}{|\boldsymbol{b}_1|\, |\boldsymbol{b}_2|} \tag{B.79}$$

Thus, its derivative es simply:

$$\frac{\partial \theta}{\partial \xi} = -\frac{\frac{\partial}{\partial \xi}\left(\frac{\boldsymbol{b}_1 \boldsymbol{b}_2}{|\boldsymbol{b}_1||\boldsymbol{b}_2|}\right)}{\sqrt{1-\left(\frac{\boldsymbol{b}_1 \boldsymbol{b}_2}{|\boldsymbol{b}_1||\boldsymbol{b}_2|}\right)}} = \frac{\left(\frac{\partial \boldsymbol{b}_1}{\partial \xi}\boldsymbol{b}_2 + \boldsymbol{b}_1 \frac{\partial \boldsymbol{b}_2}{\partial \xi}\right)|\boldsymbol{b}_1|\,|\boldsymbol{b}_2| - \boldsymbol{b}_1 \boldsymbol{b}_2 \left(\frac{\partial |\boldsymbol{b}_1|}{\partial \xi}|\boldsymbol{b}_2| + |\boldsymbol{b}_1| \frac{\partial |\boldsymbol{b}_2|}{\partial \xi}\right)}{\left(|\boldsymbol{b}_1|\,|\boldsymbol{b}_2|\right)^2} \tag{B.80}$$

where the derivative of vectors $\boldsymbol{b}_1$ and $\boldsymbol{b}_2$ are:

$$\frac{\partial \boldsymbol{b}_1}{\partial \xi} = \begin{Bmatrix} \frac{\partial x_2^{\boldsymbol{b}_1}}{\partial \xi} - \frac{\partial x_1^{\boldsymbol{b}_1}}{\partial \xi} \\ \frac{\partial y_2^{\boldsymbol{b}_1}}{\partial \xi} - \frac{\partial y_1^{\boldsymbol{b}_1}}{\partial \xi} \\ \frac{\partial z_2^{\boldsymbol{b}_1}}{\partial \xi} - \frac{\partial z_1^{\boldsymbol{b}_1}}{\partial \xi} \end{Bmatrix} = \begin{Bmatrix} \frac{\partial dx^{\boldsymbol{b}_1}}{\partial \xi} \\ \frac{\partial dy^{\boldsymbol{b}_1}}{\partial \xi} \\ \frac{\partial dz^{\boldsymbol{b}_1}}{\partial \xi} \end{Bmatrix} \qquad \frac{\partial \boldsymbol{b}_2}{\partial \xi} = \begin{Bmatrix} \frac{\partial x_2^{\boldsymbol{b}_2}}{\partial \xi} - \frac{\partial x_1^{\boldsymbol{b}_2}}{\partial \xi} \\ \frac{\partial y_2^{\boldsymbol{b}_2}}{\partial \xi} - \frac{\partial y_1^{\boldsymbol{b}_2}}{\partial \xi} \\ \frac{\partial z_2^{\boldsymbol{b}_2}}{\partial \xi} - \frac{\partial z_1^{\boldsymbol{b}_2}}{\partial \xi} \end{Bmatrix} = \begin{Bmatrix} \frac{\partial dx^{\boldsymbol{b}_2}}{\partial \xi} \\ \frac{\partial dy^{\boldsymbol{b}_2}}{\partial \xi} \\ \frac{\partial dz^{\boldsymbol{b}_2}}{\partial \xi} \end{Bmatrix} \tag{B.81}$$

in the above equation notation $x_i^{b_j}$ refers to the $x$ coordinate of joint $i$ and element $b_j$.

Additionally, the derivative of the modulus of the vectors used in (B.80) is:

$$\frac{\partial \left|\boldsymbol{b}_1\right|}{\partial \xi} = \frac{dx^{\boldsymbol{b}_1}\frac{\partial dx^{\boldsymbol{b}_1}}{\partial \xi} + dy^{\boldsymbol{b}_1}\frac{\partial dy^{\boldsymbol{b}_1}}{\partial \xi} + dz^{\boldsymbol{b}_1}\frac{\partial dz^{\boldsymbol{b}_1}}{\partial \xi}}{\sqrt{(dx^{\boldsymbol{b}_1})^2 + (dy^{\boldsymbol{b}_1})^2 + (dz^{\boldsymbol{b}_1})^2}} \tag{B.82}$$

### B.3.2. Derivative of the dimensional constraints

The derivatives of the dimensional constraints that limit the above values in order for the SCFs to be valid are:

$$\begin{gathered}
\left\{ \begin{array}{c} \frac{\partial g_{\beta m}}{\partial \xi} = -\frac{\partial \beta}{\partial \xi} \\ \frac{\partial g_{\beta M}}{\partial \xi} = \frac{\partial \beta}{\partial \xi} \end{array} \right\} \left\{ \begin{array}{c} \frac{\partial g_{\tau m}}{\partial \xi} = -\frac{\partial \tau}{\partial \xi} \\ \frac{\partial g_{\tau M}}{\partial \xi} = \frac{\partial \tau}{\partial \xi} \end{array} \right\} \\
\left\{ \begin{array}{c} \frac{\partial g_{\gamma m}}{\partial \xi} = -\frac{1}{64}\frac{\partial \gamma}{\partial \xi} \\ \frac{\partial g_{\gamma M}}{\partial \xi} = \frac{1}{64}\frac{\partial \gamma}{\partial \xi} \end{array} \right\} \left\{ \begin{array}{c} \frac{\partial g_{\alpha m}}{\partial \xi} = -\frac{1}{20}\frac{\partial \alpha}{\partial \xi} \\ \frac{\partial g_{\alpha M}}{\partial \xi} = \frac{1}{20}\frac{\partial \alpha}{\partial \xi} \end{array} \right\} \\
\left\{ \begin{array}{c} \frac{\partial g_{\theta m}}{\partial \xi} = -\frac{4}{\pi}\frac{\partial \theta}{\partial \xi} \\ \frac{\partial g_{\theta M}}{\partial \xi} = \frac{4}{\pi}\frac{\partial \theta}{\partial \xi} \end{array} \right\}
\end{gathered} \tag{B.83}$$

### B.3.3. SCFs sensitivities for T/Y joints

The derivatives of the Stress Concentration Factors for simple tubular T or Y joints are:

$$\begin{aligned}
\tfrac{\partial SCF_{T,AC,C}}{\partial \xi} = {} & 0.2\,\gamma^{-0.8}\,\tfrac{\partial \gamma}{\partial \xi}\tau\left(2.65 + 5\left(\beta - 0.65\right)^2\right) + \gamma^{0.2}\,\tfrac{\partial \tau}{\partial \xi}\,\left(2.65 + 5\left(\beta - 0.65\right)^2\right) + \\
& \gamma^{0.2}\,\tau\,\left(10\left(\beta - 0.65\right)\tfrac{\partial \beta}{\partial \xi}\right) + \tfrac{\partial \tau}{\partial \xi}\,\beta\left(0.25\,\alpha - 3\right)\,\sin(\theta) + \\
& \tau\,\tfrac{\partial \beta}{\partial \xi}\left(0.25\alpha - 3\right)\,\sin\theta + \tau\,\beta\,0.25\,\tfrac{\partial \alpha}{\partial \xi}\,\sin(\theta) + \tau\,\beta\left(0.25\alpha - 3\right)\,\cos(\theta)\tfrac{\partial \theta}{\partial \xi}
\end{aligned} \tag{B.84}$$

$$\begin{aligned}
\tfrac{\partial SCF_{T,AS,C}}{\partial \xi} = {} & \tfrac{\partial \gamma}{\partial \xi}\,\tau^{1.1}\left(1.1 - 3\left(\beta - 0.52\right)^2\right)\left(\sin(\theta)\right)^{1.6} + \\
& \gamma\,1.11\,\tau^{0.1}\,\tfrac{\partial \tau}{\partial \xi}\left(1.1 - 3\left(\beta - 0.52\right)^2\right)\left(\sin(\theta)\right)^{1.6} + \\
& \gamma\,\tau^{1.1}\left(-6\left(\beta - 0.52\right)\tfrac{\partial \beta}{\partial \xi}\right)\left(\sin(\theta)\right)^{1.6} + \\
& \gamma\,\tau^{1.1}\left(1.1 - 3\left(\beta - 0.52\right)^2\right)1.6(\sin(\theta))^{0.6}\cos(\theta)\tfrac{\partial \theta}{\partial \xi}
\end{aligned} \tag{B.85}$$

$$\begin{aligned}\frac{\partial SCF_{T,MIP,C}}{\partial \xi} = & 1.45\ \frac{\partial \beta}{\partial \xi}\ \tau^{0.85}\ \gamma^{(1-0.68\,\beta)}(\sin(\theta))^{0.7} + \\ & 1.45\ \beta\ 0.85\ \tau^{-0.15}\ \frac{\partial \tau}{\partial \xi}\ \gamma^{(1-0.68\,\beta)}(\sin(\theta))^{0.7} + \\ & 1.45\ \beta\ \tau^{0.85}\left((1-0.68\beta)\ \gamma^{-0.68\beta}\frac{\partial \gamma}{\partial \xi} + \gamma^{(1-0.68\beta)}\ln(\gamma)(-0.68\frac{\partial \beta}{\partial \xi}\right) \\ & (\sin(\theta))^{0.7} + 1.45\ \beta\ \tau^{0.8}\ \gamma^{(1-0.68\beta)}0.7(\sin(\theta))^{-0.3}\ \cos(\theta)\ \frac{\partial \theta}{\partial \xi}\end{aligned} \tag{B.86}$$

$$\begin{aligned}\frac{\partial SCF_{T,MOP,C}}{\partial \xi} = & \left(\frac{\partial \gamma}{\partial \xi}\ \tau\beta + \gamma\ \frac{\partial \tau}{\partial \xi}\ \beta + \gamma\ \tau\frac{\partial \beta}{\partial \xi}\right)\left(1.7 - 1.05\beta^3\right)(\sin(\theta))^{1.6} + \\ & \gamma\ \tau\ \beta\left(-3.15\ \beta^2\frac{\partial \beta}{\partial \xi}\right)(\sin(\theta))^{1.6} + \gamma\ \tau\ \beta\left(1.7 - 1.05\beta^3\right)1.6(\sin(\theta))^{0.6}\sin(\theta)\frac{\partial \theta}{\partial \xi}\end{aligned} \tag{B.87}$$

$$\begin{aligned}\frac{\partial SCF_{T,AC,B}}{\partial \xi} = & 1.2\ \gamma^{0.2}\frac{\partial \gamma}{\partial \xi}\left(0.12\ e^{-4\beta} + 0.011\beta^2 - 0.045\right) + \frac{\partial \beta}{\partial \xi}\ \tau\ (0.1\alpha - 1.2) + \\ & \gamma^{1.2}\left(0.12\ e^{-4\beta}(-4\frac{\partial \beta}{\partial \xi}) + 0.022\ \beta\frac{\partial \beta}{\partial \xi}\right) + \beta\ \frac{\partial \tau}{\partial \xi}(0.1\alpha - 1.2) + \beta\ \tau\ 0.1\frac{\partial \alpha}{\partial \xi}\end{aligned} \tag{B.88}$$

$$\begin{aligned}\frac{\partial SCF_{T,AS,B}}{\partial \xi} = & \frac{\partial \gamma}{\partial \xi}\ \tau^{0.52}\ \alpha^{0.1}\left(0.187 - 1.25\beta^{1.1}(\beta - 0.96)\right)(\sin(\theta))^{(2.7-0.01\alpha)} + \\ & \alpha\ 0.52\ \tau^{-0.48}\ \frac{\partial \tau}{\partial \xi}\ \alpha^{0.1}\left(0.187 - 1.25\beta^{1.1}(\beta - 0.96)\right)(\sin(\theta))^{(2.7-0.01\alpha)} + \\ & \gamma\ \tau^{0.52}\ 0.1\alpha^{-0.9}\frac{\partial \alpha}{\partial \xi}\left(0.187 - 1.25\beta^{1.1}(\beta - 0.96)\right)(\sin(\theta))^{(2.7-0.01\alpha)} + \\ & \gamma\ \tau^{0.52}\ \alpha^{0.1}\left(-1.25\ 2.1\ \beta^{1.1}\frac{\partial \beta}{\partial \xi} + 1.25\ 0.96\ 1.1\ \beta^{0.1}\frac{\partial \beta}{\partial \xi}\right)(\sin(\theta))^{(2.7-0.01\alpha)} + \\ & \gamma\ \tau^{0.52}\ \alpha^{0.1}\left(0.187 - 1.25\beta^{1.1}(\beta - 0.96)\right) \\ & \left((2.7 - 0.01\alpha)(\sin(\theta))^{(1.7-0.01\alpha)}\cos(\theta)\frac{\partial \theta}{\partial \xi} + \right. \\ & \left.(\sin\theta)^{(2.7-0.01\alpha)}\ln(\sin(\theta))\ (-0.01)\frac{\partial \alpha}{\partial \xi}\right)\end{aligned} \tag{B.89}$$

$$\begin{aligned}\frac{\partial SCF_{T,MIP,B}}{\partial \xi} = & 0.65\frac{\partial \beta}{\partial \xi}\ \tau^{0.4}\ \gamma^{(1.09-0.77\beta)}(\sin(\theta))^{(0.06\gamma-1.16)} + \\ & 0.65\ \beta\ 0.4\ \tau^{-0.6}\frac{\partial \tau}{\partial \xi}\ \gamma^{(1.09-0.77\beta)}(\sin(\theta))^{(0.06\gamma-1.16)} + 0.65\ \beta\ \tau^{0.4} \\ & \left((1.09 - 0.77\beta)\gamma^{(0.09-0.77\beta)}\frac{\partial \gamma}{\partial \xi} + \gamma^{(1.09-0.77\beta)}\ \ln(\gamma)(-0.77\frac{\partial \beta}{\partial \xi})\right) \\ & (\sin(\theta))^{(0.06\gamma-1.16)} + \\ & 0.65\ \beta\ \tau^{0.4}\ \gamma^{(1.09-0.77\beta)} \\ & \left((0.06\gamma - 1.16)(\sin(\theta))^{(0.06\alpha-2.16)}\cos(\theta)\frac{\partial \theta}{\partial \xi} + (\sin\theta)^{(0.06\gamma-1.16)}\right. \\ & \left.\ln(\sin(\theta))\ 0.06\ \frac{\partial \gamma}{\partial \xi}\right)\end{aligned} \tag{B.90}$$

$$\begin{aligned}\frac{\partial SCF_{T,MOP,B}}{\partial \xi} &= -0.54\,\tau^{-1.54}\,\frac{\partial \tau}{\partial \xi}\,\gamma^{-0.05}\left(0.99-0.47\beta+0.08\beta^4\right)SCF_{T,MIP,B}+\\ &\tau^{-0.54}\,(-0.05)\,\gamma^{-1.05}\frac{\partial \gamma}{\partial \xi}\left(0.99-0.47\beta+0.08\beta^4\right)SCF_{T,MIP,B}+\\ &\tau^{-0.54}\gamma^{-0.05}\left(-0.47\,\frac{\partial \beta}{\partial \xi}+0.32\,\beta^3\frac{\partial \beta}{\partial \xi}\right)SCF_{T,MIP,B}+\\ &\tau^{-054}\,\gamma^{-0.05}\left(0.99-0.47\,\beta+0.08\,\beta^4\right)\frac{\partial SCF_{T,7}}{\partial \xi}\end{aligned} \tag{B.91}$$

If the parameter $\alpha < 12$ then some of the coefficients need to be corrected by the short chord correction factors. Their derivatives are:

$$\begin{aligned}\frac{\partial f_{T,1}}{\partial \xi} &= -\left(0.83-1.12\,\beta\frac{\partial \beta}{\partial \xi}\right)\,\gamma^{0.23}\,e^{(-0.21\gamma^{-1.16}\alpha^{2.5})}-\\ &\left(0.83\beta-0.56\beta^2-0.02\right)0.23\gamma^{-0.77}\frac{\partial \gamma}{\partial \xi}\,e^{(-0.21\gamma^{-1.16}\alpha^{2.5})}-\\ &\left(0.83\beta-0.56\beta^2-0.02\right)\gamma^{0.23}\,e^{(-0.21\gamma^{-1.16}\alpha^{2.5})}\\ &\left(0.49\,0.89\,\gamma^{-1.89}\frac{\partial \gamma}{\partial \xi}\alpha^{1.8}-0.49\,\gamma^{-0.89}\,1.8\,\alpha^{0.8}\frac{\partial \alpha}{\partial \xi}\right)\end{aligned} \tag{B.92}$$

$$\begin{aligned}\frac{\partial f_{T,3}}{\partial \xi} &= -0.55\,1.8\,\beta^{0.8}\,\frac{\partial \beta}{\partial \xi}\,\gamma^{0.16}\,e^{(-0.49\,\gamma^{-0.89}\alpha^{1.8})}-\\ &0.55\,\beta^{1.8}\,0.16\,\gamma^{-0.84}\,\frac{\partial \gamma}{\partial \xi}\,e^{(-0.49\,\gamma^{-0.89}\alpha^{1.8})}-\\ &0.55\,\beta^{1,8}\,\gamma^{0.16}\,e^{(-0.49\,\gamma^{-0.89}\alpha^{1.8})}\\ &\left(0.49\,0.89\,\gamma^{-1.89}\frac{\partial \gamma}{\partial \xi}\alpha^{1.8}-0.49\,\gamma^{-0.89}\,1.8\,\alpha^{0.8}\frac{\partial \alpha}{\partial \xi}\right)\end{aligned} \tag{B.93}$$

Those SCFs that need to be corrected are computed as $SCF' = SCFf$, thus their derivatives are obtained as $\frac{\partial SCF'}{\partial \xi} = \frac{\partial SCF}{\partial \xi}f + SCF\frac{\partial f}{\partial \xi}$.

### B.3.4. SCFs sensitivities for X joints

$$\begin{aligned}\frac{\partial SCF_{X,AC,C}}{\partial \xi} &= 0.2\,\gamma^{-0.8}\frac{\partial \gamma}{\partial \xi}\,\tau\left(2.65+5(\beta-0.65)^2\right)-3\,\frac{\partial \tau}{\partial \xi}\beta\sin(\theta)+\\ &\gamma^{0.2}\,\frac{\partial \tau}{\partial \xi}\left(2.65+5(\beta-0.65)^2\right)-3\,\tau\frac{\partial \beta}{\partial \xi}\sin(\theta)+\\ &\gamma^{0.2}\,\tau\left(10(\beta-0.65)\frac{\partial \beta}{\partial \xi}\right)-3\,\tau\,\beta(\cos\theta)\,\frac{\partial \theta}{\partial \xi}\end{aligned} \tag{B.94}$$

$$\begin{aligned}\frac{\partial SCF_{X,AS,C}}{\partial \xi} &= \left(\frac{\partial \gamma}{\partial \xi}\,\tau\beta+\gamma\,\frac{\partial \tau}{\partial \xi}\,\beta+\gamma\,\tau\frac{\partial \beta}{\partial \xi}\right)\,3.87(1.10-\beta^{1.8})(\sin(\theta))^{1.7}+\\ &3.87\,\gamma\,\tau\,\beta(-1.8\,\beta^{0.8}\frac{\partial \beta}{\partial \xi})(\sin(\theta))^{1.7}+\\ &3.87\,\gamma\,\tau\,\beta(1.10-\beta^{1.8})\,1.7\,(\sin(\theta))^{0.7}\,\cos(\theta)\,\frac{\partial \theta}{\partial \xi}\end{aligned} \tag{B.95}$$

$$\begin{aligned}\frac{\partial SCF_{X,MIP,C}}{\partial \xi} &= 1.45\,\frac{\partial \beta}{\partial \xi}\,\tau^{0.85}\,\gamma^{(1-0.68\,\beta)}(\sin(\theta))^{0.7}+\\ &1.45\,\beta\,0.85\,\tau^{-0.15}\,\frac{\partial \tau}{\partial \xi}\,\gamma^{(1-0.68\,\beta)}(\sin(\theta))^{0.7}+\\ &1.45\,\beta\,\tau^{0.85}\left((1-0.68\beta)\,\gamma^{-0.68\beta}\frac{\partial \gamma}{\partial \xi}+\gamma^{(1-0.68\beta)}\ln(\gamma)(-0.68\frac{\partial \beta}{\partial \xi}\right)\\ &(\sin(\theta))^{0.7}+1.45\,\beta\,\tau^{0.8}\,\gamma^{(1-0.68\beta)}0.7(\sin(\theta))^{-0.3}\,\cos(\theta)\,\frac{\partial \theta}{\partial \xi}\end{aligned} \tag{B.96}$$

$$\begin{aligned}\frac{\partial SCF_{X,MOP,C}}{\partial \xi} &= \left(\frac{\partial \gamma}{\partial \xi}\,\tau\beta + \gamma\,\frac{\partial \tau}{\partial \xi}\,\beta + \gamma\,\tau\frac{\partial \beta}{\partial \xi}\right)\,(1.56 - 1.34\,\beta^4)(\sin(\theta))^{1.6} + \\ &\quad \gamma\,\tau\,\beta(-5.36\,\beta^3\,\frac{\partial \beta}{\partial \xi})(\sin(\theta))^{1.6} + \\ &\quad \gamma\,\tau\,\beta(1.56 - 1.34\,\beta^4)\,1.6\,(\sin(\theta))^{0.6}\,\cos(\theta)\,\frac{\partial \theta}{\partial \xi}\end{aligned} \tag{B.97}$$

$$\begin{aligned}\frac{\partial SCF_{X,AC,B}}{\partial \xi} &= 1.2\,\gamma^{0.2}\,\frac{\partial \gamma}{\partial \xi}\left(0.12\,e^{-4\beta} + 0.011\,\beta^2 - 0.045\right) + \\ &\quad \gamma^{1.2}\left(0.12\,e^{-4\beta}(-4\frac{\partial \beta}{\partial \xi}) + 0.022\,\beta\,\frac{\partial \beta}{\partial \xi}\right)\end{aligned} \tag{B.98}$$

$$\begin{aligned}\frac{\partial SCF_{X,AS,B}}{\partial \xi} &= 1.9\,\frac{\partial \gamma}{\partial \xi}\,\tau^{0.5}\,\beta^{0.9}\left(1.09 - \beta^{1.7}\right)(\sin(\theta))^{2.5} + \\ &\quad 1.9\,\gamma\,0.5\,\tau^{-0.5}\frac{\partial \tau}{\partial \xi}\,\beta^{0.9}\left(1.09 - \beta^{1.7}\right)(\sin(\theta))^{2.5} + \\ &\quad 1.9\,\gamma\,\tau^{0.5}\,0.9\,\beta^{-0.1}\frac{\partial \beta}{\partial \xi}\left(1.09 - \beta^{1.7}\right)(\sin(\theta))^{2.5} + \\ &\quad 1.9\,\gamma\,\tau^{0.5}\,\beta^{0.9}\left(-1.7\,\beta^{0.7}\frac{\partial \beta}{\partial \xi}\right)(\sin(\theta))^{2.5} + \\ &\quad 1.9\,\gamma\,\tau^{0.5}\,\beta^{0.9}\left(1.09 - \beta^{1.7}\right)2.5\,(\sin(\theta))^{1.5}\,\cos(\theta)\frac{\partial \theta}{\partial \xi}\end{aligned} \tag{B.99}$$

$$\begin{aligned}\frac{\partial SCF_{X,MIP,B}}{\partial \xi} &= 0.65\frac{\partial \beta}{\partial \xi}\,\tau^{0.4}\,\gamma^{(1.09-0.77\beta)}(\sin(\theta))^{(0.06\gamma-1.16)} + \\ &\quad 0.65\,\beta\,0.4\,\tau^{-0.6}\frac{\partial \tau}{\partial \xi}\,\gamma^{(1.09-0.77\beta)}(\sin(\theta))^{(0.06\gamma-1.16)} + \\ &\quad 0.65\,\beta\,\tau^{0.4}\left((1.09 - 0.77\beta)\gamma^{(0.09-0.77\beta)}\frac{\partial \gamma}{\partial \xi} + \gamma^{(1.09-0.77\beta)}\right. \\ &\quad \left.\ln(\gamma)(-0.77\frac{\partial \beta}{\partial \xi})\right)(\sin(\theta))^{(0.06\gamma-1.16)} + \\ &\quad 0.65\,\beta\,\tau^{0.4}\,\gamma^{(1.09-0.77\beta)}\left((0.06\gamma - 1.16)(\sin(\theta))^{(0.06\alpha-2.16)}\cos(\theta)\frac{\partial \theta}{\partial \xi} + \right. \\ &\quad \left.(\sin(\theta))^{(0.06\gamma-1.16)}\,\ln(\sin(\theta))\,0.06\,\frac{\partial \gamma}{\partial \xi}\right)\end{aligned} \tag{B.100}$$

$$\begin{aligned}\frac{\partial SCF_{X,MOP,B}}{\partial \xi} &= -0.54\,\tau^{-1.54}\,\frac{\partial \tau}{\partial \xi}\,\gamma^{-0.05}\left(0.99 - 0.47\beta + 0.08\beta^4\right)SCF_{X,MIP,B} + \\ &\quad \tau^{-0.54}\,(-0.05)\,\gamma^{-1.05}\frac{\partial \gamma}{\partial \xi}\left(0.99 - 0.47\beta + 0.08\beta^4\right)SCF_{X,MIP,B} + \\ &\quad \tau^{-0.54}\gamma^{-0.05}\left(-0.47\,\frac{\partial \beta}{\partial \xi} + 0.32\,\beta^3\frac{\partial \beta}{\partial \xi}\right)SCF_{X,MIP,B} + \\ &\quad \tau^{-054}\,\gamma^{-0.05}\left(0.99 - 0.47\,\beta + 0.08\,\beta^4\right)\frac{\partial SCF_{X,MIP,B}}{\partial \xi}\end{aligned} \tag{B.101}$$

### B.3.5. SCFs sensitivities for K joints

K joints need two additional parameters $\zeta$ and $x$ with derivatives:

$$\frac{\partial \zeta}{\partial \xi} = -\frac{gap\,\frac{\partial D}{\partial \xi}}{D^2} \tag{B.102}$$

$$\frac{\partial x}{\partial \xi} = \frac{\left(\frac{\partial \zeta}{\partial \xi}\sin\theta + \zeta\cos\theta\frac{\partial \theta}{\partial \xi}\right)\beta - \zeta\sin\theta\frac{\partial \beta}{\partial \xi}}{\beta^2} \tag{B.103}$$

When analyzing the Stress Concentration Factors for K joints some discontinuous parameters appear, for example $\beta_{max}$, $\beta_{min}$, $\theta_{max}$ and $\theta_{min}$. To obtain an analytic derivative of the SCF, assuming small variations of the design variables, the derivatives of those discontinuous values are taken as the derivatives of the parameters that gives the maximum or minimum value. For example, if $\beta_{max} = max(\beta_1, \beta_2)$ and $\beta_1 > \beta_2$ then the derivative of $\beta_1$ is taken as the derivative of $\beta_{max}$.

$$
\begin{aligned}
\frac{\partial SCF_{K,AC,C}}{\partial \xi} = \; & 0.9\,\tau^{-0.1}\frac{\partial \tau}{\partial \xi}\gamma^{0.5}\left(0.67-\beta^2+1.16\beta\right)\sin(\theta)\left(\frac{\sin(\theta_{max})}{\sin(\theta_{min})}\right)^{0.30}\left(\frac{\beta_{max}}{\beta_{min}}\right)^{0.30} \\
& \left(1.64+0.29\beta^{-0.38}\arctan(8\zeta)\right)+ \\
& \tau^{0.9}\,0.5\gamma^{-0.5}\frac{\partial \gamma}{\partial \xi}\left(0.67-\beta^2+1.16\beta\right)\sin(\theta)\left(\frac{\sin(\theta_{max})}{\sin(\theta_{min})}\right)^{0.30}\left(\frac{\beta_{max}}{\beta_{min}}\right)^{0.30} \\
& \left(1.64+0.29\beta^{-0.38}\arctan(8\zeta)\right)+ \\
& \tau^{0.9}\,\gamma^{0.5}\left(-2\,\beta\frac{\partial \beta}{\partial \xi}+1.16\,\frac{\partial \beta}{\partial \xi}\right)\sin(\theta)\left(\frac{\sin(\theta_{max})}{\sin(\theta_{min})}\right)^{0.30}\left(\frac{\beta_{max}}{\beta_{min}}\right)^{0.30} \\
& \left(1.64+0.29\beta^{-0.38}\arctan(8\zeta)\right)+ \\
& \tau^{0.9}\,\gamma^{0.5}\left(0.67-\beta^2+1.16\beta\right)\cos(\theta)\frac{\partial \theta}{\partial \xi}\left(\frac{\sin(\theta_{max})}{\sin(\theta_{min})}\right)^{0.30}\left(\frac{\beta_{max}}{\beta_{min}}\right)^{0.30} \\
& \left(1.64+0.29\beta^{-0.38}\arctan(8\zeta)\right)+ \\
& \tau^{0.9}\,\gamma^{0.5}\left(0.67-\beta^2+1.16\beta\right)\sin(\theta)\,0.3\left(\frac{\sin(\theta_{max})}{\sin(\theta_{min})}\right)^{-0.7} \\
& \left(\frac{\cos(\theta_{max})\frac{\partial \theta_{max}}{\partial \xi}\sin(\theta_{min})-\sin(\theta_{max})\cos(\theta_{min})\frac{\partial \theta_{min}}{\partial \xi}}{(\sin(\theta_{min}))^2}\right)\left(\frac{\beta_{max}}{\beta_{min}}\right)^{0.30} \\
& \left(1.64+0.29\beta^{-0.38}\arctan(8\zeta)\right)+ \\
& \tau^{0.9}\,\gamma^{0.5}\left(0.67-\beta^2+1.16\beta\right)\sin(\theta)\left(\frac{\sin(\theta_{max})}{\sin(\theta_{min})}\right)^{0.30}0.3\left(\frac{\beta_{max}}{\beta_{min}}\right)^{-0.7} \\
& \left(\frac{\frac{\partial \beta_{max}}{\partial \xi}\beta_{min}-\beta_{max}\frac{\partial \beta_{min}}{\partial \xi}}{\beta_{min}^2}\right)\left(1.64+0.29\beta^{-0.38}\arctan(8\zeta)\right)+ \\
& \tau^{0.9}\gamma^{0.5}\left(0.67-\beta^2+1.16\beta\right)\sin(\theta)\left(\frac{\sin(\theta_{max})}{\sin(\theta_{min})}\right)^{0.30}\left(\frac{\beta_{max}}{\beta_{min}}\right)^{0.30} \\
& \left(-0.29\,0.38\,\beta^{-1.38}\frac{\partial \beta}{\partial \xi}\arctan(8\zeta)+0.29\,\beta^{-0.38}\frac{8\frac{\partial \zeta}{\partial \xi}}{1+(8\zeta)^2}\right)
\end{aligned}
\tag{B.104}
$$

$$
\frac{\partial SCF_{K,AS,C}}{\partial \xi} = \frac{\partial SCF_{K,AC,C}}{\partial \xi} \tag{B.105}
$$

$$
\begin{aligned}
\frac{\partial SCF_{K,MIP,C}}{\partial \xi} = & \,1.45\,\frac{\partial \beta}{\partial \xi}\,\tau^{0.85}\,\gamma^{(1-0.68\,\beta)}(\sin(\theta))^{0.7}+ \\
& 1.45\,\beta\,0.85\,\tau^{-0.15}\,\frac{\partial \tau}{\partial \xi}\,\gamma^{(1-0.68\,\beta)}(\sin(\theta))^{0.7}+ \\
& 1.45\,\beta\,\tau^{0.85}\left((1-0.68\beta)\,\gamma^{-0.68\beta}\frac{\partial \gamma}{\partial \xi}+\gamma^{(1-0.68\beta)}\ln(\gamma)(-0.68\frac{\partial \beta}{\partial \xi}\right) \\
& (\sin(\theta))^{0.7}+1.45\,\beta\,\tau^{0.8}\,\gamma^{(1-0.68\beta)}0.7(\sin(\theta))^{-0.3}\,\cos(\theta)\,\frac{\partial \theta}{\partial \xi}
\end{aligned}
\tag{B.106}
$$

$$\begin{aligned}\frac{\partial SCF_{K,MOP,C}}{\partial \xi} = &\left(\left(\frac{\partial \gamma}{\partial \xi}\,\tau_a\beta_a + \gamma\,\frac{\partial \tau_a}{\partial \xi}\,\beta_a + \gamma\,\tau_a\frac{\partial \beta_a}{\partial \xi}\right)\left(1.7 - 1.05\beta_a^3\right)(\sin(\theta_a))^{1.6} + \right.\\ &\gamma\tau_a\beta_a\left(-3.15\beta_a^2\frac{\partial \beta_a}{\partial \xi}\right)(\sin(\theta_a))^{1.6} + \\ &\left.\gamma\tau_a\beta_a\left(1.7 - 1.05\beta_a^3\right)1.6(\sin(\theta_a))^{0.6}\sin(\theta_a)\frac{\partial \theta_a}{\partial \xi}\right) \\ &\left(1 - 0.08\,(\beta_b\,\gamma)^{0.5}\,e^{-0.8x}\right) + \\ &\left(\gamma\,\tau_a\,\beta_a\left(1.7 - 1.05\,\beta_a^3\right)(\sin(\theta_a))^{1.6}\right) \\ &\left(-0.08\,0.5(\beta_b\gamma)^{-0.5}(\frac{\partial \beta_b}{\partial \xi}\gamma + \beta_b\frac{\partial \gamma}{\partial \xi})e^{-0.8x} + 0.08\,0.8(\beta_b\gamma)^{0.5}e^{-0.8x}\frac{\partial x}{\partial \xi}\right) + \\ &\left(\left(\frac{\partial \gamma}{\partial \xi}\,\tau_b\beta_b + \gamma\,\frac{\partial \tau_b}{\partial \xi}\,\beta_b + \gamma\,\tau_b\frac{\partial \beta_b}{\partial \xi}\right)\left(1.7 - 1.05\beta_b^3\right)(\sin(\theta_b))^{1.6} + \right.\\ &\gamma\tau_b\beta_b\left(-3.15\beta_b^2\frac{\partial \beta_b}{\partial \xi}\right)(\sin(\theta_b))^{1.6} + \\ &\left.\gamma\tau_b\beta_b\left(1.7 - 1.05\beta_b^3\right)1.6(\sin(\theta_b))^{0.6}\sin(\theta_b)\frac{\partial \theta_b}{\partial \xi}\right) \\ &\left(1 - 0.08\,(\beta_a\,\gamma)^{0.5}\,e^{-0.8x}\right)\left(2.05\beta_{max}^{0.5}\,e^{-1.3x}\right) + \\ &\left(\gamma\,\tau_b\,\beta_b\left(1.7 - 1.05\,\beta_b^3\right)(\sin(\theta_b))^{1.6}\right) \\ &\left(-0.08\,0.5(\beta_a\gamma)^{-0.5}(\frac{\partial \beta_a}{\partial \xi} + \beta_a\frac{\partial \gamma}{\partial \xi})e^{-0.8x} + 0.08\,0.8(\beta_a\gamma)^{0.5}e^{-0.8x}\frac{\partial x}{\partial \xi}\right) \\ &\left(2.05\beta_{max}^{0.5}e^{-1.3x}\right) + \\ &\left(\gamma\,\tau_b\,\beta_b\left(1.7 - 1.05\,\beta_b^3\right)(\sin(\theta_b))^{1.6}\right) \\ &\left(1 - 0.08\,(\beta_a\,\gamma)^{0.5}\,e^{-0.8x}\right) \\ &\left(2.05\,0.5\beta_{max}^{-0.5}\frac{\partial \beta_{max}}{\partial \xi}e^{-1.3x} + 2.05\beta_{max}^{0.5}(-1.3\frac{\partial x}{\partial \xi})e^{-1.3x}\right)\end{aligned} \tag{B.107}$$

$$\begin{aligned}\frac{\partial SCF_{K,AC,B}}{\partial \xi} = &\frac{\partial SCF_{K,1}}{\partial \xi}\left(1.97 - 1.57\beta^{0.25}\right)\tau^{-0.14}(\sin(\theta))^{0.7} + \\ &SCF_{K,1}\left[-1.57\,0.25\,\beta^{-0.75}\frac{\partial \beta}{\partial \xi}\tau^{-0.14}(\sin(\theta))^{0.7} + \right.\\ &(1.97 - 1.57\beta^{0.5})(-0.14)\tau^{-1.14}\frac{\partial \tau}{\partial \xi}(\sin(\theta))^{0.7} + \\ &\left.(1.97 - 1.57\beta^{0.25})\tau^{-0.14}0.7(\sin(\theta))^{-0.3}\cos(\theta)\frac{\partial \theta}{\partial \xi}\right] + \\ &1.8(\sin(\theta))^{0.8}(\theta_{max} + \theta_{min})\cos(\theta_{max} + \theta_{min}) \\ &\left(\frac{\partial \theta_{max}}{\partial \xi} + \frac{\partial \theta_{min}}{\partial \xi}\right)(0.131 - 0.084\arctan(14\zeta + 4.2\beta))\,C\beta^{1.5}\gamma^{0.5}\tau^{-1.22} + \\ &(\sin(\theta))^{1.8}(\theta_{max} + \theta_{min})\left(\frac{-0.084}{1+(14\zeta+4.2\beta)^2}\left(14\frac{\partial \zeta}{\partial \xi} + 4.2\frac{\partial \beta}{\partial \xi}\right)\right) \\ &C\beta^{1.5}\gamma^{0.5}\tau^{-1.22} + C\left(1.5\beta^{0.5}\frac{\partial \beta}{\partial \xi}\gamma 0.5\tau^{-1.22} + \beta^{1.5}0.5\gamma^{-0.5}\frac{\partial \gamma}{\partial \xi}\tau^{-1.22}\right. \\ &\left.+\beta^{1.5}\gamma^{0.5}(-1.22)\tau^{-2.22}\frac{\partial \tau}{\partial \xi}\right) \\ &(\sin(\theta))^{1.8}(\theta_{max} + \theta_{min})\,(0.131 - 0.084\arctan(14\zeta + 4.2\beta))\end{aligned} \tag{B.108}$$

$$\frac{\partial SCF_{K,AS,B}}{\partial \xi} = \frac{\partial SCF_{K,AC,B}}{\partial \xi} \tag{B.109}$$

$$\begin{aligned}\frac{\partial SCF_{K,MIP,B}}{\partial \xi} = & 0.65 \frac{\partial \beta}{\partial \xi} \tau^{0.4} \gamma^{(1.09-0.77\beta)} (\sin(\theta))^{(0.06\gamma-1.16)} + \\ & 0.65\ \beta\ 0.4\ \tau^{-0.6} \frac{\partial \tau}{\partial \xi} \gamma^{(1.09-0.77\beta)} (\sin(\theta))^{(0.06\gamma-1.16)} + \\ & 0.65\ \beta\ \tau^{0.4} \Big( (1.09 - 0.77\beta) \gamma^{(0.09-0.77\beta)} \frac{\partial \gamma}{\partial \xi} + \gamma^{(1.09-0.77\beta)} \\ & \ln(\gamma)(-0.77 \frac{\partial \beta}{\partial \xi}) \Big) (\sin(\theta))^{(0.06\gamma-1.16)} + 0.65\ \beta\ \tau^{0.4}\ \gamma^{(1.09-0.77\beta)} \\ & \Big( (0.06\gamma - 1.16)(\sin(\theta))^{(0.06\alpha-2.16)} \cos(\theta) \frac{\partial \theta}{\partial \xi} + (\sin(\theta))^{(0.06\gamma-1.16)} \\ & \ln(\sin(\theta))\ 0.06\ \frac{\partial \gamma}{\partial \xi} \Big)\end{aligned} \tag{B.110}$$

$$\begin{aligned}\frac{\partial SCF_{K,MOP,B}}{\partial \xi} = & \frac{\partial SCF_{K,MOP,C}}{\partial \xi} \left( \tau^{-0.54} \gamma^{-0.05} \left( 0.99 - 0.47\beta + 0.08\beta^4 \right) \right) + \\ & SCF_{K,4} \Big[ -0.54 \tau^{-1.54} \frac{\partial \tau}{\partial \xi} \gamma^{-0.05} \left( 0.99 - 0.47\beta + 0.08\beta^4 \right) + \\ & \tau^{-0.54} (-0.05) \gamma^{-1.05} \frac{\partial \gamma}{\partial \xi} \left( 0.99 - 0.47\beta + 0.08\beta^4 \right) + \\ & \tau^{-0.54} \gamma^{-0.05} \left( -0.47 \frac{\partial \beta}{\partial \xi} + 0.32\beta^3 \frac{\partial \beta}{\partial \xi} \right) \Big]\end{aligned} \tag{B.111}$$

Appendix C

# Extended summary in Spanish

*"Yo soy yo y mi circunstancia, y si no la salvo a ella no me salvo yo"*
**Ortega y Gasset**, Meditaciones del Quijote.

## Introducción

Indudablemente, la energía eólica se ha convertido en una de las grandes apuestas destinadas a liderar un cambio en nuestro formato energético. No obstante, esta tesis no está centrada en las típicas turbinas eólicas. Actualmente existe una tendencia masiva de instalación de parques eólicos en instalaciones marinas u *offshore*. Estas nuevas localizaciones suponen evidentemente un alto incremento en el coste tanto de instalación como de transporte, pero están justificadas por una simple razón: el viento es más fuerte y constante en el mar. Por tanto, el beneficio en este viaje es un mejor y más eficiente aprovechamiento energético del viento.

Pero la implantación de turbinas en el medio del mar necesita del desarrollo de un método de sustentación. Mientras que el conjunto torre-góndola-palas mantiene la misma estructura y tipología que sus parientes en tierra firme, se necesitan estructuras especiales que sostengan el peso del conjunto y soporten los esfuerzos a los que se ven sometidos.

Hay distintos tipos de subestructuras para soportar las turbinas eólicas *offshore*, siendo cada uno de ellos particularmente aplicable a un rango de profundidades del mar relativamente establecido. Así como los límites de profundidad entre tipologías no están rotundamente determinados, sí que existe una gran diferencia entre dos conceptos completamente opuestos: estructuras fijas y estructuras flotantes. Los conceptos de estructuras de soporte flotantes aún están en fase de desarrollo mientras que las estructuras fijas están sólidamente avaladas por la experiencia ingenieril. El concepto es sencillo, construir una estructura que conecte físicamente la base de la torre con el fondo marino.

Existen también distintas tipologías de subestructuras fijas, siendo los mono-pilotes las más extendidas y numerosas en los parques eólicos ya instalados. No obstante, los mono-pilotes están ciertamente limitados a profundidades bajas 25 - 30 m y en cuanto a la potencia de las turbinas que pueden soportar. El desafío actual se encuentra en las profundidades intermedias 30 - 60 metros donde los *jackets* son sin duda la mejor solución. Los *jackets* son estructuras metálicas reticuladas formadas por secciones tubulares en torno a los 0.5 - 2.0 metros de diámetro, formando conjuntos de 500 a 600 toneladas. La mayoría de los proyectos en desarrollo o en previsión de parques eólicos *offshore* actuales se basan en esta tecnología.

Aun así, existen muchos aspectos tecnológicos y de diseño de los *jackets* sujetos a incertidumbre o todavía por resolver. Algo tan simple como el análisis estructural o la definición de los condicionantes que han de imponerse a la estructura es un proceso lejos de ser sencillo. Además, algunos de los fenómenos altamente relevantes para la vida estructural de los *jackets* como por ejemplo la fatiga, aún son difíciles de estimar o predecir con precisión. Además, la correcta modelización de las condiciones ambientales en el mar y las cargas derivadas de éstas implica el tener en cuenta un elevado número de casos de carga y el gestionar una cantidad inmensa de información y resultados del análisis estructural. En cuanto al diseño de los *jackets* es esencial que estén adecuadamente aprovechados estructuralmente pues el coste material individual de cada uno de ellos representa un alto porcentaje del coste total de inversión de una turbina eólica *offshore*.

Por tanto, es necesaria una metodología de análisis y diseño que permita; no solo establecer si un determinado *jacket* cumple las necesidades estructurales para resistir los esfuerzos a los que está sometido, sino también obtener el diseño más eficiente posible, o en otras palabas, el óptimo.

Y ese es el objetivo de esta tesis. Desarrollar una metodología de análisis dinámico que permita el cálculo estructural de turbinas eólicas *offshore* soportadas por *jackets* y plantear y resolver el problema de optimización estructural mediante técnicas matemáticas y numéricas. Los objetivos específicos de la tesis son:

- Establecer las características del problema dinámico de una turbina eólica *offshore* acoplada y resolver el problema estructural.
- Definir un método de estimación de la fatiga a lo largo de la vida útil sin necesidad de simulaciones numéricas excesivamente largas.
- Definición del problema de optimización acorde a los requisitos estructurales impuestos por la normativa de aplicación.
- Lograr que el problema de optimización planteado tenga una dimensión manejable.
- Resolver el problema de optimización de *jackets* para molinos eólicos *offshore*.

## Modelo estructural

El modelo estructural es un modelo completamente acoplado con todos los elementos que forman la turbina *offshore*: *jacket*, pieza de transición, torre del aerogenerador, góndola y palas. El propósito es modelar el comportamiento dinámico conjunto de toda la estructura y la interacción entre los distintos elementos.

Dada la tipología estructural de los *jackets* y del conjunto, el modelo matemático se basa en elementos finitos tipo barra con nudos rígidos. Para la resolución del problema dinámico se deducen las expresiones de las matrices de masa, amortiguamiento y rigidez. Se utiliza un modelo de masas consistente y un amortiguamiento de tipo Rayleigh.

En cuanto a las solicitaciones de la estructura, se tienen en cuenta las cargas actuantes que condicionan en mayor medida su diseño final. Tanto el peso propio de toda la estructura como el peso del recubrimiento marino sobre los tubulares y el agua en las pilas inundadas se tienen en cuenta. Se considera también por supuesto el efecto de la flotabilidad en los elementos del *jacket* por debajo de la superficie del mar.

Las cargas ambientales más relevantes y que se consideran en el modelo son el viento y el oleaje. El viento se supone actuando sobre la parte aérea de la estructura. Se modela como una fuerza de *drag* sobre la torre del generador teniendo en cuenta el efecto pantalla de las palas al pasar por delante de ésta. Las fuerzas del viento sobre las palas se obtienen mediante el método BEM (Blade Element Momentum) a partir de las características aerodinámicas de secciones discretas de las palas y dada una velocidad de rotación constante prefijada.

Por otro lado, el oleaje se considera actuando en la parte marina de la estructura, o la parte sumergida del *jacket*. Se modela según dos teorías de ola, lineal de Airy y Stokes de segundo orden y las fuerzas sobre los elementos barra se calcula mediante la fórmula de Morison. La implementación permite la consideración de oleaje direccional además de la inclusión de una velocidad de corriente.

Resulta obvio que los aerogeneradores están diseñados para moverse, o más concretamente rotar. Por lo tanto, es completamente necesario que esta rotación sea introducida en el modelo numérico con el fin de obtener una respuesta dinámica de la estructura que prevea todas las fuentes de excitación dinámicas presentes durante el funcionamiento de la turbina. En este sentido, se impone una rotación de las palas en el modelo a una velocidad constante con lo que la geometría de la estructura es variable en el tiempo. Aunque esta variación geométrica no representa una no-linealidad estructural propiamente dicha, las propiedades de la estructura son diferentes para instantes de tiempo diferentes debido a estos movimientos, y la integración numérica de las ecuaciones dinámicas ha de llevarse a cabo mediante un algoritmo no lineal. En este caso se ha usado un esquema de integración no-lineal de Newmark obteniendo resultados de movimientos y esfuerzos en la estructura en concordancia con las referencias.

Por último, el fenómeno de la fatiga se aborda desde el método de las curvas S-N que definen el número de ciclos que un elemento metálico es capaz de soportar a fatiga

con una determinada amplitud de tensiones. Con esta base según el número de ciclos a los que está sometida la estructura se puede determinar el daño a fatiga acumulado mediante la regla de Miner, considerando acumulación lineal del daño. Para ello es necesario contar estos ciclos de esfuerzos a partir del historial de tensiones en la estructura mediante algoritmos de conteo. En este caso se ha elegido el algoritmo Rainflow ya que es el más extendido y uno de los pocos que fue específicamente desarrollado para la evaluación de la fatiga en metales. Todos estos cálculos se realizan en puntos concretos de la estructura, particularmente en las uniones entre los distintos perfiles, dónde se seleccionan 8 puntos circunferencialmente equiespaciados llamados *hot-spots*. En estos puntos se considera además una concentración de tensiones mediante Factores de Concentración de Tensiones (SCF).

Sin embargo, esto no es suficiente para la evaluación del daño en la estructura y su comprobación, pues ha de comprobarse que el daño no supera los límites establecidos, pero durante toda la vida útil de la estructura, por ejemplo 20 años. Como es obvio, no es razonable realizar simulaciones numéricas con 20 años de duración por lo que es necesario establecer un método de evaluación del daño a períodos largos de tiempo a partir de simulaciones más cortas. En este caso se ha optado por extrapolar el daño a cualquier edad de la estructura linealmente a partir del daño obtenido a 300 y 600 segundos. Los resultados obtenidos se han comparado con simulaciones largas completas con buena correlación.

## Planteamiento del problema de optimización

El planteamiento de cualquier problema de optimización matemática se basa en la definición de tres aspectos determinantes: la o las funciones objetivo, las restricciones, y la determinación de los parámetros modificables o variables de diseño.

En esta tesis se plantea la optimización del coste de los *jackets* a través de la minimización de la cantidad de material o lo que es lo mismo, la optimización del peso de la estructura. Por tanto, la función objetivo es sencillamente una suma del peso de cada una de las barras que componen el *jacket*.

Las restricciones impuestas responden a tres tipos de limitaciones bien diferenciadas. Por un lado, se imponen restricciones a los estados tensionales de los distintos elementos que componen la estructura, llamadas restricciones de Estado Límite Último (ULS). Se imponen además restricciones de Estado Límite de Fatiga (FLS) para limitar el daño a fatiga durante la vida útil de la estructura en todos los *hot-spots*. Y por último, restricciones sobre las frecuencias naturales de vibración para que éstas se mantengan entre la frecuencia de vibración del rotor del aerogenerador (1P) y la frecuencia con la que una pala pasa por delante de la torre (3P).

No obstante, es de resaltar una particularidad de las restricciones ULS, y es que, dado que el problema analizado tiene una componente dinámica inherente, los resultados de tensiones y esfuerzos se obtienen para todos los instantes de tiempo analizados. Por tanto, cada una de las expresiones de Estado Límite Último se desdobla en un gran

número de restricciones que limitan el estado tensional de la estructura a lo largo de toda la simulación temporal. Esto da como resultado una cantidad ingente de información en muchos casos innecesaria y redundante para el problema de optimización. El tratamiento de restricciones que dependen del tiempo es uno de los tópicos más importantes en la optimización de la respuesta dinámica de estructuras y, aunque existen diversas formulaciones para manejar las restricciones del tiempo, no existe todavía un acuerdo en cuál de ellas es la más eficaz a la vez que representa en mejor medida la situación real de las restricciones y/o el estado tensional de la estructura.

En esta tesis se propone el uso de funciones de agregación de restricciones o una función global, habituales en otros campos de optimización como la optimización topológica de estructuras, pero nunca hasta ahora utilizadas para agregar restricciones temporales en un problema dinámico. Concretamente las restricciones dependientes del tiempo se agregan mediante la función Kreisselmeier-Steinhauser. La ventaja principal es que se reduce considerablemente el número de restricciones efectivas a la hora de plantear el diseño óptimo, pero manteniendo información sobre la activación de las distintas restricciones a lo largo de la simulación temporal.

Por último, se plantea una optimización de formas y dimensiones para lo cual se eligen como variables de diseño por un lado, el diámetro y el espesor de las secciones tubulares de las barras, y por otro lado la dimensión de las bases superior e inferior del *jacket*. De esta forma se consigue controlar tanto la sección transversal de las barras como la forma global del *jacket* sin modificar la conectividad y manteniendo la configuración de los nodos de la estructura.

## Metodología de optimización y análisis de sensibilidad

Normalmente la propia definición del problema de optimización influencia en gran medida la elección del algoritmo matemático de optimización a utilizar. Según se ha definido, nos encontramos ante un problema de optimización: mono-objetivo, pues solo tenemos una función objetivo; restringido, pues está sujeto a restricciones; determinista, pues no está sujeto a incertidumbre; y continuo, pues las variables de diseño se consideran continuas en su dominio.

Como no hay solución analítica directa para el problema propuesto, las opciones más viables para su resolución serían la transformación en un problema incondicionado o no restringido, o la reducción del problema a una sucesión de problemas más sencillos. En esta tesis se ha optado por un método de reducción, en concreto se ha resuelto la optimización mediante Programación Lineal Secuencial (SLP) dada su eficacia y robustez. Es decir, aunque el problema es no lineal tanto en su función objetivo como en sus restricciones, éste se aproxima a una secuencia de problemas lineales utilizando el análisis de sensibilidad de primer orden. Cada uno de los sub-problemas linealizados se resuelve entonces mediante Programación Lineal, en este caso cada una de las iteraciones se resuelve utilizando el algoritmo Simplex. Sin embargo, es evidente que al linealizar el problema se está resolviendo un problema ligeramente distinto al original

y con un dominio factible diferente. Para aliviar las posibles diferencias entre la región original y la linealizada se limita el tamaño del paso máximo que se puede dar en cada iteración mediante lo que se llaman límites móviles. Estos límites móviles se fijan en cada iteración y para cada una de las variables de diseño en particular en función de su valor específico.

Como se ha dicho, para la linealización de la función objetivo y de las restricciones se necesita un análisis de sensibilidad de primer orden. En este caso dado que el número de variables de diseño es considerablemente inferior al número de restricciones o variables de control se ha implementado un método de Diferenciación Directa para el cálculo de las derivadas frente al método del Estado Adjunto, claramente en desventaja para el problema planteado. Las derivadas particulares de cada una de las funciones se han calculado analíticamente a excepción de la restricción de fatiga. Debido al conteo de los ciclos de tensiones a los que está sometido cada uno de los *hot-spot* mediante el algoritmo Rainflow, la restricción de fatiga no tiene derivada analítica. Por tanto, para calcular su sensibilidad respecto a las variables de diseño ha sido necesario introducir una formulación semi-analítica con diferencias finitas utilizando la derivada analítica de los esfuerzos y de los Factores de Concentración de Tensiones.

El análisis de sensibilidad representa una de las partes más costosas computacionalmente de la metodología de optimización propuesta e implementada. De hecho, la cantidad de almacenamiento en memoria necesario para las derivadas de las distintas restricciones y de las tensiones en los *hot-spot* para la fatiga es uno de los mayores factores limitantes del código desarrollado.

## Resultados, conclusiones y futuras líneas de trabajo

La metodología de optimización desarrollada se ha aplicado a ejemplos reales de turbinas *offshore* sobre *jackets* de forma satisfactoria obteniendo reducciones importantes del peso en todos los casos.

Primeramente, se ha demostrado absolutamente necesario el considerar la rotación de las palas para captar de manera precisa todos los ciclos de tensiones a los que está sometida la estructura y evaluar correctamente el daño a fatiga que sufren los elementos metálicos del *jacket*. La estimación del daño a fatiga mediante extrapolación lineal ha permitido reducir enormemente el coste computacional del análisis a fatiga da le estructura, manteniendo la precisión de los cálculos.

Por otro lado, el algoritmo se ha mostrado robusto y eficaz ante el problema de optimización propuesto logrando reducciones sustanciales del peso en cualquiera de las estructuras propuestas, apreciando una considerable reducción de las secciones de las barras y en algunos de los casos un aumento en el ancho de las bases del *jacket*. Las funciones de agregación de restricciones para las restricciones dependientes del tiempo han demostrado su eficiencia frente a problemas con varios casos de carga y un gran coste computacional. El uso de Diferenciación Directa frente al Estado Adjunto ha sido claramente ventajoso en este caso debido al reducido número de variables de

diseño en comparación con el número de restricciones. La elección de las variables de diseño ha permitido optimizar las dimensiones y la forma de los *jackets* manteniendo su configuración, conectividad y sencillez. Por último, mencionar que también se ha planteado la optimización de los *jackets* trasladando las transiciones entre distintas secciones transversales de las barras de las uniones hacia las partes intermedias de las patas. De esta forma se evita la creación de nudos excesivamente complicados, así como la introducción de concentraciones de tensiones adicionales.

El modelo desarrollado en esta tesis abre las puertas a futuras líneas de trabajo de cara a una mejora tanto del modelo estructural como de la metodología de optimización. Las líneas futuras de investigación más prometedoras y relevantes que se señalan son: La consideración de la interacción suelo-estructura para un cálculo más real de las condiciones dinámicas de la estructura; el abordar el cálculo desde una perspectiva completamente no lineal teniendo en cuenta sobre todo la no-linealidad de las deformaciones de las palas y su impacto sobre las cargas de viento que efectivamente se desarrollan; la introducción de nuevas variables de diseño que permitan conseguir aún mayores reducciones del peso de los *jackets*; la implementación de un análisis de sensibilidad de segundo orden para lograr un algoritmo aún más eficiente. Por último, sería altamente ventajosa la aplicación de técnicas de cálculo en paralelo al código desarrollado en esta tesis; no solo para mejorar los rendimientos computacionales del algoritmo de análisis y optimización, sino también para lograr la modelización completa de todos los casos de carga de viento y oleaje en cualquier dirección que se producen en una instalación offshore real

Appendix D

# Extended summary in Galician

## Introdución

Indubidabelmente, a enerxía eólica converteuse nunha das grandes apostas destinadas a lidera-lo cambio no noso formato enerxético. Non obstante, esta tese non está centrada nas típicas turbinas eólicas. Actualmente, existe unha tendencia masiva de construción de parques eólicos en instalación mariñas ou offshore. Estas novas localizacións supoñen evidentemente un alto incremento no custo, tanto de instalación como de transporte, pero están xustificadas por unha simple razón: o vento é máis forte e constante no mar. Polo tanto, o beneficio neste viaxe é un mellor e máis eficiente aproveitamento enerxético do vento.

Mais a implantación de turbinas no medio do mar precisa do desenrolo dun método de sustentación. Mentres que o conxunto torre-góndola-palas mantén a mesma estrutura e tipoloxía que os seus parentes de terra firme, necesítanse estruturas especiais que sosteñan o peso do conxunto e soporten os esforzos aos que se ven sometidos.

Hai distintos tipos de subestruturas para soporta-las turbinas eólicas offshore, sendo cada un deles particularmente aplicable a un rango de profundidades do mar relativamente establecidos. Así coma os límites de profundidade entre tipoloxías non están rotundamente determinados, si que existe unha gran diferenza entre dous conceptos completamente opostos: estruturas fixas e estruturas flotantes. Os conceptos de estruturas de soporte flotantes aínda están en fase de desenrolo mentres que as estruturas fixas están solidamente avaladas pola experiencia. O concepto é sinxelo, construír unha estrutura que conecte fisicamente a base da torre con fondo mariño.

Existen á vez distintas tipoloxías de subestruturas fixas, sendo os mono-pilotes as máis estendidas e numerosas nos parques eólicos xa instalados. Non obstante, os mono-pilotes están certamente limitados a profundidades baixas 25 - 30 metros e en canto á potencia das turbinas que son capaces de soportar. O desafío actual encóntrase nas profundidades intermedias 30 – 60 metros onde os *jackets* son sen dúbida algunha a

mellor solución. Os *jackets* son estruturas metálicas reticuladas formadas por seccións tubulares en torno aos 0.5 – 2.0 metros de diámetro, formando conxuntos de 500 a 600 toneladas. A maioría dos proxectos en desenrolo ou en previsión de parques eólicos *offshore* actuais baséanse nesta tecnoloxía.

Pero existen moitos aspectos tecnolóxicos e do deseño dos *jackets* suxeitos a incerteza ou aínda por resolver. Algo tan simple como a análise estrutural ou a definición dos condicionantes que se teñen que impor á estrutura é un proceso lonxe de ser sinxelo. Ademais, algúns dos fenómenos altamente relevantes para a vida estrutural dos *jackets* como por exemplo a fatiga, aínda son difíciles de estimar ou predicir con precisión. O correcto modelado das condicións ambientais no mar e das cargas derivadas destas implica ter en conta un elevado número de casos de carga e xestionar unha cantidade inmensa de información e resultados da análise estrutural. En canto ao deseño dos *jackets*, é esencial que estean adecuadamente aproveitados estruturalmente pois o coste material individual de cada un deles representa unha alta porcentaxe do custo total de inversión dunha turbina eólica *offshore*.

Polo tanto, é necesaria unha metodoloxía de análise e deseño que permita; non só establecer se un determinado *jacket* cumpre as necesidades estruturais para resistilos esforzos aos que está sometido, senón tamén acadar o deseño máis eficiente posible, ou noutras palabras, o óptimo. Ése é o obxectivo desta tese. O desenvolvemento dunha metodoloxía de análise dinámico que permita e cálculo estrutural de turbinas eólicas *offshore* soportadas por *jackets* e propoñer e resolve-lo problema de optimización estrutural mediante técnicas matemáticas e numéricas. Os obxectivos específicos desta tese son:

- Establece-las características do problema dinámico dunha turbina eólica *offshore* acoplada e resolve-lo problema estrutural.
- Definir un modelo de estimación da fatiga ao longo da vida útil sen necesidade de simulacións numéricas excesivamente longas.
- Definición do problema de optimización acorde aos requisitos estruturais impostos pola normativa de aplicación.
- Lograr que o problema de optimización exposto teña una dimensión manexable.
- Resolve-lo problema de optimización de *jackets* para moliños eólicos *offshore*.

## Modelo estrutural

O modelo estrutural é un modelo completamente acoplado con tódolos elementos que forman a turbina *offshore*: *jacket*, peza de transición, torre do aeroxerador, góndola e palas. O propósito é modela-lo comportamento dinámico conxunto do toda a estrutura e a interacción entre os distintos elementos.

Dada a tipoloxía estrutural dos *jackets* e do conxunto, o modelo matemático baséase en elementos finitos tipo barra con nodos ríxidos. Para a resolución do problema dinámico dedúcense as expresións das matrices de masa, amortecemento e rixidez. Onde se utiliza un modelo de masas consistente e un amortecemento de tipo Rayleigh.

En canto ás solicitacións da estrutura, téñense en conta as cargas actuantes que condicionan en maior medida o seu deseño final. Tanto o peso propio de toda a estrutura como o peso do crecemento mariño sobre os tubulares e a auga nas pilas inundadas téñense en conta. Considérase tamén por suposto o efecto da flotación nos elementos do *jacket* por debaixo da superficie do mar.

As cargas ambientais máis relevantes e que se consideran no modelo son o vento e mailas ondas do mar. O vento suponse actuando sobre a parte aérea da estrutura. Modélase coma una forza de *drag* sobre a torre do aeroxerador tendo en conta o efecto pantalla das palas ao pasar por diante desta. As forzas do vento sobre as palas obtense mediante o método BEM (Blade Element Momentum) a partir das características aerodinámicas de seccións discretas das palas e dada unha velocidade de rotación constante prefixada.

Por outra parte, as ondas considéranse actuando na parte mariña da estrutura, ou na parte somerxida do *jacket*. Modélanse segundo dúas teorías de onda, lineal de Airy e Stokes de segundo orde e as forzas sobre os elementos barra calcúlanse mediante a fórmula de Morison. Permítese ademais a consideración de ondas cunha dirección establecida e a inclusión dunha velocidade de corrente.

Resulta obvio que os aeroxeradores están deseñados para moverse, ou máis concretamente rotar. Polo tanto, e completamente necesario que esta rotación sexa introducida no modelo numérico con fin de obter unha resposta dinámica da estrutura que prevexa tódalas fontes de excitación dinámicas presentes durante o funcionamento da turbina. Neste sentido, imponse unha rotación das palas no modelo a unha velocidade constante co que a xeometría da estrutura é variable no tempo. Aínda que esta variación xeométrica non representa una non-linearidade estrutural, as propiedades da estrutura son diferentes para instantes de tempo distintos debido a estes movementos, e a integración numérica das ecuacións dinámicas tense que facer mediante un algoritmo non-lineal. Neste caso úsase un esquema de integración non-lineal de Newmark obtendo resultados de movementos e esforzos da estrutura en concordancia coas referencias.

Por último, o fenómeno da fatiga abórdase dende o método das curvas S-N que definen o número de ciclos que un elemento metálico é capaz de soportar a fatiga cunha determinada amplitude de tensións. Con esta base, segundo o número de ciclos aos que está sometida a estrutura pódese determina-lo dano a fatiga acumulado mediante a regra de Miner, considerando acumulación lineal do dano. Para isto é necesario conta-los ciclos de esforzos a partir do historial de tensións da estrutura mediante algoritmos para contar. Neste caso elixiuse o algoritmo Rainflow xa que é o mais estendido e un dos poucos que foi especificamente creado para a cuantificación da fatiga en metais. Todos estes cálculos realízanse en puntos concretos da estrutura, particularmente nas unións entre os distintos perfiles, onde se seleccionan 8 puntos circunferencialmente equidis-

tantes chamados *hot-spots*. Nestes puntos considérase ademais unha concentración de tensións mediante Factores de Concentración de Tensións (SCF).

Sen embargo, isto non é suficiente para a cuantificación do dano na estrutura e a súa comprobación, pois o dano ten que comprobarse que non supera os límites establecidos, pero durante toda a vida útil da estrutura, por exemplo 20 anos. Como é obvio, non é razoable realizar simulacións numéricas con 20 anos de duración polo que é necesario establecer un método de cuantificación do dano a períodos longos de tempo a partir de simulacións máis curtas. Neste caso optouse por extrapola-lo dano a calquera idade da estrutura linealmente a partir do dano obtido a 300 e 600 segundos. Os resultados obtidos comprobáronse con simulacións longas completas con boa correlación.

## Formulación do problema de optimización

A formulación de calquera problema de optimización matemática baséase na definición de tres aspectos fundamentais: a ou as funcións obxectivo, as restricións, e a determinación dos parámetros modificables ou variables de deseño.

Nesta tese preséntase a optimización do custo dos *jackets* a través da minimización da cantidade de material ou o que é o mesmo, a optimización do peso da estrutura. Polo tanto, a función obxectivo é simplemente unha suma do peso de cada unha das barras que compoñen o *jacket*.

As restricións impostas responden a tres tipos de limitacións ben diferenciadas. Por un lado, impóñense restricións aos estados tensionais dos distintos elementos que compoñen a estrutura, chamadas restricións de Estado Límite Último (ULS). Impóñense ademais restricións de Estado Límite de Fatiga (FLS) para limitalo dano a fatiga durante a vida útil da estrutura en tódolos *hot-spots*. E por último, restricións sobre as frecuencias naturais de vibración para que estas manténñanse entre a frecuencia de vibración do rotor do aeroxerador (1P) e a frecuencia coa que unha pala pasa por diante da torre (3P).

Non obstante, é de resaltar unha particularidade das restricións ULS, e é que, dado que o problema analizado ten unha compoñente dinámica inherente, os resultados das tensións e esforzos obtéñense para tódolos instantes de tempo analizados. Por tanto, cada unha das expresións de Estado Límite Último desdóbrase nun gran número de restricións que limitan o estado tensional da estrutura ao longo de toda a simulación temporal. Isto dá como resultado unha cantidade inxente de información en moitos casos innecesaria e redundante para o problema de optimización. O tratamento de restricións que dependen do tempo é un dos tópicos máis importantes na optimización da resposta dinámica de estruturas e, aínda que existen diversas formulacións para o manexo das restricións dependentes do tempo, non existe acordo en cal delas é a máis eficaz e a que representa en maior medida a situación real das restricións e/ou o estado tensional da estrutura.

Nesta tese proponse o uso de funcións de agregación de restricións ou unha función global, habituais noutros campos de optimización como a optimización topolóxica de

estruturas, pero nunca ata o de agora utilizada para a agregación de restricións dependentes do tempo nun problema dinámico. Concretamente as restricións agréganse mediante a función Kreisselmeier-Steinhauser. A vantaxe principal é que se reduce considerablemente o número de restricións efectivas á hora de formulalo deseño óptimo, pero mantendo información sobre a activación das distintas restricións ao longo da simulación temporal.

Por último, formúlase un problema de optimización de formas e dimensións para o cal se elixen como variables de deseño, por un lado o diámetro e espesor das seccións tubulares das barras, e por outro lado a dimensión das bases superior e inferior do *jacket*. Desta forma conséguese controlar tanto a sección transversal das barras como a forma global do *jacket* se modificar a conectividade e mantendo a configuración dos nodos da estrutura.

## Metodoloxía de optimización e análise de sensibilidade

Normalmente a propia definición do problema de optimización influencia en gran medida a elección do algoritmo matemático de optimización a empregar. Segundo se definiu, atopámonos ante un problema de optimización: mono-obxectivo, pois so temos unha función obxectivo; restrinxido, pois está suxeito a restricións; determinista, pois non está suxeito a incerteza; e continuo, pois as variables de deseño considéranse continuas no seu dominio.

Coma non hai solución analítica directa para o problema proposto, as opcións máis viables para a súa resolución serían a transformación nun problema non condicionado ou non restrinxido, ou a redución do problema a unha sucesión de problemas máis sinxelos. Nesta tese óptase por un método de redución, en concreto a optimización resólvese mediante Programación Lineal Secuencial (SLP) dada a súa eficacia e robustez. É dicir, aínda que o problema non é lineal tanto na súa función obxectivo como nas restricións, este aproxímase a una secuencia de problemas lineais empregando a análise de sensibilidade de primeiro orde. Cada un dos sub-problemas linealizados resólvese entón mediante Programación Lineal, neste caso cada unha das iteracións soluciónase empregando o algoritmo Simplex. Sen embargo, é evidente que ao linealizar o problema estase a resolver un problema lixeiramente distinto ao orixinal e cun dominio factible diferente. Para aliviar as posibles diferencias entre a rexión orixinal e a linealizada limítase o tamaño de paso máximo que se pode dar en cada iteración mediante o que se chaman límites móbiles. Estes límites móbiles fíxanse en cada iteración e para cada unha das variables de deseño en particular en función do se valor específico.

Como xa se dixo, para a linealización da función obxectivo e das restricións necesítase a análise de sensibilidade de primeiro orde. Neste caso dado que o número de variables de deseño é considerablemente inferior ao número de restricións ou variables de control óptase por utilizar Diferenciación Directa para o cálculo das derivadas fronte ao método do Estado Adxunto, claramente en desvantaxe para o problema formulado. As derivadas particulares de cada unha das funcións calcúlanse analiticamente a excep-

ción da restrición de fatiga. Debido a que os ciclos de tensións aos que está sometido cada un dos *hot-spot* cóntanse mediante o algoritmo Rainflow, a restrición a fatiga non ten derivada analítica. Por tanto, para calcular a súa sensibilidade respecto ás variables de deseño foi necesario introducir unha formulación semi-analítica con diferencias finitas empregando as derivadas analíticas dos esforzos e dos Factores de Concentración de Tensións.

A análise de sensibilidade representa unha das partes máis custosas computacionalmente da metodoloxía de optimización proposta. De feito, a cantidade de almacenamento en memoria necesaria para as derivadas das distintas restricións e das tensións nos *hot-spots* para á fatiga é uns dos maiores factores limitadores do código programado.

## Resultados, conclusións e futuras liñas de traballo

A metodoloxía de optimización proposta aplícase a exemplos reais de turbinas *offshore* sobre *jackets* de forma satisfactoria obtendo reducións importantes do peso en tódolos casos.

Primeiramente, amósase absolutamente necesaria a consideración da rotación das palas para captar de maneira precisa tódolos ciclos de tensións aos que está sometida a estrutura e así cuantificar correctamente o dano a fatiga que sofren os elementos metálicos do *jacket*. A estimación do dano a fatiga mediante a extrapolación lineal permitiu reducilo custo computacional da análise a fatiga da estrutura, mantendo a precisión dos cálculos.

Por outra banda, o algoritmo amosouse robusto e eficaz ante o problema de optimización proposto acadando reducións substanciais do peso en calquera das estruturas propostas, apreciando unha considerable redución das seccións das barras e nalgúns dos casos un aumento no ancho das bases do *jacket*. As funcións de agregación de restricións para as restricións dependentes do tempo demostrouse eficaz fronte a problemas con varios casos de carga e un grande coste computacional. O uso de Diferenciación Directa fronte a Estado Adxunto foi claramente vantaxoso neste caso debido ao reducido número de variables de deseño en comparación co número de restricións. A elección das variables de deseño permitiu optimiza-las dimensións e forma dos *jackets* mantendo a súa configuración, conectividade e sinxeleza. Por último, mencionar que tamén se propón a optimización dos *jackets* trasladando as transicións entre as distintas seccións transversais das barras das unións cara as partes intermedias das patas do *jacket*. Deste modo evítase a xeración de nodos excesivamente complicados así como a introdución de concentracións de tensións adicionais.

O modelo formulado nesta tese abre as portas a futuras liñas de traballo de cara a unha mellora tanto do modelo estrutural como da metodoloxía de optimización. As liñas futuras de investigación máis prometedoras e relevantes que se sinalan son: A consideración da interacción solo-estrutura para un cálculo máis real das condicións dinámicas da estrutura; aborda-lo cálculo dende unha perspectiva completamente non-lineal tendo en conta sobre todo a non-linealidade na deformación das palas e o seu

impacto sobre as cargas de vento que efectivamente se producen; a introdución de novas variables de deseño que permitan acadar aínda meirandes reducións do peso dos *jackets*; o cálculo da análise de sensibilidade de segundo orde para lograr un algoritmo aínda máis eficiente. Por último, sería altamente vantaxoso a aplicación de técnicas de cálculo en paralelo ao código desenvolto testa tese; non so para mellora-los rendementos computacionais do algoritmo de análise e optimización, senón tamén para lograr un modelado completo de tódolos casos de carga de vento e ondas en calquera dirección que se poden producir nunha instalación *offshore*.

*"We have to go. I'm almost happy here."*
**Orson Scott Card**, Ender's Game.

# Bibliography


ABS (2003). *Fatigue assessment of offshore structures*. American Bureau of Shipping. ↑50 , ↑163

Adhikari, S. (2000). *Damping Models for Structural Vibration*. PhD thesis, Cambridge University. ↑25

Ahmadi, H. & Lotfollahi-Yaghin, M. A. (2012). Geometrically parametric study of central brace scfs in offshore three-planar tubular kt-joints. *Journal of Constructional Steel Research*, 71, 149–161. ↑163

Ahmadi, H., Lotfollahi-Yaghin, M. A., & Aminfar, M. H. (2011). Distribution of weld toe stress concentration factors on the central brace in two-planar chs dkt-connections of steel offshore structures. *Thin-Walled Structures*, 49(10), 1225–1236. ↑163

Ahmadi, H., Lotfollahi-Yaghin, M. A., & Aminfar, M. H. (2012). The development of fatigue design formulas for the outer brace scfs in offshore three-planar tubular kt-joints. *Thin-Walled Structures*, 58, 67–68. ↑163

Aliabadi, M. (2002). *The Boundary Element Method: Volume 2: Applications in Solids and Structures*. Wiley. ↑28

API-RP-2A-LRFD (1993). *Planning, designing and constructing fixed offshore platforms - Load and resistnace factor design*. American Petroleum Institute. ↑67

Arora, J. (1989). *Introduction to optimum design*. McGraw-Hill. ↑114

ASTM-E1049-85(2011)e1 (2011). *Standard Practice for Cycle Counting in Fatigue Analysis*. American Society for Testing and Materials. ↑53

Bai, Y., Liang, R., & Yang, Z. (2016). Splitting augmented lagrangian method for optimization problems with a cardinality constraint and semicontinuous variables. *Optimization Methods and Software*, 31(5), 1089–1109. ↑110

Bathe, K. & Noh, G. (2012). Insight into an implicit time integration scheme for structural dynamics. *Computers and Structures*, 98-99, 1–6. ↑42

Bathe, K. & Wilson, E. (1973). Stability and accuracy analysis of direct integration methods. *Earthquake Engineering and Structural Dynamics*, 1, 283–291. ↑42

Betz, A. (1919). Schraubenpropeller mit geringstem energieverlust. *Gottinger Nachr.* ↑29

Birgin, E. & Martínez, J. (2014). *Practical Augmented Lagrangian Methods for Constrained Optimization*. SIAM. ↑109

Brebbia, C. & Domínguez, J. (1992). *Boundary elements: An introductory course*. WIT Press. ↑28

Burton, T., Sharpe, D., Jenkins, N., & Bossanyi, E. (2001). *Wind Energy Handbook*. John Wiley & Sons, Inc. ↑28 , ↑30 , ↑31 , ↑48

Carrera, E., Giunta, G., & Petrolo, M. (2011). *Beam Structures. Classical and advanced theories*. John Wiley & Sons, Inc. ↑18

Caughey, T. & O'Kelly, M. (1965). Classical normal modes in damped linear dynamic systems. *Transactions of ASME, Journal of Applied Mechanics*, 32, 583–588. ↑25

Chakrabarti, S. (2005). *Handbook of Offshore Engineering.*, volume 1. Elsevier. ↑5 , ↑34 , ↑35

Chang, S.-Y. (2004a). Studies of newmark method for solving nonlinear systems: I basic analysis. *Journal of the Chinese Institute of Engineers*, 27(5), 651–662. ↑46

Chang, S.-Y. (2004b). Studies of newmark method for solving nonlinear systems: Ii verification and guideline. *Journal of the Chinese Institute of Engineers*, 27(5), 663–675. ↑46

Chen, T.-Y. (1993). Calculation of the move limits for the sequential linear programming method. *International Journal for Numerical Methods in Engineering*, 36, 2661–2679. ↑114

Cheng, F. Y. (2001). *Matrix Analysis of Structural Dynamics*. Marcel Dekker, Inc. ↑23 , ↑24

Chew, K. H., Muskulus, M., Narasimalu, S., Tai, K., & Ng, E. (2015). Fatigue sensitivity analysis of offshore wind turbine structures. In *11th Congress On Structural and Multidisciplinary Optimization* Sydney, Australia. ↑100

Chew, K. H., Muskulus, M., Zwick, D., Ng, E., & Tai, K. (2013). Structural optimization and parametric study of offshore wind turbine jacket substructure. In *Proceedings of the Twenty-third International Offshore and Polar Engineering* Anchorage, Alaska, USA. ↑8 , ↑9 , ↑100

Chew, K.-H., Tai, K., Ng, E., & Muskulus, M. (2016). Analytical gradient-based optimization of offshore wind turbine substructures under fatigue and extreme loads. *Marine Structures*, 47, 23–41. ↑8 , ↑9 , ↑100 , ↑111 , ↑137 , ↑138

Chiew, S.-P., Soh, C.-K., & Wu, N.-W. (1999). Experimental and numerical stress analyses of tubular xt-joints. *Journal of Structural Engineering, ASCE*, 125(11), 1239–1248. ↑163

Choi, K. K. & Kim, N.-H. (2005). *Structural Sensitivity Analysis and Optimization*, volume 2. Springer. ↑100

Chong, E. K. & Zak, S. H. (2001). *An Introduction to Optimization*. Wiley. ↑108

Chopra, A. K. (1995). *Dynamics of Structures. Theory and applications to earthquake engineering*. Prentice Hall. ↑25 , ↑46

Clough, R. W. & Penzien, J. (1995). *Dynamics of Structures*. Computers and Structures, Inc. ↑23

Cui, W., Huang, X., & Wang, F. (2014). *Towards a Unified Fatigue Life Prediction Method for Marine Structures*. Springer. ↑50

Curtis, F. E., Jiang, H., & Robinson, D. P. (2015). An adaptive augmented lagrangian method for large-scale constrained optimization. *Mathematical Programming*, 152(1-2), 201–245. ↑110

Dalrymple, R. & Heideman, J. (1989). Non-linear water waves on a vertically-sheared current. In *E & P Forum Workshop* Paris. ↑38

Dantzig, G. (1987). *Origins of the Simplex Method.* Technical report, Department of Operations Research, Standfor University. ↑114

Dantzig, G. B. & Thapa, M. N. (1997a). *Linear Programming I: Introduction*. Springer. ↑114

Dantzig, G. B. & Thapa, M. N. (1997b). *Linear Programming II: Theory and Extensions*. Springer. ↑114

de Vries, W. (2011). *Final report WP 4.2: Support structure concepts for deep water sites: Deliverable D4.2.8*. Technical report, UpWind Project. ↑122 , ↑151

Dentcheva, D., Martínez, G., & Wolfhagen, E. (2016). Augmented lagrangian methods for solving optimization problems with stochastic-order constraints. *Operations Research*, 64(6), 1451–1456. ↑110

DIN EN 10220:2002 (2002). *Seamless and welded steel tubes*. European Standard. ↑138

Dirlik, T. (1985). *Applications of Computers in Fatigue Analysis*. PhD thesis, University of Warwick. ↑53

DNV-OS-C101 (2014). *Design of offshore steel structures, general (LRFD method)*. Det Norske Veritas. ↑7 , ↑25 , ↑35 , ↑61 , ↑67

DNV-OS-J101 (2010). *Design of offshore wind turbine structures*. Det Norske Veritas. ↑36 , ↑42

DNV-RP-C203 (2011). *Fatigue design of offshore steel structures*. Det Norske Veritas. ↑50 , ↑51 , ↑52 , ↑133 , ↑145 , ↑146 , ↑149 , ↑152 , ↑161 , ↑162 , ↑163 , ↑164 , ↑169

DNV-RP-C205 (2010). *Environmental Conditions and Environmental Loads*. Det Norske Veritas. ↑42

Dolan, D. S. & Lehn, P. W. (2006). Simulation model of wind turbine 3p torque oscillations due to wind shear and tower shadow. *IEEE Transactions on Energy Conversion*, 21(3), 717–723. ↑33

Duysinx, P. & Sigmund, O. (1998). New developments in handling stress constraints in optimal material distributions. In *7th AIAA/USAF/NASA/ISSMO Symposium on Multidisciplinary Design Optimization* St Louis, Missouri, USA. ↑73

Efthymiou, M. (1988). Development of scf formulae and generalised influence functions for use in fatigue analysis. In *Offshore Tubular Joints Conference on Recent Developments in Tubular Joints Technology* London. ↑164

El-Reedy, M. A. (2015). *Marine Structural Design Calculations*. Elsevier. ↑5 , ↑24

Elshafey, A. A., Haddara, M. R., & Marzouk, H. (2009). Dynamic response of offshore jacket structures under random loads. *Marine Structures*, 22, 504–521. ↑25

Endo, T., Matsuishi, M., Mitsunaga, K., Kobayashi, K., & Takahashi, K. (1974). Rain flow method - the proposal and the applications. *Memoir Kyushu Institute Technical Engineering*. ↑53

Endo, T., Mitsunaga, K., & Nakgawa, H. (1967a). Fatigue of metals subjected to varying stress - prediction of fatigue lives. In *Preliminary Proceedings of The Chugoku-Shikoku District Meeting, The Japan Society of Mechanica Engineers*. ↑53

Endo, T., Mitsunaga, K., Nakgawa, H., & Ikeda, K. (1967b). Fatigue of metals subjected to varying stress - low cycle, middle cycle fatigue. In *Preliminary Proceedings of The Chugoku-Shikoku District Meeting, The Japan Society of Mechanica Engineers*. ↑53

Fletcher, R. (2000). *Practical Methods of Optimization*. Wiley. ↑108

Gans, H. D. & Anderson, W. J. (1991). Structural optimization including centrifugal effects. *Finite Elements in Analysis and Design*, 7, 317–324. ↑48

Geradin, M. & Kill, N. (1984). A new approach to finite element modelling of flexible rotors. *Engineering Computations*, 1(1), 52–64. ↑48

Gill, P. E., Murray, W., & Wright, M. H. (1989). *Practical Optimization*. Academic Press. ↑109

Glauert, H. (1935). Airplane propellers. *Aerodynamic Theory*, 4, 169–360. ↑30

Griffith, R. & Stewart, R. (1961). A nonlinear programming technique for the optimization of continuous processing systems. *Management Sciencie*, 7, 379–392. ↑113

Guizán, R. (2018). *A general formulation for computational design of grounding systems in underground electrical substations*. PhD thesis, University of A Coruña. ↑28

Hafka, R., Gurdal, Z., & Kamat, M. (1990). *Elements of structural optimization*. Kluwer. ↑114

Hamdi, H., Mrad, C., Hamdi, A., & Nasri, R. (2014). Dynamic response of an horizontal axis wind turbine blade under aerodynamic, gravity and gyroscopic effects. *Applied Acoustics*, 86, 154–164. ↑48

Hansen, M. O. (2015). *Aerodynamics of Wind Turbines*. Routledge. ↑28 , ↑31

Haritos, N. (2007). Introduction to the analysis and design of offshore structures - an overview. *Electronic Journal of Structural Engineering, Special Issue: Loading on Structures*, (pp. 55–65). ↑37

Hau, E. (2006). *Wind Turbines. Fundamentals, Technologies, Application, Economics*. Springer. ↑2 , ↑28 , ↑34

Hernández, S. (1990). *Métodos de Diseño Óptimo de Estructuras*. Colegio de Ingenieros de Caminos, Canales y Puertos, PARANINFO. ↑108 , ↑113

Hsieh, C. & Arora, J. S. (1984). Design sensitivity analysis and optimization of dynamic response. *Computer Methods in Applied Mechanics and Engineering*, 43, 195–219. ↑72

Hughes, T. J. (1987). *The Finite Element Method. Linear Static and Dynamic Finite Element Analysis*. Prentice-Hall, Inc. ↑42

ISO19901-1 (2005). *BS EN ISO 19901-1: Petroleum and natural gas industries - Specific requirements for offshore structures - Part 1: Metaocean design and operating considerations*. British Standard. ↑38

ISO19902:2007 (2013). *BS EN ISO 19902:2007+A1:2013: Petroleum and natural gas industries - Fixed steel offshore structures*. British Standard. ↑24 , ↑25 , ↑35 , ↑61

James, K. A., Hansen, J. S., & Martins, J. R. (2009). Structural topology optimization for multiple load cases using a dynamic aggregation technique. *Engineering Optimization*, 41(12), 1103–1118. ↑74

Jia, J. (2014). Investigations of a practical wind-induced fatigue calculation based on nonlinear time domain dynamic analysis and a full wind-directional scatter diagram. *Ships and Offshore Structures*, 9(3), 272–296. ↑55

Jonkman, J., Butterfield, S., Musial, W., & Scott, G. (2009). *Definition of a 5-MW reference wind turbine for offshore system development.* Technical report, NREL: National Renewable Energy Laboratory. ↑32 , ↑122 , ↑123 , ↑138 , ↑148

Kang, B.-S., Park, G.-J., & Arora, J. S. (2006). A review of optimization of structures subjected to transient loads. *Structural and Multidisciplinary Optimization*, 31, 81–95. ↑72

Karadeniz, H., Toğan, V., Daloğlu, A., & Vrouwenvelder, T. (2010). Reliability-based optimisation of offshore jacket-type structures with an integrated-algurithms system. *Ships and Offshore Structures*, 5(1), 67–74. ↑8 , ↑111

Karamanos, S. A., Romeijn, A., & Wardenier, J. (1999). Stress concentrations in multi-planar welded chs xx-connections. *Journal of Constructional Steel Research*, 50, 259–282. ↑163

Karimirad, M. (2014). *Offshore Energy Structures.* Springer. ↑3

Kassimali, A. (2012). *Matrix analysis of structures.* Cengage Learning. ↑15

King, J., Cordle, A., & McCann, G. (2013). Cost reductions in offshore wind turbine jacket design using integrated analysis and advanced control. In *Proceedings of the Twenty-third International Offshore and Polar Engineering* Anchorage, Alaska, USA. ↑8

Kreisselmeier, G. & Steinhauser, R. (1979). Systematic control design by optimizing a vector performance indicator. In *Symposium on Computer-Aided Design of Control Systems, IFAC* Zurich, Switzerland. ↑73

Kvittem, M. I. & Moan, T. (2015). Time domain analysis procedures for fatigue assessment of a semi-submersible wind turbine. *Marine Structures*, 40, 38–59. ↑55

Lalanne, C. (1999). *Mechanical Vibration and Shock Analysis. Volume 4: Fatigue Damage.* Wiley. ↑51 , ↑52

Lambe, A. B., graeme J. Kennedy, & Martins, J. R. (2017). An evaluation of constraint aggregation strategies for wing box mass minimization. *Structural and Multidisciplinary Optimization*, 55, 257–277. ↑73

Lamberti, L. & Pappalettere, C. (2000). Comparison of the numerical efficiency of different sequential linear programming based algorithms for structural optimisation problems. *Computers & Structures*, 76, 713–728. ↑114 , ↑128

Lamberti, L. & Pappalettere, C. (2003). Move limits definition in structural optimization with sequential linear programming. part i: Optimization algorithm. *Computers & Structures*, 81, 197–213. ↑114

Lee, K. Y. & El-Sharkawi, M. A. (2008). *Modern Heuristic Optimization Techniques*. IEE Press, Wiley. ↑108

Lee, Y.-S., González, J. A., Lee, J. H., young II Kim, Park, K., & Han, S. (2016). Structural topology optimization of the transition piece for an offshore wind turbine with jacket foundation. *Renewable Energy*, 85, 1214–1225. ↑124

Lindenburg, C. (2002). *Aeroelastic modelling of the LMH64-5 blade*. Technical report, DOWEC-02-KL-083/0. ↑25

Marsh, G., Wignall, C., Thies, P. R., Barltrop, N., Incenik, A., Venugopal, V., & Johanning, L. (2016). Review and application of rainflow residue processing techniques for accurate fatigue damage estimation. *International Journal of Fatigue*, 82, 757–765. ↑53

Martens, J. H. (2014). *Topology Optimization of a Jacket for an Offshore Wind Turbine*. PhD thesis, Norwegian University of Science and Technology. ↑55

Martínez, S. (2012). *Optimización mixta de estructuras de apoyo de líneas de transporte de engergía*. PhD thesis, University of A Coruña. ↑70 , ↑107

Méhauté, B. L. (1976). *An Introduction to Hydrodynamics and Water Waves*. Springer. ↑35

Mohammadi, S. F., GAlgoul, N. S., Starossek, U., & Videiro, P. M. (2016). An efficient time domain fatigue analysis and its comparison to spectral fatigue assessment for an offshore jacket structure. *Marine Structures*, 49, 97–115. ↑54

Morison, J., O'Brien, M., Johnson, J., & Schaaf, S. (1950). The force exerted by surface waves on piles. *Petroleum Transactions*, 189, 149–154. ↑36

Murakami, Y. (1992). *The rainflow method in fatigue - The Tatsuo Endo memorial volume*. Butterworth-Heinemann. ↑53

Musial, W., Butterfield, S., & Sam, B. (2006). Energy from offshore wind. *NREL/CP-500-39450*. ↑10

Muskulus, M. & Schafhirt, S. (2014). Design optimization of wind turbine support structures - a review. *Journal of Oceand and Wind Energy*, 1(1), 12–22. ↑8

Myers, A., Arwade, S., Valamanesh, V., Hallowell, S., & Carswell, W. (2015). Strength, stiffness, resonance and the design of offshore wind turbine monopiles. *Engineering Structures*, 100, 332–341. ↑69

Nasseri, T., Shabakhty, N., & Afshar, M. H. (2014). Study of fixed jacket offshore platform in the optimization design process under environmental loads. *International Journal of Maritime Technology*, 2, 75–84. ↑8 , ↑111

Navarrina, F. & Casteleiro, M. (1991). A general methodological analysis for optimum design. *International Journal for Numerical Methods in Engineering*, 31, 85–111. ↑78

Navarrina, F., Gómez, H., París, J., & Colominas, I. (2012). Isogeometric shape sensitivity analysis. *Computer Aided Optimum Design in Engineering XII*, 125, 119–130. ↑80

Navarrina, F., López-Fontán, S., Colominas, I., Bendito, E., & Casteleiro, M. (2000). High order shape design sensitivity: a unified approach. *Computer Methods in Applied Mechanics and Engineering*, 188, 681–696. ↑81

Newmark, N. M. (1959). A method of computation for structural dynamics. *Journal of the Engineering Mechanics Division, Proceedings of the American Society of Civil Engineers*, 1, 67–94. ↑42

Norsok (2004). *Design of steel structures*. Standards Norway. ↑61 , ↑169

Oñate, E. (1992). *Cálculo de Estructuras por el Método de Elementos Finitos*. CIMNE. ↑18

Oest, J., Sorensen, R., Overgaard, L. C. T., & Lund, E. (2017). Structural optimization with fatigue and ultimate limit constraints of jacket structures for large offshore wind turbines. *Structural and Multidisciplinary Optimization*, 55(33), 779–793. ↑9 , ↑92 , ↑111

Palmgren, A. (1924). Die lebensdauer von kugellagern. *VDI-Zeitschrift*, 68, 339–341. ↑50

París, J. (2007). *Restricciones en tensión y minimización del peso: una metodología general para la optimización topológica de estructuras*. PhD thesis, University of A Coruña. ↑73 , ↑114 , ↑120

París, J., Navarrina, F., Colominas, I., & Casteleiro, M. (2009). Topology optimization of continuum structures with local and global stress constraints. *Structural and Multidisciplinary Optimization*, 39, 419–437. ↑73

París, J., Navarrina, F., Colominas, I., & Casteleiro, M. (2010). Block aggregation of stress constraints in topology optimization of structures. *Advances in Engineering Software*, 41, 433–441. ↑73

Passon, P. & Branner, K. (2014). Load calculation methods for offshore wind turbine foundations. *Ships and Offshore Structures*, 9(4), 433–449. ↑44

Paz, M. (2003). *Structural Dynamics*. Kluwer Academic Publishers. ↑23

Pérez-Collazo, C., Greaves, D., & Iglesias, G. (2015). A review of combined wave and offshore wind energy. *Renewable and Sustainable Energy Reviews*, 42, 141–153. ↑3

Pilkey, W. D. (2005). *Formulas for stress, strain, and structural matrices*. John Wiley & Sons, Inc. ↑18

Popko, W., Vorphal, F., Zuga, A., Kohlmeier, M., Jonkman, J., Robertson, A., Larsen, T. J., Yde, A., Sætertrø, K., Okstad, K. M., Nichols, J., Nygaard, T. A., Gao, Z., Manolas, D., Kim, K., Yu, Q., Shi, W., Park, H., Vásquez-Rojas, A., Dubois, J., Kaufer, D., Thomassen, P., de Ruiter, M. J., van der Zee, T., Peeringa, J. M., Zhiwen, H., & von Waaden, H. (2014). Offshore code comparison collaboration continuation (oc4), phase i—results of coupled simulations of an offshore wind turbine with jacket support structure. *Journal of Ocean and Wind Energy*, 1, 1–11. ↑41 , ↑43 , ↑122

Przemieniecki, J. S. (1968). *Theory of Matrix Structural Analysis*. Dover Publications, Inc. ↑48

Ragan, P. & Manuel, L. (2007). Comparing estimates of wind turbine fagtigue loads usint time-domain and spectral methods. *Wind Engineering*, 31(2), 83–99. ↑54

Ramírez, L. (2015). *High-order finite volume methods based on moving least squares for computational fluid dynamics. Application to all-speed and incompressible flows on unstructured grids*. PhD thesis, University of A Coruña. ↑31

Rayleigh, L. (1877). *Theory of Sound*. Dover Publications. ↑25

Rockafellar, R. T. (1973). The multiplier method of hestenes and powell applied to convex programming. *Journal of Optimization Theroy and Applications*, 12, 555–562. ↑72 , ↑109

Saini, D. S., Karmakar, D., & Ray-Chaudhuri, S. (2016). A review of stress concentration factors in tubular and non-tubular joints for design of offshore installations. *Journal of Ocean Engineering and Science*, 1, 186–202. ↑162

Sauer, G. & Wolf, M. (1989). Finite element analysis of gyroscopic effects. *Finite Elements in Analysis and Design*, 5, 131–140. ↑48

Schafhirt, S., Zwick, D., & Muskulus, M. (2014). Reanalysis of jacket support structure for computer-aided optimization of offshore wind turbines with a genetic algorithm. *Journal of Ocean and Wind Energy*, 1(4), 209–216. ↑8 , ↑9

Schafhirt, S., Zwick, D., & Muskulus, M. (2016). Two-stage local optimization of lattice type support structures for offshore wind turbines. *Ocean Engineering*, 117, 163–173. ↑8 , ↑9 , ↑111

Shabana, A. A. (1997). Flexible multibody dynamics: Review of past and recent develompments. *Multibody System Dynamics*, 1, 189–222. ↑44

Spera, D. (1994). *Wind Turbine Technology.* ASME Press. ↑32

Spera, D. A. (2008). *Models of Lift and Drag Coefficients of Stalled and Unstalled Airfoils in Wind Turbines and Wind Tunnels.* Technical report, NASA/CR-2008-215434. ↑31

Stieng, L. E. S., Hetland, R., Schafhirt, S., & Muskulus, M. (2015). Relative assessment of fatigue loads for offshore wind turbine support structures. In *Energy Procedia. 12th Deep Sea Offshore Wind R&D Conference* Norway. ↑55

Toprac, A. & Beale, A. (1967). Analysis of in-plane t, y and k welded tubular connections. *Welding Research Council 125.* ↑161

UK-HSE (1997). *OTH 354: Stress concentration factors for simple tubular joints. Assessment of existing and development of new parametric formulae.* Technical report, Health and Safety Executive, Prepared by Lloyd's Register of Shipping. ↑164

van der Tempel, J. & Molenaar, D.-P. (2002). Wind turbine structural dynamics – a review of the principles for modern power generation, onshore and offshore. *Wind Engineering*, 6(4), 211–220. ↑39

von Mises, R. & Pollaczek-Geiringer, H. (1929). Praktische verfahren der gleichungsauflösung. *Zeitschrift für Angewandte Mathematik und Mechanik*, 9, 152–164. ↑39 , ↑40

Vorpahl, F. & Popko, W. (2012). *Description of the load cases and output sensors to be simulated in the OC4 project under IEA Wind Annex XXX.* Technical report, Fraunhofer Institute for Wind Energy and Energy System Technology IWES. ↑122

Vorpahl, F., Popko, W., & Kaufer, D. (2012). *Description of a basic model of the UpWind reference jacket for code comparison in the OC4 project under IEA Wind Annex XXX.* Technical report, Fraunhofer Institute for Wind Energy and Energy System Technology IWES. ↑122 , ↑123

Wallrapp, O. & Schwertassek, R. (1991). Representation of geometric stiffening in multibody system simulationi. *International Journal for Numerical Methods in Engineering*, 32, 1833–1850. ↑48

Wang, Q. & Arora, J. S. (2005). Alternative formulations for transient dynamic response optimization. *American Institute of Aeronautics and Astronautics Journal*, 43(10), 2188–2195. ↑72

Wang, Q. & Arora, J. S. (2009). Several simultaneous formulations for transient dynamic response optimization: An evaluation. *International Journal for Numerical Methods in Engineering*, 80, 631–650. ↑72

Weaver, W. & Gere, J. M. (1990). *Matrix Analysis of Framed Structures*. Computers and Structures, Inc. ↑38

Wilson, E. L. (2001). *Three-dimensional static and dynamic analysis of structures*. Van Nostrand Reinhold. ↑18

Wilson, J. F. (2003). *Dynamics of Offshore Structures*. John Wiley & Sons, Inc. ↑5

Woghiren, C. & Brennan, F. (2009). Weld toe stress concentrations in multi-planar stiffened tubular kk joints. *International Journal of Fatigue*, 31(1), 164–172. ↑163

Yan, Q., Zhang, Z., Cui, L., & Wang, Y. (2010). Structural optimization of offshore jacket platform based on ansys. *Advanced Materials Research*, 163-167, 3029–3033. ↑8

Yeter, B., Garbatov, Y., & Soares, C. G. (2015). Fatigue damage assessment of fixed offshore wind turbine tripod support structures. *Engineering Structures*, 101, 518–528. ↑44 , ↑55

Yoshida, S. (2006). Wind turbine tower optimization method using a genetic algorithm. *Wind Engineering*, 30(6), 453–470. ↑8 , ↑111

Zengah, S., Aid, A., & Benguediab, M. (2013). Comparative study of fatigue damage models using different number of classes combined with the rainflow method. *Engineering, Technology & Applied Science Research*, 3(3), 446–451. ↑53

Zhu, Y. (2014). *Sensitivity Analysis and Optimization of Multibody Systems*. PhD thesis, Virginia Polytechnic Institute and State University. ↑44

Zoutendijk, G. (1960). *Methods of Feasible Directions*. Elsevier. ↑110

Zwick, D. (2015). *Simulation and optimization in offshore wind turbine structural analysis*. PhD thesis, Norwegian University of Science and Technology. ↑55

Zwick, D., Muskulus, M., & Moe, G. (2012). Iterative optimization approach for the design of full-height lattice towers for offshore wind turbines. *Energy Procedia*, 24, 297–304. ↑8 , ↑111